QUANTIFYING FLUVIAL RESISTANCE OF STREAMBANKS USING JET EROSION TESTS

By

ERIN REBECCA DALY

Bachelor of Science in Biosystems Engineering
Clemson University
Clemson, SC
2010

Master of Science in Biosystems and Agricultural Engineering
Oklahoma State University
Stillwater, OK
2012

Submitted to the Faculty of the
Graduate College of the
Oklahoma State University
in partial fulfillment of
the requirements for
the Degree of
DOCTOR OF PHILOSOPHY
December, 2014

QUANTIFYING FLUVIAL RESISTANCE OF

STREAMBANKS USING JET EROSION TESTS

Dissertation Approved:

Dr. Garey Fox

Dissertation Adviser

Dr. Daniel Storm

Dr. Sherry Hunt

Dr. Rifat Bulut

ACKNOWLEDGEMENTS

I would like to acknowledge the financial support of the Buchanan Family Trust through the Buchanan Endowed Chair at Oklahoma State University. My committee was incredible to work with and supported and challenged me along the way. I am especially grateful of my advisor, Dr. Garey Fox. I could not have asked for a better role model and mentor. Through Dr. Fox's encouragement, guidance, and support I have gained irreplaceable knowledge on what it means to be an outstanding researcher, teacher, mentor, family member, and friend. Thank you also to Dr. Dan Storm, who provided me with valuable guidance, Dr. Sherry Hunt, who served as a wonderful professional role model for myself, and Dr. Rifat Bulut, who provided support along the way. A sincere thank you to my committee who helped me to grow so much over these two years.

I am also appreciative to all of the students who helped me in the field, lab, and office – Anish Khanal, Holly Enlow, Rebecca Purvis, Whitney Lisenbee, Kate Klavon, and Yan (Joey) Zhou. I would have never been able to finish without their unending support and laughter. I could not have asked for a more special and talented group to work with and they will forever be my "Fox Family."

I would also like to thank my parents, Frank and Lynne Daly, who provided love and encouragement throughout this process. Finally, I am indescribably appreciative of my fiancé, Wesley Porter. His endless encouragement, support, and love made all of this possible. He gives everything in my life purpose and will always drive me to be my best.

Name: Erin R. Daly

Date of Degree: DECEMBER, 2014

Title of Study: QUANTIFYING FLUVIAL RESISTANCE OF STREAMBANKS USING JET EROSION TESTS

Major Field: Biosystems and Agricultural Engineering

Abstract: The United States has over forty-thousand impaired water bodies with sediment listed as one of the top five causes of impairment. Recent research has found that more than 50% of fine sediment in watersheds originates from channel sources. This highlights the need for watershed management strategies geared towards channel erosion, specifically in the form of streambank erosion. Process-based models are often used to study streambank erosion mechanisms and predict erosion in order to work towards more comprehensive watershed management solutions. The fluvial erosion component of these models is based on the excess shear stress equation dependent on the erodibility parameters – the critical shear stress (τ_c) and the erodibility coefficient (k_d). One of the most commonly used methods of measuring the erodibility parameters is the Jet Erosion Test (JET). However, there has been discussion recently regarding the derivation of the erodibility parameters from JET data, the variability of results, and the effects of subaerial processes on parameter estimation. There remains a large gap in the knowledge with regard to these points. In order to begin addressing some of these gaps, the overall objectives of this research were (1) to evaluate new solution methodologies for the derivation of the erodibility parameters, τ_c and k_d, from the JET, (2) investigate the erodibility parameters using all three techniques by considering parameter uniformity, correlations between the derived parameters and physical soil properties, and the applicability of currently proposed relationships to estimate the erodibility parameters at both a site and watershed scale, and (3) to apply the results from JET data to composite streambanks within a process-based modeling framework. The new solution methodologies, the scour depth and iterative solutions, were found to provide improved fits over the Blaisdell solution and incorporated into an automated spreadsheet. The erodibililty parameters were explored at both a site and watershed scale and found to vary spatially and temporally by orders of magnitude. This large amount of variation, coupled with the new solution techniques, have shown currently used empirical relationships to estimate the erodibility parameters to be generally invalid for the systems included in this study. This research highlights the need to measure the erodibility parameters *in situ* and the continued research into parameter variability and the role of subaerial processes in cohesive streambank erosion.

TABLE OF CONTENTS

Chapter Page

I. CHAPTER 1
INTRODUCTION 1

1.1 Background 1
1.2 Objectives and Overview 3

II. CHAPTER 2
A SCOUR DEPTH APPROACH FOR DERIVING ERODIBILITY PARAMETERS FROM JET EROSION TESTS 5

2.1 Abstract 5
2.2 Introduction 6
2.3 Materials and Methods 11
2.3.1 Solution Techniques 11
2.3.2 JET Spreadsheet 14
2.3.3 Field Data 18
2.4 Results and Discussion 21
2.5 Conclusions 23
2.6 Acknowledgements 24

III. CHAPTER 3
VARIABILITY OF FLUVIAL ERODIBILITY PARAMETERS FOR STREAMBANKS ON A WATERSHED SCALE 25

3.1 Abstract 25
3.2 Introduction 26
3.3 Materials and Methods 30
3.3.1 Watershed Description 30
3.3.2 Data Collection 31
3.3.3 Derivation of Erodibility Parameters 32
3.3.4 Evaluating Existing Relationships 33

3.3.5 Statistical Analysis 35
3.4 Results and Discussion 36
3.4.1 Variability and Correlations 36
3.4.2 Estimating the Critical Shear Stress 41
3.4.3 Estimating the Erodibility Coefficient 46
3.4.4 Wilson Model Parameters 50
3.5 Conclusions 52
3.6 Acknowledgements 54

IV. CHAPTER 4
SITE-SCALE VARIABILITY OF STREAMBANK FLUVIAL ERODIBILITY PARAMETERS AS MEASURED WITH A JET EROSION TEST 55

4.1 Abstract 55
4.2 Introduction 56
4.3 Materials and Methods 59
4.3.1 Site Descriptions 59
4.3.2 Data Collection 61
4.3.3 Derivation of Erodibility Parameters 62
4.3.4 Statistical Analysis 66
4.3.5 Evaluating Empirical Relationships 68
4.4 Results and Discussion 70
4.4.1 Variability in JET Measurements 70
4.4.2 Sample Size Determination 80
4.4.3 Spatial Variability 91
4.4.4 Evaluating Empirical Relationships 95
4.5 Conclusions 103
4.6 Acknowledgements 104

V. CHAPTER 5
CORRELATING ERODIBILITY PARAMETERS FROM JET EROSION TESTS TO SOIL PROPERTIES ON A SITE SCALE 105

5.1 Abstract 105
5.2 Introduction 106
5.3 Materials and Methods 114
5.3.1 Site Descriptions 114
5.3.2 Data Collection 116

5.3.3 Evaluating Empirical Relationships 118
5.3.4 Statistical Analysis 119
5.4 Results and Discussion 120
5.5 Conclusions 138
5.6 Acknowledgements 139

VI. CHAPTER 6
MODELING STREAMBANK EROSION AND FAILURE ALONG PROTECTED AND UNPROTECTED COMPOSITE STREAMBANKS 140

6.1 Abstract 140
6.2 Introduction 141
6.2.1 BSTEM Model Description 143
6.2.2 Influence of Riparian Vegetation 148
6.2.3 Objectives 149
6.3 Materials and Methods 151
6.3.1 Description of Study Sites 151
6.3.2 Streambank Testing 154
6.3.3 Aerial Imagery Analysis 156
6.3.4 Model Calibration 157
6.3.5 Root Biomass and Cohesion 162
6.3.6 Critical Study Period 163
6.4 Results and Discussion 164
6.4.1 Aerial Imagery Analysis of Bank Retreat 164
6.4.2 Bank Stability Modeling 167
6.4.3 Field Monitoring of Streambank Erosion Rates 174
6.5 Conclusions 177
6.6 Acknowledgements 178

VII. CHAPTER 7
CONCLUSIONS 179

7.1 Conclusions 179
7.2 Recommendations for Future Research 183

VIII. CHAPTER 8
REFERENCES 186

LIST OF TABLES

Table Page

Table 2.1. Solutions based on varying initial guesses of τ_c and k_d for the Blaisdell solution and the scour depth solution. See Figure 2.4 for an example solution for both approaches..... 21

Table 2.2. Solutions based on varying initial guesses of τ_c and k_d for the Blaisdell solution and the scour depth solution. 22

Table 3.1. Summary statistics for average parameters measured at 13 sites within the Illinois River watershed. 39

Table 3.2. Results of the Mann-Whitney rank sum test for estimates of τ_c. The Blaisdell and scour depth values measured from the JET were compared to estimates based on the silt-clay content (*SC*), mean particle size (d_{50}), and clay content (P_c). Estimate methods that were significantly different from the measured values (α = 0.05) are indicated by *..... 44

Table 3.3. Results of the Mann-Whitney rank sum test for estimates of k_d. The Blaisdell and scour depth values measured from the JET were compared to estimates based on Hanson and Simon (*HS*), Simon et al. (*S*), and the National Engineering Handbook (*NEH*). Estimate methods that were significantly different from the measured values (α = 0.05) are indicated by *. 49

Table 4.1. Summary statistics for erodibility parameters at each site derived from the Blaisdell solution ($\tau_{c\text{-}BL}$, $k_{d\text{-}BL}$), scour depth solution ($\tau_{c\text{-}SD}$, $k_{d\text{-}SD}$), and iterative solution ($\tau_{c\text{-}IT}$, $k_{d\text{-}IT}$)..... 74

Table 4.2. Anderson-Darling (AD) test statistics and respective p-values for all 18 parameters analyzed for both the normal and log-normal distributions. Non-significant results (α = 0.05) are highlighted in red, indicating the best distribution fit. 79

Table 4.3. Example of required sample sizes to guarantee with 95% confidence that the observed mean is within a certain range of error using the Blaisdell (BL), scour depth (SD), and iterative (IT) solutions. Calculations assume that parameters follow a normal distribution..... 84

Table 4.4. Example of required sample sizes to guarantee with 95% confidence that the observed mean is within a certain range of error using the Blaisdell (BL), scour depth (SD), and iterative (IT) solutions. Calculations assume that parameters follow a log-normal distribution. 88

Table 4.5. Precision achieved for sample sizes of three and five JETs assuming parameters follow a normal or log-normal distribution. Calculations are shown for a 95% confidence level (Z = 1.96). Blaisdell solution ($\tau_{c\text{-}BL}$, $k_{d\text{-}BL}$), scour depth solution ($\tau_{c\text{-}SD}$, $k_{d\text{-}SD}$), and iterative solution ($\tau_{c\text{-}IT}$, $k_{d\text{-}IT}$). 90

Table 4.6. Amount of precision achieved using various methods assuming parameters follow a normal distribution. Calculations are shown for a 95% confidence level (Z = 1.96) and a sample size, n = 3. Blaisdell solution ($\tau_{c\text{-}BL}$, $k_{d\text{-}BL}$), scour depth solution ($\tau_{c\text{-}SD}$, $k_{d\text{-}SD}$), and iterative solution ($\tau_{c\text{-}IT}$, $k_{d\text{-}IT}$). 99

Table 4.7. Amount of precision achieved using various methods assuming parameters follow a log-normal distribution. Calculations are shown for a 95% confidence level (Z = 1.96) and a sample size, n = 3. Blaisdell solution ($\tau_{c\text{-}BL}$, $k_{d\text{-}BL}$), scour depth solution ($\tau_{c\text{-}SD}$, $k_{d\text{-}SD}$), and iterative solution ($\tau_{c\text{-}IT}$, $k_{d\text{-}IT}$). 100

Table 4.8. Amount of precision achieved using various methods assuming parameters follow a log-normal distribution. Calculations are shown for a 95% confidence level (Z = 1.96) and a sample size, n = 3. Blaisdell solution ($\tau_{c\text{-}BL}$, $k_{d\text{-}BL}$), scour depth solution ($\tau_{c\text{-}SD}$, $k_{d\text{-}SD}$), and iterative solution ($\tau_{c\text{-}IT}$, $k_{d\text{-}IT}$). 101

Table 4.9. Amount of precision achieved using various methods assuming parameters follow a log-normal distribution. Calculations are shown for a 95% confidence level (Z = 1.96) and a sample size, n = 3. Blaisdell solution ($\tau_{c\text{-}BL}$, $k_{d\text{-}BL}$), scour depth solution ($\tau_{c\text{-}SD}$, $k_{d\text{-}SD}$), and iterative solution ($\tau_{c\text{-}IT}$, $k_{d\text{-}IT}$). 102

Table 5.1. Summary statistics for erodibility parameters at each site derived from the Blaisdell solution ($\tau_{c\text{-}BL}$, $k_{d\text{-}BL}$), scour depth solution ($\tau_{c\text{-}SD}$, $k_{d\text{-}SD}$), and iterative solution ($\tau_{c\text{-}IT}$, $k_{d\text{-}IT}$)..... 122

Table 5.2. Linear regressions for prediction of erodibility parameters at Barren Fork. . 133

Table 5.3. Linear regressions for prediction of erodibility parameters at Cow Creek.... 134

Table 5.4. Linear regressions for prediction of erodibility parameters at Five Mile. 134

Table 6.1. Equations used to calculate root cohesion (c_r)..... 163

Table 6.2. Surveyed characteristics of study sites. 166

Table 6.3. Calibrated and original (base case) BSTEM model parameter values for Barren Fork Creek sites. Note that ϕ' is internal angle of friction, c' is cohesion, S_w is saturated weight of soil, τ_c is critical shear stress, k_d is soil erodibility, α is a factor that accounts for the stream radius of curvature at the site, and c_r is root cohesion based on the tree root biomass estimate. Historically unprotected sites have no c_r calibration. 169

LIST OF FIGURES

Figure Page

Figure 2.1. Example of the Data Input sheet from the updated spreadsheet routine. Required input data are highlighted in orange. 15

Figure 2.2. Example of the Solve sheet from the updated spreadsheet routine. 17

Figure 2.3. Example dimensionless scour function optimization using the Blaisdell solution (left) and the scour depth solution (right). J^* is a dimensionless scour depth and T^* is dimensionless time. 17

Figure 2.4. Example of observed and predicted scour depths using the Blaisdell solution and scour depth solution. 18

Figure 2.5. The Illinois River basin (Oklahoma only) with 13 sites (circles) at which JETs were conducted. 20

Figure 2.6. Example of "mini" JET being performed (right) and example of typical bank profile (left). 20

Figure 2.7. Correlation between k_d and τ_c (solid line) for the Illinois River watershed JET tests (triangles are derived from the Blaisdell solution, and circles are derived from the scour depth solution) and comparison to previously proposed relationships by Hanson and Simon (2001) (dashed line) and Simon et al. (2011) (dotted line). 23

Figure 3.1. The Illinois River basin (Oklahoma only) and location of the 13 sampling sites (left). Example of a typical bank profile showing a cohesive top layer and unconsolidated gravel bottom layer (right). JETs were conducted only in the cohesive layer. 32

Figure 3.2. Boxplots of variation at a site scale in (a) τ_c and (b) k_d using both solution techniques at four sites with at least three JETs performed. IR = Illinois River; BF = Barren Fork Creek; U = Upstream; and D = Downstream. 37

Figure 3.3. Boxplots of variation at a watershed scale in τ_c (left) and k_d (right) for both the Blaisdell solution (*BL*) and the scour depth solution (*SD*). 40

Figure 3.4. Spearman's rho (r_s) between k_d (right) or τ_c (left) for (a) the Blaisdell solution (*BL*) and (b) the scour depth solution (*SD*) and bulk density (*BD*), average particulate size (d_{50}), and percent clay, silt, sand, and silt-clay (*SC*). 41

Figure 3.5. Measured τ_c and silt-clay content with the Julian and Torres (2006) relationship indicated by the dotted line (left), and measured versus predicted τ_c using the Julian and Torres (2006) relationship (right). 42

Figure 3.6. Measured τ_c and d_{50} with the Smerdon and Beasley (1961) relationship indicated by the dotted line (left), and measured versus predicted τ_c using the Smerdon and Beasley (1961) relationship (right). 43

Figure 3.7. Measured τ_c and P_c with the Smerdon and Beasley (1961) relationship indicated by the dotted line (left), and measured versus predicted τ_c using the Smerdon and Beasley (1961) relationship (right). 44

Figure 3.8. Pairwise differences in τ_c values measured with the JET using the Blaisdell solution (BL) or the scour depth solution (SD) and estimated using silt-clay content (SC), mean particle size (d_{50}) and percent clay (Pc). 45

Figure 3.9. Measured k_d using the NEH (2011) relationship indicated by the dotted and solid lines (left), and measured versus predicted k_d using the NEH (2011) relationship (right). 46

Figure 3.10. Correlation between site-averaged k_d and τ_c for the Blaisdell solution (solid line) and the scour depth solution (long-dashed line) from multiple JETs (circles) and comparison to previously proposed relationships by Hanson and Simon (2001) (dotted line) and Simon et al. (2011) (short-dashed line). 47

Figure 3.11. Measured versus predicted k_d using the Hanson and Simon (2001) relationship for the Blaisdell (left) and scour depth (right) solutions. 48

Figure 3.12. Measured versus predicted k_d using the Simon et al. (2011) relationship for the Blaisdell (left) and scour depth (right) solutions. 48

Figure 3.13. Pairwise differences in k_d values measured with the JET using the Blaisdell solution (BL) or the scour depth solution (SD) and estimated using the Hanson and Simon (2001) relationship (HS), Simon et al. (2011) relationship (S), and the NEH (2011) relationship (NEH). 50

Figure 3.14. Correlation between Wilson Model parameters b_0 and b_1 for the in-situ JETs at 13 sites..... 51

Figure 3.15. Correlation between Wilson Model parameter b_0 and the erodibility coefficient, k_d, from the excess shear stress model (top) and between Wilson Model parameter b_1 and the critical shear stress, τ_c, from the excess shear stress model (bottom)..... 52

Figure 4.1. Location of Five Mile Creek, Cow Creek, and Barren Fork Creek in Oklahoma as sites chosen for variability studies (top). Pictures of banks sampled (bottom) at Five Mile Creek (left), Cow Creek (middle), and Barren Fork Creek (right) sites. 60

Figure 4.2. Soil textures for samples from (a) Barren Fork Creek, (b) Cow Creek, and (c) Five Mile Creek. 71

Figure 4.3. Bulk densities (top) and volumetric water contents (bottom) from samples at Barren Fork Creek, Cow Creek, and Five Mile Creek. 71

Figure 4.4. Range in erodibility parameters derived using the Blaisdell, scour depth, and iterative solution methodologies at Barren Fork Creek, Cow Creek, and Five Mile Creek. 73

Figure 4.5. Probability plots of the original and transformed τ_c and k_d derived using the Blaisdell (top), scour depth (middle), and iterative (bottom) solutions at Barren Fork Creek. 76

Figure 4.6. Probability plots of the original and transformed τ_c and k_d derived using the Blaisdell (top), scour depth (middle), and iterative (bottom) solutions at Cow Creek. 77

Figure 4.7. Probability plots of the original and transformed τ_c and k_d derived using the Blaisdell (top), scour depth (middle), and iterative (bottom) solutions at Five Mile Creek. 78

Figure 4.8. Sample size requirements for Barren Fork Creek for the erodibility parameters assuming a normal distribution for specified levels of confidence (legend) and precision unit deviation about the true mean (Δ). 81

Figure 4.9. Sample size requirements for Cow Creek for the erodibility parameters assuming a normal distribution for specified levels of confidence (legend) and precision unit deviation about the true mean (Δ). 82

Figure 4.10. Sample size requirements for Five Mile Creek for the erodibility parameters assuming a normal distribution for specified levels of confidence (legend) and precision unit deviation about the true mean (Δ). 83

Figure 4.11. Sample size requirements for Barren Fork Creek for the erodibility parameters assuming a log-normal distribution for specified levels of confidence (legend) and deviation percentage about the true mean (P). 85

Figure 4.12. Sample size requirements for Cow Creek for the erodibility parameters assuming a log-normal distribution for specified levels of confidence (legend) and deviation percentage about the true mean (P)..... 86

Figure 4.13. Sample size requirements for Five Mile Creek for the erodibility parameters assuming a log-normal distribution for specified levels of confidence (legend) and deviation percentage about the true mean (P)..... 87

Figure 4.14. Spatial variability at Barren Fork Creek in derived (a) τ_c (Pa) and (b) k_d (cm^3/Ns). JET sample points are indicated as black dots. 92

Figure 4.15. Spatial variability at Cow Creek in derived (a) τ_c (Pa) and (b) k_d (cm^3/Ns). JET sample points are indicated as black dots. The hatched area indicates an area of the bank that was heavily vegetated and thus not sampled. 93

Figure 4.16. Spatial variability at Five Mile Creek in derived (a) τ_c (Pa) and (b) k_d (cm^3/Ns). JET sample points are indicated as black dots. 94

Figure 4.17. Measured τ_c and silt-clay content with the *Julian* and *Torres* [2006] relationship indicated by the dotted line (left), and measured versus predicted τ_c using the *Julian* and *Torres* [2006] relationship (right). Data compiled from all three sites, totaling 74 JETs. 96

Figure 4.18. Coefficient of determination (R^2) between k_d and τ_c for each solution technique from 74 JETs (circles) compiled from all three sites (Barren Fork Creek, Cow Creek, and Five Mile Creek) and comparison to previously proposed relationships by *Hanson* and *Simon* [2001] (dashed line) and *Simon* et al. [2011] (dotted line). 97

Figure 5.1. Location of Five Mile Creek, Cow Creek, and Barren Fork Creek in Oklahoma as sites chosen for variability studies (top). Pictures of banks sampled (bottom) at Five Mile Creek (left), Cow Creek (middle), and Barren Fork Creek (right) sites. 108

Figure 5.2. Location of Five Mile Creek, Cow Creek, and Barren Fork Creek in Oklahoma as sites chosen for variability studies (top). Pictures of banks sampled (bottom) at Five Mile Creek (left), Cow Creek (middle), and Barren Fork Creek (right) sites. 115

Figure 5.3. Range in soil textures from samples at Barren Fork Creek, Cow Creek, and Five Mile Creek. 121

Figure 5.4. Range in volumetric water contents (left) and bulk densities (right) from samples at Barren Fork Creek, Cow Creek, and Five Mile Creek. 121

Figure 5.5. Range in erodibility parameters derived using the Blaisdell, scour depth, and iterative solution methodologies at (a) Barren Fork Creek, (b) Cow Creek, and (c) Five Mile Creek. 124

Figure 5.6. Contour plots showing (a) τ_c (Pa), (b) k_d (cm^3/Ns), and (c) soil texture at Barren Fork Creek. 125

Figure 5.7. Contour plots showing (a) τ_c (Pa), (b) k_d (cm^3/Ns), and (c) soil texture at Cow Creek. The hatched area indicates an area of the bank that was heavily vegetated and thus not sampled. 126

Figure 5.8. Contour plots showing (a) τ_c (Pa), (b) k_d (cm^3/Ns), and (c) soil texture at Five Mile Creek. 127

Figure 5.9. Spearman's rho (r_s) between τ_c or k_d for each solution technique and the horizontal coordinate (*x*), vertical coordinate (*y*), soil temperature (*Ts*), water temperature (*Tw*), bulk density (*BD*), volumetric moisture content (*MC*), porosity (*n*), degree of saturation (*S*), void ratio (*e*), % sand (*SN*), % silt (*SL*), % clay (*CL*), and silt-clay content (*SC*) for Barren Fork Creek. Parameters that are significantly correlated are shown in red. 129

Figure 5.10. Spearman's rho (r_s) between τ_c or k_d for each solution technique and the horizontal coordinate (*x*), vertical coordinate (*y*), soil temperature (*Ts*), water temperature (*Tw*), bulk density (*BD*), volumetric moisture content (*MC*), porosity (*n*), degree of saturation (*S*), void ratio (*e*), % sand (*SN*), % silt (*SL*), % clay (*CL*), and silt-clay content (*SC*) for Cow Creek. Parameters that are significantly correlated are shown in red. 130

Figure 5.11. Spearman's rho (r_s) between τ_c or k_d for each solution technique and the horizontal coordinate (*x*), vertical coordinate (*y*), soil temperature (*Ts*), water temperature (*Tw*), bulk density (*BD*), volumetric moisture content (*MC*), porosity

(*n*), degree of saturation (*S*), void ratio (*e*), % sand (*SN*), % silt (*SL*), % clay (*CL*), and silt-clay content (*SC*) for Five Mile Creek. Parameters that are significantly correlated are shown in red. 131

Figure 5.12. Spearman's rho (r_s) between τ_c or k_d for each solution technique and the horizontal coordinate (*x*), vertical coordinate (*y*), soil temperature (*Ts*), water temperature (*Tw*), bulk density (*BD*), volumetric moisture content (*MC*), porosity (*n*), degree of saturation (*S*), void ratio (*e*), % sand (*SN*), % silt (*SL*), % clay (*CL*), and silt-clay content (*SC*) for all three sites combined. Parameters that are significantly correlated are shown in red. 132

Figure 5.13. Measured τ_c and silt-clay content with the Julian and Torres (2006) relationship indicated by the dotted line (left), and measured versus predicted τ_c using the Julian and Torres (2006) relationship (right). Data compiled from all three sites, totaling 74 JETs. 137

Figure 5.14. Correlations between k_d and τ_c for each solution technique from 74 JETs (circles) compiled from all three sites and comparison to previously proposed relationships by Hanson and Simon (2001) (dashed line) and Simon et al. (2011) (dotted line). 138

Figure 6.1. Segmentation of local flow areas and determination of the hydraulic radii in the calculation of the applied fluvial stress in the Bank Stability and Toe Erosion Model (BSTEM). Source: BSTEM technical documentation [20] and Simon et al. [34]. 144

Figure 6.2. Barren Fork Creek watershed in Oklahoma and Arkansas, and study site locations. 152

Figure 6.3. A Barren Fork Creek composite bank showing typical layers: (a) silt-loam topsoil, (b) packed gravel, and (c) loose gravel toe. Recent stream migration has eroded into (d) root zone of riparian tree near bank edge (not shown) (Midgley et al., 2012). Note that roots occupy only the cohesive soil layer, and do not extend into gravel layer. The steep bank profile is typical, and indicates that mass failure is the dominant mechanism of streambank erosion, which in this case is controlled by both the rate of fluvial undercutting of the gravel layers, and the strength of cohesive soil and tree roots (if present). 153

Figure 6.4. Pictures of Barren Fork Creek streambank sites, showing typically steep bank faces, cohesive topsoil, and coarse gravel subsoil. At some sites (G, H and I) riparian trees eroded from the bank top are visible at the bank toe. 154

Figure 6.5. NAIP aerial imagery (2008) at Site A showing the bank retreat from 2003 to 2010 157

Figure 6.6. Site-specific hydrographs used for calibration. The dashed line represents bank height (m). 158

Figure 6.7. Box plot of the total bank retreat (RT) for the seven historically protected (HP) and three historically unprotected (HUP) study sites. The median value is designated by the solid, central line, the 1st and 3rd quartiles by the box extent, the whiskers indicate the 10th and 90th percentiles, and the mean value is shown

as the dashed line. A t-test for the difference between the groups was not statistically significant ($P = 0.067$, $\alpha = 0.05$). 165

Figure 6.8. Comparison of measured bank retreat (R_T) from aerial imagery to predicted retreat estimates from BSTEM based on (a) linear regression and (b) box plots. Perfect agreement is shown as the dashed line in (a). 171

Figure 6.9. (a) Radius of curvature (ROC, estimated from aerial imagery) and the average annual bank retreat (m/yr) for historically protected (HP) and historically unprotected (HUP) sites, showing that the range of ROC and bank retreat was broad for both types of sites. (b) BSTEM α (dimensionless) versus the standard deviation of radius of curvature (ROC_{SD}, solid symbol) estimated from aerial imagery and BSTEM modeled bank retreat (hollow symbol). 173

Figure 6.10. Erosion rates averaged over 1, 2, and 3 yrs at the historically unprotected sites. The dashed line represents the 6 yr averaged erosion rate. 175

Figure 6.11. Erosion rates averaged over 1, 2, and 3 yrs at the historically protected sites. The dashed line represents the 6 yr averaged erosion rate. 176

LIST OF VARIABLES

Symbol	*Variable*	*Units*
τ_c	critical shear stress	Pa
k_d	erodibility coefficient	$cm^3\ N^{-1}\ s^{-1}$
ε_r	erosion rate	$m\ s^{-1}$
τ	applied shear stress	Pa
J	scour depth	cm
J_p	potential core length	cm
J_e	equilibrium scour depth	cm
τ_0	maximum shear stress at jet nozzle	Pa
C_f	coefficient of friction	-
ρ_w	density of water	$kg\ m^{-3}$
U_o	jet velocity at the orifice	$cm\ s^{-1}$
d_0	nozzle diameter	cm
C_d	diffusion constant	-
J^*	dimensionless scour depth (J/Je)	-
T_r	reference time	s
T^*	dimensionless time (t/Tr)	-
t	time of scour depth measurement	s
d_{50}	average particle size	m
b_0	Wilson model parameter	$g\ m^{-1}\ s^{-1}\ N^{-0.5}$
b_1	Wilson model parameter	Pa
$\tau_{c\text{-}BL}$	critical shear stress using Blaisdell solution	Pa
$\tau_{c\text{-}SD}$	critical shear stress using scour depth solution	Pa
$\tau_{c\text{-}IT}$	critical shear stress using iterative solution	Pa
$k_{d\text{-}BL}$	erodibility coefficient using Blaisdell solution	$cm^3\ N^{-1}\ s^{-1}$
$k_{d\text{-}SD}$	erodibility coefficient using scour depth solution	$cm^3\ N^{-1}\ s^{-1}$
$k_{d\text{-}IT}$	erodibility coefficient using iterative solution	$cm^3\ N^{-1}\ s^{-1}$
$SC\%$	percent silt-clay content	-
Pc	percent clay content	-
ρ_d	bulk density	$kg\ m^{-3}$
$c\%$	percent clay content	-
r_s	Spearman's rank correlation coefficient	-
BD	bulk density	$kg\ m^{-3}$
t_m	calculated measured time	s
T_s	soil temperature	°C
T_w	water temperature	°C

MC	volumetric moisture content	$cm^3\ cm^{-3}$
n	porosity	-
S	degree of saturation	-
e	void ratio	-
SN	percent sand content	-
SL	percent silt content	-
CL	percent clay content	-
s_r	shear strength of soil	kPa
c'	effective cohesion	kPa
σ	normal stress	kPa
ϕ'	effective internal angle of friction	°
ψ	matric suction	kPa
ϕ_b	angle between shear and matric suction	°
W	weight of soil block per unit area	$kN\ m^{-2}$
β	failure plane angle	°
P_i	hydrostatic confining force	$kN\ m^{-1}$
U_i	hydrostatic uplift force	$kN\ m^{-1}$
α	local bank angle	°
F_r	resistive forces	kPa
L	length of failure plane	m
s_d	driving force	kPa
F_d	driving forces	kPa
FoS	factor of safety	-
c_r	root cohesion	kPa
AGB	above ground biomass	kg
BGB	below ground biomass	kg
θ	bank angle	°
g	gravitational acceleration	$m\ s^{-2}$
LR	reach length	m
ROC	radius of curvature	m
RT	total retreat	m
DBH	diameter at breast height	m

CHAPTER 1

INTRODUCTION

1.1 Background

The United States has over forty-thousand impaired water bodies according to the most recent survey by the Environmental Protection Agency (EPA). These are reported under the Clean Water Act which mandates, under section 303(d), that all states, territories, and authorized tribes are required to maintain a list of impaired waters that are too degraded or polluted to meet water quality standards (USEPA, 2011). In the national summary tables for available water quality data in the United States, the EPA lists sediment as one of the top five causes of impairment for 303(d) listed waters (USEPA, 2011). While suspended sediment, erosion, and deposition are natural processes, an excess amount of sediment in streams has many adverse effects on both humans and the surrounding ecosystems. Sediments in streams cause excess turbidity and can carry excess amount of nutrients or even toxic pollutants downstream. Also, stream instability caused by excess erosion can harm aquatic life and affect recreation, navigation, water treatment, water quality, and water storage. Furthermore, streambank erosion itself is important economically from the standpoint of land loss and the undermining of structures within the floodplain.

Recent research has found that more than 50% of fine sediment in watersheds

originates from channel sources (Wilson et al., 2014). This highlights the need for watershed management strategies geared towards channel erosion, specifically in the form of streambank erosion. In general, streambank erosion can be attributed to three primary mechanisms: mass failure, fluvial erosion, and subaerial processes (Couper and Maddock, 2001; Couper 2003). Mass failures are episodic in nature and occur when there is a force imbalance. Fluvial erosion is a continuous process when shear stresses exceed the soil's critical shear stress and is caused by the shearing of particles by the water flow. Subaerial erosion is climate related and occurs when there is a reduction in soil strength due to subaerial processes that induce direct erosion or make the bank more susceptible to erosion. There is strong interaction between each of these three mechanisms, but they can also be simplified into a series process. Subaerial erosion is commonly thought of as a preparatory process that weakens the bank making it more susceptible to fluvial erosion, and then fluvial erosion may undercut the bank or scour the bed to create streambank instability and cause mass failures (Fox and Wilson, 2010; Midgley et al., 2012).

Process-based models are often used to study streambank erosion mechanisms and predict erosion in order to work towards more comprehensive watershed management solutions. Current models generally view streambank erosion in terms of fluvial erosion by stream flow and the resulting mass failures by gravity (Fox et al., 2007). With this approach, subaerial processes are largely ignored. However, research is continually suggesting that subaerial processes can have a significant effect on the resistance of cohesive streambanks to fluvial erosion (Couper and Maddock, 2001; Clark and Wynn, 2007; Grabowski et al., 2011).

Predicting cohesive streambank erosion has remained difficult, although there is a large amount of research on the topic (Smerdon and Beasley, 1961; Julian and Torres, 2006; Clark and Wynn, 2007; Utley and Wynn, 2008). The complex interactions that govern cohesive soil erosion have made it problematic to estimate the erodibility parameters. There are many factors that can influence the erodibility of cohesive soils such as soil texture, structure, unit weight, and water content (Grabowski et al., 2011). One of the most commonly used methods of measuring the erodibility parameters, τ_c and k_d, is the Jet Erosion Test (JET). The submerged JET was developed for measuring these parameters *in situ* as well as in the laboratory (Hanson, 1990b; Hanson and Cook, 1997; Hanson and Simon, 2001).

The JET has been essential to measure the erodibility parameters *in situ* for input into process-based models. However, there has been discussion recently regarding the derivation of the erodibility parameters from JET data, the variability of results, and the effects of subaerial processes on parameter estimation. There remains a large gap in the knowledge with regard to these points.

1.2 Objectives and Overview

In order to begin addressing some of these gaps, the overall objectives of this research were (1) to evaluate new solution methodologies for the derivation of the erodibility parameters, τ_c and k_d, from the JET, (2) investigate the erodibility parameters using all three techniques by considering parameter uniformity, correlations between the derived parameters and physical soil properties, and the applicability of currently proposed relationships to estimate the erodibility parameters at both a site and watershed

scale, and (3) to apply the results from JET data to composite streambanks within a process-based modeling framework.

First a new solution methodology was incorporated into an automatic spreadsheet tool to derive the erodibility parameters from the JET (Chapter 2). The scour depth solution was introduced and evaluated in terms of the ability to predict the observed scour depth data from the JET. Differences in the predicted erodibility parameters from the two approaches were quantified and compared. The Blaisdell solution and scour depth solution were then evaluated at a watershed scale (Chapter 3). Parameters derived using both solution techniques were evaluated by considering parameter uniformity, correlations between the derived parameters and physical soil properties, and the applicability of currently proposed relationships to estimate the erodibility parameters. The applicability of the Wilson model using field JET data was also demonstrated. This evaluation was then taken from the watershed scale to the site scale (Chapter 4). The site scale study investigated the variability of JET results from an assumed homogenous streambank layer in order to provide guidance to users of the technique regarding the number of JETs needed in order to accurately characterize a streambank. The site scale study also addressed the variability in the erodibility parameters derived from JETs at a site scale with respect to soil parameter correlations, temporal variability, spatial variability, and testing variability (Chapter 5). Finally, results from JETs were applied within the framework of a process-based model (Chapter 6). The model was applied to a series of composite streambanks in order to assess the ability of the model to simulate observed lateral retreat rates based on measured parameters with respect to composite banks and sinuous channels.

CHAPTER 2

A SCOUR DEPTH APPROACH FOR DERIVING ERODIBILITY PARAMETERS FROM JET EROSION TESTS[1]

2.1 Abstract

Typically, the erosion rate of cohesive soils is modeled using the excess shear stress equation, which includes two soil parameters: the erodibility coefficient (k_d) and the critical shear stress (τ_c). A jet erosion test (JET) is a standardized method available for deriving the erodibility of cohesive soils. The JET data are typically analyzed using a Blaisdell solution approach. A second solution approach based on direct parameter optimization to the measured scour depth data has recently been proposed but with limited evaluation. Therefore, the objectives of this research were to: (1) develop a new spreadsheet tool that simultaneously solves for the erodibility parameters using both solution approaches, (2) evaluate the solutions in terms of their ability to predict the observed scour depth data, and (3) quantify differences in the predicted erodibility parameters from the two approaches. A series of JETs conducted across the Illinois River watershed in eastern Oklahoma were used to evaluate the performance of the spreadsheet

[1] Published in *Transactions of the ASABE*:
Daly, E.R., G.A. Fox, A.T. Al-Madhhachi, and R.B. Miller. 2013. A scour depth approach for deriving erodibility parameters from Jet Erosion Tests. *Transactions of the ASABE* 56(6): 1343-1351.

and the solution methodologies. The new scour depth solution provided improved fits to the original scour depth data along with being more stable in converging to a solution as a function of the initial parameter estimates. The automated spreadsheet provides an easy-to-use tool for deriving erodibility parameters from JETs.

2.2 Introduction

Streambank erosion is known to be a significant source of sediment in many impaired streams (Simon et al., 2000; Wilson et al., 2008; Fox and Wilson, 2010). Particle detachment models are often employed to predict rates of streambank erosion due to fluvial processes within a basin. Commonly, the erosion rate of cohesive streambanks is simulated using the excess shear stress equation (Partheniades, 1965; Hanson, 1990a, 1990b), which is defined as:

$$\varepsilon_r = k_d \left(\tau - \tau_c\right)^a \tag{2.1}$$

where ε_r is the erosion rate (cm s^{-1}), k_d is the erodibility coefficient (cm^3 N^{-1} s^{-1}), τ is the average hydraulic boundary shear stress (Pa), τ_c is the critical shear stress (Pa), and a is an empirical exponent commonly assumed to be unity (Hanson, 1990a, 1990b; Hanson and Cook, 2004). Using this model, erosion initiates once τ exceeds τ_c, and k_d defines the rate at which particles are detached after erosion is initiated.

Numerous studies have derived k_d and τ_c for cohesive soils using different techniques: large flumes (Hanson, 1990a; Hanson and Cook, 1997), small flumes (Briaud et al., 2001), laboratory hole erosion test (Wan and Fell, 2004), and a submerged jet test (Hanson and Cook, 1997; Mazurek, 2010; Marot et al., 2011; Al-Madhhachi et al., 2013a, 2013b, 2013c). The submerged jet erosion test (JET) was developed for measuring these

parameters *in situ* as well as in the laboratory (Hanson, 1990b; Hanson and Cook, 1997; Hanson and Simon, 2001). The JET device consists of an impinging jet connected to a constant water source, a "can" that serves to both hold the JET in position and to submerge the test soil in water, and a point gauge to measure the depth of scour produced by the JET. A detailed description of the JET and the testing methodology has been presented by numerous studies (Hanson and Cook, 1997; Hanson and Simon, 2001; Al-Madhhachi et al., 2013a).

Hanson and Cook (1997) and Hanson et al. (2002) developed the analytical methods to directly estimate k_d and τ_c based on diffusion principles using an Excel spreadsheet routine. The analytical methods were based on diffusion principles developed by Stein and Nett (1997). The rate of variation in the depth of scour was assumed to be the erosion rate as a function of the maximum stress at the boundary. The maximum shear stress was based on determining the diameter of the jet nozzle and the distance from the jet origin to the initial cohesive soil surface. Accordingly, τ_c was assumed to occur when the rate of scour was equal to zero at the equilibrium depth. Blaisdell et al. (1981) developed a hyperbolic function for predicting the equilibrium depth, which was used in the spreadsheet to calculate τ_c. The k_d was then determined depending on the measured scour depth, time, predetermined τ_c, and a dimensionless time function (Hanson et al., 2002).

Several flume studies have been conducted to measure the erosion of cohesive soils in order to verify the use of the JET (Hanson, 1990a; Hanson and Cook, 1997; Hanson and Simon, 2001). Hanson (1990a) measured soil erodibility in large outdoor channels with soil material placed throughout the entire length of the channel beds. Six

channels were constructed (0.91 m wide and 30.5 m long) with different slopes: 0.5%, 1.5%, and 3%. Hanson (1990b) empirically related JET index values determined from the three soils to the soil erodibility values determined from the flume studies of Hanson (1990a). Hanson and Cook (1999) performed two open-channel flow tests in a large outdoor open channel (1.8 m wide and 29 m long with 2.4 m sidewalls) on compacted samples of lean clay and silty clay. The k_d and τ_c determined from those flume tests verified the use of *in situ* and laboratory JET experiments. This study as well as other studies (Hanson et al., 2002; Hanson and Cook, 2004) have verified the use of the JET to predict the rates of erosion for headcut migration, impinging jet scour, and embankment breach formation and widening.

In addition to the original JET, a new miniature version of the JET device, which is referred to as the "mini" JET, was recently developed by Hanson (Al-Madhhachi et al., 2013a). The "mini" JET device is smaller (975 cm^3) and lighter (4.2 kg) than the original JET device (28,130 cm^3 and 12.6 kg) and thus can be more easily handled in the field as well as in the laboratory (Al-Madhhachi et al., 2013a). The "mini" JET device was first used by Simon et al. (2010) in the field, where they performed 279 tests using the "mini" JET to measure k_d and τ_c utilizing the methods of testing and analysis developed for the original JET. They compared the "mini" JET results with the original JET device at 35 sites in the Tualatin River basin, Oregon, and observed good agreement in derived values of τ_c but observed differences in k_d and the k_d-τ_c relationships between the two JET devices (Simon et al., 2010). They hypothesized that the observed differences in results were due to differences in the size of the submergence cans between the original and "mini" JET devices. These tests were conducted *in situ* at side-by-side locations, but Al-

Madhhachi et al. (2013a) hypothesized that the results were likely influenced by *in situ* heterogeneity and possible differences in methodology and setup.

Al-Madhhachi et al. (2013a) compared measured excess shear stress parameters using the two JET devices in a more controlled laboratory setting using two cohesive soils (clayey sand and silty sand). Statistically equivalent k_d values were derived by the two JET devices for both soils based on Mann-Whitney rank sum tests, but the τ_c values derived by the "mini" JET were consistently lower. Al-Madhhachi et al. (2013a) hypothesized that the measured differences in τ_c were due to the relative scale of the two submerged jets in comparison to the inherent soil structure created by the compaction method. Adjusting the equilibrium depth of the "mini" JET by a coefficient in the analysis resulted in insignificant differences in the estimated τ_c between the two JET devices. Al-Madhhachi et al. (2013a) concluded that the "mini" JET measurements, based on the excess stress model parameters, provided erosion rate predictions equivalent to the original JET. Al-Madhhachi et al. (2013b, 2013c) compared both the *in situ* original and "mini" JET devices with flume tests to predict soil erodibility on two cohesive soils. With these modifications, they concluded that the flume and both JET devices provided statistically equivalent soil erodibility estimates.

In order to estimate k_d as a function of τ_c for cohesive soils, Hanson and Simon (2001) suggested an inverse relationship between k_d and τ_c:

$$k_d = 0.2\tau_c^{-0.5} \tag{2.2}$$

Hanson and Simon (2001) derived their relationship based on 83 *in situ* JETs conducted on cohesive streambeds in the Midwestern U.S. A wide data range was observed, with τ_c spanning six orders of magnitude and k_d spanning four orders of magnitude. A general

inverse relationship was observed between τ_c and k_d, suggesting that soils with a low τ_c have a high k_d and vice versa. Their relationship predicted the data with a coefficient of determination (R^2) of 0.64 and was incorporated into streambank erosion and stability models, such as the Bank Stability and Toe Erosion Model (BSTEM), as a tool for estimating k_d from τ_c (Midgley et al., 2012). This relationship was recently updated from Simon et al. (2011) based on hundreds of JETs on streambanks across the U.S.:

$$k_d = 1.62\tau_c^{-0.838} \tag{2.3}$$

However, in many cases, it has been reported that the Blaisdell equilibrium scour depth solution approach that forms the basis for deriving erodibility parameters does not always converge to a reasonable solution (Simon et al., 2010). A second solution approach based on direct parameter optimization to the measured scour depth data has recently been proposed by Robert Thomas (Department of Geography, University of Hull, U.K.) but with limited evaluation (Simon et al., 2010; Cossette et al., 2012; Daly et al., 2013). In fact, such an iterative solution was originally proposed by Hanson and Cook (1997) as "method 1," but the solver routine never converged to a stable solution and was therefore not investigated further. Simon et al. (2010) found that this solution methodology provided a reduction in the scatter of the k_d-τ_c relationship, but the values obtained led to an overprediction of erosion during simulations, while the original Blaisdell solution underpredicted erosion. Cossette et al. (2012) evaluated this optimized solution methodology along with the original methodology of Hanson and Cook (2004), a visual assessment methodology, and an equilibrium state methodology. The results suggested varying critical shear stress values based on the four methodologies, although the relative ranking between different soils tested was consistent. They concluded that

there is a need for a review of the theoretical framework of the JET and its underlying assumptions. While the Blaisdell solution methodology continues to be the default method for analyzing JET data at the present time, these current research studies have raised questions about the accuracy of values obtained from this analysis. Therefore, the objectives of this research were to: (1) develop a new spreadsheet tool that simultaneously solves for the erodibility parameters using two solution approaches, (2) evaluate the solution methodologies in terms of their ability to predict the observed scour depth data, and (3) quantify differences in the predicted erodibility parameters from the two approaches. This research utilized a series of JETs conducted across the Illinois River watershed in eastern Oklahoma.

2.3 Materials and Methods

2.3.1 Solution Techniques

Analytical methods for the JET were first presented by Hanson and Cook (1997, 2004), assuming that the rate of variation in the depth of scour (dJ/dt) was the erosion rate as a function of the maximum stress at the boundary, which was determined by the diameter of the jet nozzle and the distance from jet origin to the initial channel bed. Therefore, the erosion rate equation for jet scour is written as (Hanson and Cook, 1997):

$$\frac{dJ}{dt} = k_d \left[\frac{\tau_0 J_p^{\,2}}{J^2} - \tau_c \right] \text{ for } J \geq J_p \tag{2.4}$$

where J is the scour depth (cm), and J_p is the potential core length from jet origin (cm). Accordingly, τ_c was assumed to occur when the rate of scour was equal to zero at the equilibrium scour depth (J_e):

$$\tau_c = \tau_0 \left(\frac{J_p}{J_e} \right)^2 \tag{2.5}$$

where $\tau_o = C_f \rho_w U_o^2$ is the maximum shear stress due to the jet velocity at the nozzle (Pa), C_f = 0.00416 is the coefficient of friction, ρ_w is water density (kg m^{-3}), U_o is the jet velocity at the orifice (cm s^{-1}), $J_p = C_d d_o$, d_o is the nozzle diameter (cm), and C_d = 6.3 is the diffusion constant. Equations 2.4 and 2.5 can be incorporated in a dimensionless form as the following equation:

$$\frac{dJ^*}{dT^*} = \frac{1 - J^{*2}}{J^{*2}} \tag{2.6}$$

where $J^* = J/J_e$ and $J_p{}^* = J_p/J_e$. Stein and Nett (1997) presented the reference time (T_r) as follows:

$$T_r = \frac{J_e}{k_d \tau_c} \tag{2.7}$$

and the dimensional time (T^*) was given as:

$$T^* = \frac{t}{T_r} \tag{2.8}$$

where t is the time of a data reading or scour depth measurement.

Equation 2.6 refers to the change in scour depth with time, for time T^*. Integration of equation 2.6 gives the following equation:

$$T^* - T_p{}^* = -J^* + 0.5 \ln \left(\frac{1 + J^*}{1 - J^*} \right) + J_p{}^* - 0.5 \ln \left(\frac{1 + J_p{}^*}{1 - J_p{}^*} \right) \tag{2.9}$$

The Excel spreadsheet discussed by Hanson and Cook (2004) using equations 2.4 through 2.9 was used to determine τ_c and k_d. The critical stress (τ_c) was determined from equation 2.5 based on the equilibrium scour depth (J_e). Blaisdell et al. (1981) noted that it

was difficult to determine the equilibrium scour depth due to the large time required to reach J_e. Therefore, the spreadsheet calculated the equilibrium scour depth using the scour depth data versus time and a hyperbolic function for determining the equilibrium scour depth developed by Blaisdell et al. (1981). The general form of this equation is:

$$\left(f - f_0\right)^2 - x^2 = A_1^{\,2} \tag{2.10}$$

where A_1 is the value for the semi-transfer and semi-conjugate of the hyperbola, $f = \log(J/d_o) - x$, $x = \log[(U_o t)/d_o]$, and $f_o = \log(J_e/d_o)$. From fitting the scour depth data based on plotting f versus x, the coefficients A_1 and f_o can be determined using Microsoft Excel Solver, and then J_e can be determined ($J_e = d_o 10^{fo}$). The spreadsheet was then used to calculate k_d by fitting the curve of measured data based on equation 2.9. The k_d depends on the measured scour depth, time, pre-estimated τ_c, and the dimensional time function (Hanson et al., 2002).

A second solution of the excess shear stress equation has been proposed by multiple researchers (Simon et al., 2010; Daly et al., 2013). The proposed alternative plotted the original scour depth versus time as derived from the JETs. Then, using the applied shear stress and the initial parameter estimates, k_d and τ_c were fit to the observed scour depth data using the solver routine in Microsoft Excel (generalized reduced gradient method) to minimize the sum of squared errors between the measured scour data and the solution of the excess shear stress equation. This procedure mimics the approach used by Al-Madhhachi et al. (2013b, 2014) for a mechanistic detachment model.

While this solution approach has been proposed previously by Hanson and Cook (1997), it was originally found to be unstable, as it allowed for multiple solutions depending on the initial iteration values, and therefore was neglected in favor of the

Blaisdell solution. In order to check convergence, the scour depth and Blaisdell solution approaches were both tested using a series of initial guesses for the k_d and τ_c values. Various initial values of τ_c were selected with the corresponding initial value of k_d determined using the Simon et al. (2011) relationship shown in equation 2.3.

2.3.2 JET Spreadsheet

To incorporate the recently proposed scour depth solution approach, an automated spreadsheet routine has been created following the original spreadsheet routine developed by Hanson and Cook (2004). This updated routine includes both the Blaisdell solution as well as the scour depth solution approach. The Data Input sheet allows the user to directly input field data from the JET without conversion factors (Figure 2.1). The required input includes the time between readings, the point gauge readings, the head setting, the point gauge reading at the nozzle, the nozzle diameter, and initial parameter estimates for τ_c and k_d (Figure 2.1). If the user does not have an initial estimate, a value of 1 may be entered for both parameters, or the suggested values of k_d as a function of τ_c may be used (Hanson and Simon, 2001; Simon et al., 2011). These initial parameter estimates are utilized to aid in solution convergence using the generalized reduced gradient method solver routine.

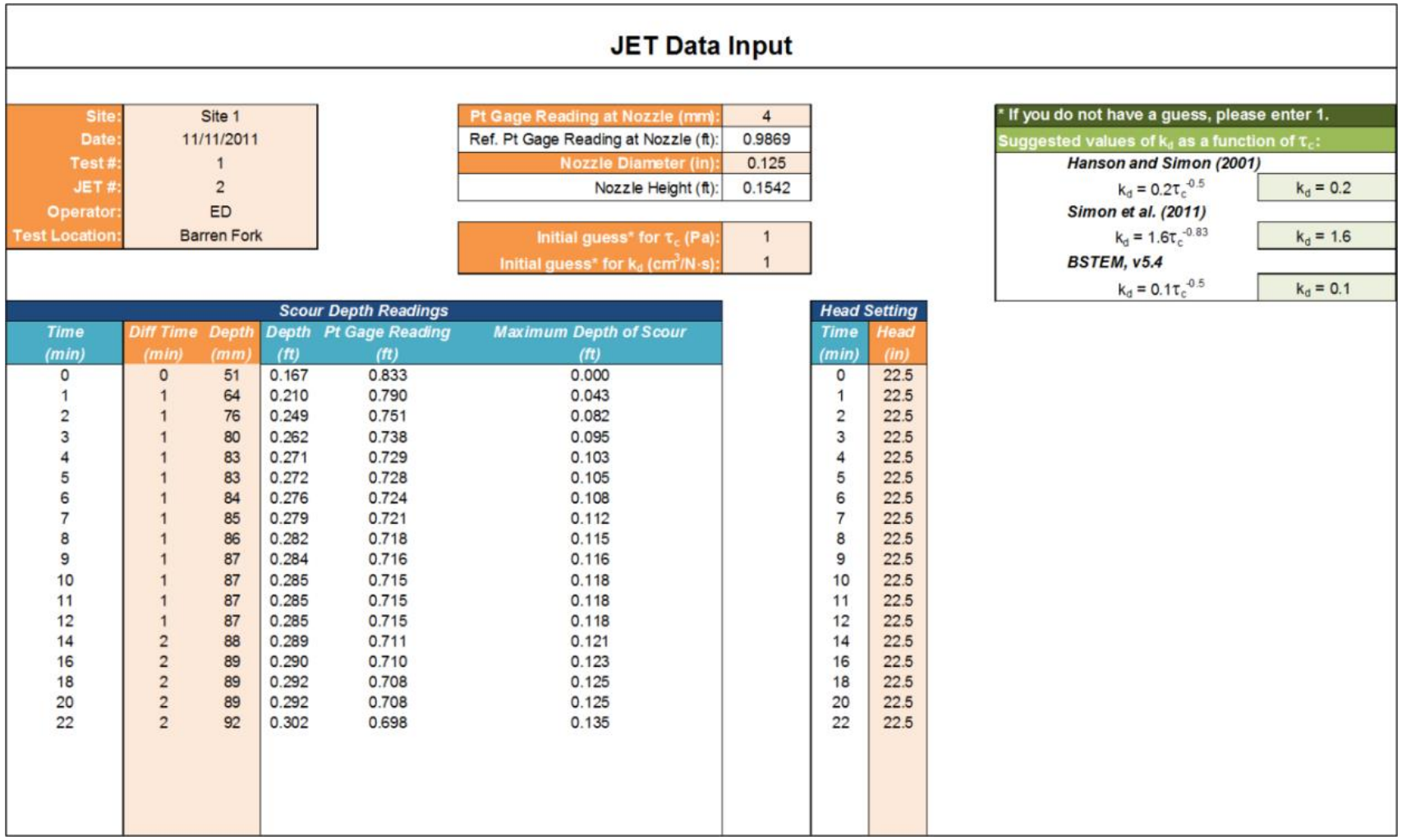

JET Data Input

Site:	Site 1
Date:	11/11/2011
Test #:	1
JET #:	2
Operator:	ED
Test Location:	Barren Fork

Pt Gage Reading at Nozzle (mm):	4
Ref. Pt Gage Reading at Nozzle (ft):	0.9869
Nozzle Diameter (in):	0.125
Nozzle Height (ft):	0.1542

Initial guess* for τ_c (Pa):	1
Initial guess* for k_d ($cm^3/N{\cdot}s$):	1

* If you do not have a guess, please enter 1.

Suggested values of k_d as a function of τ_c:

Hanson and Simon (2001)	
$k_d = 0.2\tau_c^{-0.5}$	k_d = 0.2
Simon et al. (2011)	
$k_d = 1.6\tau_c^{-0.83}$	k_d = 1.6
BSTEM, v5.4	
$k_d = 0.1\tau_c^{-0.5}$	k_d = 0.1

Scour Depth Readings

Time (min)	Diff Time (min)	Depth (mm)	Depth (ft)	Pt Gage Reading (ft)	Maximum Depth of Scour (ft)
0	0	51	0.167	0.833	0.000
1	1	64	0.210	0.790	0.043
2	1	76	0.249	0.751	0.082
3	1	80	0.262	0.738	0.095
4	1	83	0.271	0.729	0.103
5	1	83	0.272	0.728	0.105
6	1	84	0.276	0.724	0.108
7	1	85	0.279	0.721	0.112
8	1	86	0.282	0.718	0.115
9	1	87	0.284	0.716	0.116
10	1	87	0.285	0.715	0.118
11	1	87	0.285	0.715	0.118
12	1	87	0.285	0.715	0.118
14	2	88	0.289	0.711	0.121
16	2	89	0.290	0.710	0.123
18	2	89	0.292	0.708	0.125
20	2	89	0.292	0.708	0.125
22	2	92	0.302	0.698	0.135

Head Setting

Time (min)	Head (in)
0	22.5
1	22.5
2	22.5
3	22.5
4	22.5
5	22.5
6	22.5
7	22.5
8	22.5
9	22.5
10	22.5
11	22.5
12	22.5
14	22.5
16	22.5
18	22.5
20	22.5
22	22.5

Figure 2.1. Example of the Data Input sheet from the updated spreadsheet routine. Required input data are highlighted in orange.

After the user has input all required data, the Solve tab is used. A button at the top of the worksheet labeled "Solve Workbook" activates the automated routine. Solver routines for both solution approaches are iteratively performed three times to ensure convergence. The routine first estimates the erodibility parameters using the Blaisdell solution following the original methodology as outlined by Hanson and Cook (2004). The results of this solution are shown in the box labeled "Blaisdell Solution" (Figure 2.2). The routine then derives erodibility parameters using the scour depth solution and reports its results in the box labeled "Scour Depth Solution" (Figure 2.2). After the scour depth solution approach is completed, the routine back-calculates the Blaisdell solution with the new τ_c and k_d solutions by updating the equilibrium scour depth (J_e) and the parameter f_o. With a fixed f_o and J_e, A is solved for using the solver routine in Microsoft Excel (generalized reduced gradient method). From here, an updated J^* and T^* are calculated and displayed as the dimensionless scour function optimization. For comparison, the dimensionless scour function optimization plot is shown for both the Blaisdell solution and the scour depth solution (Figure 2.3). Also for comparison, the observed and predicted scour depths are plotted and displayed on the Solve sheet (Figure 2.4).

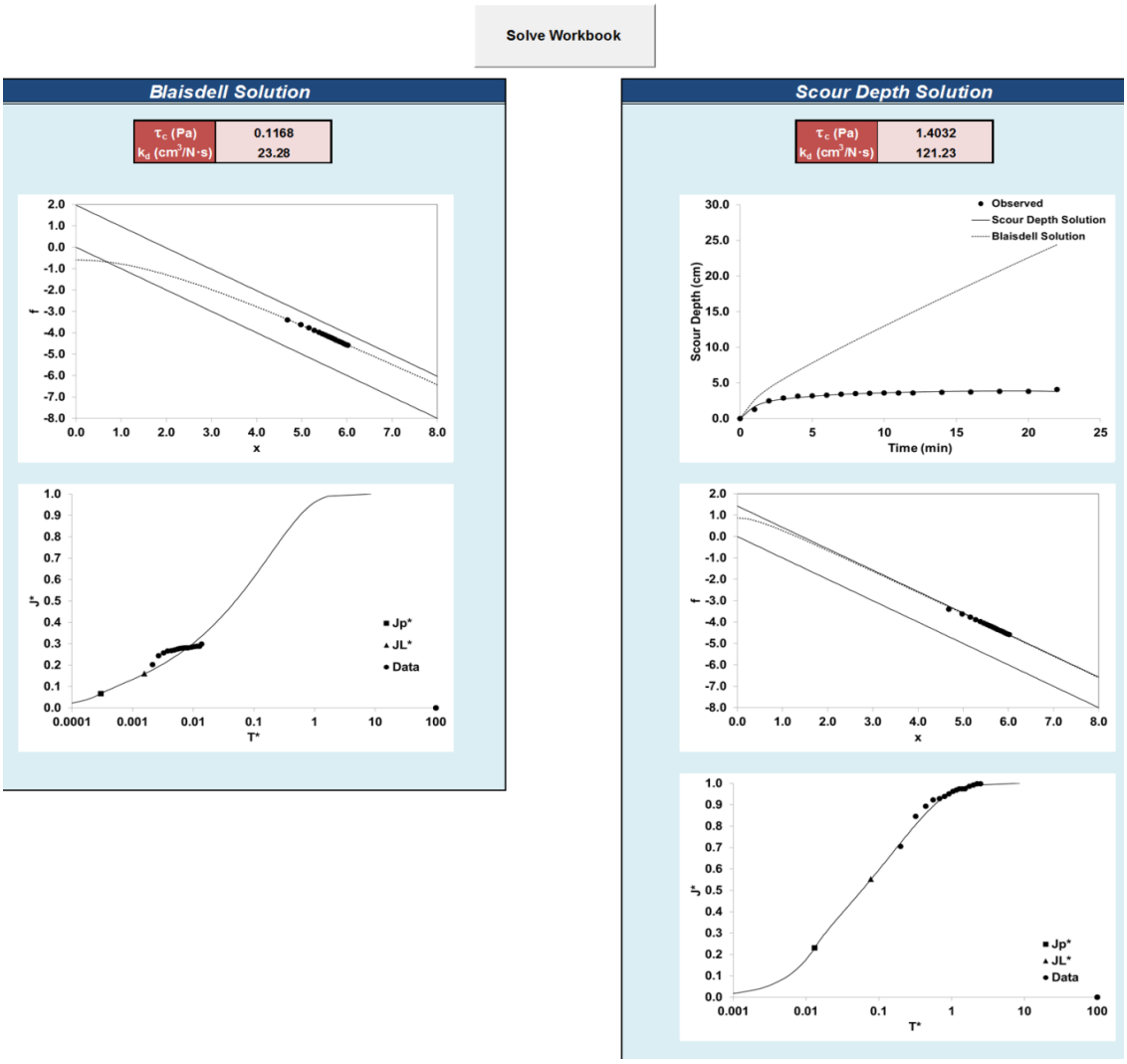

Figure 2.2. Example of the Solve sheet from the updated spreadsheet routine.

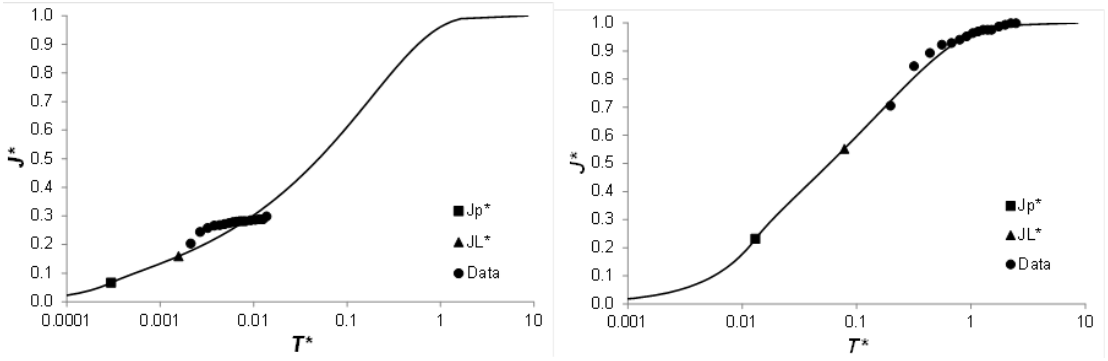

Figure 2.3. Example dimensionless scour function optimization using the Blaisdell solution (left) and the scour depth solution (right). *J is a dimensionless scour depth and *T** is dimensionless time.**

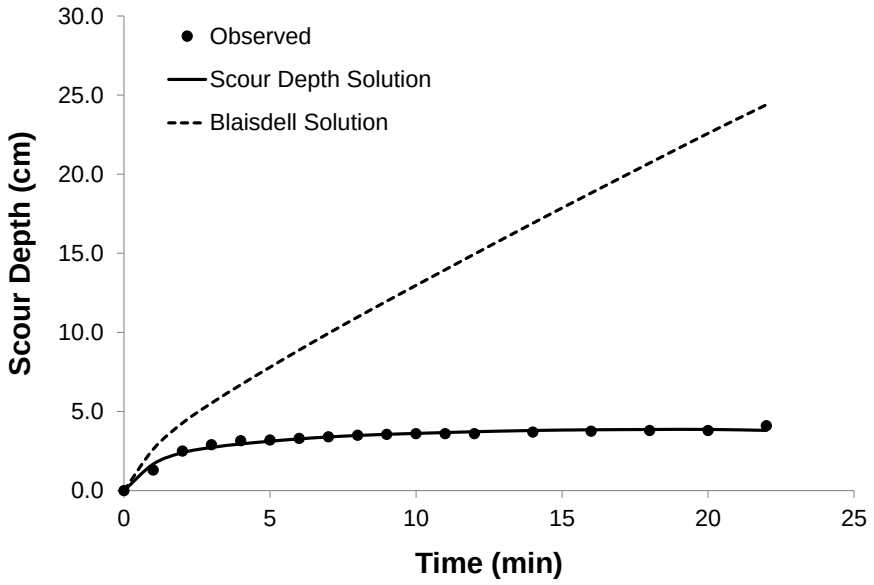

Figure 2.4. Example of observed and predicted scour depths using the Blaisdell solution and scour depth solution.

2.3.3 Field Data

The *in situ* JETs were performed on streambanks in the Illinois River basin in northeastern Oklahoma, one of the state's high-priority basins. The basin falls within the Ozark Highlands ecoregion, which typically contains streams that are riffle and pool dominated, clear, and have coarse gravel, cobble, or bedrock substrates. Banks are typically composite and include a silty loam top layer with an unconsolidated gravel bottom layer and toe (Fox et al., 2011; Heeren et al., 2012; Midgley et al., 2012).

Detailed stream reach data were collected at 13 sites within the Illinois River basin (Figure 2.5). Sites were distributed over a variety of stream orders. Locations for data collection were chosen based on accessibility. Data collection at each site included soil samples from the cohesive layers of the streambank and "mini" JETs along a representative stream reach (Al-Madhhachi et al., 2013a, 2013b, 2014). At least one JET

was performed (Figure 2.6) *in situ* at each site where the streambanks had a cohesive soil layer. The "mini" JETs were set up and operated following procedures outlined by Al-Madhhachi et al. (2013a, 2013b).

The parameters derived from each solution approach were used to predict the scour depth over time within the excess shear stress equation. The normalized objective function (NOF) (Fox et al., 2006; Al-Madhhachi et al., 2013a, 2013b) was calculated to quantify the goodness of fit. The NOF is the ratio of the standard deviation (STDD) of differences between observed and predicted data to the overall mean (X_a) of the observed data:

$$NOF = \frac{STDD}{X_a} = \frac{\sqrt{\frac{\sum_{i=1}^{N}(x_i - y_i)^2}{N}}}{X_a} \tag{2.11}$$

where x_i and y_i are the observed and predicted data, respectively, and N is the number of observations. In general, 1%, 10%, and 100% deviations from the observed values result in NOF values of 0.01, 0.1, and 1.0, respectively (Fox et al., 2006).

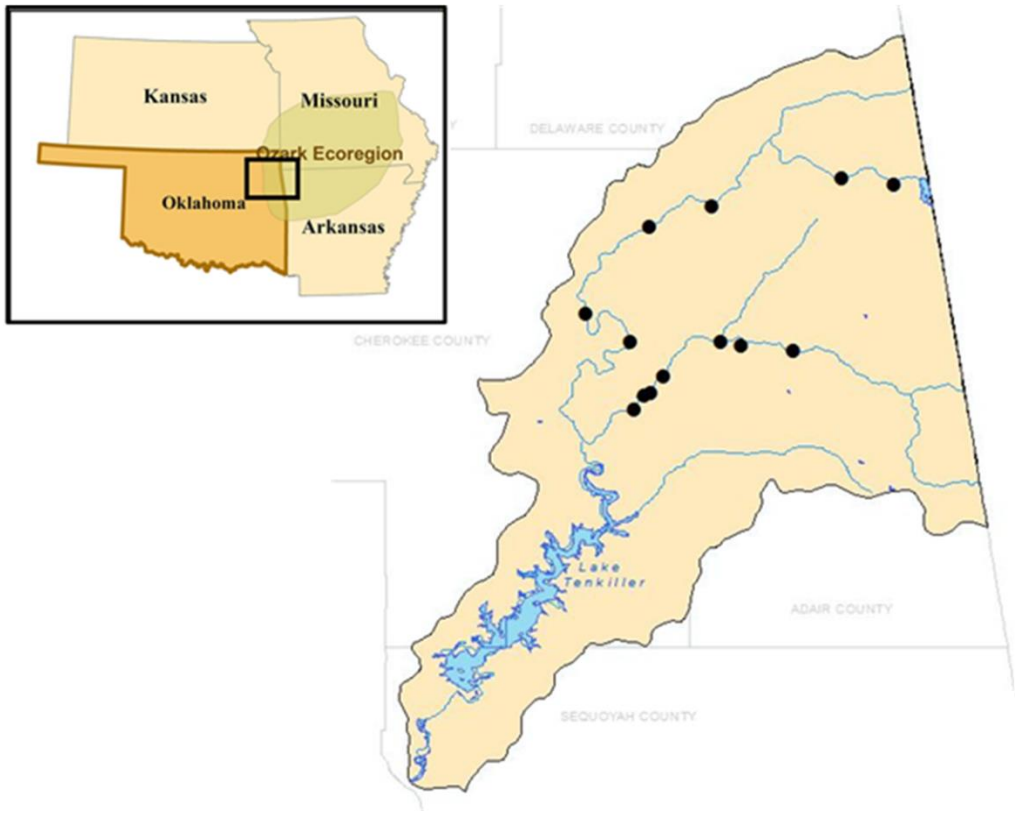

Figure 2.5. The Illinois River basin (Oklahoma only) with 13 sites (circles) at which JETs were conducted.

Figure 2.6. Example of "mini" JET being performed (right) and example of typical bank profile (left).

2.4 Results and Discussion

For most of the in-field JETs, the original spreadsheet routine proposed by Hanson and Cook (2004) did not always converge to a reasonable solution based on a visual observation of the J^* versus T^* plot (see Figure 2.3 as an example). The scour depth solution provided much improved fits of J^* versus T^* (Figure 2.3) and therefore much improved fits (lower NOF values) to the original scour depth data measured during the JET (Table 2.1). Typically, the Hanson and Cook (2004) approach resulted in a lower τ_c and a corresponding k_d that resulted in an overestimation of the scour depth over time (Table 2.1). An analytical method that overpredicts scour depth may be viewed as a conservative approach from a design standpoint, but it poses drawbacks for testing and understanding erosion processes.

Table 2.1. Solutions based on varying initial guesses of τ_c and k_d for the Blaisdell solution and the scour depth solution. See Figure 2.4 for an example solution for both approaches.

	Blaisdell Solution (Hanson and Cook, 2004)			Scour Depth Solution		
Site #	k_d (cm^3/Ns)	τ_c (Pa)	NOF	k_d (cm^3/Ns)	τ_c (Pa)	NOF
1	23.3	0.1	3.4[a]	121.2	1.4	0.1
2	13.2	<0.1	0.2	12.1	<0.1	0.2
3	4.4	0.4	4.6[a]	27.5	2.8	0.1
4	3.6	0.0	0.8[a]	6.6	3.1	0.1
5	1.1	1.3	3.3[a]	6.6	14.3	0.1
6	4.1	0.1	2.5[a]	17.6	3.1	0.1
7	28.6	0.3	5.3[a]	210.8	1.2	0.1
8	1.4	0.0	0.5[a]	2.0	2.8	0.2
9	7.7	0.4	4.6[a]	50.8	2.5	0.1
10	22.1	1.3	5.8[a]	194.1	2.3	0.1
11	11.0	0.5	4.8[a]	74.7	2.2	0.1
12	0.3	1.3	1.9[a]	0.9	16.4	0.1
13	3.1	0.9	5.4[a]	21.9	5.6	0.1

[a] Solution over predicted the observed scour depth data, similar to the example in Figure 2.4.

The scour depth solution was found to be stable regardless of the initial parameter estimates (Table 2.2). This analysis was performed on a JET test from two of the 13 sites representing a range of expected τ_c and k_d values. For Barren Fork Site 1 (the more

erodible case, with slightly cohesive silt loam soil), both the Blaisdell solution and the scour depth solution converged on the same parameter values each time, although unique from each other (Table 2.2). For Barren Fork Site 2 (the less erodible case, with cemented silt loam soil), the scour depth solution was found to be stable, converging on the same answer with each initial parameter estimate; however, the Blaisdell solution was not always able to converge on a solution for k_d, specifically for the lower initial τ_c values (Table 2.2).

Table 2.2. Solutions based on varying initial guesses of τ_c and k_d for the Blaisdell solution and the scour depth solution.

Barren Fork Creek – Site 1						Barren Fork Creek – Site 2					
Initial Guess		Blaisdell Solution		Scour Depth Solution		Initial Guess		Blaisdell Solution		Scour Depth Solution	
τ_c (Pa)	k_d (cm^3/Ns)	τ_c (Pa)	k_d (cm^3/Ns)	τ_c (Pa)	k_d (cm^3/Ns)	τ_c (Pa)	k_d (cm^3/Ns)	τ_c (Pa)	k_d (cm^3/Ns)	τ_c (Pa)	k_d (cm^3/Ns)
0.01	73.1	0.1	23.3	1.4	121.2	0.01	73.1	1.3	Error	14.3	6.6
0.1	10.8	0.1	23.3	1.4	121.2	0.1	10.8	1.3	Error	14.3	6.6
1	1.6	0.1	23.3	1.4	121.2	1	1.6	1.3	1.1	14.3	6.6
10	0.2	0.1	23.3	1.4	121.2	10	0.2	1.3	1.1	14.3	6.6

Using the scour depth solutions for this limited data set, an inverse relationship was observed between the two erodibility parameters (k_d and τ_c) in the excess shear stress equation (Figure 2.7). A power law relationship estimated k_d as a function of τ_c with R^2 = 0.56 for the parameters derived from the scour depth solution approach. Note that the updated Simon et al. (2011) relationship adequately predicted the k_d-τ_c relationship when the parameters were derived with the Blaisdell solution approach. While there was a similar trend between the measured data and the Hanson and Simon (2001) relationship for the k_d-τ_c relationship when derived from the scour depth approach, k_d calculated using the Hanson and Simon (2001) relationship would have been underestimated. Erosion rate

predictions would consequently have been underestimated as well. With the new scour depth solution approach, previous relationships may need to be revisited.

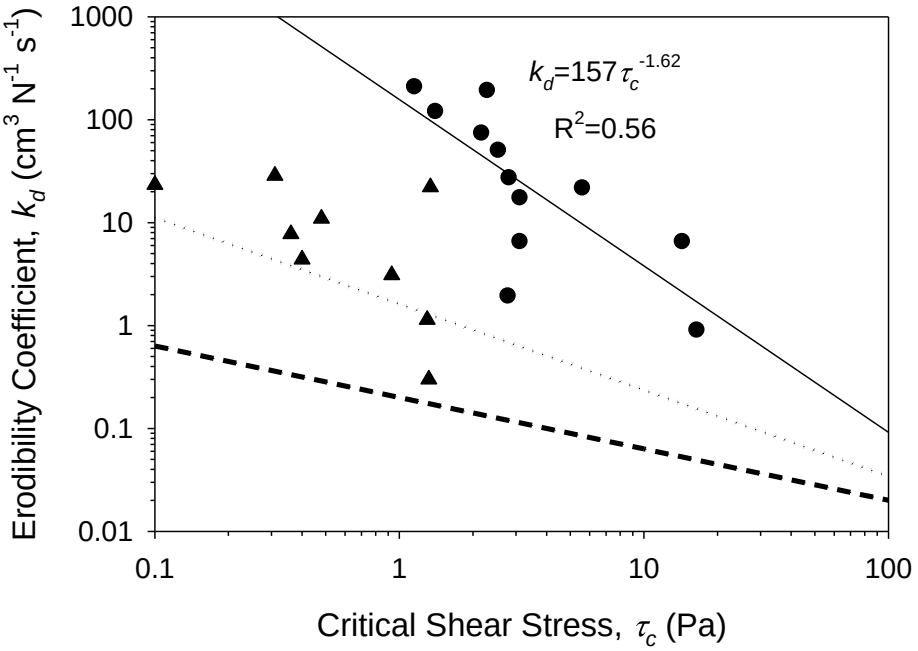

Figure 2.7. Correlation between k_d and τ_c (solid line) for the Illinois River watershed JET tests (triangles are derived from the Blaisdell solution, and circles are derived from the scour depth solution) and comparison to previously proposed relationships by Hanson and Simon (2001) (dashed line) and Simon et al. (2011) (dotted line).

2.5 Conclusions

The routines in the original JET spreadsheet did not always converge to a reasonable solution based on a visual observation of the dimensionless scour versus time. Therefore, a new spreadsheet tool has been developed to incorporate an automated scour depth solution approach similar to that proposed by Hanson and Cook (1997) and Simon et al. (2010). This tool provides both the Blaisdell solution and the scour depth solution approaches for use at the discretion of the user. The scour depth solution was stable within the ranges tested and converged on the same solution despite different initial

parameter estimates. The scour depth solution fit the dimensionless scour function optimization better than the original Blaisdell solution, which tended to underpredict the critical shear stress. With the corresponding erodibility coefficient, the Blaisdell solution overpredicted the resulting scour depth (a conservative design approach). Overprediction of scour depth may be valuable in situations such as dam construction where a large factor of safety is an engineering requirement, but a solution that more accurately represents the physical properties of the soil is preferable from a scientific and engineering standpoint. Results from the new scour depth solution showed similar trends in relationships between erodibility parameters as reported by previous research; however, these trends may need to be revisited with the alternative solution approach.

2.6 Acknowledgements

This research is based upon work supported by the National Science Foundation under Grant No. 0943491. Any opinions, findings, and conclusions or recommendations expressed in this material are those of the authors and do not necessarily reflect the views of the National Science Foundation. The work is also supported by funding support provided by the Buchanan Family Trust as part of the Buchanan Endowed Chair in Biosystems and Agricultural Engineering at Oklahoma State University. The authors also acknowledge Dr. Greg Hanson, Retired, USDA-ARS, for guidance on the use and analysis of Jet Erosion Tests (JETs).

CHAPTER 3

VARIABILITY OF FLUVIAL ERODIBILITY PARAMETERS FOR STREAMBANKS ON A WATERSHED SCALE[2]

3.1 Abstract

Typically the erosion rate of cohesive soils is modeled using the excess shear stress equation, which includes two soil parameters: the erodibility coefficient (k_d) and the critical shear stress (τ_c). Alternatively, a mechanistic detachment rate model, the Wilson Model, was recently developed to predict the erosion rate of cohesive soils, also based on two soil parameters: b_0 and b_1. The Wilson Model is proposed as advantageous in terms of being a more mechanistic, fundamentally based erosion equation. The objective of this research was to derive the excess shear stress model parameters (k_d and τ_c) from field jet erosion tests (JETs) on numerous streambanks across the Illinois River watershed in Oklahoma to investigate (i) erodibility parameter variability or uniformity at a river basin scale, (ii) correlations between the derived parameters and soil texture, (iii) influence of solution technique on the estimated erodibility parameters, and (iv) the applicability of predictive relationships between k_d and τ_c. The second objective was to demonstrate the applicability of the mechanistic Wilson Model using field JET data and

[2] Submitted to *Geomorphology*:
Daly, E.R., G.A. Fox, A.T. Al-Madhhachi, and D.E. Storm. 2014. Variability of fluvial erodibility parameters for streambanks on a watershed scale. *Geomorphology*.

investigate correlations between the excess shear stress model parameters, k_d and τ_c, and the Wilson Model parameters, b_0 and b_1. Erodibility parameters for streambanks of varying soil texture were measured using a miniature version of the JET device ("mini" JET). Data from the JETs were used to derive the erodibility parameters using both a Blaisdell and scour depth approach. Soil samples were acquired at locations of the JETs to quantify particle size distribution, average particle size (d_{50}) and bulk density. No significant relationships existed between k_d or τ_c and bulk density, d_{50}, percent clay, silt, or sand, or percent clay-silt. Existing empirical relationships should be used with caution considering the variability between the results observed in this research and previous relationships proposed in the literature. Strong correlations were observed between b_0 and k_d (R^2 = 0.62 to 0.89) and between b_1 and τ_c (R^2 = 0.31 to 0.96). Therefore, the Wilson model parameters closely resemble the empirical excess shear stress parameters.

3.2 Introduction

Streambank erosion is known to be a significant source of sediment in many impaired streams (Simon et al., 2000; Cancienne et al., 2008; Fox and Wilson, 2010). These streambank sediments are often higher in nutrients as well, contributing to the nutrient loading of the stream (Miller et al., 2014). Detachment models are often employed to predict rates of degradation due to fluvial processes within a basin. Typically the erosion rate of cohesive streambanks is simulated using an excess shear stress model. The excess shear stress equation (Partheniades, 1965; Hanson, 1990a, 1990b) is defined as:

$$\varepsilon_r = k_d\left(\tau - \tau_c\right)^a \tag{3.1}$$

where ε_r is the erosion rate (cm s^{-1}), k_d is the erodibility coefficient (cm^3 N^{-1} s^{-1}), τ is the average hydraulic boundary shear stress (Pa), τ_c is the critical shear stress (Pa), and a is an empirical exponent commonly assumed to be unity (Hanson, 1990a, 1990b; Hanson and Cook, 2004).

Predicting cohesive streambank erosion has remained difficult despite the large amount of research on the topic. The complex interactions that govern cohesive soil erosion have made it problematic to estimate the erodibility parameters. There are many factors that can influence the erodibility of cohesive soils such as soil texture, structure, unit weight, and water content (Grabowski et al., 2011). Previous research has attempted to correlate soil physical and erodibility parameters from the excess shear stress model (Smerdon and Beasley, 1961; Julian and Torres, 2006; Clark and Wynn, 2007; Utley and Wynn, 2008). While there are several relationships to estimate τ_c based on soil properties, there are no widely-tested and verified relationships between k_d and soil physical properties. Inverse power-law relationships have been suggested in order to estimate k_d as a function of τ_c for cohesive soils (Hanson and Simon, 2001; Simon et al., 2010). More research is needed to verify these relationships in a wide variety of cohesive soils. More specifically, how successful are these relationships in accurately representing k_d-τ_c in a unique watershed from which they were derived? Many widely used erosion models utilize these relationships, either by embedding them into the model or suggesting the relationships to the user, to calculate the erodibility parameters. Users of erosion models, such as the Bank Stability and Toe Erosion Model (BSTEM), Water Erosion Prediction Project (WEPP), Soil and Water Assessment Tool (SWAT), and CONservational

Channel Evolution and Pollutant Transport Systesm (CONCEPTS), routinely estimate the erodibility parameters using these relationships despite being able to measure the parameters *in situ* (Langendoen, 2000; Ulrich and Nieber, 2008; Abaci and Papanicolaou, 2009; NEH, 2011; Neitsch et al., 2011; Midgley et al., 2012).

When considering multiple forces influencing soil erodibility, the disadvantage of using an excess shear stress model is the lack of mechanistic predictions of its parameters for specific soil and hydraulic conditions. A more fundamentally-based, mechanistic detachment model may be preferred for modeling the range of environmental conditions experienced during fluvial erosion. Wilson (1993a, 1993b) developed a mechanistic detachment model to provide a general framework for studying soil and fluid characteristics and their impact on cohesive soil erodibility. The model was developed based on a simple two-dimensional representation of particles to predict soil erodibility:

$$\varepsilon_r = b_0 \sqrt{\tau_j} \left[1 - \exp\{-\exp(3 - \frac{b_1}{\tau_j})\} \right] \tag{3.2}$$

where τ_j is the applied shear stress, b_0 and b_1 are the two fundamental, mechanistically-derived parameters of the model. The b_0 has dimensions of $(M\ L^{-3})^{0.5}$ and b_1 has dimensions of $M\ T^{-2}L^{-1}$. The benefit of this detachment model is that it is not restricted to modeling on a single particle scale. The mechanistic nature of the Wilson model allows for the analysis to be applied for aggregates, which may be a more appropriate approach to cohesive soil erosion. Unfortunately, at this time, several variables in the Wilson model must be measured rather than simply being estimated from characteristics.

Therefore, whether the excess shear stress model or the Wilson model is used, these models ultimately must be tied back to measured parameters. For cohesive soils, the parameters for the excess shear stress model, k_d and τ_c, can be estimated using a Jet

Erosion Test (JET). The JET works by shooting a small jet of water into the streambank at a constant pressure and measuring the amount of material eroded over time in the scour hole (Hanson, 1990b; Hanson et al., 1990; Hanson et al., 2002). The τ_c is estimated from these tests based on the predicted equilibrium scour hole depth and k_d is estimated from the relationship between scour hole depth and the time to reach equilibrium. A miniature version of a submerged JET device, which is referred to as the "mini" JET, was recently developed (Al-Madhhachi et al., 2013a, 2013b). The "mini" JET device is smaller, lighter, and requires less water compared to the original JET device and can be more easily used in the field as well as in laboratory. The "mini" JET provides essentially equivalent results to the original JET (Simon et al., 2010; Al-Madhhachi et al., 2013b). Recently Al-Madhhachi et al. (2013b) incorporated the hydraulic analysis of JET devices into the Wilson model. Based on results from JET and flume tests, they concluded that the more fundamentally-based detachment model can be used in the place of the excess shear stress equation with parameters that can be estimated using existing JET techniques.

Knowing that both the excess shear stress model and the Wilson model can be applied based on the two parameters computed from the JET, k_d and τ_c or b_0 and b_1, the importance of accurately measuring and understanding these parameters in the field becomes critical. While the excess shear stress model is widely used and accepted, there are a still uncertainties involved when deriving the erosion parameters. There have been only a few studies that have looked at parameter uniformity for streambanks at a watershed scale and parameter correlations with soil texture (Clark and Wynn, 2007).

Therefore, the first objective of this research was to further investigate the erosion parameters used in the excess shear stress model by considering parameter uniformity, correlations between the derived parameters and physical soil properties, and the applicability of currently proposed relationships to estimate the erodibility parameters. The second objective of this study was to demonstrate the applicability of the Wilson model using field JET data. If a shift to the more fundamentally based Wilson model is expected, similar investigations into parameter uniformity and correlations are needed. This study also investigated correlations between the excess shear stress model parameters, k_d and τ_c, and the Wilson model parameters, b_0 and b_1.

3.3 Materials and Methods

3.3.1 Watershed Description

This study focused on the Illinois River Basin in northeastern Oklahoma, one of the state's high priority basins. The basin has some of the state's most treasured streams and rivers as well as Tenkiller Ferry Lake, an important reservoir that serves as the drinking water source for a large portion of that region. The basin is also home to designated scenic rivers that are protected for their natural scenic beauty and recreational values. This unique resource has created a thriving recreational and tourism industry that attracts thousands of visitors to the basin each year.

The Illinois River basin covers 4,330 km^2 spanning the northeastern Oklahoma-Arkansas border. Approximately 54% of this basin is located within Oklahoma. The basin falls within the Ozark Highlands ecoregion, which typically contains streams that are riffle and pool dominated, clear, and have coarse gravel, cobble, or bedrock substrates. Banks are typically composite and include a silty loam top layer with an

unconsolidated gravel bottom layer and toe (Heeren et al., 2012; Midgley et al., 2012). Banks tested in this study ranged from 1 to 8 m in height with a cohesive top layer and gravel bottom layer and toe. The cohesive top layer was typically 0.5 to 3 m thick with the remaining bank being gravel. The cohesive layer that was the focus of the study is generally classified as a Healing silt loam. The dominating land uses in the basin are forest and hay production or pasture with the major agricultural industries being poultry and cattle (OCC, 2010). Historical data indicate good water quality in the Illinois River basin up to the early 1970s. After this time nutrient loading and eutrophication became and continue to be an issue. The annual Oklahoma 303(d) list for impaired and threatened waters generally cites phosphorus, bacteria, and sediment as the impairment causes for the waters in this basin (OCC, 2010).

3.3.2 Data Collection

Detailed stream reach data were collected at 13 sites within the Illinois River basin (Figure 3.1). Data collection occurred between October 2011 and April 2012. Sites were distributed over a variety of stream orders in order to properly characterize the basin. Locations for data collection were chosen based on accessibility. Data collection at each site included soil samples from the cohesive layers of the streambank and "mini" JETs along a representative stream reach (Al-Madhhachi et al., 2013a, 2013b). Small soil cores extracted from the streambanks were analyzed for bulk density. Disturbed bulk soil samples were brought back to the laboratory where sieve and hydrometer tests were performed to quantify the particle size distributions and d_{50} (ASTM, 2003). A minimum of two JETs were performed in situ at each site in the cohesive soil layer. In some cases

as many as five or six JETs were performed if time allowed. The "mini" JETs were setup and operated following procedures outlined by Hanson and Cook (2004) and Al-Madhhachi et al. (2013a, 2013b). Because the data used in this study were intended for an alternate study, analysis was restricted to the soil parameters measured and number of JETs performed.

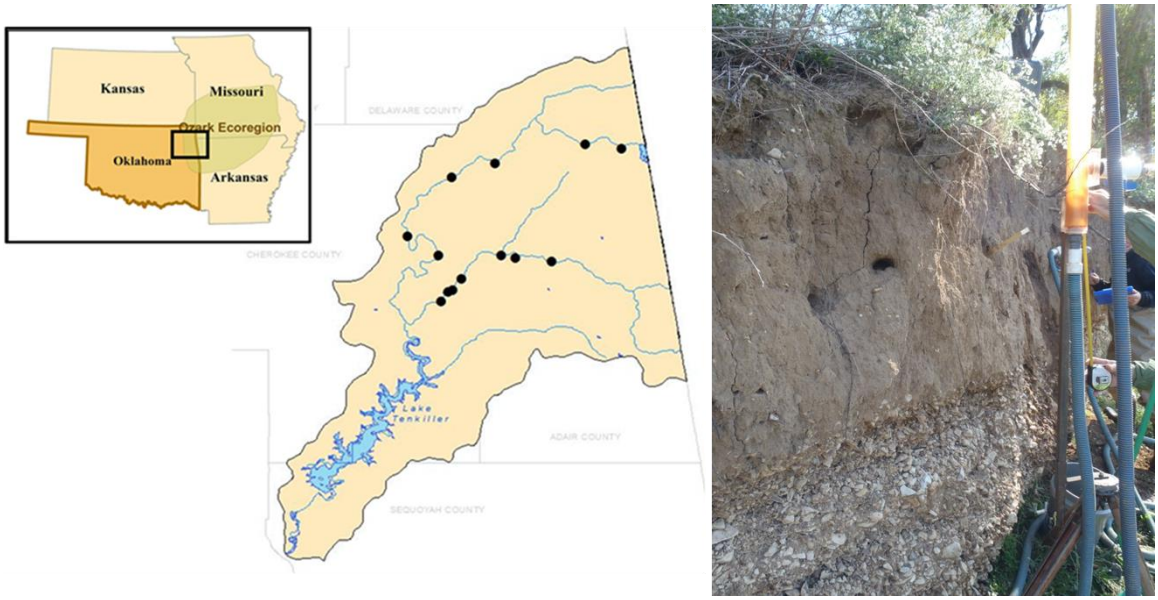

Figure 3.1. The Illinois River basin (Oklahoma only) and location of the 13 sampling sites (left). Example of a typical bank profile showing a cohesive top layer and unconsolidated gravel bottom layer (right). JETs were conducted only in the cohesive layer.

3.3.3 Derivation of Erodibility Parameters

Methods of analysis for deriving k_d and τ_c (equation 3.1) and the Wilson Model parameters (equation 3.2) followed Al-Madhhachi et al. (2013a, 2013b). Analytical methods for the JET were first presented by Hanson and Cook (1997, 2004) based on diffusion principles developed by Blaisdell et al. (1981) and Stein and Nett (1997). For these in-field JETs, the routines in the JET spreadsheet did not always converge to a reasonable solution. In fact, this was the case for many of the JETs performed in the

Illinois River watershed. Therefore, this research utilized both the original Blaisdell solution technique (*BL*) and a second solution of the excess shear stress equation based on the scour depth approach (*SD*) described by Daly et al. (2013). The Wilson model parameters (b_0 and b_1) were also derived from observed JET data using an iterative solution of the parameters using Microsoft Excel solver (generalized gradient method) to minimize the error between the measured data and the functional solutions of the equations.

3.3.4 Evaluating Existing Relationships

There are, however, many relationships suggested in the literature relating soil texture parameters to the erodibility parameters: τ_c and k_d. This research utilized the data collected from streambanks at a watershed scale to evaluate many of the commonly used relationships. This evaluation is similar to that conducted by Clark and Wynn (2007), but within a unique watershed and expanded to two solution techniques and two detachment models. There are several empirical relationships that are widely used to estimate τ_c from physical soil parameters. Julian and Torres (2006) suggested a relationship relating τ_c to the silt-clay content of cohesive soils. The relationship is a third-order polynomial trend line based on the assumption that τ_c would be at a maximum value at 100% silt-clay content and that τ_c would be at a minimum value at 0% silt-clay content. Based on the lower limit of the Shield's curve (Shields, 1936) and observations by Dunn (1959), Julian and Torres (2006) developed the following relationship (R^2=0.91):

$$\tau_c = 0.1 + 0.1779(SC\%) + 0.0028(SC\%)^2 - 2.34E-5(SC\%)^3 \quad (3.3)$$

Smerdon and Beasley (1961) suggested multiple relationships relating τ_c to basic soil properties. Using a flume study, measured τ_c values for cohesive soils were related to the plasticity index, dispersion ratio, mean particle size, and percent clay. For the purposes of this study, only the relationships using the mean particle size (d_{50}) and percent clay were analyzed (P_c). The empirical relationships were reported as:

$$\tau_c = 3.54 \times 10^{-28.1 d_{50}} \quad (3.4)$$

$$\tau_c = 0.493 \times 10^{0.0182 P_c} \quad (3.5)$$

These three relationships to estimate τ_c (equations 3.3 to 3.5) were evaluated specifically using the soil texture data and JET-derived τ_c in this study using both the *BL* and *SD* solution techniques.

Predicting k_d from basic soil properties has proved to be more difficult and there are few relationships available. An equation relating the percent clay content and bulk density for estimating k_d is presented in the National Engineering Handbook (NEH, 2011) as:

$$k_d = \frac{5.66 \rho_w}{\rho_d} \exp\left[-0.121 c_{\%}^{\,0.406} \left(\frac{\rho_d}{\rho_w} \right)^{3.1} \right] \quad (3.6)$$

where ρ_w is the unit weight of water (g cm^{-3}), ρ_d is the soil bulk density (g cm^{-3}), and $c_{\%}$ is the percent clay content. This relationship was evaluated using soil properties and JET-derived k_d values.

Also, inverse relationships have been suggested (Hanson and Simon, 2001) in order to estimate k_d as a function of τ_c for cohesive soils rather than specific soil properties:

$$k_d = 0.2\tau_c^{-0.5} \quad (3.7)$$

Hanson and Simon (2001) derived their relationship based on 83 in situ JETs. These tests were conducted in cohesive streambeds in the Midwestern United States. Results showed a wide range of data with τ_c spanning six orders of magnitude and k_d spanning four orders of magnitude. However, a general inverse relationship was observed between τ_c and k_d suggesting that soils with a low τ_c have a high k_d and vice versa. Their relationship predicted 64% of the variation within their data and was incorporated into streambank erosion and stability models, such as the Bank Stability and Toe Erosion Model (BSTEM), as a tool for estimating k_d from τ_c. This relationship was recently updated (Simon et al., 2011) based on hundreds of JETs on streambanks across the United States and given as:

$$k_d = 1.62\tau_c^{-0.838} \quad (3.8)$$

Relationships were plotted between k_d and τ_c as derived from the JETs in the Illinois River watershed and compared to equations (3.7) and (3.8).

3.3.5 Statistical Analysis

The data collected in this study created a small sample size and did not follow a Gaussian distribution. Therefore, non-parametric tests were used to evaluate results. In order to assess the correlation between measured soil parameters and erodibility parameters, the Spearman's rank correlation coefficient, or Spearman's rho, was calculated using SigmaPlot 12.5 (Systat Software, Inc., Germany). Using the same program the Mann-Whitney rank sum test was used to quantify the differences in the estimated and measured erodibility parameters. Non-parametric pairwise differences

between each of the methods were also calculated. A significance level of $\alpha = 0.05$ was assumed for all tests. This statistical analysis is similar to that undertaken by Clark and Wynn (2007) for reasons of comparison.

3.4 Results and Discussion

3.4.1 Variability and Correlations

Variability was explored at both the site and watershed scale. Four sites were chosen that had three or more JETs performed in order to investigate site variability. Two sites from the Illinois River, one upstream (IR-U, five JETs) and one downstream (IR-D, six JETs), and two sites from Barren Fork Creek, one upstream (BF-U, four JETs) and one downstream (BF-D, three JETs), were selected (Figure 3.2). The τ_c varied as much as three orders of magnitude and k_d varied as much as three orders of magnitude at a single site comparing multiple JETs and for both the *BL* and *SD* solutions.

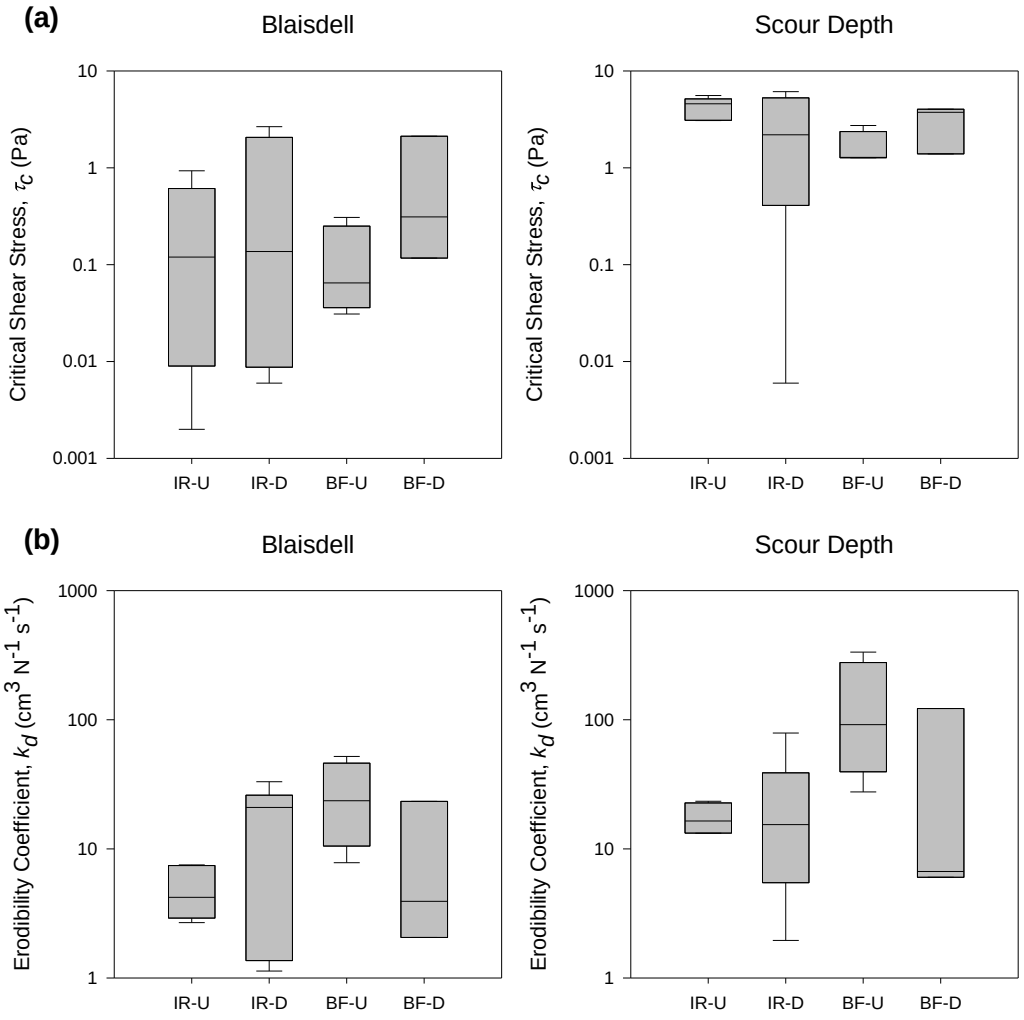

Figure 3.2. Boxplots of variation at a site scale in (a) τ_c and (b) k_d using both solution techniques at four sites with at least three JETs performed. IR = Illinois River; BF = Barren Fork Creek; U = Upstream; and D = Downstream.

There are a variety of variables that could cause this variability, such as the presence of gravel or roots at the JET site, differences in moisture content, or soil heterogeneity. This amount of variability causes less confidence in an average value being the most representative parameter for erosion predictions at a site. There have been numerous studies that have found similar degrees of variability at a site scale (Hanson and Simon, 2001; Wynn and Mostaghimi, 2006; Wynn et al., 2008; Layzell and Mandel, 2014). These studies cite both subaerial processes and soil heterogeneity as the most

likely causes of the variability. More research is needed to test variability on a site scale in order to create a standard operating procedure for the number of JETs needed to obtain reliable parameter estimates.

For purposes of comparison for the remainder of this study, at sites where more than one JET was performed, results were averaged in order to have a single set of erodibility parameters per site. When considering parameter uniformity across the 13 sites, it was found that the derived parameters from the JET using both solution techniques varied throughout the watershed (Figure 3.3). At the watershed scale, both τ_c and k_d varied by as much as three orders of magnitude across the 13 sites. While many studies have verified the wide range in erodibility on a site scale, there are still models that attempt to estimate the erodibility parameters on both a site and, furthermore, a watershed scale. Similar to this study, Thoman and Niezgoda (2008) reported large amounts of variability at a watershed scale. For this study, the measured soil texture parameters varied throughout the watershed as well (Table 3.1). Although soil parameters were expected to be similar due to the uniformity of the soils in the watershed, both soil texture parameters and erodibility parameters were highly variable. For τ_c and k_d, the standard deviations were greater than their respective averages.

Table 3.1. Summary statistics for average parameters measured at 13 sites within the Illinois River watershed.

	$\tau_{c\text{-}BL}$ (Pa)	$k_{d\text{-}BL}$ ($cm^3\ N^{-1}\ s^{-1}$)	$\tau_{c\text{-}SD}$ (Pa)	$k_{d\text{-}SD}$ ($cm^3\ N^{-1}\ s^{-1}$)	ρ_b ($kg\ m^{-3}$)	d_{50} (mm)	% Clay (< 0.002 mm)	% Silt (0.002 – 0.062 mm)	% Sand (0.063 – 2 mm)	% Gravel (2 – 64 mm)
Mean	0.53	9.8	4.4	43.2	1785	0.05	15.8	53.9	28.3	2.1
Median	0.29	7.5	2.6	23.9	1801	0.04	16.7	54.8	23.0	0.6
Range	1.8	26.4	15.4	152	130	0.12	11.7	53.4	60.1	8.5
Std. Dev.	0.55	7.7	5.0	47.9	41	0.03	3.4	16.6	18.2	2.8
Count	13	13	13	13	11	13	13	13	13	13

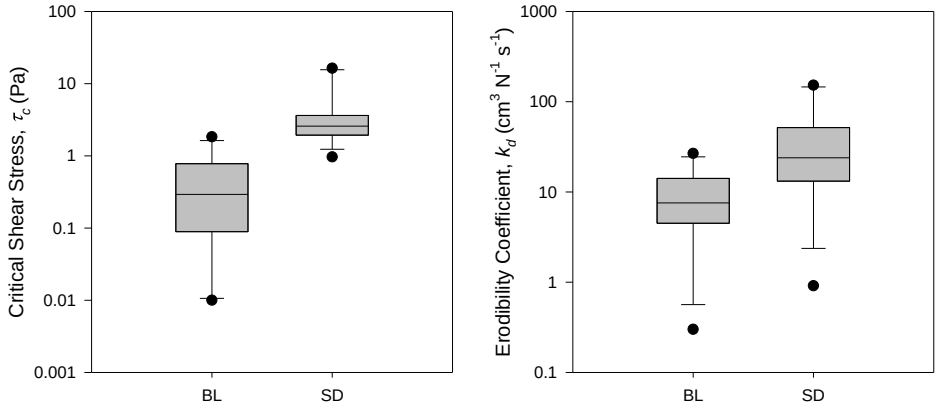

Figure 3.3. Boxplots of variation at a watershed scale in τ_c (left) and k_d (right) for both the Blaisdell solution (*BL*) and the scour depth solution (*SD*).

For the average values at each of the 13 sites, Spearman's rank correlation coefficient (r_s) was calculated considering the relationship between k_d or τ_c with bulk density, soil texture, and the percent silt-clay (< 0.063 mm) for both solution techniques. All of the correlation coefficients ranged between approximately ±0.0–0.5 suggesting only weak correlations between any of the parameters. In fact, no significant correlations were reported as all p values were greater than 0.05 (Figure 3.4). This indicates that, within this system, the erodibility parameters, k_d and τ_c, cannot be accurately predicted using soil physical parameters such as soil texture alone.

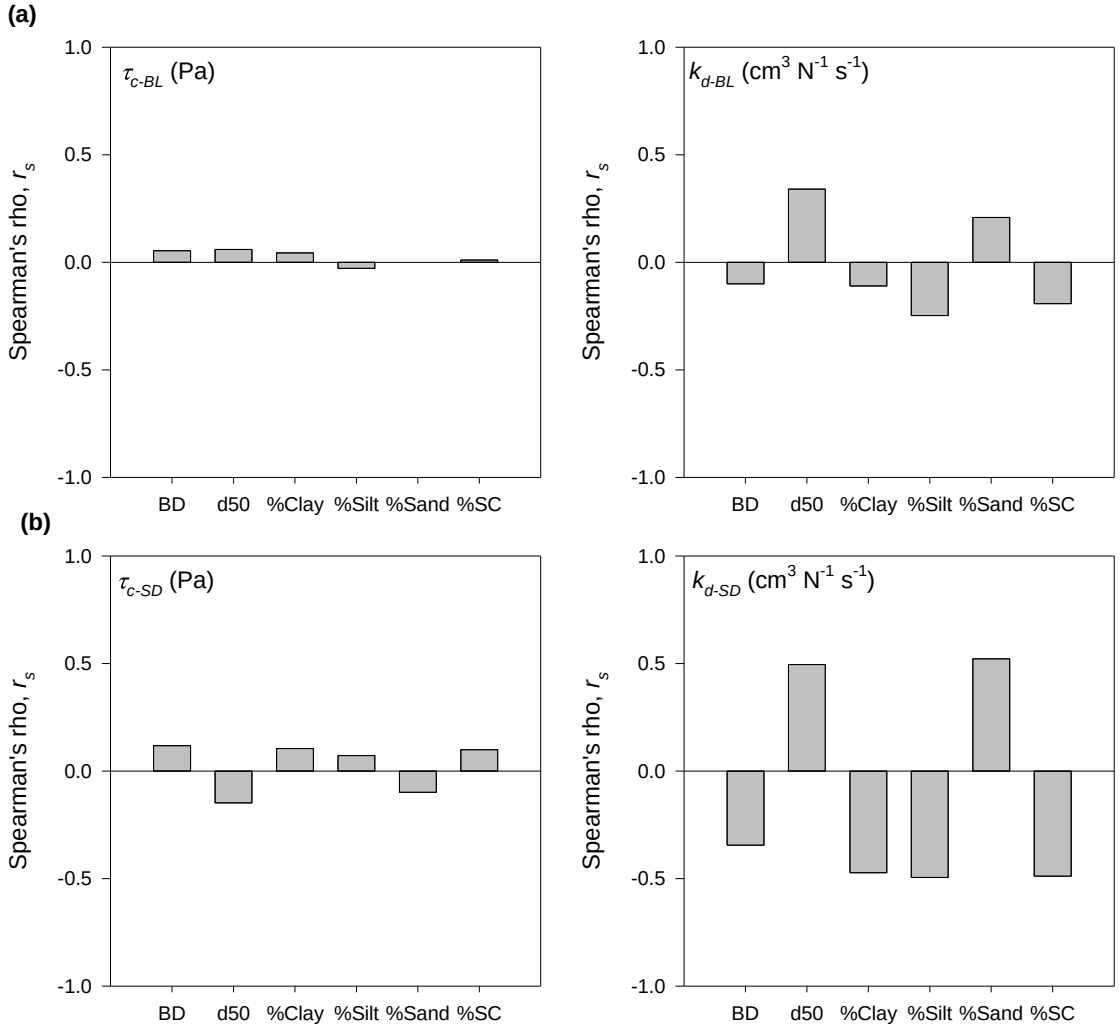

Figure 3.4. Spearman's rho (r_s) between k_d (right) or τ_c (left) for (a) the Blaisdell solution (*BL*) and (b) the scour depth solution (*SD*) and bulk density (*BD*), average particulate size (d_{50}), and percent clay, silt, sand, and silt-clay (*SC*).

3.4.2 Estimating the Critical Shear Stress

Three empirical relationships used to estimate τ_c were compared to the τ_c derived from *in situ* JETs using both solution techniques at each of the 13 sites. The Julian and Torres (2006) relationship correlating τ_c to the silt-clay content of cohesive soils (equation 3.3) was applied to the measured data (Figure 3.5) and over predicted τ_c at all sites in the watershed. In fact, the measured τ_c values spanned three orders of magnitude

while the Julian and Torres (2006) relationship predicted a smaller range of values over a large range of silt-clay contents. The Julian and Torres (2006) relationship was derived using a range of silt-clay contents of approximately 5 to 95%. The silt-clay contents in this study ranged between 28 and 93%. Even with this large range in silt-clay contents, the Julian and Torres (2006) relationship predicted a small range in τ_c values. More research is needed in order to investigate the applicability of such relationships in a wide range of systems. For example, the mineralogy of the system may be a key factor when using such relationships. The clay-sized particles in this study were mainly weathered chert (Miller, 2012; Miller et al., 2014) while the clay-sized particles in the Julian and Torres (2006) study were clay particles. Thus, it was expected that the Julian and Torres (2006) relationship would over predict τ_c for a given silt-clay content. With these relationships, the clay mineralogy may be a more controlling factor than the percent clay content.

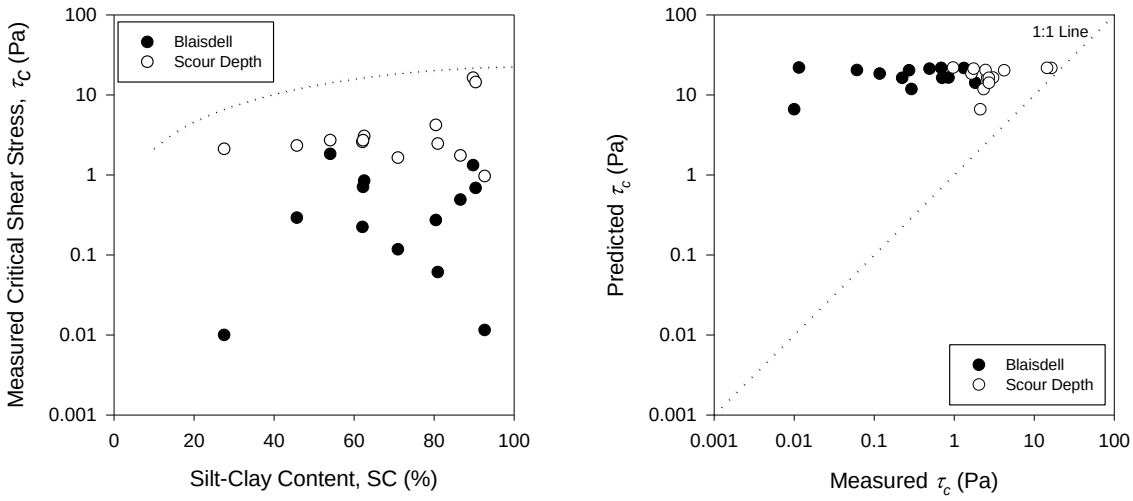

Figure 3.5. Measured τ_c and silt-clay content with the Julian and Torres (2006) relationship indicated by the dotted line (left), and measured versus predicted τ_c using the Julian and Torres (2006) relationship (right).

The Smerdon and Beasley (1961) relationships estimating τ_c from the d_{50} (equation 3.4) or P_c (equation 3.5) was also applied to the measured data and compared to the *in situ* measures of τ_c from the JETs. Estimating τ_c from the d_{50} generally over predicted τ_c when compared to the measured parameter (Figure 3.6). Predicting τ_c from P_c generally over predicted τ_c using the *BL* solution and under predicted τ_c using the *SD* solution (Figure 3.7). Again, these relationships predicted a very narrow range of τ_c values over a large range of d_{50} and P_c while the measured values of τ_c spanned three orders of magnitude. This once again strengthens the idea of subaerial processes and other biological or chemical soil parameters playing a major role in determining cohesive soil erodibility.

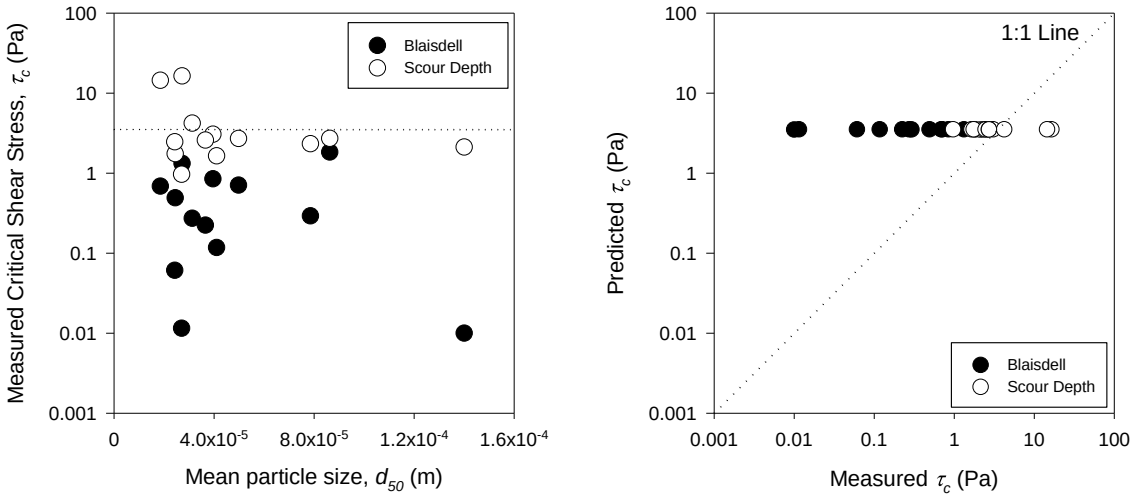

Figure 3.6. Measured τ_c and d_{50} with the Smerdon and Beasley (1961) relationship indicated by the dotted line (left), and measured versus predicted τ_c using the Smerdon and Beasley (1961) relationship (right).

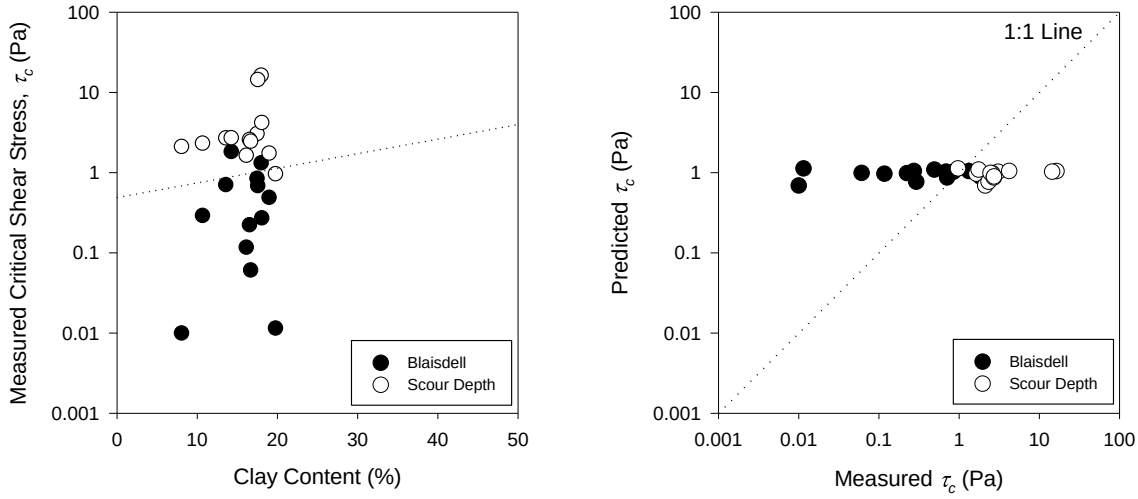

Figure 3.7. Measured τ_c and P_c with the Smerdon and Beasley (1961) relationship indicated by the dotted line (left), and measured versus predicted τ_c using the Smerdon and Beasley (1961) relationship (right).

Table 3.2. Results of the Mann-Whitney rank sum test for estimates of τ_c. The Blaisdell and scour depth values measured from the JET were compared to estimates based on the silt-clay content (*SC*), mean particle size (d_{50}), and clay content (P_c). Estimate methods that were significantly different from the measured values ($\alpha = 0.05$) are indicated by *.

Blaisdell	U-Statistic	P-Value
SC	57	0.166
d_{50}*	0	<0.001
P_c*	29	0.005
Scour Depth	**U-Statistic**	**P-Value**
*SC**	20	0.001
d_{50}*	39	0.021
P_c*	29	0.005

The Mann-Whitney rank sum test was used to quantify the differences in the estimated and measured τ_c values from both solution techniques and all three empirical models. Using this test, it was found that the τ_c estimated using the Julien and Torres

(2006) relationship was not statistically different than the τ_c values measured using the JET and derived using the *BL* solution (Table 3.2).

All of the remaining methods of estimating τ_c were significantly different than the measured values using both the *BL* and *SD* solutions. This is evidenced further when considering the pairwise differences between the two JET solution techniques and the three empirical estimates (Figure 3.8). The three empirical estimates generally predicted much higher τ_c values than the measured data using the *BL* solution and predicted much lower values than the measured data using the *SD* solution. It was expected that these empirical relationships would not be good predictors of the measured τ_c values derived from the *SD* solution due to the fact that the relationships were developed based on values derived from the *BL* solution.

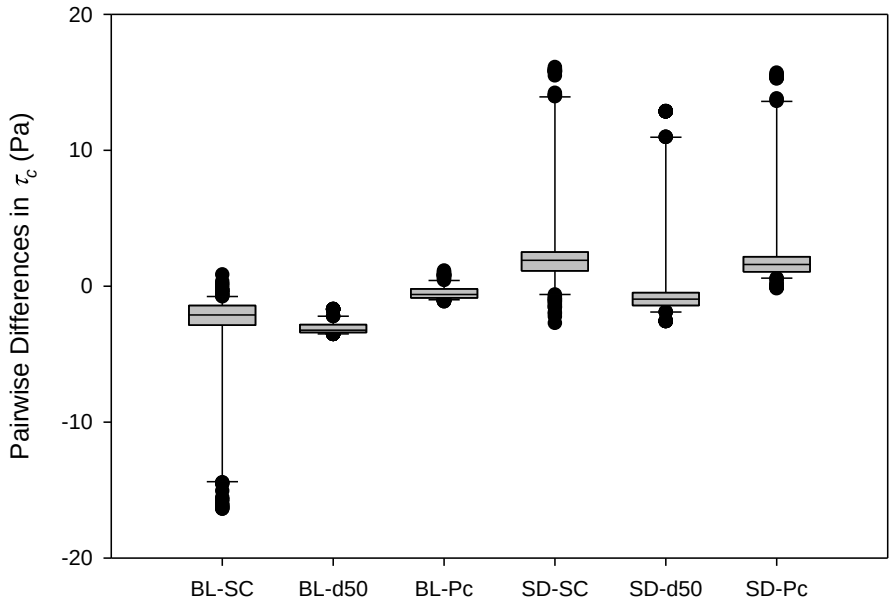

Figure 3.8. Pairwise differences in τ_c values measured with the JET using the Blaisdell solution (BL) or the scour depth solution (SD) and estimated using silt-clay content (SC), mean particle size (d_{50}) and percent clay (Pc).

3.4.3 Estimating the Erodibility Coefficient

Three empirical relationships used to estimate k_d were compared to the k_d derived from *in situ* JETs using both solution techniques at each of the 13 sites. The NEH (2011) relationship between k_d and the clay content and bulk density (equation 3.6) was applied to the measured data and generally under predicted k_d for both solution techniques (Figure 3.9). Again, note that a small range of k_d values was predicted using an empirical relationship compared to the large range measured *in situ*.

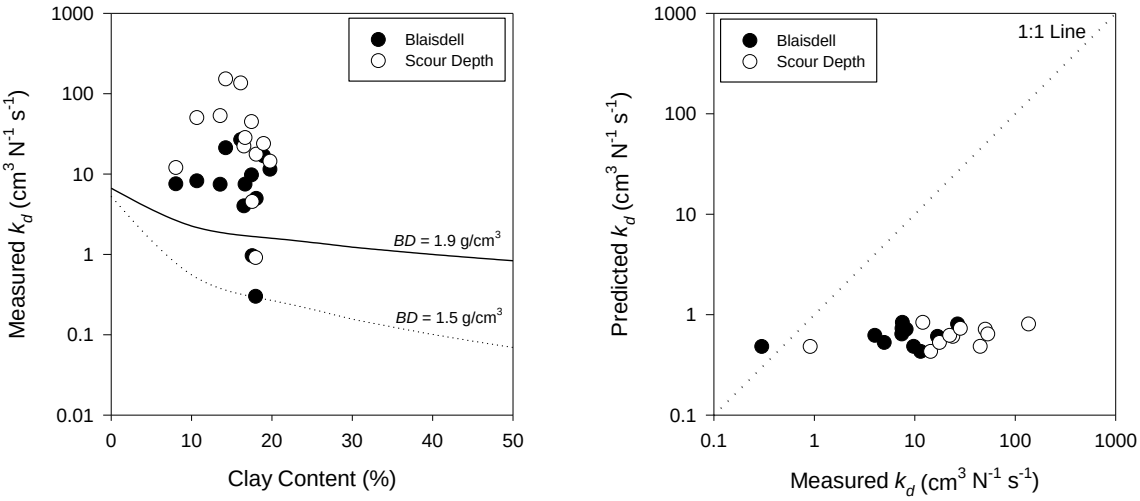

Figure 3.9. Measured k_d using the NEH (2011) relationship indicated by the dotted and solid lines (left), and measured versus predicted k_d using the NEH (2011) relationship (right).

Similar to other studies (Hanson and Simon 2001; Thoman and Niezgoda, 2008; Karmaker and Dutta, 2011; Simon et al., 2011; Layzell and Mandel, 2014), an inverse relationship was observed between the two erodibility parameters, k_d and τ_c, in the excess shear stress equation (Figure 3.10). A power law relationship estimated k_d as a function of τ_c with a coefficient of determination, R^2, of 0.08 and 0.47 for the *BL* and *SD* solutions, respectively:

$$k_{d-BL} = 4.62\tau_{c-BL}^{-0.207} \quad (3.9)$$

$$k_{d-SD} = 84.3\tau_{c-SD}^{-1.17} \quad (3.10)$$

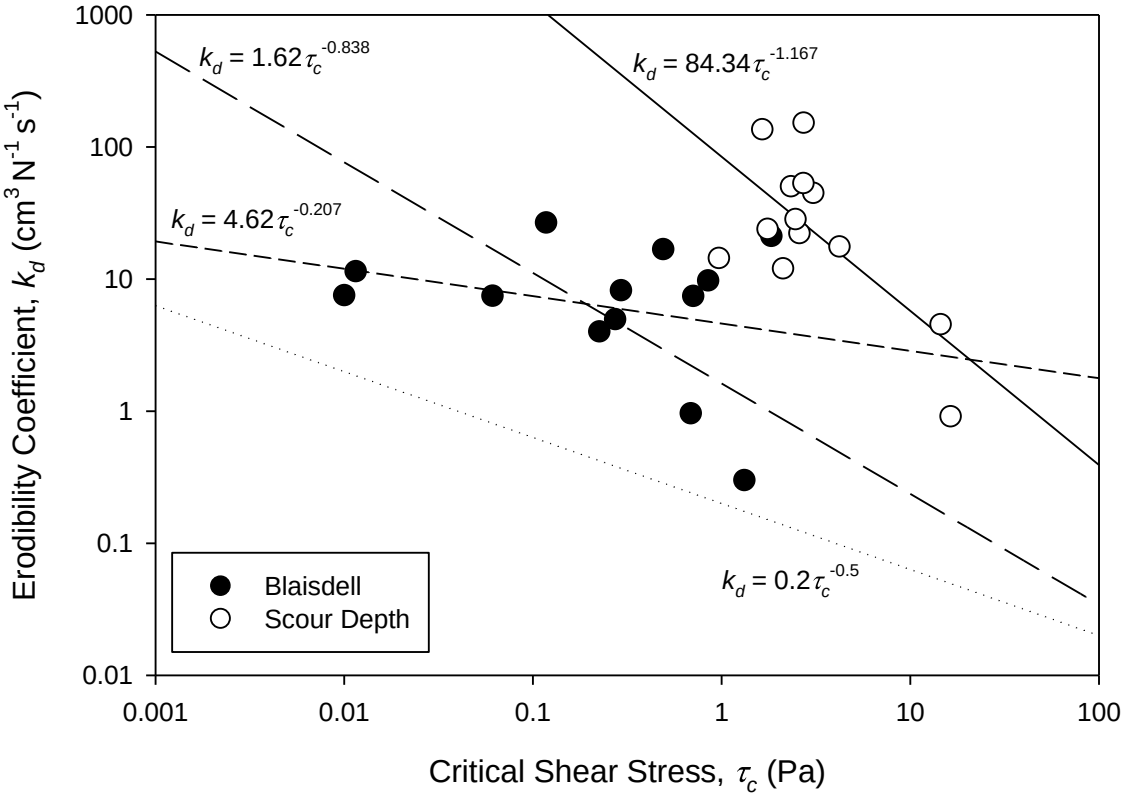

Figure 3.10. Correlation between site-averaged k_d and τ_c for the Blaisdell solution (solid line) and the scour depth solution (long-dashed line) from multiple JETs (circles) and comparison to previously proposed relationships by Hanson and Simon (2001) (dotted line) and Simon et al. (2011) (short-dashed line).

Existing empirical relationships proposed in the literature should be used with caution (Figure 3.10). While there was a similar trend between the measured data using the *BL* solution and the Hanson and Simon (2001) relationship (equation 3.7), k_d calculated using the Hanson and Simon (2001) relationship would have been underestimated (Figure 3.11). This result is similar to that found by Clark and Wynn (2007) and Karmaker and Dutta (2011). Similarly, there was a comparable trend between

the measured data using the *SD* solution and the Simon et al. (2011) relationship (equation 3.8), but k_d calculated using the Simon et al. (2011) relationship would have been underestimated (Figure 3.12). Erosion rate predictions would consequently have been underestimated as well using either solution technique or relationship. The updated Simon et al. (2011) relationship was a better predictor of k_d based on τ_c for this system (Figure 3.10).

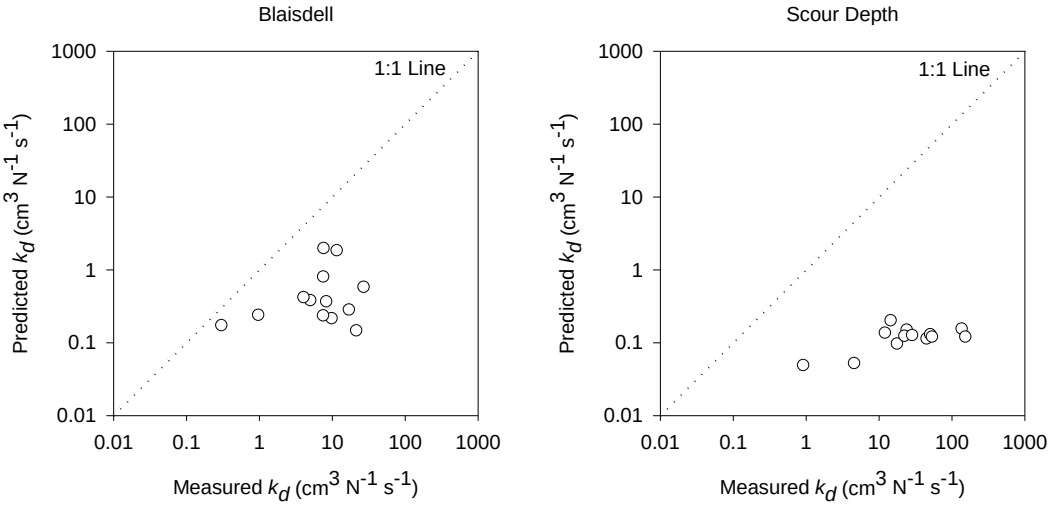

Figure 3.11. Measured versus predicted k_d using the Hanson and Simon (2001) relationship for the Blaisdell (left) and scour depth (right) solutions.

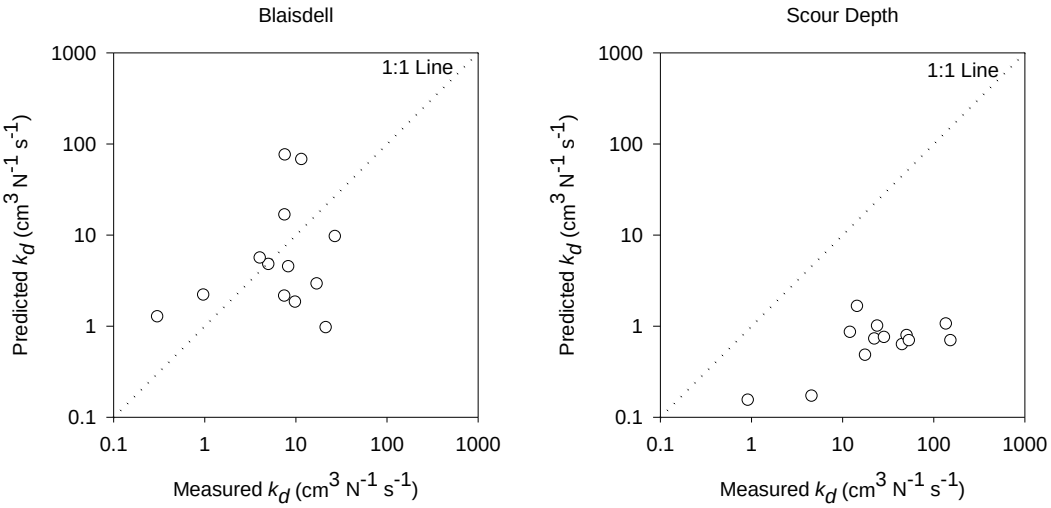

Figure 3.12. Measured versus predicted k_d using the Simon et al. (2011) relationship for the Blaisdell (left) and scour depth (right) solutions.

The original Hanson and Simon (2001) relationship classified soils based on their position on the k_d-τ_c plot as ranging from very resistant to very erodible. Very erodible soils had a low τ_c and a high k_d while very resistant soils had a high τ_c and a low k_d. All of the soils in this study fall within the ranges specified for erodible to very erodible soils. The updated Simon et al. (2011) relationship may be more valid for erodible to very erodible soils. More research is needed to determine whether a better approach would be to develop separate k_d-τ_c relationships for soils within different erodibility classes (very erodible, erodible, resistant, and very resistant).

The Mann-Whitney rank sum test was used to quantify the differences in the estimated and measured k_d values from both solution techniques and all three empirical models. Using this test, it was found that the k_d estimated using the Hanson and Simon (2001) relationship was not statistically different than the k_d values measured using the JET and derived using the *BL* solution (Table 3.3).

Table 3.3. Results of the Mann-Whitney rank sum test for estimates of k_d. The Blaisdell and scour depth values measured from the JET were compared to estimates based on Hanson and Simon (*HS*), Simon et al. (*S*), and the National Engineering Handbook (*NEH*). Estimate methods that were significantly different from the measured values ($\alpha = 0.05$) are indicated by *.

Blaisdell	U-Statistic	P-Value
*HS**	9	<0.001
S	68	0.412
*NEH**	11	<0.001
Scour Depth	U-Statistic	P-Value
*HS**	0	<0.001
*S**	3	<0.001
*NEH**	0	<0.001

All of the remaining methods of estimating k_d were significantly different than the measured values using both the *BL* and *SD* solutions. This is evidenced further when considering the pairwise differences between the two JET solution techniques and the three empirical estimates (Figure 3.13). The three empirical models predicted much lower values of k_d than those derived using the *SD* solution. Again, this was expected as the relationships were developed based on values derived from the *BL* solution.

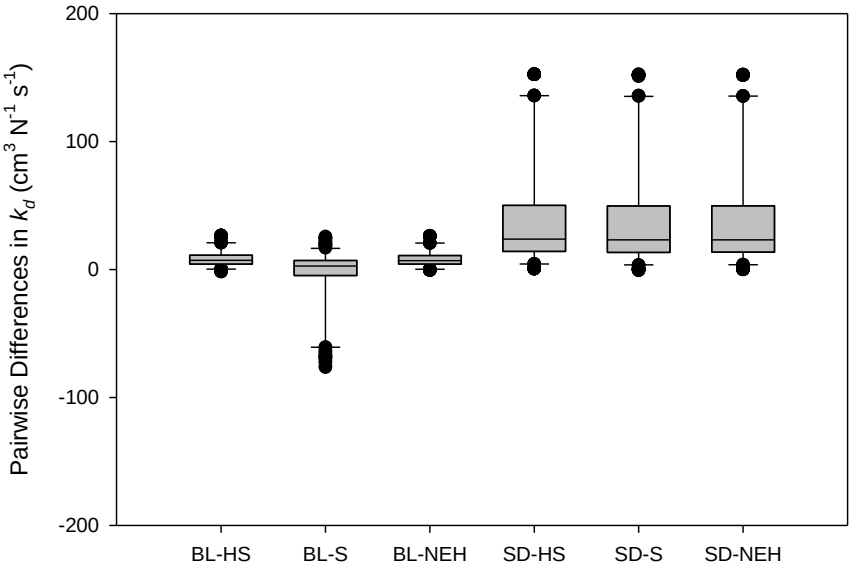

Figure 3.13. Pairwise differences in k_d values measured with the JET using the Blaisdell solution (BL) or the scour depth solution (SD) and estimated using the Hanson and Simon (2001) relationship (HS), Simon et al. (2011) relationship (S), and the NEH (2011) relationship (NEH).

3.4.4 Wilson Model Parameters

While k_d and τ_c were found to be only slightly related using a power law relationship in this study, a similar relationship was observed between the Wilson model parameters b_0 and b_1 (Figure 3.14). These results again suggest the need for site-specific measurements to quantify fluvial resistance to erosion.

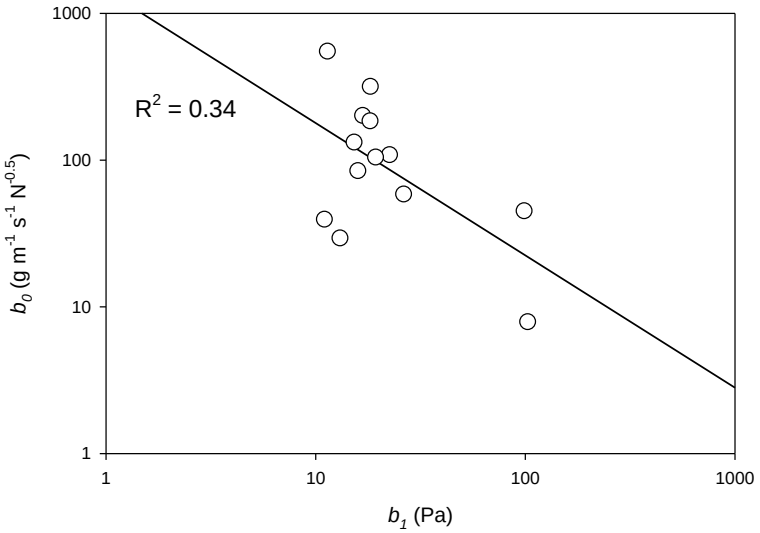

Figure 3.14. Correlation between Wilson Model parameters b_0 and b_1 for the in-situ JETs at 13 sites.

When using parameters derived with the scour depth solution, strong relationships were observed between b_0 and k_d (R^2 = 0.62 to 0.89, Figure 3.15) and between b_1 and τ_c (R^2 = 0.31 to 0.96, Figure 3.15). Therefore, the Wilson model parameters closely resembled the empirical excess shear stress parameters, particularly those derived using the *SD* solution, but with different magnitudes. Note that the Wilson Model parameters were derived with a similar solution approach as the *SD* solution for the excess shear stress parameters. This is similar to reported observations by Al-Madhhachi et al. (2013b) for JETs and flume tests. Even though there are factors in b_0 and b_1 that depend on hydraulic conditions, both of the Wilson model parameters are primarily soil material parameters that depend on properties of the soil particle or aggregate, such as its orientation and the soil cohesion (Al-Madhhachi et al., 2013b). The Wilson model may be advantageous across large applied shear stresses due to its nonlinear detachment prediction, as noted by Wahl et al. (2008).

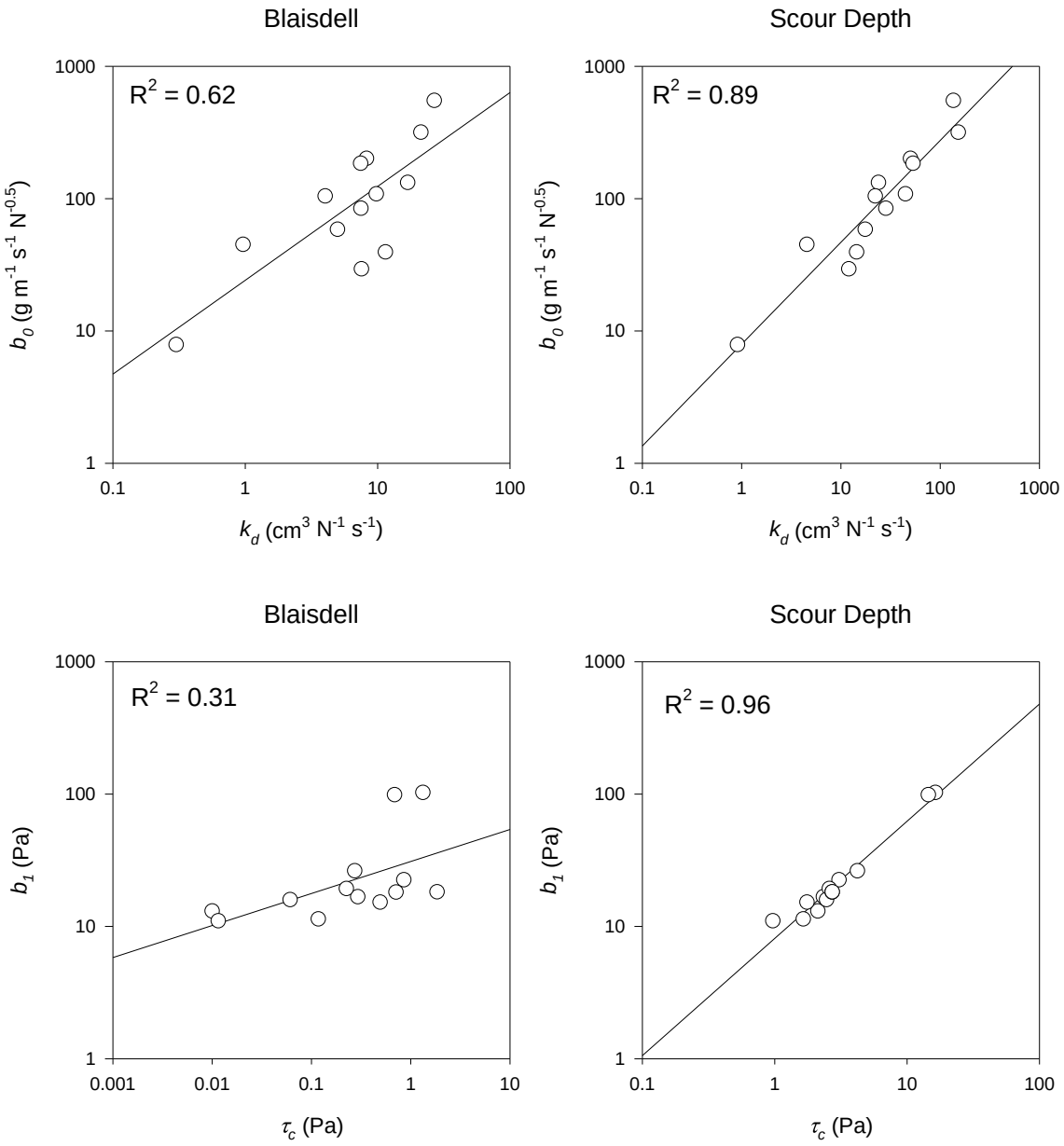

Figure 3.15. Correlation between Wilson Model parameter b_0 and the erodibility coefficient, k_d, from the excess shear stress model (top) and between Wilson Model parameter b_1 and the critical shear stress, τ_c, from the excess shear stress model (bottom).

3.5 Conclusions

Estimating fluvial erosion parameters, τ_c and k_d, is an obstacle in predicting the fluvial entrainment of cohesive particles or aggregates. While JETs provide a measured estimate of the parameters, the wide range in variability from test to test leads to an

uncertain approximation. More research is needed to evaluate parameter variability at the site scale in order to determine if there is a need for a standard operating procedure. Variability was also explored on the watershed scale. The results from averaged JETs at each of the 13 sites showed a wide range in variability throughout the watershed in both the estimated erosion parameters and the soil characterization. This highlights the fact that, while upon observation many of the soils seem uniform across the watershed, they are actually different from an erosion perspective and produce different values for τ_c and k_d or b_0 and b_1. This study demonstrated similarities between the excess shear stress parameters, k_d and τ_c, and the Wilson model parameters, b_0 and b_1, as applied to field data. The variability observed at both a site and watershed scale in these parameters may be due to subaerial processes and more research is needed in order to quantify the spatial and temporal effects of these processes on the erodibility parameters. Therefore, using default or general values to characterize erosion rates at multiple sites across a watershed may not produce the most representative result. Site-specific measurements are needed in order to properly quantify fluvial resistance to erosion.

While there are several relationships to estimate τ_c based on soil properties, there are no acceptable simple relationships between k_d and basic soil properties. The Julian and Torres (2006) relationship relating the silt-clay content to τ_c was found to be a poor predictor of the variable for this system and estimated τ_c values much higher than those measured in the field. This would lead to an under prediction of erosion rates due to fluvial processes. This result was also true for the Smerdon and Beasley (1961) relationships predicting τ_c from clay content or mean particle size. Currently proposed relationships between k_d and τ_c were also poor predictors of k_d for this watershed. Both

the Hanson and Simon (2001) and updated Simon et al. (2011) relationship under predicted k_d based on measured τ_c values. This was also true of the NEH (2011) relationship that predicts k_d from the bulk density and clay content.

The relationships analyzed in this study are used to estimate τ_c or k_d within the predictive framework of erosion models; however, they lack validation outside of their original derivation and are largely applied for lack of a better estimate. In fact, in many cases τ_c may be estimated using one of these relationships and then k_d is estimated using the empirically derived τ_c. This has the potential to lead to compounding errors when these relationships are applied at either a site- or watershed-scale. Site-specific measurements are necessary when characterizing the erodibility of cohesive soils. Also, progress towards a mechanistic approach to modeling cohesive soil erosion is needed.

3.6 Acknowledgements

This research is based upon work supported by the National Science Foundation under Grant No. 0943491. Any opinions, findings, and conclusions or recommendations expressed in this material are those of the authors and do not necessarily reflect the views of the National Science Foundation.

CHAPTER 4

SITE-SCALE VARIABILITY OF STREAMBANK FLUVIAL ERODIBILITY PARAMETERS AS MEASURED WITH A JET EROSION TEST[3]

4.1 Abstract

The erosion rate of cohesive streambanks is typically modeled using the excess shear stress equation, dependent on two erodibility parameters: critical shear stress and erodibility coefficient. The Jet Erosion Test (JET) has become the most common method for estimating these erodibility parameters in situ. Typically, results from a few JETs are averaged to acquire a single set of parameters for characterizing a streambank layer; however, this may be inadequate for accurately characterizing erodibility. The research objectives were to investigate the variability of JET results from assumed homogeneous streambank layers and to estimate the number of JETs required to accurately characterize erodibility for use in predictive models. On three unique streambanks in Oklahoma and across a range of erodibility, 20 to 30 JETs were conducted over the span of three days. Each JET was analyzed using the Blaisdell, scour depth, and iterative solutions. The required sample size to accurately estimate the erodibility parameters depended on the JET solution technique, the parameter being estimated, and the degrees of precision and

[3] Submitted to *Water Resources Research*:
Daly, E.R., G.A. Fox, H.K. Enlow, D.E. Storm, and S.L. Hunt. 2014. Site-Scale Variability of Streambank Fluvial Erodibility Parameters as Measured with a Jet Erosion Test. *Water Resources Research*.

confidence. Conducting three to five JETs per soil layer on a streambank typically provided an order of magnitude estimate of the erodibility parameters. Because the parameters were log-normally distributed, using empirical equations to predict erosion properties based on soil characteristics will likely contain high uncertainty and thus should be used with caution. This study exemplifies the need to conduct in situ measurements using the JET in order to accurately characterize streambank resistance to fluvial erosion.

4.2 Introduction

Streambank erosion is known to be a significant source of sediment and nutrients in many impaired streams (Odgaard, 1987; Pizzuto and Meckelnburg, 1989; Simon et al., 2000; Papanicolaou et al., 2007; Rinaldi et al., 2008; Wilson et al., 2008; Fox and Wilson, 2010; Miller et al., 2014). Particle detachment models are often employed to predict rates of streambank erosion due to fluvial processes within a basin. Commonly, the erosion rate of cohesive streambanks is simulated using the excess shear stress equation [Partheniades, 1965; Hanson, 1990a, 1990b], which is defined as:

$$\varepsilon_r = k_d(\tau - \tau_c)^a \tag{4.1}$$

where ε_r is the erosion rate (cm s^{-1}), k_d is the erodibility coefficient (cm^3 N^{-1} s^{-1}), τ is the average hydraulic boundary shear stress (Pa), τ_c is the critical shear stress (Pa), and a is an empirical exponent commonly assumed to be unity (Hanson, 1990a, 1990b; Hanson and Cook, 2004). Using this model, erosion initiates once τ exceeds τ_c, and k_d defines the rate at which particles are detached after erosion is initiated.

One of the most commonly used methods of measuring the erodibility parameters, τ_c and k_d, is the Jet Erosion Test (JET). The submerged JET was developed for measuring these parameters in situ as well as in the laboratory (Hanson, 1990b; Hanson and Cook, 1997; Hanson and Simon, 2001). The JET device consists of an impinging jet connected to a constant water source, a "can" that serves to both hold the JET in position and to submerge the test soil and water jet, and a point gauge to measure the depth of scour produced by the water jet. A detailed description of the JET and the testing methodology has been presented by numerous studies (Hanson and Cook, 1997; Hanson and Simon, 2001; Al-Madhhachi et al., 2013a).

Hanson and Cook (1997) and Hanson et al. (2002) developed the analytical methods to directly estimate k_d and τ_c based on diffusion principles using an Excel spreadsheet routine. The analytical methods were based on diffusion principles developed by Stein and Nett (1997). The rate of variation in the depth of scour was assumed to be the erosion rate as a function of the maximum stress at the boundary. The maximum shear stress was based on determining the diameter of the jet nozzle and the distance from the jet origin to the initial cohesive soil surface. Accordingly, τ_c was assumed to occur when the rate of scour was equal to zero at the equilibrium depth. Blaisdell et al. (1981) developed a hyperbolic function for predicting the equilibrium depth, which was used in the spreadsheet to calculate τ_c. The k_d was then determined depending on the measured scour depth, time, predetermined τ_c, and a dimensionless time function (Hanson et al., 2002).

Recently, two alternative solution techniques have been proposed to estimate the erodibility parameters from the JET. Simon et al. (2010) proposed an iterative solution

which iteratively solves for τ_c and k_d based on a dimensionless time (T^*) and dimensionless scour depth (J^*). The iterative solution is confined by an upper bound on τ_c to prevent the solution from exceeding the equilibrium scour depth. Daly et al. (2013) proposed another solution technique that iteratively solves for τ_c and k_d to fit to the observed scour depth data to minimize the sum of squared errors between the measured scour data and the solution of the excess shear stress equation. Both the iterative solution and the scour depth solution have shown improved fits over the Blaisdell solution to the observed data; however, limited testing and analysis has been performed on the two new solution techniques. Also, there has been limited comparison of the three solver routines and the three sets of erodibility parameters derived by these routines. All three solution techniques have been incorporated into an automated spreadsheet routine to solve for the erodibility parameters using JET data (Daly et al., 2013).

Despite the ability to measure these parameters in situ using the JET, predicting cohesive streambank erosion has remained difficult. Although there is a large amount of research on the topic, the complex interactions that govern cohesive soil erosion have made it problematic to estimate the erodibility parameters. There are many factors that can influence the erodibility of cohesive soils such as soil texture, structure, unit weight, and water content (Grabowski et al., 2011). The influence of these factors is not captured by conducting a JET at one discrete point in time and at one discrete location on the streambank. Typically, the erodibility of a streambank is characterized by conducting two to three JETs per layer. Parameters derived from these tests are then averaged and then used as input in predictive models. However, the temporal and spatial scales of variability

of these parameters on the streambank are not well understood, so this method may lead to a substantial over- or under-estimation of the erodibility parameters.

The overall goal of this study was address one of these current gaps in the knowledge of cohesive streambank erosion. In particular, this study investigated the variability of JET results from an assumed homogenous streambank layer in order to provide guidance to users of the technique regarding the number of JETs needed in order to accurately characterize a streambank.

4.3 Materials and Methods

4.3.1 Site Descriptions

Three sites were selected for variability studies. Sites were chosen from three different regions in Oklahoma and included sites on Barren Fork Creek, Cow Creek, and Five Mile Creek (Figure 4.1).

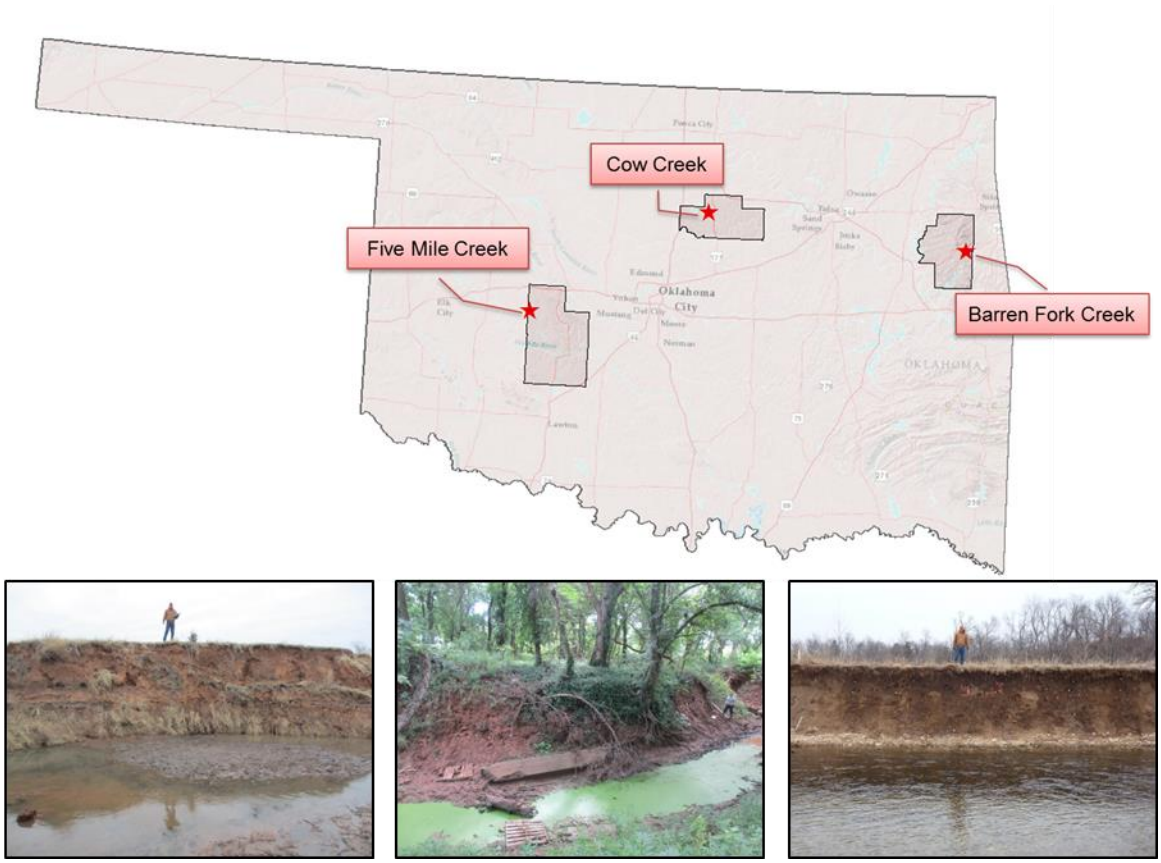

Figure 4.1. Location of Five Mile Creek, Cow Creek, and Barren Fork Creek in Oklahoma as sites chosen for variability studies (top). Pictures of banks sampled (bottom) at Five Mile Creek (left), Cow Creek (middle), and Barren Fork Creek (right) sites.

The Barren Fork Creek, located in northeastern Oklahoma in Cherokee County, is a fourth order stream part of the Illinois River watershed. The watershed covers 4,330 km^2 spanning the northeastern Oklahoma-Arkansas border. Approximately 54% of this basin is located within Oklahoma. The watershed falls within the Ozark Highlands ecoregion, which typically contains streams that are riffle and pool dominated, clear, and have coarse gravel, cobble, or bedrock substrates. Banks are typically composite and include a silty loam top layer with an unconsolidated gravel bottom layer and toe (Fox et al., 2011; Midgley et al., 2012). The dominating land uses in the basin are forest and hay production or pasture with the major agricultural industry being poultry and cattle (OCC,

2010). The streambanks at this site had little vegetation, but there were roots present especially towards the top of the bank.

Cow Creek, located in north central Oklahoma in Payne County, is located in the Central Great Plains Ecoregion. The watershed, covering approximately 30 km^2, has both rural and urban portions with a significant portion devoted to Oklahoma State University's research farms. Cow Creek is an intermittent stream where it is not dammed. The streambanks are comprised of a single layer of loam and sandy loam soils (Midgley et al., 2013). The majority of the creek has significant riparian areas as well. The streambanks at this site had the largest amount of vegetation across the bank face.

The Fort Cobb watershed, including Five Mile Creek located in Caddo County, lies in the Central Great Plains Ecoregion of western Oklahoma. The watershed, which covers 813 km^2, is used for mostly agricultural purposes with 51% used for crops and 40% pastures. Much of the pasture provides uncontrolled access for cattle to riparian areas (Storm et al., 2003). This watershed drains to the Fort Cobb Reservoir, which provides public water supply, flood control, recreation, and wildlife habitat, but it does not meet water quality standards based on sediment. Streambank erosion from the Fort Cobb watershed is one of the primary contributors of sediment loading to the reservoir. Streambanks in this watershed consist of sand or sandy loam topsoil (approximately 1 m) overlying a layer with higher clay content. Streambanks at this site had little vegetation.

4.3.2 Data Collection

Data was collected at each of the three sites between February and July of 2014. Data at each site was collected over a span of three days. A homogeneous layer was

selected on the critical bank at each site for testing. If the critical bank had multiple apparent soil layers, a single layer was chosen for testing. The JETs at each site were completed using two "mini" JETs that were setup and operated following the procedures outlined by Hanson and Cook (2004) and Al-Madhhachi et al. (2013a, 2013b).

Prior to each test, the soil foundation ring was secured to the bank. After placement of the foundation ring, a 5 cm diameter by 5 cm long cylindrical soil core sample was inserted approximately 15 cm to the right of the foundation ring, and a sample was extracted from the streambank. The soil core was used to analyze bulk density and moisture content at each test location. At the conclusion of each test, a bag sample of the soil was taken from the center of the foundation ring for determination of soil texture. Particle size analyses were conducted with a sieve analysis and hydrometer test according to ASTM Standards D421 (2002) and D422 (2002). Vertical and horizontal spatial coordinates for each test location were estimated using a surveying tape, surveying rod, and laser level.

4.3.3 Derivation of Erodibility Parameters

Analytical methods for the JET were first presented by Hanson and Cook (1997, 2004), assuming that the rate of variation in the depth of scour (dJ/dt) was the erosion rate as a function of the maximum stress at the boundary, which was determined by the diameter of the jet nozzle and the distance from jet origin to the initial channel bed. Therefore, the erosion rate equation for jet scour is written as (Hanson and Cook, 1997):

$$\frac{dJ}{dt} = k_d \left[\frac{\tau_o J_p{}^2}{J^2} - \tau_c \right] \text{ for } J \geq J_p \tag{4.2}$$

where J is the scour depth (cm), and J_p is the potential core length from jet origin (cm). Accordingly, τ_c was assumed to occur when the rate of scour was equal to zero at the equilibrium scour depth (J_e):

$$\tau_c = \tau_o \left(\frac{J_p}{J_e} \right)^2 \tag{4.3}$$

where $\tau_o = C_f \rho_w U_o{}^2$ is the maximum shear stress due to the jet velocity at the nozzle (Pa), C_f = 0.00416 is the coefficient of friction, ρ_w is water density (kg m^{-3}), U_o is the jet velocity at the orifice (cm s^{-1}), $J_p = C_d d_o$, d_o is the nozzle diameter (cm), and C_d = 6.3 is the diffusion constant. Equations 4.2 and 4.3 can be incorporated in a dimensionless form as the following equation:

$$\frac{dJ^*}{dT^*} = \frac{1 - J^{*2}}{J^{*2}} \tag{4.4}$$

where $J^* = J/J_e$ and $J_p{}^* = J_p/J_e$. Stein and Nett (1997) presented the reference time (T_r) as follows:

$$T_r = \frac{J_e}{k_d \tau_c} \tag{4.5}$$

and the dimensional time (T^*) was given as:

$$T^* = \frac{t}{T_r} \tag{4.6}$$

where t is the time of a data reading or scour depth measurement.

Equation 4.4 refers to the change in scour depth with T^*. Integration of equation 4.4 gives the following equation:

$$T^* - T_p{}^* = -J^* + 0.5\ln\left(\frac{1+J^*}{1-J^*}\right) + J_p{}^* - 0.5\ln\left(\frac{1+J_p{}^*}{1-J_p{}^*}\right) \quad (4.7)$$

The Excel spreadsheet, discussed by Hanson and Cook (2004) and utilizing equations 4.2 through 4.7, was used to determine τ_c and k_d. The critical shear stress (τ_c) was determined from equation 4.3 based on the equilibrium scour depth (J_e). Blaisdell et al. (1981) noted that it was difficult to determine the equilibrium scour depth due to the large time required to reach J_e. Therefore, the spreadsheet calculated the equilibrium scour depth using the scour depth data versus time and a hyperbolic function for determining the equilibrium scour depth developed by Blaisdell et al. (1981). The general form of this equation is:

$$\left(f - f_o\right)^2 - x^2 = A_1{}^2 \quad (4.8)$$

where A_1 is the value for the semi-transfer and semi-conjugate of the hyperbola, $f = \log(J/d_o) - x$, $x = \log[(U_o t)/d_o]$, and $f_o = \log(J_e/d_o)$. From fitting the scour depth data based on plotting f versus x, the coefficients A_1 and f_o can be determined using Microsoft Excel Solver, and then J_e can be determined ($J_e = d_o 10^{fo}$). The spreadsheet was then used to calculate k_d by fitting the curve of measured data based on equation 4.7. The k_d depends on the measured scour depth, time, pre-estimated τ_c, and the dimensional time function (Hanson et al., 2002). For the remainder of this paper, this solution approach will be referred to as the Blaisdell Solution.

An alternative solution methodology of the excess shear stress equation has been proposed by multiple researchers (Simon et al., 2010; Daly et al., 2013). One proposed solution approach outlined by Simon et al. (2010) as the iterative solution, was incorporated into the most recent version of the automated spreadsheet tool (Daly et al.,

2013). Using data from hundreds of JETs, Simon found that the dimensionless time reached at the end of the test (T^*) was highly variable suggesting that the results of the JET test are sensitive to the length of time the test is performed. The iterative solution was developed based on "Method 1" from Hanson and Cook (1997) in which τ_c and k_d are iteratively determined based on T^* and the dimensionless scour depth (J^*). The iterative solution is initialized with the τ_c and k_d values determined using the Blaisdell Solution and the parameters are then simultaneously solved for iteratively to minimize the root-mean-square-error between the measured and predicted time. The iterative solution is confined by an upper bound on τ_c that is a function of the water pressure at the nozzle (τ_o), the nozzle diameter (d_o), and the maximum scour depth observed during the test (J_e). This upper bound is included to prevent the solution from exceeding the equilibrium scour depth. The maximum τ_c constraint was set as:

$$\tau_{c-\max} = \tau_0 \left(\frac{C_d d_0}{J_e} \right)^2 \tag{4.9}$$

where C_d is the diffusion constant with a value of 6.2 (Hanson and Cook, 1997). The updated JET spreadsheet tool includes the iterative solution by using the solver routine in Microsoft Excel (generalized reduced gradient method) to minimize the error between the measured time during the test and the calculated measured time (t_m) following the equation by Hanson and Cook (1997):

$$t_m = T_r \left[0.5 \ln\left(\frac{1+J^*}{1-J^*} \right) - J^* - 0.5 \ln\left(\frac{1+J_i^*}{1-J_i^*} \right) + J_i^* \right] \tag{4.10}$$

A third proposed alternative, referred to as the scour depth solution, plots the original scour depth versus time as derived from the JETs (Daly et al., 2013). Then, using the applied shear stress and the initial parameter estimates, k_d and τ_c are fit to the

observed scour depth data using the solver routine in Microsoft Excel (generalized reduced gradient method) to minimize the sum of squared errors between the measured scour data and the solution of the excess shear stress equation. This procedure mimics the approach used by Al-Madhhachi et al. (2013b, 2014) for a mechanistic detachment model.

Data collected at each site was analyzed using the JET spreadsheet tool that incorporates all three solution techniques (Daly et al., 2013). Solutions for k_d and τ_c derived using the Blaisdell, scour depth, and iterative solutions were reported for each JET conducted. The solution technique used to derive each parameter is indicated by "BL" for the Blaisdell solution, "SD" for the scour depth solution, and "IT" for the iterative solution.

4.3.4 Statistical Analysis

The τ_c and k_d values derived from the BL, SD and IT solutions were analyzed for each of the three sites. First, the Anderson-Darling normality test was used to determine whether the parameters were normally distributed. This is a one-sample hypothesis test that tests the null hypothesis that the population follows a normal distribution. The alternative hypothesis states that the population is non-normal. The test compares the empirical cumulative distribution function of the sample data with the distribution that would be expected if the data were normal. The Anderson-Darling statistic (AD) is a weighted squared distance from the observations to the fitted line for the normal distribution. Therefore, smaller AD statistics denote that the data fits a normal distribution and larger AD values denote a poor fit. A p-value is also reported with this

test. These tests were completed using MiniTab 16 Statistical Software (MiniTab Inc., 2009).

The purpose of conducting JETs *in situ* is to estimate the erodibility parameters for a streambank. When planning a study in order to estimate a parameter, it is important to know the minimum sample size required to obtain a certain amount of precision and confidence. If it is assumed that the erodibility parameters follow a normal distribution, traditional methods of estimating sample size can be utilized. Assuming the sample standard deviation (S) to be equal to the population standard deviation (σ), the minimum sample size (n) to estimate the true mean within a certain precision unit (Δ) with a certain amount of confidence (function of Z) can be estimated based on the standard error (Borradaile, 2003):

$$n = \left(\frac{ZS}{\Delta} \right)^2 \tag{4.11}$$

However, many environmental variables fail to fit a normal distribution. Hale (1972) presented a simple method for determining the sample size necessary to obtain an estimate of the mean of a parameter that follows a log normal distribution. Assuming that each observed value is independent, the sample size required to estimate the true mean within a predetermined fraction and a given level of confidence is given as:

$$n = \frac{Z^2 S^2}{\ln^2 (P+1)} \tag{4.12}$$

where n is the sample size required, Z is the normal deviate corresponding to the upper percentage point for a specified level of confidence, S is the standard deviation of the logarithms of the original observations, and P is the fraction of the observed geometric mean by which it can differ from the true geometric mean with specified probability.

Hale (1972) states that this method of determining sample size is applicable to the case of determining the number of sampling locations to estimate a mean value over a geographical area, such as the case in this study. This method has been used multiple times in the literature concerning environmental data following a log-normal distribution (e.g., Bunzl et al., 2001; Wu et al., 2013). Note the difference between the margin of error measurements (Δ and P) for the two techniques. Under the assumptions of a normal distribution Δ is a margin of error with units of the parameter being investigated. Under the assumptions of a log-normal distribution, P is a margin of error reported in a percentage deviation from the mean.

4.3.5 Evaluating Empirical Relationships

This research also compared measuring the erodibility parameters in situ using the JET and estimating the erodibility parameters using empirical relationships. There are many relationships suggested in the literature relating soil texture parameters to erodibility parameters. Typically, τ_c is estimated from a soil texture parameter and k_d is then estimated from τ_c. Julian and Torres (2006) suggested a relationship relating τ_c to the silt-clay content ($SC\%$) of cohesive soils. The relationship assumes τ_c is at a maximum value at 100% silt-clay content and a minimum value at 0% silt-clay content. Based on the lower limit of the Shield's curve (Shields, 1936) and observations by Dunn (1959), Julian and Torres (2006) developed the following relationship (R^2=0.91):

$$\tau_c = 0.1 + 0.1779(SC\%) + 0.0028(SC\%)^2 - 2.34\times10^{-5}(SC\%)^3 \qquad (4.13)$$

This relationship was evaluated specifically using the soil texture and JET-derived τ_c using each solution technique in this study.

Inverse relationships have been developed (Hanson and Simon, 2001) to estimate k_d as a function of τ_c for cohesive soils:

$$k_d = 0.2\tau_c^{-0.5} \tag{4.14}$$

Hanson and Simon (2001) derived their relationship based on 83 *in situ* JETs. These tests were conducted in cohesive streambeds in the Midwestern United States. Results showed a wide range with τ_c spanning six orders of magnitude and k_d spanning four orders of magnitude. However, a general inverse relationship was observed between τ_c and k_d suggesting that soils with a low τ_c have a high k_d and vice versa. Their relationship predicted 64% of the variation within their data and was incorporated into streambank erosion and stability models, such as the Bank Stability and Toe Erosion Model (BSTEM), as a tool for estimating k_d from τ_c. This relationship was recently updated (Simon et al., 2011) based on hundreds of JETs on streambanks across the United States and given as:

$$k_d = 1.62\tau_c^{-0.838} \tag{4.15}$$

New relationships were developed between k_d and τ_c using JET test data at each site using the three solution techniques and compared to equations 14 and 15. These equations relating τ_c and k_d were originally developed based on the Blaisdell solution. These relationships were chosen for comparison because users of erosion models, such as BSTEM, Water Erosion Prediction Project (WEPP), Soil and Water Assessment Tool (SWAT), and CONservational Channel Evolution and Pollutant Transport System (CONCEPTS), routinely estimate the erodibility parameters using these relationships (equations 4.13 to 4.15) (Langendoen, 2000; Abaci and Papanicolaou, 2009; Neitsch et al., 2011; Midgley et al., 2012).

In order to compare the values derived from the JET and those derived from these empirical relationships (equations 4.13 to 4.15) it was assumed that the sample mean at each site for each solution technique was the "true mean" or population mean. Therefore, the standard deviation (*S*) calculated for use in equations 4.11 and 4.12 for the empirical relationships was the deviation of each estimated value from the average JET value for each solution technique conducted at each site:

$$S = \sqrt{\frac{1}{n}\sum_{i=1}^{n}(x_i - \bar{x})^2} \tag{4.16}$$

where n is the number of JETs conducted or soil samples collected at that site, x_i is the individual estimate from one of the empirical equations, and $\bar{x}$ is the mean of the JETs conducted at that site for the respective solution technique. Using S of the estimated values from the mean JET measured values, the Δ or P was calculated and a range was defined. The range illustrates the uncertainty of the empirical equation and was compared to the range from the JETs.

4.4 Results and Discussion

4.4.1 Variability in JET Measurements

A total of 74 JETs were completed for this study: 30 JETs at Barren Fork Creek, 20 at Cow Creek, and 24 at Five Mile Creek. The texture analysis conducted for each of the 74 JETs showed a variety of soil textures present at each of the sites. The Barren Fork Creek and Cow Creek sites had a mixture of loam, sandy loam, and silt loam textures. Five Mile Creek had a mixture of loam, sand, sandy loam, and sandy clay loam textures (Figure 4.2). The bulk density and volumetric moisture content of each sample was also measured. Bulk densities ranged from 1.1 to 1.5 g/cm^3 and volumetric water contents

ranged from 0.08 to 0.33 cm^3/cm^3 across the three sites (Figure 4.3). From strictly an observation of texture, it would be expected that Cow Creek had the most erodible soil and Five Mile Creek had the most resistant soil.

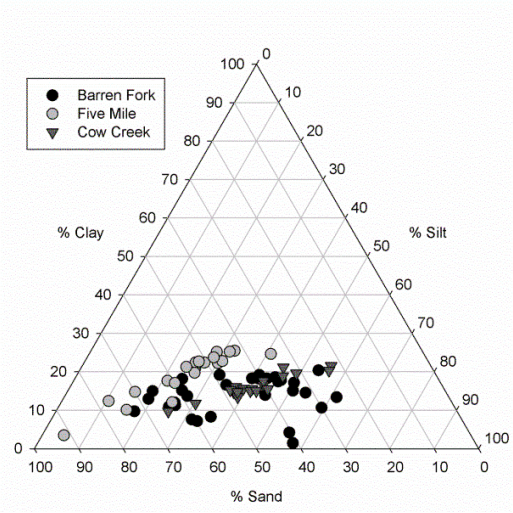

Figure 4.2. Soil textures for samples from (a) Barren Fork Creek, (b) Cow Creek, and (c) Five Mile Creek.

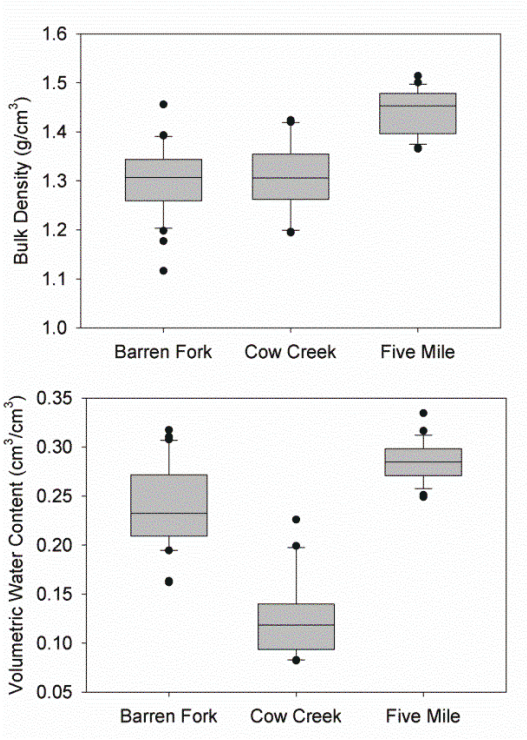

Figure 4.3. Bulk densities (top) and volumetric water contents (bottom) from samples at Barren Fork Creek, Cow Creek, and Five Mile Creek.

Variability in derived erodibility parameters was dependent on both site and solution technique (Figure 4.4). In terms of solution techniques, the BL solution predicted lower k_d and τ_c compared to the SD and IT solutions. Daly et al. (2013) observed a similar pattern with respect to the solutions, noting that the lower τ_c by the BL solution results in a conservative approach for predicting scour.

Cow Creek was the most variable site in terms of k_d. The k_d at this site spanned one, three, and two orders of magnitude for the BL, SD, and IT solutions, respectively. This high degree of variability in k_d at Cow Creek was expected due to its characterization as the site with the most erodible soil. Five Mile Creek was the most variable site in terms of τ_c with each solution producing a variation of one order of magnitude. Again, this was expected due to Five Mile Creek's characterization as the site with the most resistive soil. The τ_c results from Barren Fork Creek were the most uniform with every solution technique producing results within the same order of magnitude. There are a number of variables that could cause the presence or lack of variability, such as the presence of gravel or roots at the JET site, differences in moisture content, or soil texture heterogeneity. This amount of variability causes less confidence in an average value being the most representative parameter for erosion predictions at a site.

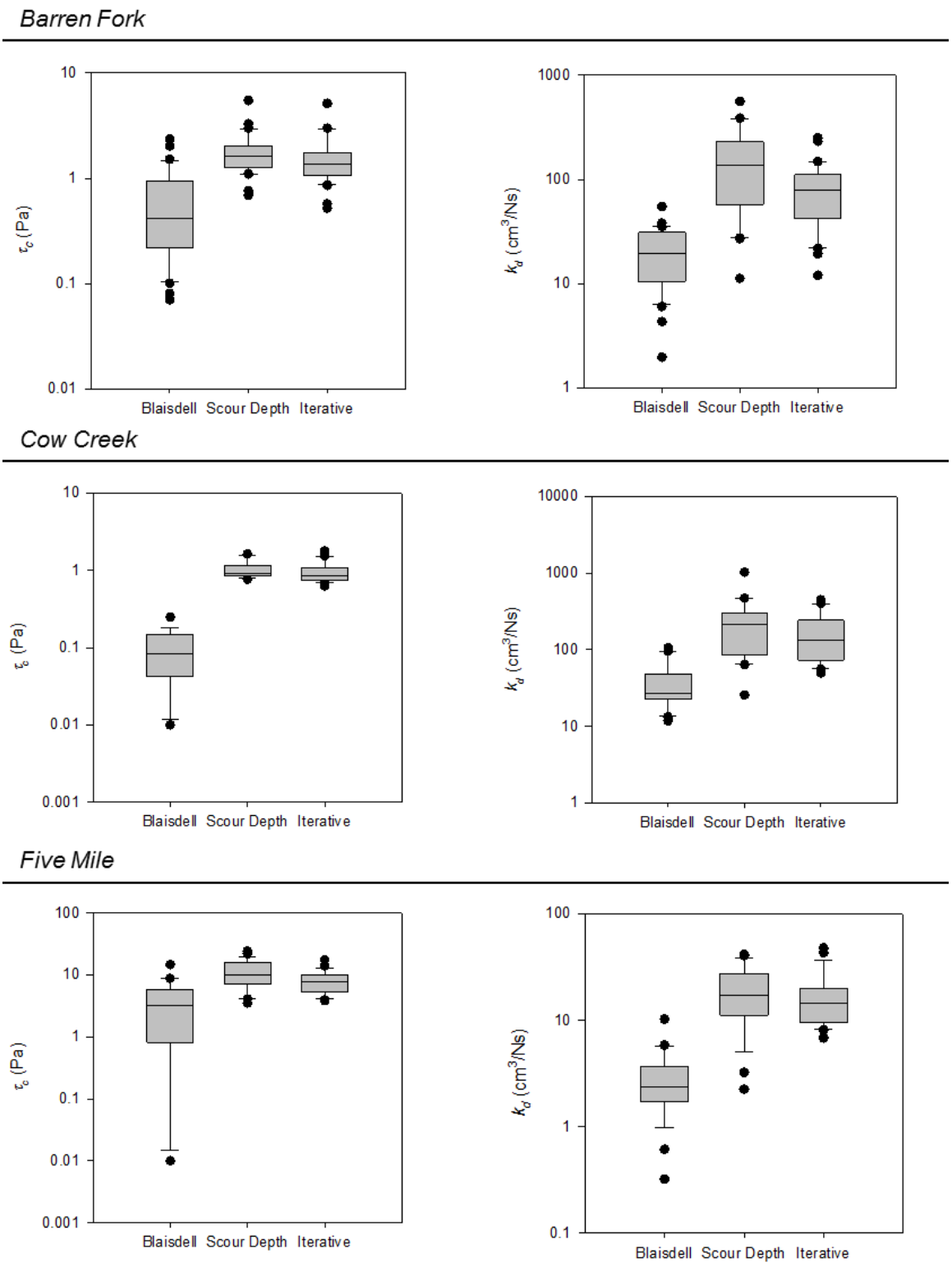

Figure 4.4. Range in erodibility parameters derived using the Blaisdell, scour depth, and iterative solution methodologies at Barren Fork Creek, Cow Creek, and Five Mile Creek.

To explore the variability further, summary statistics were calculated for results of each solution technique at each site (Table 4.1). From the summary statistics there seems to be a moderate degree of variability in all six parameters at each site as the standard deviation is generally on the same order of magnitude as the mean. The high coefficients of variation also illustrate this point.

Table 4.1. Summary statistics for erodibility parameters at each site derived from the Blaisdell solution ($\tau_{c\text{-}BL}$, $k_{d\text{-}BL}$), scour depth solution ($\tau_{c\text{-}SD}$, $k_{d\text{-}SD}$), and iterative solution ($\tau_{c\text{-}IT}$, $k_{d\text{-}IT}$).

	$\tau_{c\text{-}BL}$ (Pa)	$\tau_{c\text{-}SD}$ (Pa)	$\tau_{c\text{-}IT}$ (Pa)	$k_{d\text{-}BL}$ (cm^3/Ns)	$k_{d\text{-}SD}$ (cm^3/Ns)	$k_{d\text{-}IT}$ (cm^3/Ns)
Barren Fork						
Mean	0.62	1.82	1.59	20.0	163	85.2
Standard Deviation	0.56	0.92	0.89	12.1	129	57.8
Coeff. of Variation	0.90	0.51	0.56	0.60	0.79	0.68
Minimum	0.07	0.69	0.52	1.97	11.2	12.0
Maximum	2.36	5.49	5.15	54.9	559	251
Range	2.29	4.80	4.63	53.0	548	239
Cow Creek						
Mean	0.10	1.05	0.95	39.5	245	170
Standard Deviation	0.07	0.27	0.31	28.2	219	122
Coeff. of Variation	0.69	0.26	0.32	0.72	0.90	0.72
Minimum	0.01	0.77	0.63	11.7	25.5	49.1
Maximum	0.25	1.64	1.80	107	1029	447
Range	0.24	0.87	1.17	94.8	1004	398
Five Mile						
Mean	3.81	11.3	8.03	2.90	19.2	17.3
Standard Deviation	3.73	5.61	3.33	2.06	10.8	10.5
Coeff. of Variation	0.98	0.50	0.42	0.71	0.56	0.60
Minimum	0.01	3.52	3.84	0.32	2.24	6.80
Maximum	14.6	24.3	17.6	10.2	41.3	47.5
Range	14.6	20.7	13.7	9.89	39.0	40.7

In order to determine the most appropriate means to estimate sample size, the Anderson-Darling normality test was utilized. Results from this test indicated, at α = 0.05, that only 5 of the 18 parameters fit a normal distribution. These included $k_{d\text{-}BL}$ at

Barren Fork, $\tau_{c\text{-}BL}$ at Cow Creek, and $\tau_{c\text{-}SD}$, $k_{d\text{-}SD}$, and $\tau_{c\text{-}IT}$ at Five Mile. The data for all 18 parameters were transformed using the natural log and the Anderson-Darling normality test was rerun to test how well the transformed data fit a normal distribution. Results indicated that 15 of the 18 tests were not significant ($\alpha = 0.05$) suggesting that the data fit a log-normal distribution. Probability plots were created for both the original and transformed data for all parameters (Figure 4.5 to 4.7). A summary of the Anderson-Darling test statistics and respective p-values for the original and log-transformed data is reported in Table 4.2. Results from the Anderson-Darling tests indicated that all of the parameters followed a log-normal distribution with the exception of $\tau_{c\text{-}BL}$ at Cow Creek and Five Mile and $k_{d\text{-}SD}$ at Five Mile.

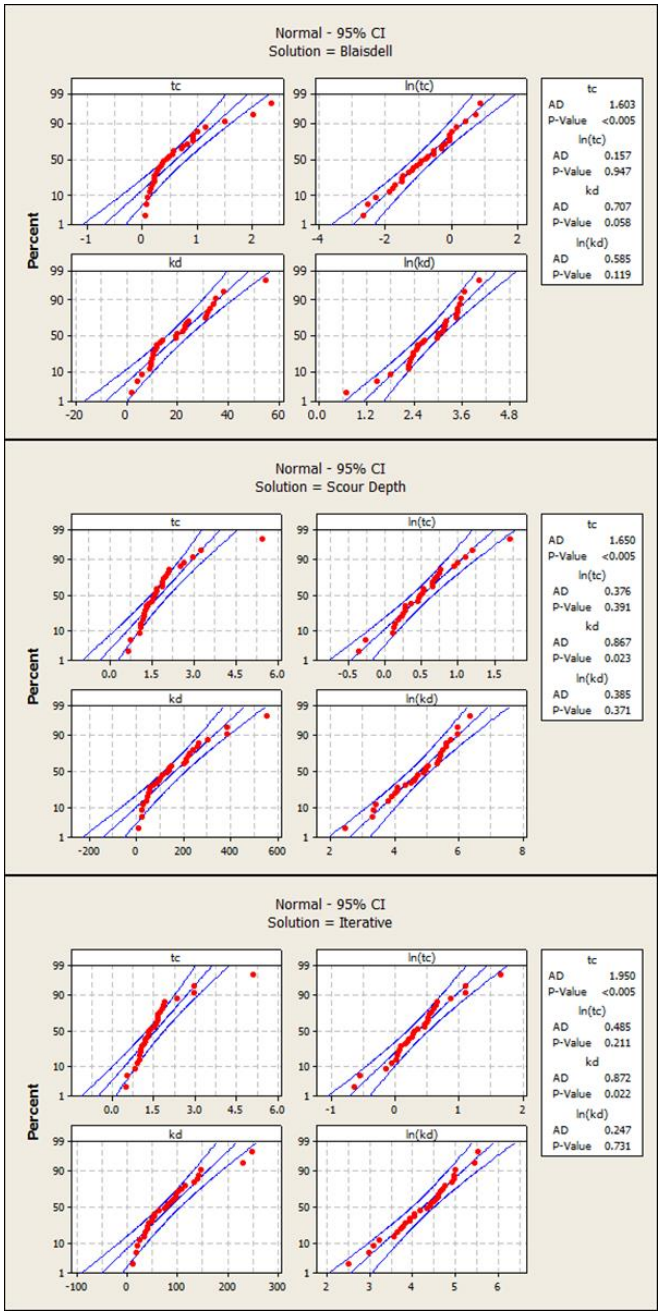

Figure 4.5. Probability plots of the original and transformed τ_c and k_d derived using the Blaisdell (top), scour depth (middle), and iterative (bottom) solutions at Barren Fork Creek.

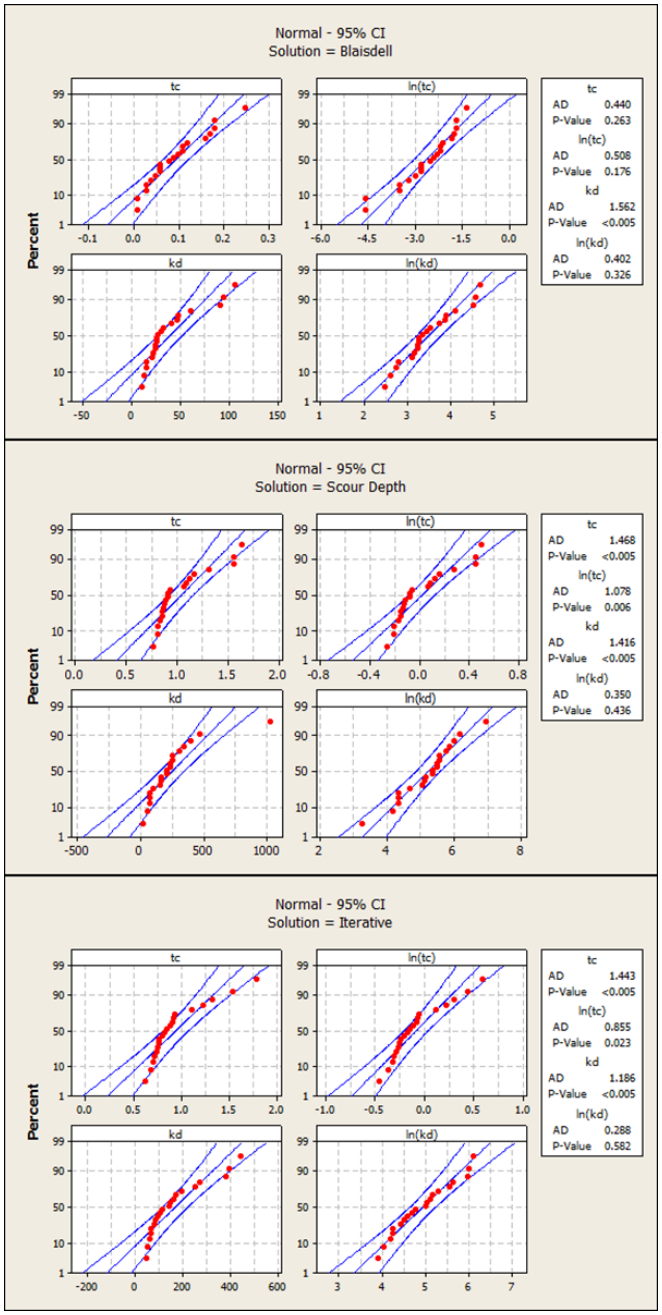

Figure 4.6. Probability plots of the original and transformed τ_c and k_d derived using the Blaisdell (top), scour depth (middle), and iterative (bottom) solutions at Cow Creek.

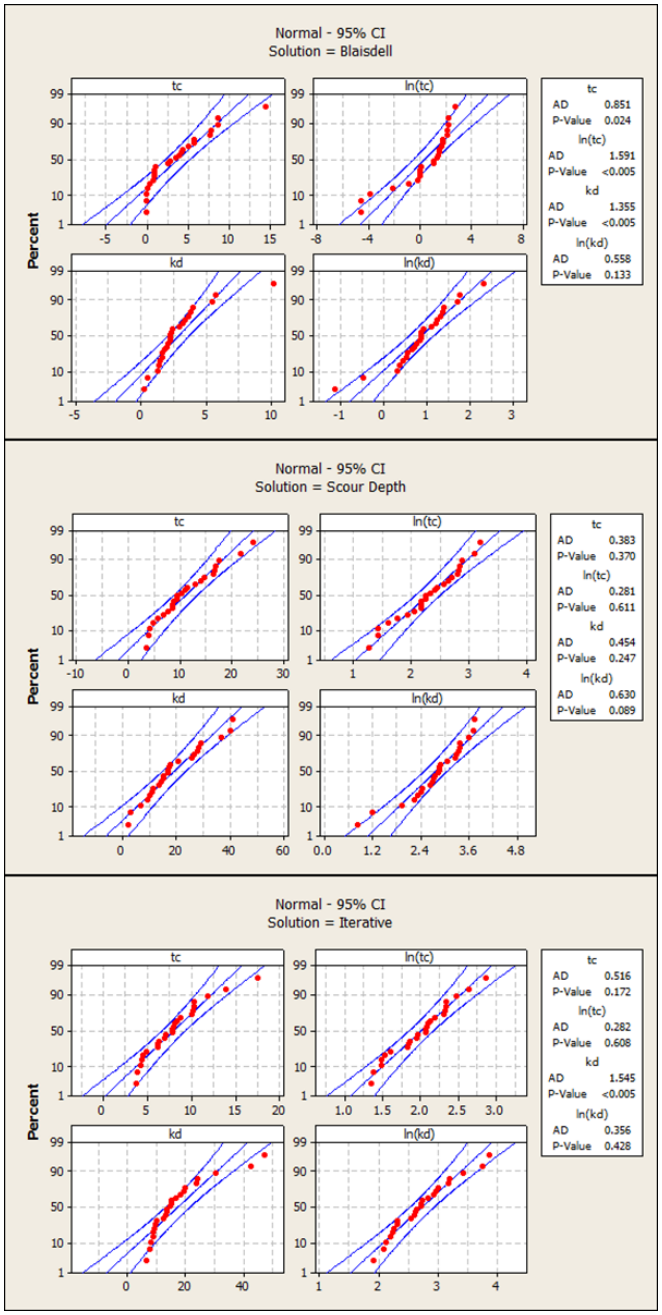

Figure 4.7. Probability plots of the original and transformed τ_c and k_d derived using the Blaisdell (top), scour depth (middle), and iterative (bottom) solutions at Five Mile Creek.

Table 4.2. Anderson-Darling (AD) test statistics and respective p-values for all 18 parameters analyzed for both the normal and log-normal distributions. Non-significant results ($\alpha = 0.05$) are highlighted in red, indicating the best distribution fit.

	$\tau_{c\text{-}BL}$ (Pa)		$\tau_{c\text{-}SD}$ (Pa)		$\tau_{c\text{-}IT}$ (Pa)		$k_{d\text{-}BL}$ (cm^3/Ns)		$k_{d\text{-}SD}$ (cm^3/Ns)		$k_{d\text{-}IT}$ (cm^3/Ns)	
	Normal	Log	Normal	Log	Normal	Log	Normal	Log	Normal	Log	Normal	Log
Barren Fork												
AD	1.60	0.16	1.65	0.38	1.95	0.49	0.71	0.59	0.87	0.39	0.87	0.25
P-Value	<0.005	0.95	<0.005	0.39	<0.005	0.21	0.06	0.12	0.02	0.37	0.02	0.73
Cow Creek												
AD	0.44	0.51	1.47	1.08	1.44	0.86	1.56	0.40	1.42	0.35	1.19	0.29
P-Value	0.26	0.18	<0.005	0.01*	<0.005	0.02*	<0.005	0.33	<0.005	0.44	<0.005	0.58
Five Mile												
AD	0.85	1.59	0.38	0.28	0.52	0.28	1.36	0.56	0.45	0.63	1.55	0.36
P-Value	0.02*	<0.005	0.37	0.61	0.17	0.61	<0.005	0.13	0.25	0.09	<0.005	0.43

* Results are significant at $\alpha = 0.05$, however this distribution has an improved fit over the alternative.

4.4.2 Sample Size Determination

Sample sizes were estimated for each parameter for both the assumption of a normal and log-normal distribution. Assuming a normal distribution and a 95% confidence level, sample sizes were calculated using the sample standard deviation and a Δ ranging from 0.01 to 10 Pa for τ_c and 1 to 100 cm^3/Ns for k_d. Results indicated a wide range in required sample sizes dependent on site, the parameter being estimated, the level of confidence required, and the Δ needing to be achieved (Figures 4.8 to 4.10). In general, Five Mile Creek required the most samples to obtain a certain amount of confidence and precision for τ_c and Cow Creek required the most samples for estimating k_d. This is likely due to the magnitude of the variability in these parameters at these sites. Five Mile Creek was characterized as the most resistant site, with the highest values of τ_c and lowest values of k_d, while Cow Creek was the least resistant site with the lowest values of τ_c and the highest values of k_d. This suggests that resistant soils may need more samples in order to properly characterize τ_c and erodible soils may need more samples in order to properly characterize k_d. As an example, Table 4.3 illustrates the magnitude of the required sample sizes and the differences between sites and solution techniques for a given confidence of 95% and a Δ of 0.1 and 1.0 Pa for τ_c and 5 and 10 cm^3/Ns for k_d.

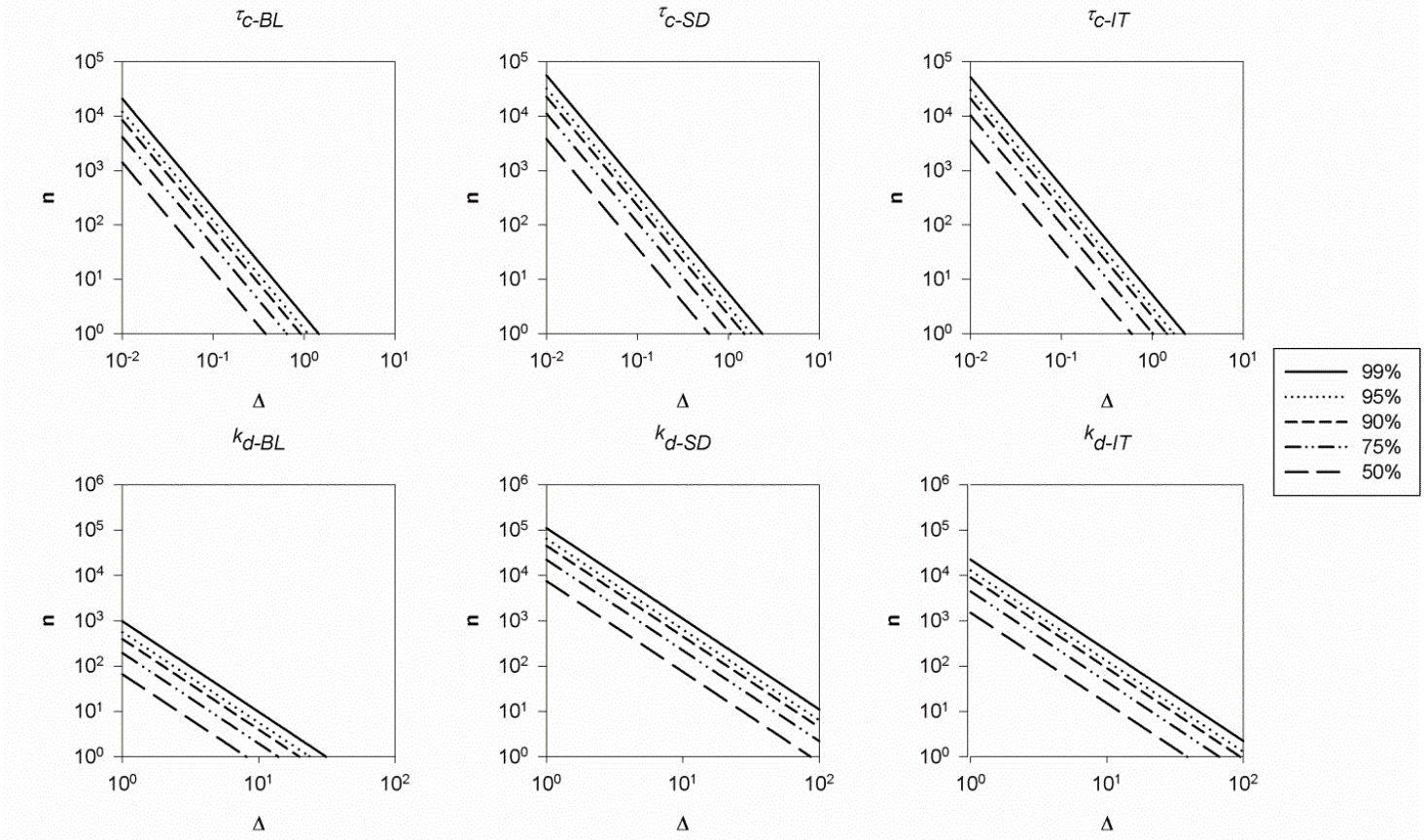

Figure 4.8. Sample size requirements for Barren Fork Creek for the erodibility parameters assuming a normal distribution for specified levels of confidence (legend) and precision unit deviation about the true mean (Δ).

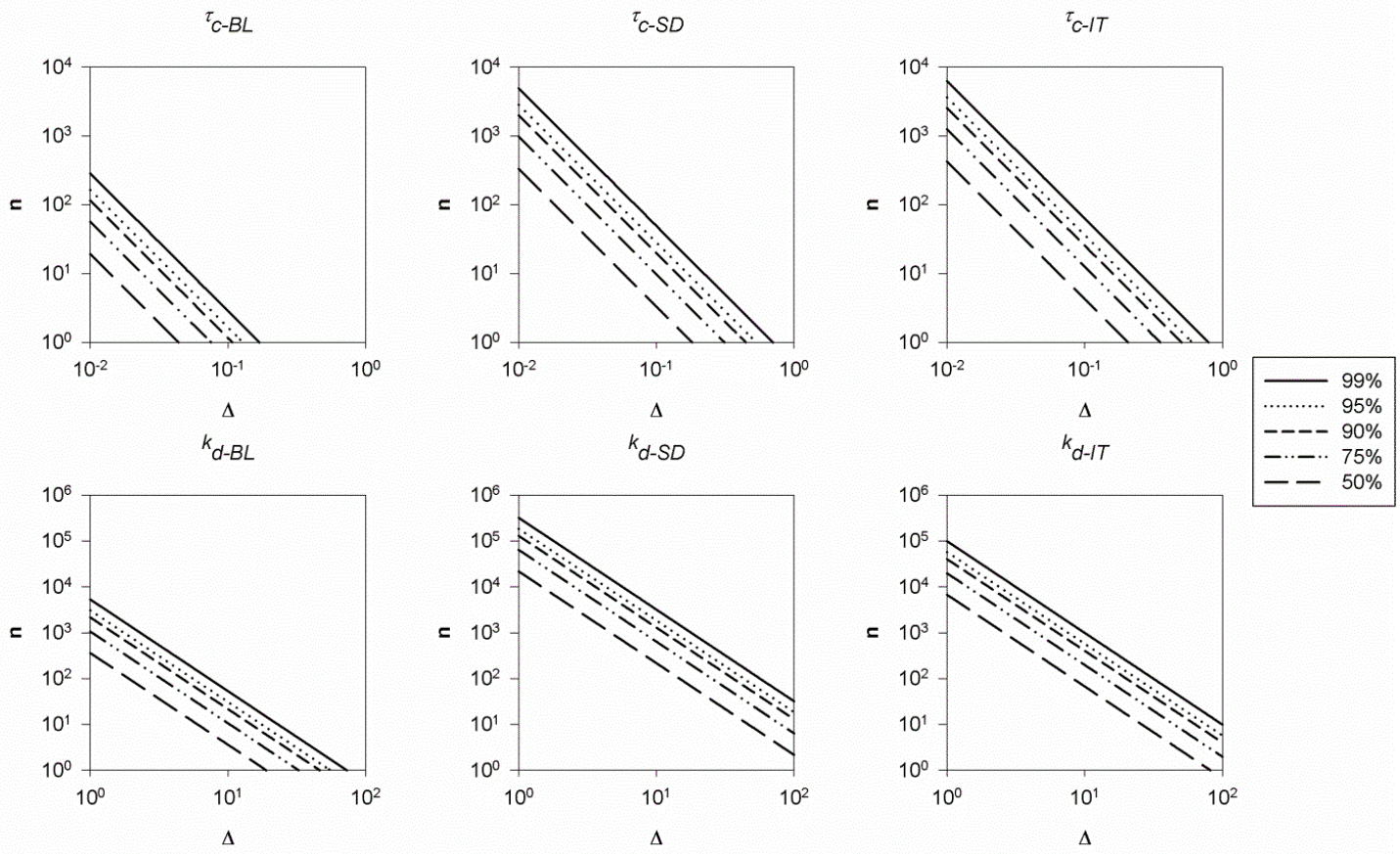

Figure 4.9. Sample size requirements for Cow Creek for the erodibility parameters assuming a normal distribution for specified levels of confidence (legend) and precision unit deviation about the true mean (Δ).

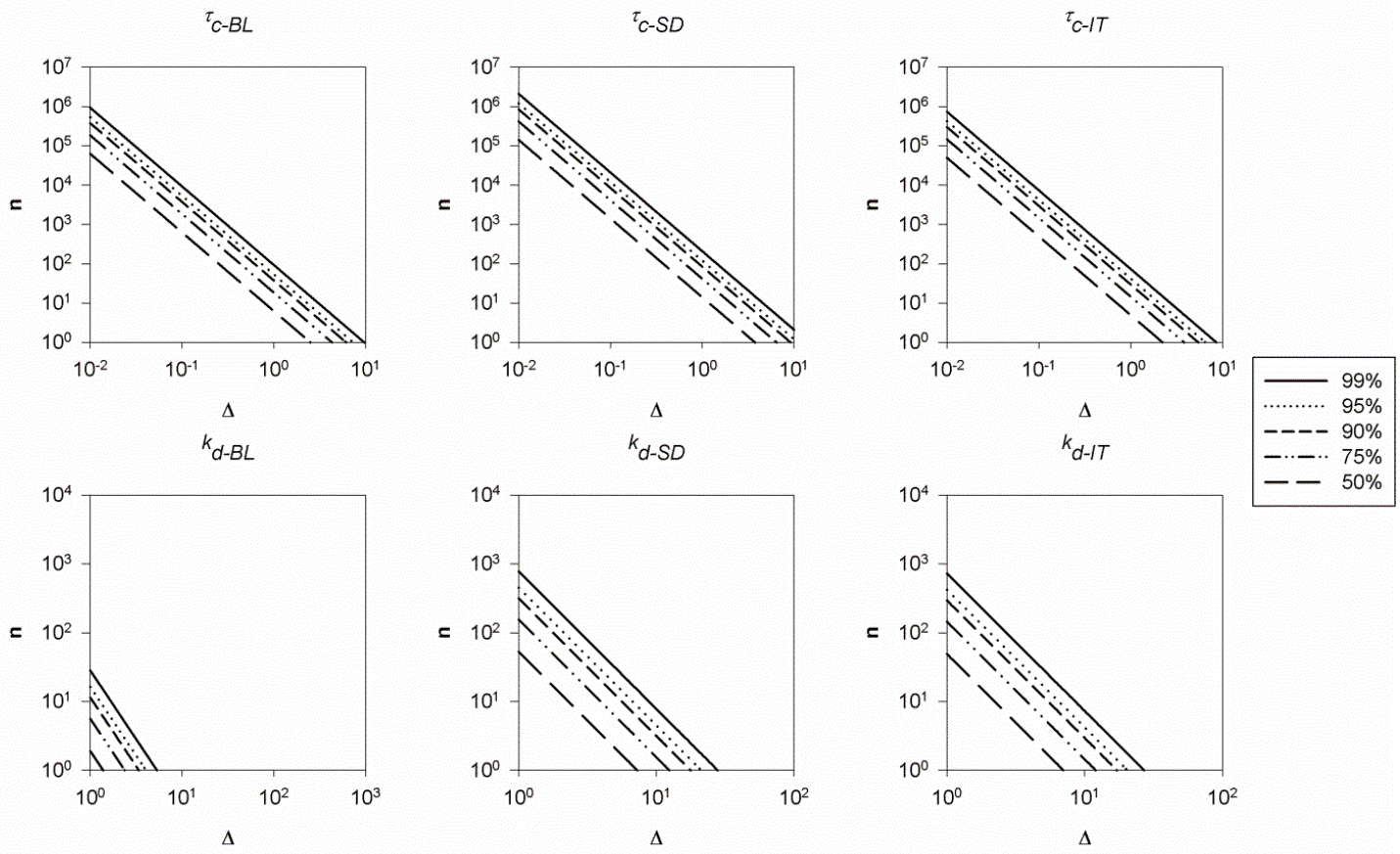

Figure 4.10. Sample size requirements for Five Mile Creek for the erodibility parameters assuming a normal distribution for specified levels of confidence (legend) and precision unit deviation about the true mean (Δ).

Table 4.3. Example of required sample sizes to guarantee with 95% confidence that the observed mean is within a certain range of error using the Blaisdell (BL), scour depth (SD), and iterative (IT) solutions. Calculations assume that parameters follow a normal distribution.

	τ_c (Pa)			k_d (cm^3/Ns)		
	Barren Fork	Cow Creek	Five Mile	Barren Fork	Cow Creek	Five Mile
Error		± 0.1 Pa			± 5 cm^3/Ns	
BL	121	2	5,342	22	122	1
SD	326	28	12,074	2,558	7,377	18
IT	302	36	4,258	513	2,286	17
Error		± 1.0 Pa			± 10 cm^3/Ns	
BL	1	1	53	6	31	1
SD	3	1	121	639	1,844	4
IT	3	1	43	128	572	4

Assuming a log-normal distribution, sample sizes were calculated using the standard deviations of the logarithms of the sample data and a P ranging from 5% to 50% (or 0.05 to 0.50) for both k_d and τ_c. Results again indicated a wide range in required sample sizes dependent on site, parameter being estimated, level of confidence required, and P needing to be achieved (Figures 4.11 to 4.13). Required sample sizes did not follow a general pattern with respect to soil erodibility as was the case under the assumption of normality. As an example, Table 4.4 illustrates the magnitude of the required sample sizes and the differences between sites and solutions techniques for a given confidence of 95% and a P of 5%, 10%, and 25% for both τ_c and k_d.

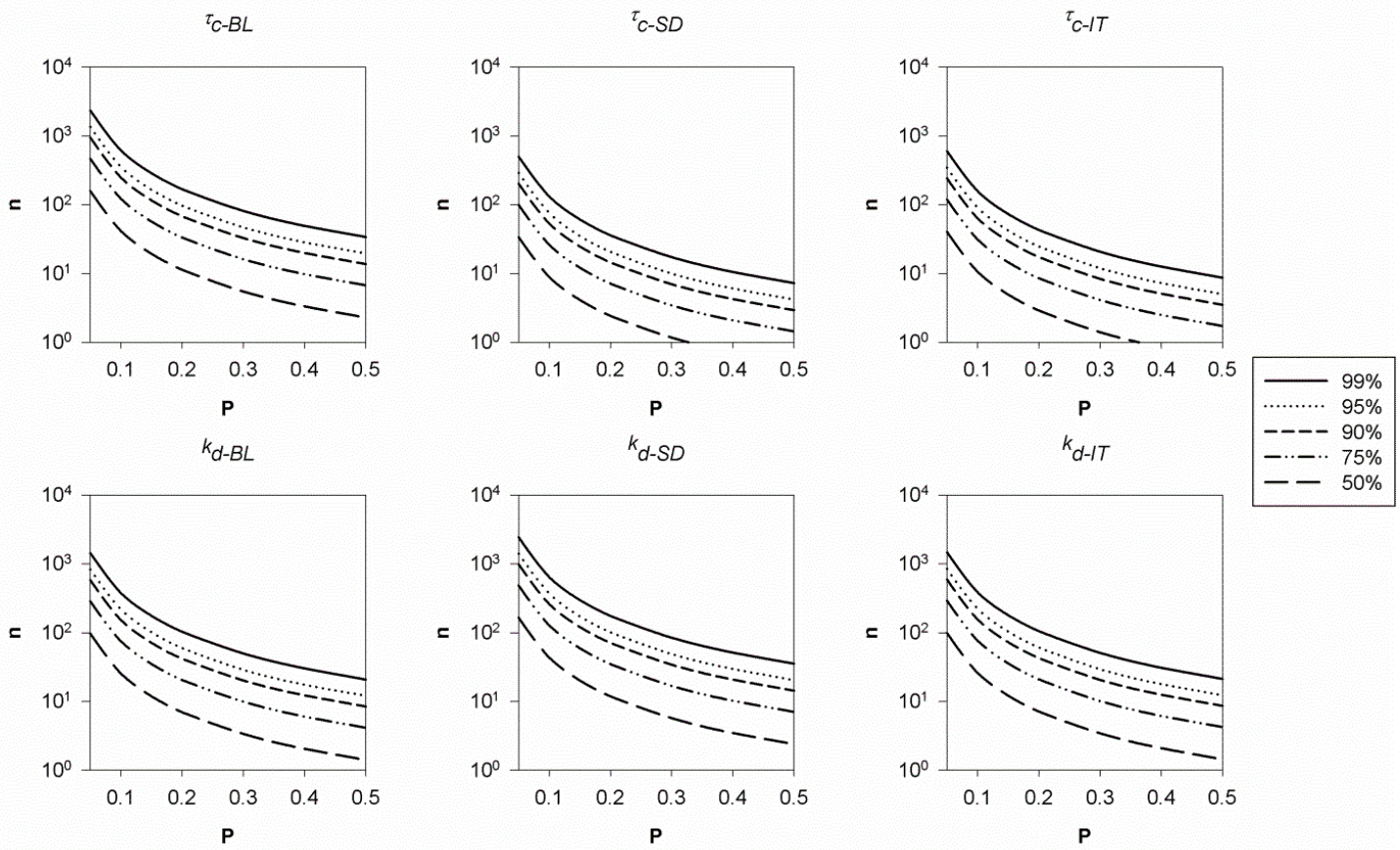

Figure 4.11. Sample size requirements for Barren Fork Creek for the erodibility parameters assuming a log-normal distribution for specified levels of confidence (legend) and deviation percentage about the true mean (*P*).

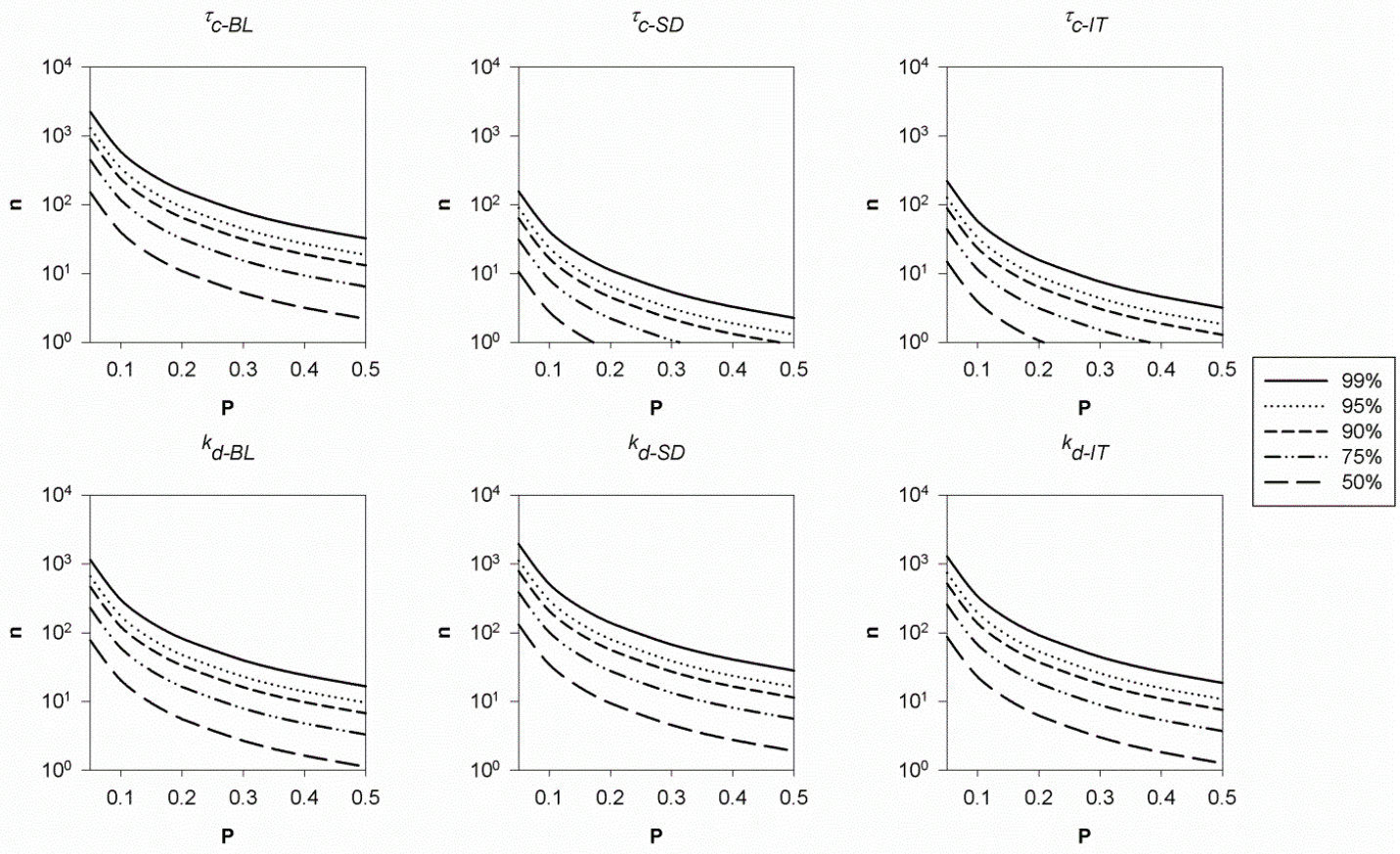

Figure 4.12. Sample size requirements for Cow Creek for the erodibility parameters assuming a log-normal distribution for specified levels of confidence (legend) and deviation percentage about the true mean (*P*).

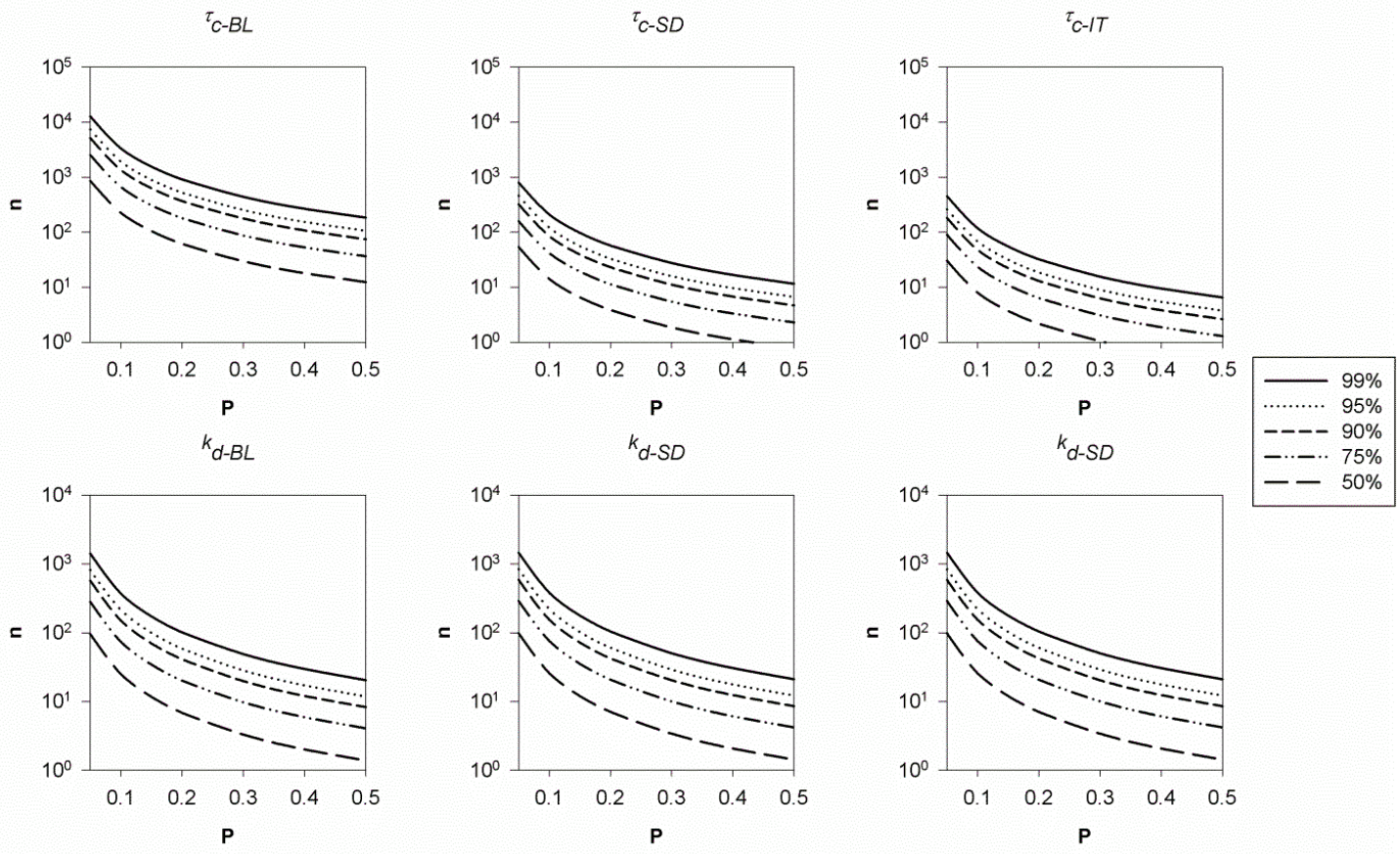

Figure 4.13. Sample size requirements for Five Mile Creek for the erodibility parameters assuming a log-normal distribution for specified levels of confidence (legend) and deviation percentage about the true mean (*P*).

Table 4.4. Example of required sample sizes to guarantee with 95% confidence that the observed mean is within a certain range of error using the Blaisdell (BL), scour depth (SD), and iterative (IT) solutions. Calculations assume that parameters follow a log-normal distribution.

	τ_c (Pa)			k_d (cm^3/Ns)		
	Barren Fork	Cow Creek	Five Mile	Barren Fork	Cow Creek	Five Mile
Error	5%					
BL	1,357	1,299	7,370	829	661	814
SD	290	90	463	1,406	1,119	839
IT	347	127	261	847	742	426
Error	10%					
BL	356	340	1,931	217	173	213
SD	76	24	121	369	293	220
IT	91	33	68	222	195	112
Error	25%					
BL	65	62	352	40	32	39
SD	14	4	22	67	53	40
IT	17	6	12	40	35	20

The required sample sizes at these sites for a reasonable amount of confidence and precision is astounding for both distributions. Very few cases require less than 10 samples for a reasonable amount of confidence. This raises two pertinent questions that need to be addressed with continued research: (1) what amount of precision is actually needed in order to use these parameters successfully within the framework of prediction modeling, and (2) how can the site-scale variability in these parameters be addressed in order to sample a site effectively.

With these questions in mind, current sampling techniques were evaluated for each of the three sites. The current practice has typically been to characterize a streambank by conducting multiple JETs and averaging the results. The amount of precision obtained for sample sizes of three and five JETs, with a 95% confidence level, under the assumption of a normal distribution and a log-normal distribution were calculated (Table 4.5). Results indicated a range of precision depending on solution technique and site. For example, assuming a normal distribution at Barren Fork Creek,

three JETs would be within ±14 cm^3/Ns using the Blaisdell solution, ±146 cm^3/Ns using the scour depth solution, and ±65 cm^3/Ns using the iterative solution for estimating k_d.

This trend is consistent when considering the results assuming a log-normal distribution. The margin of error is highly dependent on solution technique and site. It should be noted that, assuming a log-normal distribution, increasing the sample size by two JETs from three to five results in a large reduction in the margin of error. For example, if three JETs were conducted at Five Mile Creek and results for τ_c were analyzed using the scour depth solution, the margin of error would be 83%. Conducting just two more JETs for a total sample size of five reduces that margin of error to 60%. It should also be noted that conducting three to five JETs using any of the solution techniques at any of these sites produces a margin of error much greater than 50% for the majority of the parameters, with one parameter producing a margin of error of over 1000%.

Table 4.5. Precision achieved for sample sizes of three and five JETs assuming parameters follow a normal or log-normal distribution. Calculations are shown for a 95% confidence level (Z = 1.96). Blaisdell solution ($\tau_{c\text{-}BL}$, $k_{d\text{-}BL}$), scour depth solution ($\tau_{c\text{-}SD}$, $k_{d\text{-}SD}$), and iterative solution ($\tau_{c\text{-}IT}$, $k_{d\text{-}IT}$).

BARREN FORK									
Parameter	**Mean**	**Normal**				**Log-normal**			
		n = 3		*n = 5*		*n = 3*		*n = 5*	
		Δ	Range	Δ	Range	*P*	Range	*P*	Range
$\tau_{c\text{-}BL}$ (Pa)	0.62	0.64	0.0 – 1.3	0.49	0.1 – 1.1	182%	0.0 – 1.8	123%	0.0 – 1.4
$\tau_{c\text{-}SD}$ (Pa)	1.82	1.04	0.8 – 2.9	0.81	1.0 – 2.6	61%	0.7 – 3.0	45%	1.0 – 2.6
$\tau_{c\text{-}IT}$ (Pa)	1.59	1.00	0.6 – 2.6	0.78	0.8 – 2.4	69%	0.5 – 2.7	50%	0.8 – 2.4
$k_{d\text{-}BL}$ (cm^3/Ns)	20.0	13.7	6.4 - 34	10.6	9.4 – 31	125%	0.0 – 45	87%	2.5 – 38
$k_{d\text{-}SD}$ (cm^3/Ns)	163	146	17 - 309	113	50 – 276	188%	0.0 – 470	127%	0.0 – 370
$k_{d\text{-}IT}$ (cm^3/Ns)	85.2	65.4	20 - 151	50.6	35 – 136	127%	0.0 – 193	89%	9.6 – 161
COW CREEK									
Parameter	**Mean**	**Normal**				**Log-normal**			
		n = 3		*n = 5*		*n = 3*		*n = 5*	
		Δ	Range	Δ	Range	*P*	Range	*P*	Range
$\tau_{c\text{-}BL}$ (Pa)	0.10	0.07	0.0 – 0.2	0.06	0.0 – 0.2	176%	0.0 – 0.3	120%	0.0 – 0.2
$\tau_{c\text{-}SD}$ (Pa)	1.05	0.31	0.7 – 1.4	0.24	0.8 – 1.3	31%	0.7 – 1.4	23%	0.8 – 1.3
$\tau_{c\text{-}IT}$ (Pa)	0.95	0.35	0.6 – 1.3	0.27	0.7 – 1.2	37%	0.6 – 1.3	28%	0.6 – 1.2
$k_{d\text{-}BL}$ (cm^3/Ns)	39.5	31.9	7.6 – 71	24.7	15 – 64	106%	0.0 – 81	75%	9.8 – 69
$k_{d\text{-}SD}$ (cm^3/Ns)	245	248	0.0 – 493	192	53 – 437	157%	0.0 – 628	107%	0.0 – 508
$k_{d\text{-}IT}$ (cm^3/Ns)	170	138	32 – 308	107	63 – 277	115%	0.0 – 367	81%	32 – 308
FIVE MILE									
Parameter	**Mean**	**Normal**				**Log-normal**			
		n = 3		*n = 5*		*n = 3*		*n = 5*	
		Δ	Range	Δ	Range	*P*	Range	*P*	Range
$\tau_{c\text{-}BL}$ (Pa)	3.81	4.22	0.0 – 8.0	3.27	0.5 – 7.1	1023%	0.0 – 43	551%	0.0 – 25
$\tau_{c\text{-}SD}$ (Pa)	11.3	6.34	4.9 – 18	4.91	6.4 – 16	83%	1.9 – 21	60%	4.5 – 18
$\tau_{c\text{-}IT}$ (Pa)	8.03	3.77	4.3 – 12	2.92	5.1 – 11	58%	3.4 – 13	42%	4.6 – 11
$k_{d\text{-}BL}$ (cm^3/Ns)	2.90	2.33	0.6 – 5.2	1.80	1.1 – 4.7	123%	0.0 – 6.5	86%	0.4 – 5.4
$k_{d\text{-}SD}$ (cm^3/Ns)	19.2	12.2	6.9 – 31	9.48	9.7 – 29	126%	0.0 – 43	88%	2.3 – 36
$k_{d\text{-}IT}$ (cm^3/Ns)	17.3	11.8	5.5 – 29	9.16	8.2 – 26	79%	3.7 – 31	57%	7.5 – 27

4.4.3 Spatial Variability

From these analyses, it is apparent that the number of JETs conducted can yield variable results in parameter estimation depending on the site and the assumptions being made. The spatial variability was investigated as well to infer whether the location of these tests on the streambank may additionally influence parameter estimation. Assumptions made to estimate sample size requirements do not take into account the possible spatial dependency of erodibility parameters. Contour plots for each of the parameters were produced using the Surfer 8 kriging routine (Figures 4.14 through 4.16). These plots vary from site to site and suggest that there is not a strong spatial dependence when estimating the erodibility parameters. This may be due, in part, to the limited sample sizes at each site and inconsistent sample densities from different spatial regions. A more intensive study is needed in order to extrapolate any spatial correlations that may exist with respect to the erodibility parameters. For example, the spatial variability of τ_c at Barren Fork Creek (all solutions) suggests a gradient of high to low τ_c values in the vertical direction moving from the top of the bank towards the bank toe. At the Barren Fork Creek site, tests conducted towards the top of the bank may have encroached into the root zone of the grasses present. This pattern could be indicative of roots having a quantifiable influence on the erodibility of streambank soils. A similar pattern, although not as definitive, was present at Cow Creek. This site and the Five Mile Creek site had a greater amount of vegetation present across the entire bank face when compared to the Barren Fork Creek site.

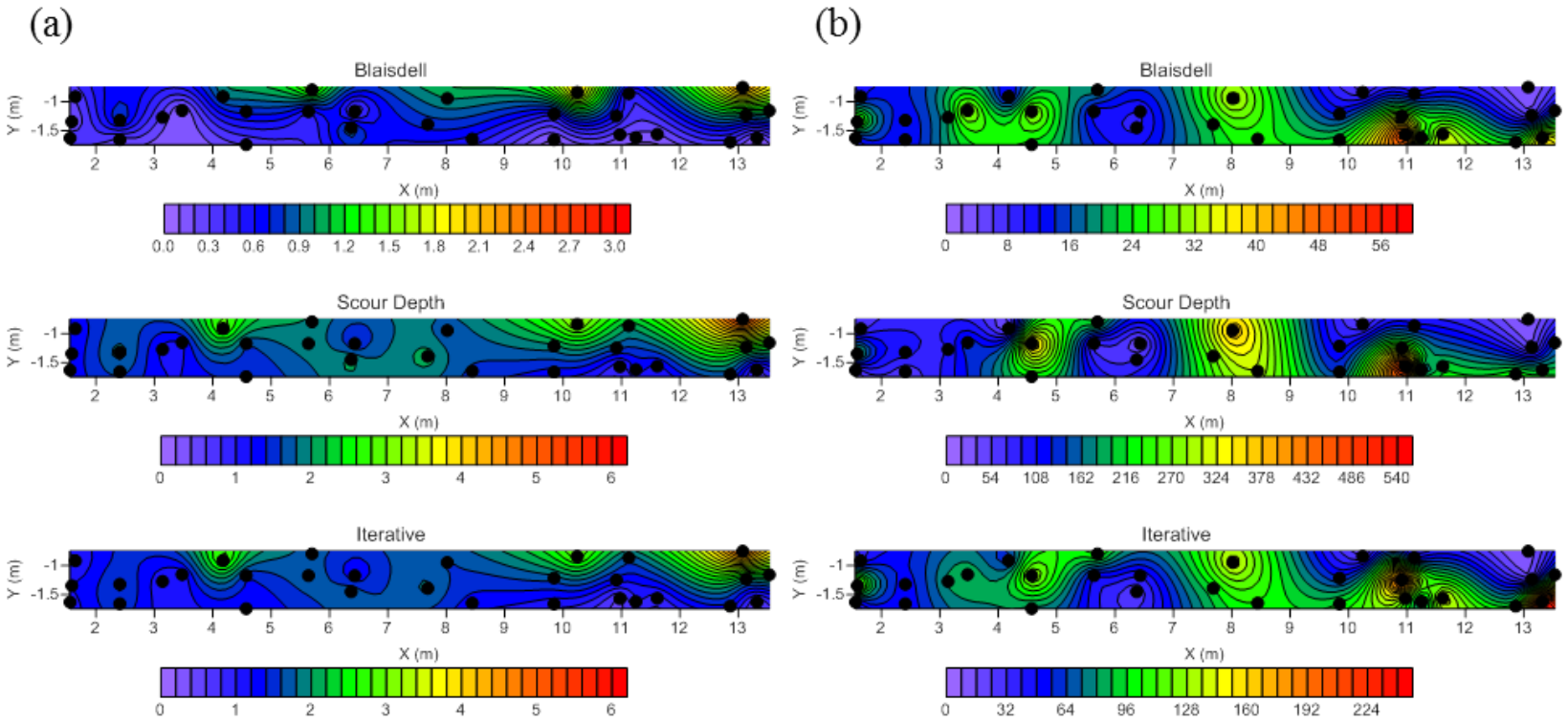

Figure 4.14. Spatial variability at Barren Fork Creek in derived (a) τ_c (Pa) and (b) k_d (cm^3/Ns). JET sample points are indicated as black dots.

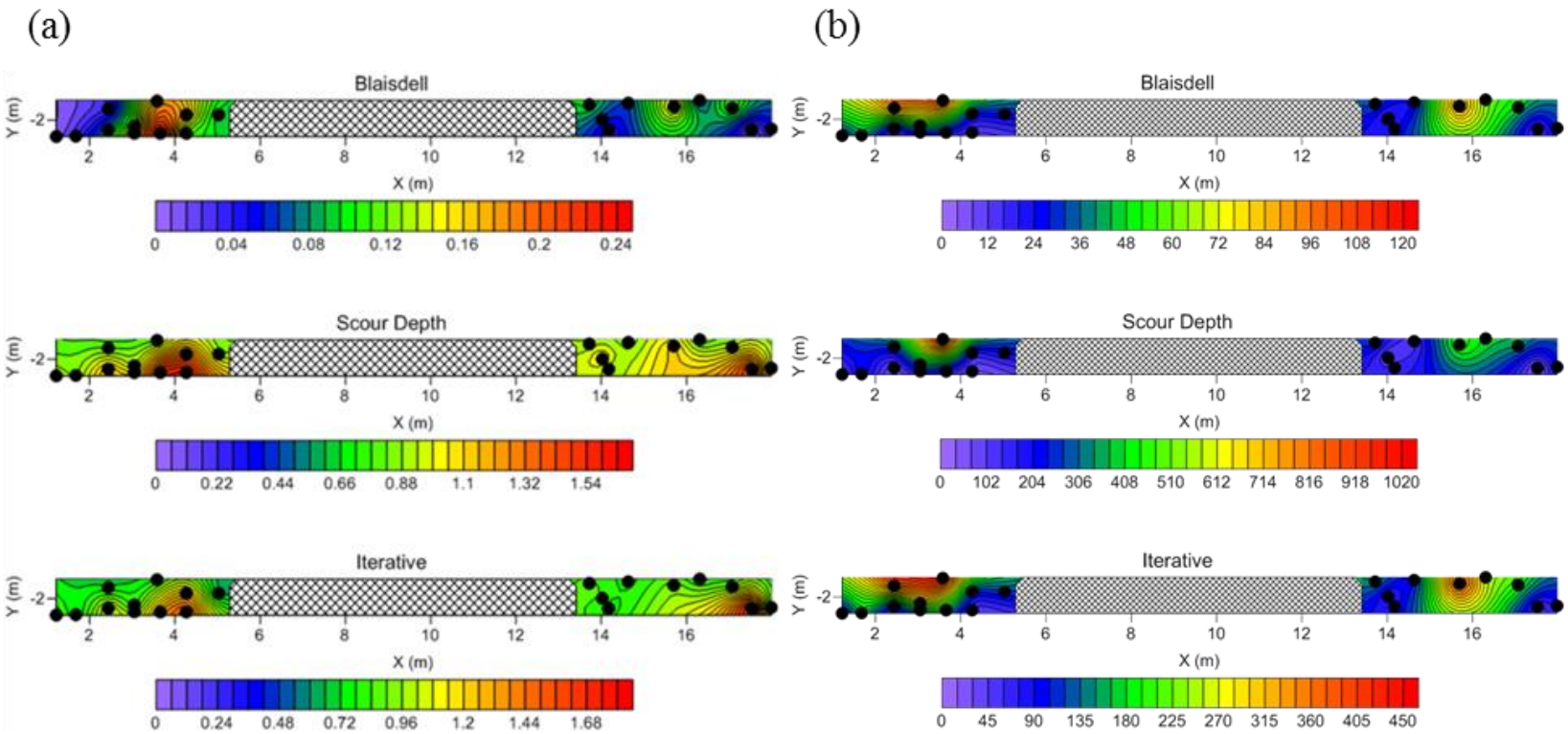

Figure 4.15. Spatial variability at Cow Creek in derived (a) τ_c (Pa) and (b) k_d (cm^3/Ns). JET sample points are indicated as black dots. The hatched area indicates an area of the bank that was heavily vegetated and thus not sampled.

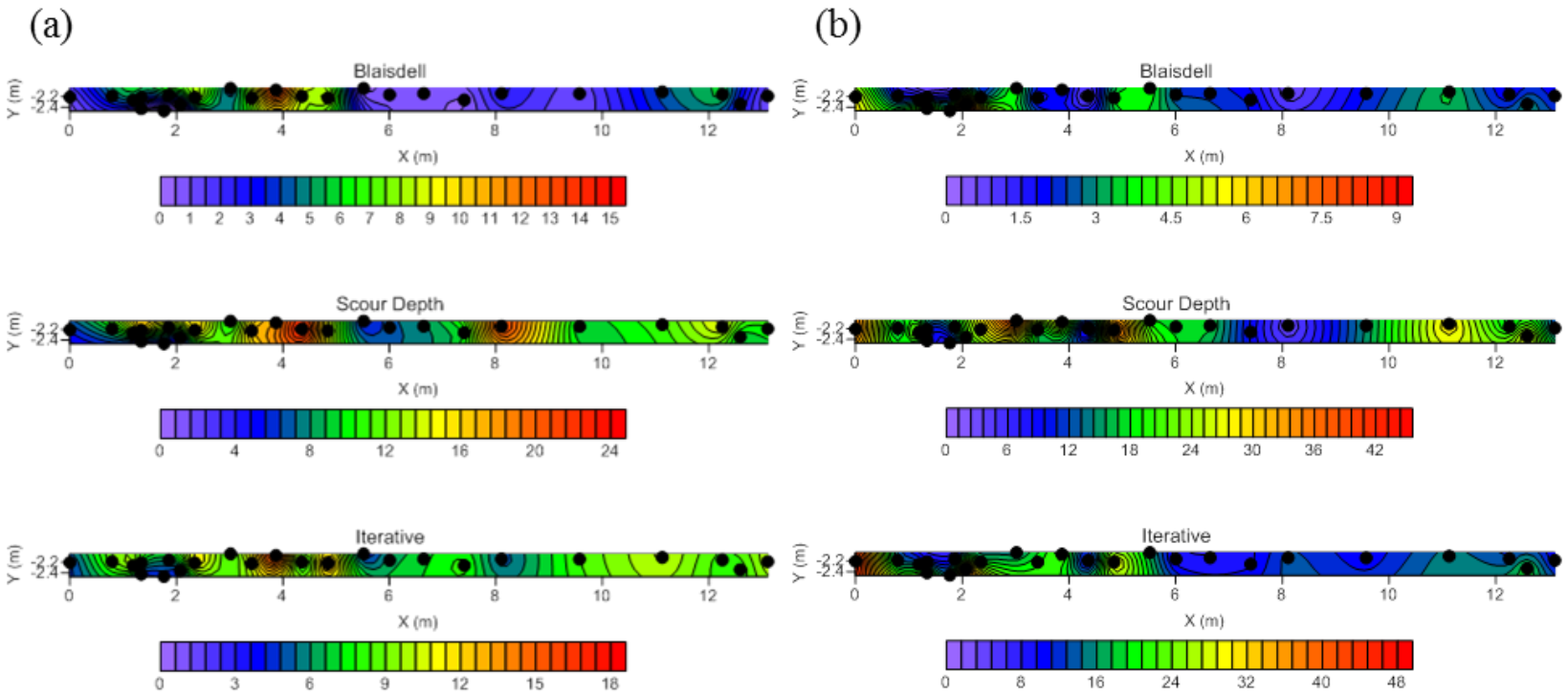

Figure 4.16. Spatial variability at Five Mile Creek in derived (a) τ_c (Pa) and (b) k_d (cm^3/Ns). JET sample points are indicated as black dots.

4.4.4 Evaluating Empirical Relationships

Visualizing the spatial variability of the erodibility parameters and soil textures at each site leads to the suggestion that empirical relationships may provide an improved estimate due to the fact that these relationships are based on a physical soil property and would thus capture the soil heterogeneity. To evaluate this, the *Julian* and *Torres* [2006] relationship based on the silt-clay content of the soil was used to estimate τ_c for each of the sample points at each site. These values were then compared the values obtained using each of the solution techniques using the JET. Likewise, k_d was estimated based on the measured τ_c for each of the sample points at each site using the *Hanson* and *Simon* [2001] and *Simon* et al. [2011] relationships. These values were then compared to those derived from the JET. It is important to note in these analyses that the empirical relationships evaluated in this study were based on the Blaisdell solution derivation of the JET data.

Results from estimating τ_c based on the silt-clay content of the soil using the *Julian* and *Torres* [2006] relationship showed a poor fit to the measured JET data using any of the three solution techniques (Figure 4.17). The *Julian* and *Torres* [2006] relationship generally over-predicted τ_c, which would lead to an underestimation of erosion. It is also important to note that the measured τ_c values spanned three orders of magnitude while the *Julian* and *Torres* [2006] relationship predicted a smaller range of values over a large range of silt-clay contents. The *Julian* and *Torres* [2006] relationship was derived using a range of silt-clay contents of approximately 5 to 95%. The silt-clay contents in this study ranged between 28 and 93%. Even with this large range in silt-clay contents, the *Julian* and *Torres* [2006] relationship predicted a small range in τ_c values.

More research is needed in order to investigate the applicability of such relationships in a wide range of systems.

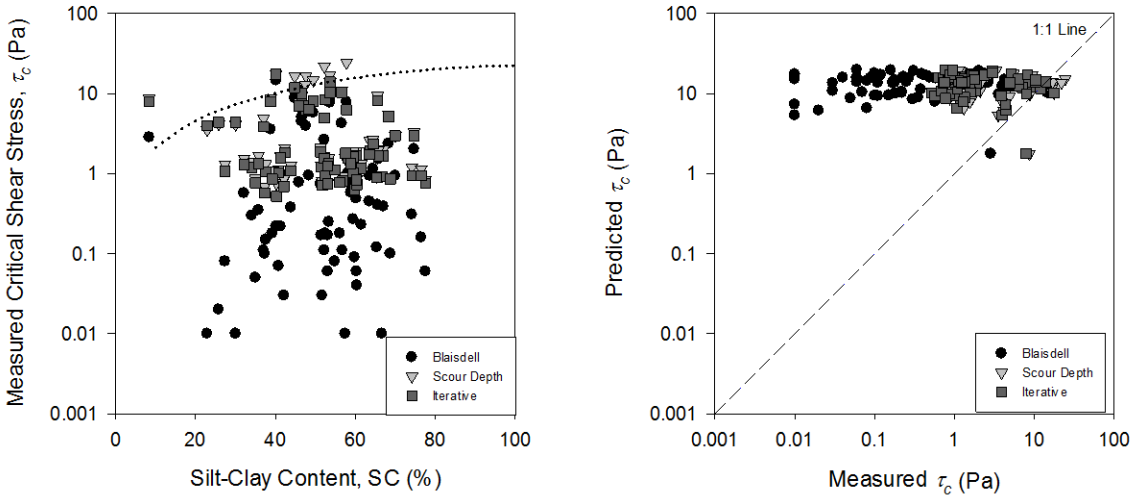

Figure 4.17. Measured τ_c and silt-clay content with the *Julian* and *Torres* [2006] relationship indicated by the dotted line (left), and measured versus predicted τ_c using the *Julian* and *Torres* [2006] relationship (right). Data compiled from all three sites, totaling 74 JETs.

The *Hanson* and *Simon* [2001] and *Simon* et al. [2011] relationships predicting k_d from τ_c were plotted alongside the measured erodibility parameters (Figure 4.18). While there was a similar trend between the measured data using the Blaisdell solution and the *Hanson* and *Simon* [2001] relationship, k_d calculated using the *Hanson* and *Simon* [2001] relationship would have been generally underestimated. This result is similar to that found by *Clark* and *Wynn* [2007] and *Karmaker and Dutta* [2011]. Similarly, there was a comparable trend between the measured data using the scour depth and iterative solutions and the *Simon* et al. [2011] relationship, but k_d calculated using the *Simon* et al. [2011] relationship would have been underestimated as well. Erosion rate predictions would consequently have been underestimated as well using either solution technique or relationship. The updated *Simon* et al. [2011] relationship was a better predictor of k_d

based on τ_c for this study although it would have still resulted in underestimation of the parameters.

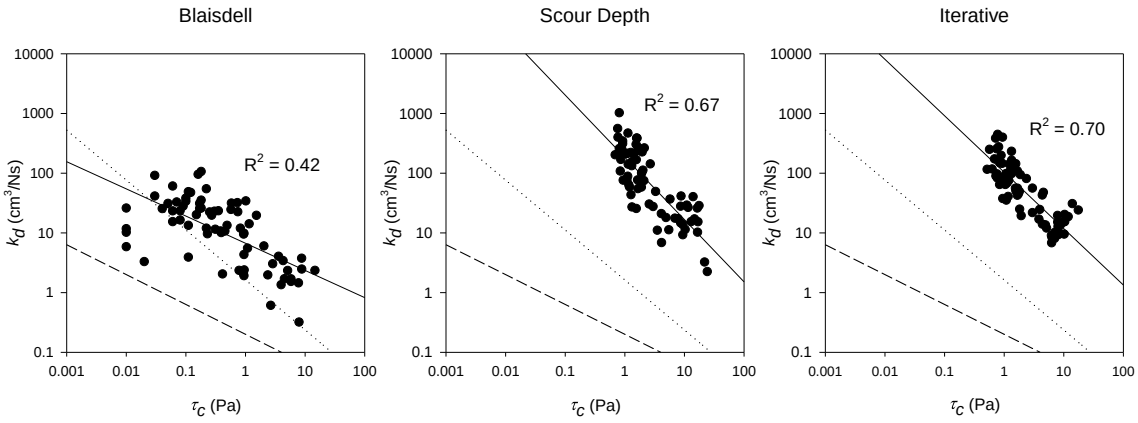

Figure 4.18. Coefficient of determination (R^2) between k_d and τ_c for each solution technique from 74 JETs (circles) compiled from all three sites (Barren Fork Creek, Cow Creek, and Five Mile Creek) and comparison to previously proposed relationships by *Hanson* and *Simon* [2001] (dashed line) and *Simon* et al. [2011] (dotted line).

In order to compare the precision achieved using one of these empirical relationships to estimate the erodibility parameters to that achieved measuring the parameters using the JET, the margins of error (Δ or P) were calculated for each solution technique. The margins of error and the resulting estimation ranges were compared to those calculated using the JET for the specified sample size for both a normal (Table 4.6 and 4.8) and log-normal (Table 4.7 and 4.9) distribution assumption. Considering first the case of a normal distribution assumption, the margins of error and ranges of values are not comparable between the JET and empirical relationships. The *Julian* and *Torres* [2006] relationship produces a range of τ_c within two orders of magnitude of the measured value, but using this estimate would cause large overestimations of the soil resistance and, consequently, a large under prediction of erosion rates. The smaller ranges of the k_d values between the JET and empirical relationships is largely an artifact of the τ_c

value input into the empirical relationships. The *Hanson* and *Simon* [2001] and *Simon* et al. [2011] relationships estimate k_d from a value of τ_c. The ranges reported in Tables 4.6 through 4.9 for these relationships use the JET measured τ_c as input to estimate k_d. If an empirical estimate of k_d was input into these relationships to estimate τ_c, which is often the case, the margins of error would be much greater. Under the assumption of normality, a user would be able to estimate τ_c within two orders of magnitude and k_d would be compounded by this error using the empirical relationships explored in this study. With this in mind, there exists a major advantage to measuring the parameters *in situ* as the empirical relationships generally would over predict the parameters.

Table 4.6. Amount of precision achieved using various methods assuming parameters follow a normal distribution. Calculations are shown for a 95% confidence level (Z = 1.96) and a sample size, n = 3. Blaisdell solution ($\tau_{c\text{-}BL}$, $k_{d\text{-}BL}$), scour depth solution ($\tau_{c\text{-}SD}$, $k_{d\text{-}SD}$), and iterative solution ($\tau_{c\text{-}IT}$, $k_{d\text{-}IT}$).

BARREN FORK									
Parameter	**Mean**	*JET*		*Julian and Torres (2006)*		*Hanson and Simon (2001)*		*Simon et al. (2010)*	
		Δ	Range	Δ	Range	Δ	Range	Δ	Range
$\tau_{c\text{-}BL}$ (Pa)	0.62	0.64	0.0 – 1.3	15	0 - 16				
$\tau_{c\text{-}SD}$ (Pa)	1.82	1.04	0.8 – 2.9	14	0 - 16				
$\tau_{c\text{-}IT}$ (Pa)	1.59	1.00	0.6 – 2.6	14	0 - 16				
$k_{d\text{-}BL}$ (cm^3/Ns)	20	13.7	6.4 - 34			22	0 - 42	18	2 - 38
$k_{d\text{-}SD}$ (cm^3/Ns)	163	146	17 - 309			185	0 - 348	184	0 - 347
$k_{d\text{-}IT}$ (cm^3/Ns)	85.2	65.4	20 - 151			96	0 - 181	95	0 - 180
COW CREEK									
Parameter	**Mean**	*JET*				*Hanson and Simon (2001)*		*Simon et al. (2010)*	
		Δ	Range	Δ	Range	Δ	Range	Δ	Range
$\tau_{c\text{-}BL}$ (Pa)	0.1	0.07	0.0 – 0.2	17	0 - 17				
$\tau_{c\text{-}SD}$ (Pa)	1.05	0.31	0.7 – 1.4	16	0 - 17				
$\tau_{c\text{-}IT}$ (Pa)	0.95	0.35	0.6 – 1.3	16	0 - 17				
$k_{d\text{-}BL}$ (cm^3/Ns)	39.5	31.9	7.6 – 71			44	0 - 83	31	8 - 71
$k_{d\text{-}SD}$ (cm^3/Ns)	245	248	0.0 – 493			277	0 - 522	275	0 - 520
$k_{d\text{-}IT}$ (cm^3/Ns)	170	138	32 – 308			192	0 - 362	192	0 - 362
FIVE MILE									
Parameter	**Mean**	*JET*				*Hanson and Simon (2001)*		*Simon et al. (2010)*	
		Δ	Range	Δ	Range	Δ	Range	Δ	Range
$\tau_{c\text{-}BL}$ (Pa)	3.81	4.22	0.0 – 8.0	9.1	0 - 13				
$\tau_{c\text{-}SD}$ (Pa)	11.3	6.34	4.9 – 18	3.8	7 - 15				
$\tau_{c\text{-}IT}$ (Pa)	8.03	3.77	4.3 – 12	5.3	3 - 13				
$k_{d\text{-}BL}$ (cm^3/Ns)	2.9	2.33	0.6 – 5.2			2.9	0 - 6	26	0 - 29
$k_{d\text{-}SD}$ (cm^3/Ns)	19.2	12.2	6.9 – 31			22	0 - 41	21	0 - 41
$k_{d\text{-}IT}$ (cm^3/Ns)	17.3	11.8	5.5 – 29			20	0 - 37	19	0 - 37

Table 4.7. Amount of precision achieved using various methods assuming parameters follow a log-normal distribution. Calculations are shown for a 95% confidence level (Z = 1.96) and a sample size, n = 3. Blaisdell solution ($\tau_{c\text{-}BL}$, $k_{d\text{-}BL}$), scour depth solution ($\tau_{c\text{-}SD}$, $k_{d\text{-}SD}$), and iterative solution ($\tau_{c\text{-}IT}$, $k_{d\text{-}IT}$).

BARREN FORK									
Parameter	**Mean**	*JET*		*Julian and Torres (2006)*		*Hanson and Simon (2001)*		*Simon et al. (2010)*	
		P	Range	*P*	Range	*P*	Range	*P*	Range
$\tau_{c\text{-}BL}$ (Pa)	0.62	182%	0.0 – 1.8	>> 10,000%	0 - 3E6				
$\tau_{c\text{-}SD}$ (Pa)	1.82	61%	0.7 – 3.0	>> 10,000%	0 - 2E6				
$\tau_{c\text{-}IT}$ (Pa)	1.59	69%	0.5 – 2.7	>> 10,000%	0 - 3E6				
$k_{d\text{-}BL}$ (cm^3/Ns)	20	125%	0.0 – 45			>> 10,000%	0 - 10E10	>> 10,000%	0 - 2E9
$k_{d\text{-}SD}$ (cm^3/Ns)	163	188%	0.0 – 470			>> 10,000%	0 - 3E82	>> 10,000%	0 - 8E81
$k_{d\text{-}IT}$ (cm^3/Ns)	85.2	127%	0.0 – 193			>> 10,000%	0 - 5E43	>> 10,000%	0 - 1E43
COW CREEK									
Parameter	**Mean**	*JET*				*Hanson and Simon (2001)*		*Simon et al. (2010)*	
		P	Range	*P*	Range	*P*	Range	*P*	Range
$\tau_{c\text{-}BL}$ (Pa)	0.1	176%	0.0 – 0.3	>> 10,000%	0 - 3E6				
$\tau_{c\text{-}SD}$ (Pa)	1.05	31%	0.7 – 1.4	>> 10,000%	0 - 1E7				
$\tau_{c\text{-}IT}$ (Pa)	0.95	37%	0.6 – 1.3	>> 10,000%	0 - 1E7				
$k_{d\text{-}BL}$ (cm^3/Ns)	39.5	106%	0.0 – 81			>> 10,000%	0 - 4E20	>> 10,000%	0 - 2E15
$k_{d\text{-}SD}$ (cm^3/Ns)	245	157%	0.0 – 628			>> 10,000%	0 - 4E122	>> 10,000%	0 - 8E121
$k_{d\text{-}IT}$ (cm^3/Ns)	170	115%	0.0 – 367			>> 10,000%	0 - 6E85	>> 10,000%	0 - 3E85
FIVE MILE									
Parameter	**Mean**	*JET*				*Hanson and Simon (2001)*		*Simon et al. (2010)*	
		P	Range	*P*	Range	*P*	Range	*P*	Range
$\tau_{c\text{-}BL}$ (Pa)	3.81	1023%	0.0 – 43	>> 10,000%	0 - 3E4				
$\tau_{c\text{-}SD}$ (Pa)	11.3	83%	1.9 – 21	4,484%	0 - 5E2				
$\tau_{c\text{-}IT}$ (Pa)	8.03	58%	3.4 – 13	>> 10,000%	0 - 2E3				
$k_{d\text{-}BL}$ (cm^3/Ns)	2.9	123%	0.0 – 6.5			1,799%	0 - 6E1	>> 10,000%	0 - 6E11
$k_{d\text{-}SD}$ (cm^3/Ns)	19.2	126%	0.0 – 43			>> 10,000%	0 - 5E10	>> 10,000%	0 - 4E10
$k_{d\text{-}IT}$ (cm^3/Ns)	17.3	79%	3.7 – 31			>> 10,000%	0 - 5E9	>> 10,000%	0 - 4E9

Table 4.8. Amount of precision achieved using various methods assuming parameters follow a log-normal distribution. Calculations are shown for a 95% confidence level (Z = 1.96) and a sample size, n = 3. Blaisdell solution ($\tau_{c\text{-}BL}$, $k_{d\text{-}BL}$), scour depth solution ($\tau_{c\text{-}SD}$, $k_{d\text{-}SD}$), and iterative solution ($\tau_{c\text{-}IT}$, $k_{d\text{-}IT}$).

BARREN FORK									
Parameter	**Mean**	*JET*		*Julian and Torres (2006)*		*Hanson and Simon (2001)*		*Simon et al. (2010)*	
		Δ	Range	Δ	Range	Δ	Range	Δ	Range
$\tau_{c\text{-}BL}$ (Pa)	0.62	0.49	0.1 – 1.1	12	0 - 13				
$\tau_{c\text{-}SD}$ (Pa)	1.82	0.81	1.0 – 2.6	11	0 - 13				
$\tau_{c\text{-}IT}$ (Pa)	1.59	0.78	0.8 – 2.4	11	0 - 13				
$k_{d\text{-}BL}$ (cm^3/Ns)	20	10.6	9.4 – 31			17	3 - 38	14	6 - 34
$k_{d\text{-}SD}$ (cm^3/Ns)	163	113	50 – 276			143	20 - 306	142	21 - 305
$k_{d\text{-}IT}$ (cm^3/Ns)	85.2	50.6	35 – 136			75	11 - 160	74	12 - 159
COW CREEK									
Parameter	**Mean**	*JET*				*Hanson and Simon (2001)*		*Simon et al. (2010)*	
		Δ	Range	Δ	Range	Δ	Range	Δ	Range
$\tau_{c\text{-}BL}$ (Pa)	0.1	0.06	0.0 – 0.2	13	0 - 13				
$\tau_{c\text{-}SD}$ (Pa)	1.05	0.24	0.8 – 1.3	12	0 - 14				
$\tau_{c\text{-}IT}$ (Pa)	0.95	0.27	0.7 – 1.2	13	0 - 14				
$k_{d\text{-}BL}$ (cm^3/Ns)	39.5	24.7	15 – 64			34	6 - 73	24	15 - 64
$k_{d\text{-}SD}$ (cm^3/Ns)	245	192	53 – 437			214	31 - 460	213	32 - 458
$k_{d\text{-}IT}$ (cm^3/Ns)	170	107	63 – 277			149	21 - 319	149	21 - 319
FIVE MILE									
Parameter	**Mean**	*JET*				*Hanson and Simon (2001)*		*Simon et al. (2010)*	
		Δ	Range	Δ	Range	Δ	Range	Δ	Range
$\tau_{c\text{-}BL}$ (Pa)	3.81	3.27	0.5 – 7.1	7.0	0 - 11				
$\tau_{c\text{-}SD}$ (Pa)	11.3	4.91	6.4 – 16	3.0	8 - 14				
$\tau_{c\text{-}IT}$ (Pa)	8.03	2.92	5.1 – 11	4.1	4 - 12				
$k_{d\text{-}BL}$ (cm^3/Ns)	2.9	1.8	1.1 – 4.7			2.3	0.6 - 5	20	0 - 23
$k_{d\text{-}SD}$ (cm^3/Ns)	19.2	9.48	9.7 – 29			17	2 - 36	17	3 - 36
$k_{d\text{-}IT}$ (cm^3/Ns)	17.3	9.16	8.2 – 26			15	2 - 32	15	2 - 32

Table 4.9. Amount of precision achieved using various methods assuming parameters follow a log-normal distribution. Calculations are shown for a 95% confidence level (Z = 1.96) and a sample size, n = 3. Blaisdell solution ($\tau_{c\text{-}BL}$, $k_{d\text{-}BL}$), scour depth solution ($\tau_{c\text{-}SD}$, $k_{d\text{-}SD}$), and iterative solution ($\tau_{c\text{-}IT}$, $k_{d\text{-}IT}$).

BARREN FORK									
Parameter	**Mean**	*JET*		*Julian and Torres (2006)*		*Hanson and Simon (2001)*		*Simon et al. (2010)*	
		P	Range	*P*	Range	*P*	Range	*P*	Range
$\tau_{c\text{-}BL}$ (Pa)	0.62	123%	0.0 – 1.4	>> 10,000%	0 - 9E4				
$\tau_{c\text{-}SD}$ (Pa)	1.82	45%	1.0 – 2.6	>> 10,000%	0 - 1E5				
$\tau_{c\text{-}IT}$ (Pa)	1.59	50%	0.8 – 2.4	>> 10,000%	0 - 1E5				
$k_{d\text{-}BL}$ (cm^3/Ns)	20	87%	2.5 – 38			>> 10,000%	0 - 6E8	>> 10,000%	0 - 3E7
$k_{d\text{-}SD}$ (cm^3/Ns)	163	127%	0.0 – 370			>> 10,000%	0 - 2E64	>> 10,000%	0 - 9E63
$k_{d\text{-}IT}$ (cm^3/Ns)	85.2	89%	9.6 – 161			>> 10,000%	0 - 2E34	>> 10,000%	0 - 7E33
COW CREEK									
Parameter	**Mean**	*JET*				*Hanson and Simon (2001)*		*Simon et al. (2010)*	
		P	Range	*P*	Range	*P*	Range	*P*	Range
$\tau_{c\text{-}BL}$ (Pa)	0.1	120%	0.0 – 0.2	>> 10,000%	0 - 6E4				
$\tau_{c\text{-}SD}$ (Pa)	1.05	23%	0.8 – 1.3	>> 10,000%	0 - 3E5				
$\tau_{c\text{-}IT}$ (Pa)	0.95	28%	0.6 – 1.2	>> 10,000%	0 - 3E5				
$k_{d\text{-}BL}$ (cm^3/Ns)	39.5	75%	9.8 – 69			>> 10,000%	0 - 2E16	>> 10,000%	0 - 1E12
$k_{d\text{-}SD}$ (cm^3/Ns)	245	107%	0.0 – 508			>> 10,000%	0 - 3E95	>> 10,000%	0 - 9E94
$k_{d\text{-}IT}$ (cm^3/Ns)	170	81%	32 – 308			>> 10,000%	0 - 9E66	>> 10,000%	0 - 5E66
FIVE MILE									
Parameter	**Mean**	*JET*				*Hanson and Simon (2001)*		*Simon et al. (2010)*	
		P	Range	*P*	Range	*P*	Range	*P*	Range
$\tau_{c\text{-}BL}$ (Pa)	3.81	551%	0.0 – 25	>> 10,000%	0 - 4E3				
$\tau_{c\text{-}SD}$ (Pa)	11.3	60%	4.5 – 18	1,835%	0 - 2E2				
$\tau_{c\text{-}IT}$ (Pa)	8.03	42%	4.6 – 11	5,924%	0 - 2E2				
$k_{d\text{-}BL}$ (cm^3/Ns)	2.9	86%	0.4 – 5.4			878%	0 - 3E1	>> 10,000%	0 - 2E9
$k_{d\text{-}SD}$ (cm^3/Ns)	19.2	88%	2.3 – 36			>> 10,000%	0 - 4E8	>> 10,000%	0 - 3E8
$k_{d\text{-}IT}$ (cm^3/Ns)	17.3	57%	7.5 – 27			>> 10,000%	0 - 6E7	>> 10,000%	0 - 5E7

When considering the case of a log-normal distribution assumption, a more reasonable assumption (Table 4.2), there is an even greater difference in the precision achieved using the JET and empirical relationships. Compared to the error expected when measuring the parameters with the JET, the empirical relationships provide an unreasonable range for both k_d and τ_c. The margins of error and ranges provided by the empirical relationships produce estimates that are no more beneficial than choosing a value at random. Under the assumption of a log-normal distribution, it is clear that measuring the erodibility parameters *in situ* is necessary in order to utilize a reasonable estimate in modeling applications.

4.5 Conclusions

Determining the sample size required to accurately estimate erodibility parameters derived from the JET depends on the solution technique, the parameter being estimated, the desired degrees of precision and confidence, and the presence of spatial dependency. In general, the iterative and scour depth methods may require more samples than the Blaisdell solution for the equivalent amount of precision and confidence due to the larger variance in parameter values. Estimating k_d, regardless of solution technique, requires more samples than would be needed for estimating τ_c with the same amount of precision and confidence due to the larger magnitude and range in values. The amount of precision needed for both of these variables may be different. Understanding the variability in these parameters and the amount of precision necessary is a major gap in this field of work at the current time. The presence of spatial dependency should be taken into account in order to properly estimate the minimum number of samples needed to properly characterize the erodibility of a bank. The current data set, with the limited

analysis, does not support a strong spatial dependency with the erodibility parameters. This study highlights the need for conducting *in situ* measurements of the erodibility parameters rather than relying on commonly used empirical relationships. The JET is able to provide parameter estimates with much smaller margins of error. Utilizing current practices of conducting three to five JETs per soil layer at a site is generally able to provide users with a one order of magnitude estimate of the erodibility parameters. Assuming a log-normal distribution for the parameters, the empirical relationships analyzed in this study produced unreasonable margins of error. This exemplifies the need to conduct *in situ* measurements using the JET in order to acquire reasonable estimates of the soil resistance to fluvial erosion.

4.6 Acknowledgements

Data used in this project is available upon request from the author. The authors acknowledge the financial support of the Buchanan Family Trust through the Buchanan Endowed Chair at Oklahoma State University. This project was also supported by Agriculture and Food Research Initiative Competitive Grant no. 2013-51130-21484 from the USDA National Institute of Food and Agriculture and through a FY 2012 319(h) Special Project #C9-00F56701.

CHAPTER 5

CORRELATING ERODIBILITY PARAMETERS FROM JET EROSION TESTS TO SOIL PROPERTIES ON A SITE SCALE

5.1 Abstract

One of the most commonly used methods of measuring erodibility parameters (critical shear stress, τ_c, and erodibility coefficient, k_d) of cohesive soils in situ is the Jet Erosion Test (JET). There are many factors that can influence the erodibility of cohesive soils, but the influence of these factors is not captured by conducting one or a few JETs at one discrete point in time and at one location on the streambank. Current practice in streambank erosion modeling largely ignores the parameter, spatial, and temporal relationships with erodibility. Furthermore, in many cases the erodibility parameters are not characterized in situ, but estimated empirically with relationships that may not be good predictors for all streambanks. The objectives of this study were to build upon previous research studies and further address the variability in the erodibility parameters across a range of soil erodibility as derived from JETs at a site scale with respect to soil parameter correlations, temporal variability, spatial variability, and testing variability. A total of 74 JETs were conducted within visually homogeneous streambank layers at three sites in Oklahoma along with measurements of soil physical parameters such as texture, bulk density, and moisture content. At the site scale τ_c and k_d varied by up to three orders

of magnitude. While there were correlations between the erodibility parameters and measured soil variables, there were no reliable relationships with strong predictive capabilities at any of the sites for any of the variables. Also, there were no significant multiple linear regressions to predict τ_c and k_d based on more than one soil parameter. Erodibility parameters measured in this study could not be predicted based on existing, widely used empirical models. It was concluded that τ_c and k_d must be measured in situ and cannot be estimated from empirical relationships due to the heterogeneous nature of soil and the variability in subaerial processes even within visually homogeneous streambank layers. More research is needed in order to quantify the role of subaerial processes on erodibility in order to incorporate temporal and spatial variation in the erodibility into stability and channel evolution models.

5.2 Introduction

Streambank erosion is known to be a significant source of sediment and nutrients in many impaired streams (Simon et al., 2000; Wilson et al., 2008; Fox and Wilson, 2010; Miller et al., 2014). Predicting the detachment of cohesive soils has remained difficult despite the large amount of research on the subject. The complex interactions that govern cohesive soil erosion have made it problematic to estimate erodibility parameters to predict detachment rates.

In general, streambank erosion can be attributed to three primary mechanisms: mass failure, fluvial erosion, and subaerial processes (Couper and Maddock, 2001; Couper 2003). Mass failures are episodic in nature and occur when there is a force imbalance. Fluvial erosion is a continuous process when shear stresses exceed the soil's critical shear stress and is caused by the shearing of particles by the water flow. Subaerial

erosion is climate related and occurs when there is a reduction in soil strength due to subaerial processes that induce direct erosion or make the bank more susceptible to erosion. There is strong interaction between each of these three mechanisms, but they can also be simplified into a series process. Subaerial erosion is commonly thought of as a preparatory process that weakens the bank making it more susceptible to fluvial erosion, and then fluvial erosion may undercut the bank or scour the bed to create streambank instability and cause mass failures (Fox and Wilson, 2010; Midgley et al., 2012).

Particle detachment models are often employed to predict rates of streambank erosion due to fluvial processes within a basin. Commonly, the erosion rate of cohesive streambanks is simulated using the excess shear stress equation (Partheniades, 1965; Hanson, 1990a, 1990b), which is defined as:

$$\varepsilon_r = k_d(\tau - \tau_c)^a \tag{5.1}$$

where ε_r is the erosion rate (cm s^{-1}), k_d is the erodibility coefficient (cm^3 N^{-1} s^{-1}), τ is the average hydraulic boundary shear stress (Pa), τ_c is the critical shear stress (Pa), and a is an empirical exponent commonly assumed to be unity (Hanson, 1990a, 1990b; Hanson and Cook, 2004). Using this model, erosion initiates once τ exceeds τ_c, and k_d defines the rate at which particles are detached after erosion is initiated.

One of the most commonly used methods of measuring the erodibility parameters, τ_c and k_d, is the Jet Erosion Test (JET). The submerged JET was developed for measuring these parameters *in situ* as well as in the laboratory (Hanson, 1990b; Hanson and Cook, 1997; Hanson and Simon, 2001). The JET device consists of an impinging jet connected to a constant water source, a tank that serves to both hold the JET in position and to submerge the test soil and jet, and a point gauge to measure the

depth of scour produced by the jet. A detailed description of the JET and the testing methodology has been presented by numerous studies (Hanson and Cook, 1997; Hanson and Simon, 2001; Al-Madhhachi et al., 2013a).

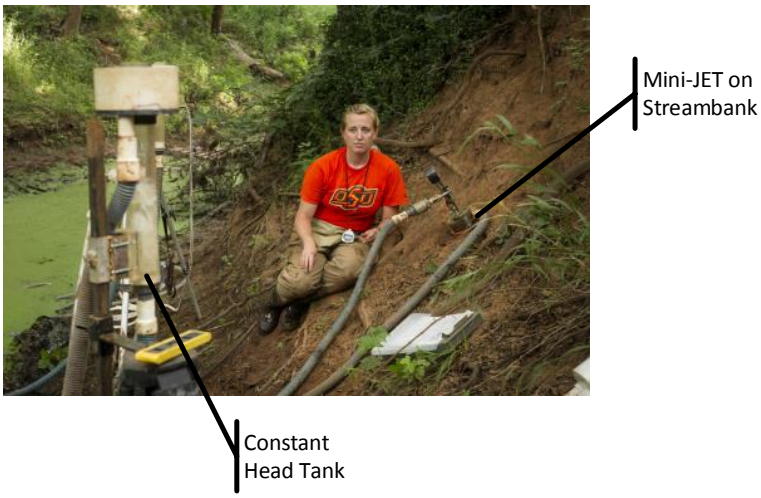

Figure 5.1. Location of Five Mile Creek, Cow Creek, and Barren Fork Creek in Oklahoma as sites chosen for variability studies (top). Pictures of banks sampled (bottom) at Five Mile Creek (left), Cow Creek (middle), and Barren Fork Creek (right) sites.

Hanson and Cook (1997) and Hanson et al. (2002) developed the analytical methods to directly estimate k_d and τ_c based on diffusion principles using an Excel spreadsheet routine. The analytical methods were based on diffusion principles developed by Stein and Nett (1997). The rate of variation in the depth of scour was assumed to be the erosion rate as a function of the maximum stress at the boundary. The maximum τ was based on determining the diameter of the jet nozzle and the distance from the jet origin to the initial cohesive soil surface. Accordingly, τ_c was assumed to occur when the rate of scour was equal to zero at the equilibrium depth. Blaisdell et al. (1981) developed a hyperbolic function for predicting the equilibrium depth, which was used in the spreadsheet to calculate τ_c. The k_d was then determined depending on the measured scour depth, time, predetermined τ_c, and a dimensionless time function (Hanson et al., 2002).

Recently, two alternative solution techniques have been proposed to estimate the erodibility parameters from the JET. Simon et al. (2010) has proposed the iterative solution which iteratively solves for τ_c and k_d based on the dimensionless time (T^*) and dimensionless scour depth (J^*). The iterative solution is confined by an upper bound on τ_c to prevent the solution from exceeding the equilibrium scour depth. Daly et al. (2013) has proposed another solution technique that iteratively solves for τ_c and k_d to fit to the observed scour depth data to minimize the sum of squared errors between the measured scour data and the solution of the excess shear stress equation. Both the iterative solution and the scour depth solution have shown improved fits over the Blaisdell solution to the observed data; however, the two new solution techniques have had limited testing and analysis. There has been limited comparison of the three solver routines and the three sets of erodibility parameters derived by these routines. All three solution techniques have been incorporated into an automated spreadsheet routine to solve for the erodibility parameters using JET data (Daly et al., 2013).

There has been discussion recently on the validity of the JET and the sensitivity of results to differences in operation (Simon et al., 2010; Charonko and Wynn, 2010; Mercier et al., 2014). Due to the complexity of cohesive soil erosion, there were questions concerning whether or not the simplified model used by the JET was accurately predicting the erodibility parameters. Mercier et al. (2014) conducted computational fluid dynamic simulations and concluded that the model of Hanson and Cook (2004) to interpret JET results was relevant. With the theory behind the JET substantiated, discussion has focused on the operation of the JET. Many studies have reported large amounts of variability in the derived parameters (Hanson and Simon, 2001; Wynn and

Mostaghimi, 2006). In order to determine if the variability was due to natural soil variability or errors in the test operation or device, Charonko and Wynn (2010) studied the variability in both lab and field scale studies. They found the variability to be significantly smaller in lab performed JETs and concluded the JET technique to be reliable with variability being attributed to soil heterogeneity and subaerial processes.

These studies have verified the use of the JET to estimate the erodibility parameters; however, Simon et al. (2010) has also pointed out that uncertainty and variability in JET results may also be dependent on the length of time the test is conducted. Using data from hundreds of JETs, Simon et al. (2010) found that the dimensionless time reached at the end of the test (T*) was highly variable sugesting that the results of the JET test are sensitive to the length of time the test is performed. Therefore, Simon et al. (2010) expanded on the iterative solution by suggesting a T* filter to check the validity of test data. Simon states that larger values of T^* correspond to increased reliability of the Blaisdell curve fitting methodology as it indicates that the length of time the test was run has neared the theoretical time need to reach the equilibrium scour depth. Using the same data set of hundreds of JETs, Simon found a T^* of 0.25 to be the optimum cutoff value. Simon's data sets show less spread in the data and an increased r2 value for the τ_c - k_d relationship when the T^* filter of 0.25 is applied.

Predicting cohesive streambank erosion has remained difficult, although there is a large amount of research on the topic (Smerdon and Beasley, 1961; Julian and Torres, 2006; Clark and Wynn, 2007; Utley and Wynn, 2008). The complex interactions that govern cohesive soil erosion have made it problematic to estimate the erodibility parameters. There are many factors that can influence the erodibility of cohesive soils

such as soil texture, structure, unit weight, and water content (Grabowski et al., 2011). The influence of these factors is not captured by conducting a JET at one discrete point in time and at one discrete location on the streambank. This variability in fluvial erosion parameters, τ_c and k_d, as a function of soil parameters leads to subaerial erosion as a preparatory process to systematically weaken the bank and make it more susceptible to fluvial erosion due to its impact on the governing parameters.

Subaerial processes leading directly or indirectly to erosion focus on the soil moisture conditions and can include the wetting and drying of the soil, desiccation, and freeze-thaw activity (Couper and Maddock, 2001). All of these processes can weaken the bank surface causing an increase in the efficacy of fluvial erosion. Also, cohesive banks are typically poorly drained due to their high percentages of *SL* and *CL* which can lead to excess pore water pressures and, consequently, increased subaerial erosion (Julian and Torres, 2006). Banks with high *CL* may also be more susceptible to desiccation cracking and slaking which also leads to increased subaerial erosion.

It has been recognized that subaerial erosion may be significant in predicting streambank erosion, especially in unison with fluvial erosion; however, there is little research supporting field investigations of subaerial erosion and correlating these effects to changes in τ_c and k_d. While many studies have investigated the influence of soil parameters in a laboratory setting, fewer studies have performed intensive testing in the field that encompasses the effects of subaerial processes. The effects of subaerial processes can be more broadly described with its dependency on three components: soil variability, temporal, and spatial. Soil variability encompasses the heterogeneity of parameters such as soil type, mineralogy, bulk density, or moisture content that may

dictate subaerial erosion effects. Temporal dependency encompasses the effects of changes in parameters such as vegetative cover, bank angle, or temperature that change over time and effect wetting/drying and freeze/thaw cycles. Finally, the spatial dependency encompasses the first two components where variations in soil parameters and temporal changes cause spatial variations as well.

Clark and Wynn (2007) studied overall variability, without isolating a particular streambank layer, by conducting 142 JETs across 25 sites in southwest Virginia. They compared the JET results to the parameters estimated from empirical relationships. Their study reported a large amount of variability and a poor agreement between the measured and empirically estimated parameters. They concluded that the parameters may be influenced by multiple soil properties, not just a single dependent parameter, and that k_d and τ_c are site-specific and should be measured in situ. Wynn and Mostaghimi (2008) studied parameter variability on vegetated streambanks and found bulk density to be the most significant parameter for determining k_d and τ_c. They concluded that bulk density was likely an important factor due to it being a function of multiple other soil properties such as soil texture, organic matter content, and root density. Thoman and Niezgoda (2008) also looked at correlations between k_d and τ_c and soil parameters and found activity, dispersion ratio, soil pH, percent organics, and cation exchange capacity to be significantly correlated to τ_c; however, none were sufficient in explaining τ_c with a linear regression. They did conclude, however, that a significant relationship between the erodibility parameters and cohesive soil properties could be developed for specific regions.

Moving beyond the straight correlation with soil variability, Wynn et al. (2008) sought to estimate the temporal variability by conducting monthly JETs over the course of a year on a streambank. They found that streambank kd and τ_c varied significantly monthly and seasonally. They noted temporal changes in both parameters and correlations with the number of freeze-thaw cycles occurring between measurements. This strengthens the evidence of subaerial erosion having a significant impact on soil erodibility.

Couper (2003) investigated the spatial variability of erodibility parameters by conducting a laboratory study mimicking subaerial processes that would be seen in the field. The study found that streambanks with high silt-clay content were most susceptible to erosion or weakening by subaerial processes due to the swelling/shrinking that can occur with wetting/drying and freeze/thaw cycles. With respect to a spatial correlation, the study concluded that a "vertical zoning" of bank erosion occurs with subaerial processes acting on the upper bank and fluvial processes acting on the lower bank.

Current practice in streambank erosion modeling largely ignores the parameter, spatial, and temporal relationships with erodibility. Current models assume that soil erodibility remains constant temporally. Many models can incorporate various bank layers to take into account spatial variability, however these are usually layered by changing soil type with the assumption that a certain soil type will behave uniformly with respect to erodibility. This lack in the temporal and spatial variability of streambanks often results in intensive calibration processes or the use of lumped calibration factors that skew the erodibility parameters. Furthermore, in many cases the erodibility parameters are not characterized in situ, but estimated empirically with relationships that

may not be good predictors in unique systems (Clark and Wynn, 2006). With these considerations in mind, the objectives of this study were to address the variability in the erodibility parameters derived from JETs at a site scale with respect to soil parameter correlations, temporal variability, spatial variability, and testing variability. Unique to this study was the selected of a visually homogeneous streambank layer in which approximately 30 JETs were performed. Therefore, JETs conducted within each layer were expected to provide site-specific measurements of erodibility, as opposed to measurements at the watershed scale where greater variability may be expected due to changes in soil type, layering, and subaerial processes (Clark and Wynn, 2007; Daly et al., in review).

5.3 Materials and Methods

5.3.1 Site Descriptions

Three sites were selected for sampling. Sites were chosen from three different regions in Oklahoma and included sites on Barren Fork Creek, Cow Creek, and Five Mile Creek (Figure 2). The Barren Fork Creek, located in northeastern Oklahoma in Cherokee County, is a fourth order stream part of the Illinois River watershed. The watershed covers 4,330 km^2 spanning the northeastern Oklahoma-Arkansas border. Approximately 54% of this basin is located within Oklahoma. The watershed falls within the Ozark Highlands ecoregion, which typically contains streams that are riffle and pool dominated, clear, and have coarse gravel, cobble, or bedrock substrates. Banks are typically composite and include a silty loam top layer with an unconsolidated gravel bottom layer and toe (Fox et al., 2011; Midgley et al., 2012). The dominating land uses in the basin are forest and hay production or pasture with the major agricultural industry being poultry

and cattle (OCC, 2010). The streambanks at this site had little vegetation, but there were roots present especially towards the top of the bank.

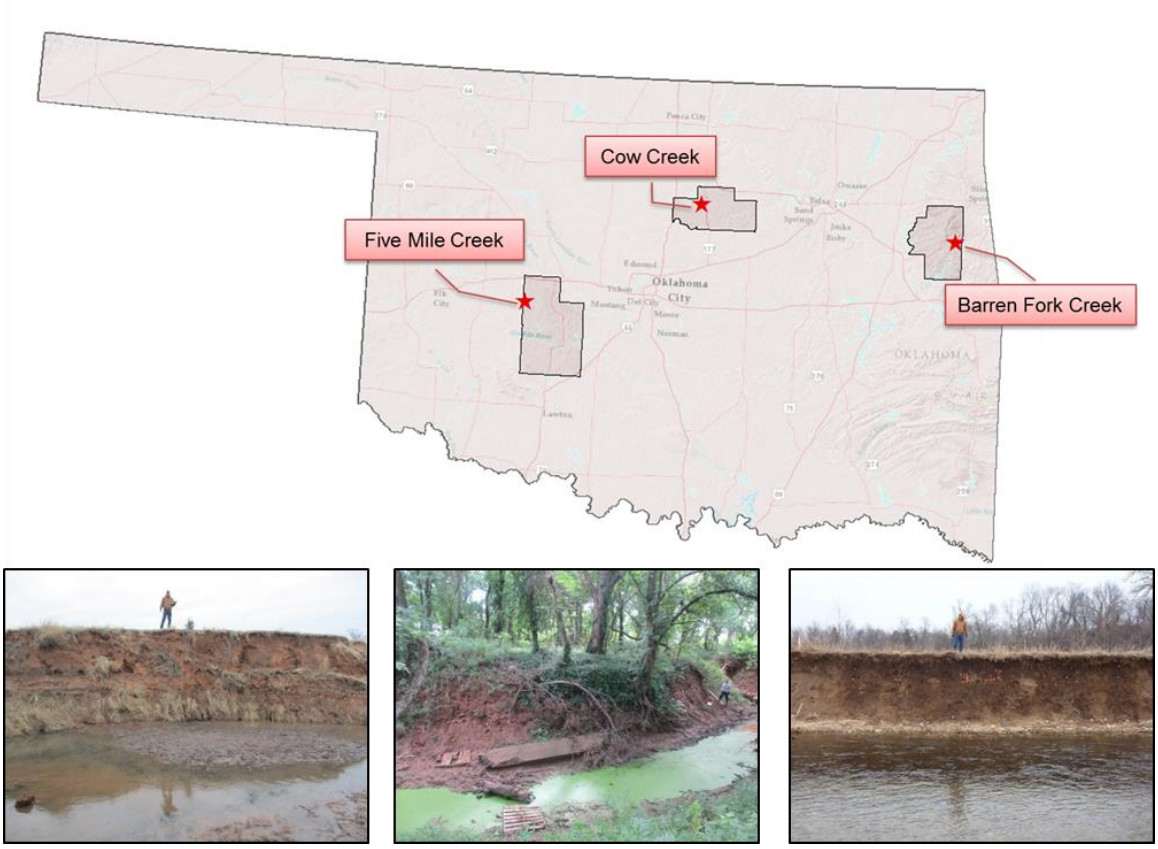

Figure 5.2. Location of Five Mile Creek, Cow Creek, and Barren Fork Creek in Oklahoma as sites chosen for variability studies (top). Pictures of banks sampled (bottom) at Five Mile Creek (left), Cow Creek (middle), and Barren Fork Creek (right) sites.

Cow Creek, located in north central Oklahoma in Payne County, is located in the Central Great Plains Ecoregion. The watershed, covering approximately 30 km^2, has both rural and urban portions with a significant portion devoted to Oklahoma State University's research farms. Cow Creek is an intermittent stream where it is not dammed. The streambanks are comprised of a single layer of loam and sandy loam soils (Midgley et al., 2013). The majority of the creek has significant riparian areas as well. The streambanks at this site had the largest amount of vegetation across the bank face.

The Fort Cobb watershed, including Five Mile Creek located in Caddo County, lies in the Central Great Plains Ecoregion of western Oklahoma. The watershed, which covers 813 km^2, is used for mostly agricultural purposes with 51% used for crops and 40% pastures. Much of the pasture provides uncontrolled access for cattle to riparian areas (Storm et al., 2003). This watershed drains to the Fort Cobb Reservoir, which provides public water supply, flood control, recreation, and wildlife habitat, but does not meet water quality standards based on sediment. Streambank erosion from the Fort Cobb watershed is one of the primary contributors of sediment loading to the reservoir. Streambanks in this watershed consist of sand or sandy loam topsoil (approximately 1 m) overlying a layer with higher clay content. Streambanks at this site had little vegetation.

5.3.2 Data Collection

Data was collected at each of the three sites between February and July 2014 over a span of three days. A homogeneous layer was selected on the critical (i.e., eroding) bank at each site for testing. If the critical bank had multiple apparent soil layers, a single layer was chosen for testing. The JETs at each site were completed using two "mini" JETs that were setup and operated following the procedures outlined by Hanson and Cook (2004) and Al-Madhhachi et al. (2013a, 2013b). A total of 74 JETs were completed for this study: 30 JETs at Barren Fork Creek, 20 at Cow Creek, and 24 at Five Mile Creek.

Prior to each test the soil foundation ring was secured to the bank. After placement of the foundation ring a 5 cm by 5 cm cylindrical soil core sample was taken approximately 15 cm to the right of the foundation ring. The soil core was used to

analyze bulk density (*BD*) and volumetric moisture content (*MC*) of the soil at each test location. Using these two parameters the porosity (*n*), degree of saturation (*S*), and void ratio (*e*) were also calculated. A soil temperature probe was then placed 3 cm to the left of the foundation ring to record the soil temperature (*Ts*) at the start of the test. Water temperature (*Tw*) was recorded from the stream where water was being pulled from for the JETs using an automated logger (HoboWare, Onset Computer Corp., Cape Cod, Mass.). Water temperature was recorded every 15 minutes. At the conclusion of each test, a bag sample of the soil was taken from the center of the foundation ring for determination of soil texture. Particle size analyses were conducted with a sieve analysis and hydrometer test according to ASTM Standards D421 (2002) and D422 (2002). Results were used to calculate the percent sand (*SN*), silt (*SL*), clay (*CL*), and silt-clay (*SC*) contents of the soil tested. Vertical (*y*) and horizontal (*x*) spatial coordinates for each test location were estimated using a surveying tape, surveying rod, and laser level. Measurements were made using the top of the bank as the datum.

Data collected by the JET at each site was analyzed using the JET spreadsheet tool that incorporates three solution techniques (Daly et al., 2013). Solutions for k_d and τ_c derived using the Blaisdell, scour depth, and iterative solutions were reported for each JET conducted. The solution technique used to derive each parameter is indicated by "BL" for the Blaisdell solution, "SD" for the scour depth solution, and "IT" for the iterative solution.

5.3.3 Evaluating Empirical Relationships

This research utilized the data collected from streambanks at a site scale to evaluate of the most commonly used relationships to estimate k_d and τ_c. There are many relationships suggested in the literature relating soil texture parameters to erodibility parameters. Typically, τ_c is estimated from a soil texture parameter and k_d is then estimated from τ_c. Julian and Torres (2006) suggested a relationship relating τ_c to the *SC* of cohesive soils. The relationship is a third-order polynomial trend line based on the assumption that τ_c would be at a maximum value at 100% *SC* and a minimum value at 0% *SC*. Based on the lower limit of the Shield's curve (Shields, 1936) and observations by Dunn (1959), Julian and Torres (2006) developed the following relationship (R^2=0.91):

$$\tau_c = 0.1 + 0.1779(SC\%) + 0.0028(SC\%)^2 - 2.34E-5(SC\%)^3 \quad (5.2)$$

This relationship was evaluated specifically using the soil texture and JET-derived τ_c in this study.

Also, inverse relationships have been suggested (Hanson and Simon, 2001) in order to estimate k_d as a function of τ_c for cohesive soils:

$$k_d = 0.2\tau_c^{-0.5} \quad (5.3)$$

Hanson and Simon (2001) derived their relationship based on 83 in situ JETs. These tests were conducted in cohesive streambeds in the Midwestern United States. Results showed a wide range of data with τ_c spanning six orders of magnitude and k_d spanning four orders of magnitude. However, a general inverse relationship was observed between τ_c and k_d suggesting that soils with a low τ_c have a high k_d and vice versa. Their relationship predicted 64% of the variation within their data and was incorporated into

streambank erosion and stability models, such as the Bank Stability and Toe Erosion Model (BSTEM), as a tool for estimating k_d from τ_c. This relationship was recently updated (Simon et al., 2011) based on hundreds of JETs on streambanks across the United States and given as:

$$k_d = 1.62\tau_c^{-0.838} \quad (5.4)$$

Relationships were plotted between k_d and τ_c as derived from the JETs in the Illinois River watershed and compared to equations 4.3 and 4.4. These equations relating τ_c and k_d were originally developed based on the Blaisdell solution. These relationships were chosen for comparison because users of erosion models, such as the Bank Stability and Toe Erosion Model (BSTEM), Water Erosion Prediction Project (WEPP), Soil and Water Assessment Tool (SWAT), and CONservational Channel Evolution and Pollutant Transport Systesm (CONCEPTS), routinely estimate the erodibility parameters using these relationships (equations 2 to 4) despite being able to measure the parameters in situ (Langendoen, 2000; Ulrich and Nieber, 2008; Abaci and Papanicolaou, 2009; Neitsch et al., 2011; Midgley et al., 2012).

5.3.4 Statistical Analysis

The data collected in this study created a relatively small sample size and generally did not follow a Gaussian distribution. In order to assess the correlation between measured soil parameters and erodibility parameters, the Spearman's rank correlation coefficient, or Spearman's rho, was calculated using SigmaPlot 12.5 (Systat Software, Inc., Germany) both at specific sites and then across all three sites. At each site, parameters that were found to be correlated to the erodibility parameters were analyzed

with a simple linear regression. Before analysis, data was transformed according to the ladder of powers (Helsel and Hirsch, 1992). Results from each site were reported and compared using the adjusted R^2 and PRESS. If there was a correlation present, data was transformed according to the ladder of powers to improve distribution symmetry (Helsel and Hirsch, 1992). Once each of the parameters were evaluated independently, a standard stepwise multiple linear regression was conducted using all measured parameters for each erodibility parameter. A significance level of $\alpha = 0.05$ was assumed for all tests.

5.4 Results and Discussion

The texture analysis conducted for each of the 74 JETs showed a variety of soil textures present at each of the visually homogenous streambank layers. The Barren Fork Creek and Cow Creek sites had a mixture of loam, sandy loam, and silt loam textures. Five Mile Creek had a mixture of loam, sand, sandy loam, and sandy clay loam textures (Figure 3). The *BD* and volumetric MC of each sample was also measured. Bulk densities ranged from 1.1 to 1.5 g/cm^3 and volumetric water contents ranged from 0.08 to 0.33 cm^3/cm^3 across the three sites (Figure 4). From strictly an observation of texture, it would be expected that Cow Creek had the most erodible soil and Five Mile Creek had the most resistant soil.

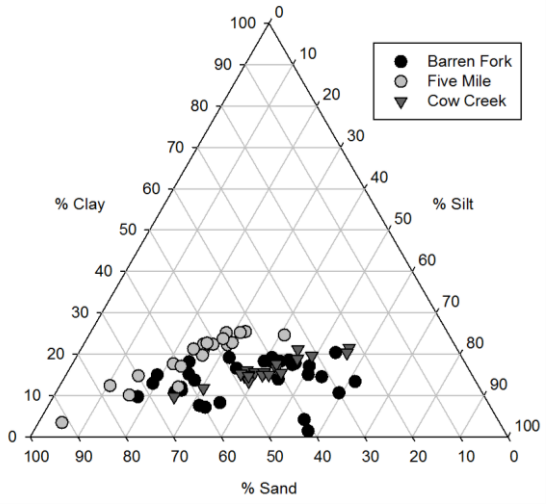

Figure 5.3. Range in soil textures from samples at Barren Fork Creek, Cow Creek, and Five Mile Creek.

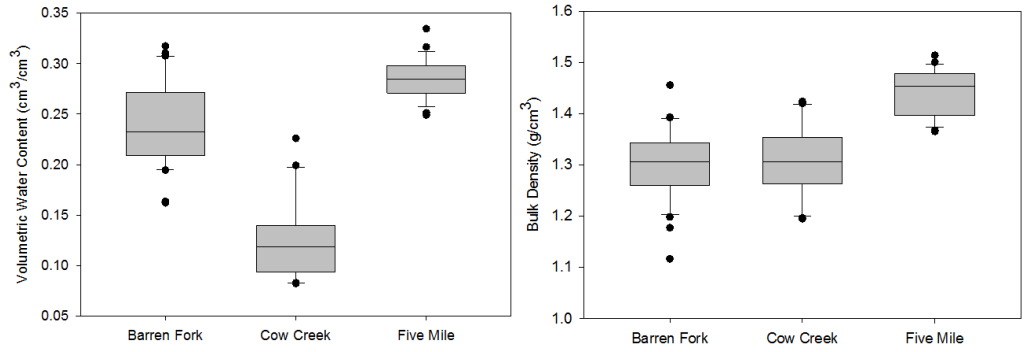

Figure 5.4. Range in volumetric water contents (left) and bulk densities (right) from samples at Barren Fork Creek, Cow Creek, and Five Mile Creek.

Variability in derived erodibility parameters was dependent on both site and solution technique (Figure 5, Table 1). In terms of solution techniques, the BL solution predicted lower k_d and τ_c compared to the SD and IT solutions. Daly et al. (2013) observed a similar pattern with respect to the solutions, noting that the lower τ_c by the BL solution results in a conservative approach for predicting scour.

Table 5.1. Summary statistics for erodibility parameters at each site derived from the Blaisdell solution ($\tau_{c\text{-}BL}$, $k_{d\text{-}BL}$), scour depth solution ($\tau_{c\text{-}SD}$, $k_{d\text{-}SD}$), and iterative solution ($\tau_{c\text{-}IT}$, $k_{d\text{-}IT}$).

	$\tau_{c\text{-}BL}$ (Pa)	$\tau_{c\text{-}SD}$ (Pa)	$\tau_{c\text{-}IT}$ (Pa)	$k_{d\text{-}BL}$ (cm^3/Ns)	$k_{d\text{-}SD}$ (cm^3/Ns)	$k_{d\text{-}IT}$ (cm^3/Ns)
Barren Fork						
Mean	0.62	1.82	1.59	20.0	163	85.2
Standard Deviation	0.56	0.92	0.89	12.1	129	57.8
Coeff. of Variation	0.90	0.51	0.56	0.60	0.79	0.68
Minimum	0.07	0.69	0.52	1.97	11.2	12.0
Maximum	2.36	5.49	5.15	54.9	559	251
Range	2.29	4.80	4.63	53.0	548	239
Cow Creek						
Mean	0.10	1.05	0.95	39.5	245	170
Standard Deviation	0.07	0.27	0.31	28.2	219	122
Coeff. of Variation	0.69	0.26	0.32	0.72	0.90	0.72
Minimum	0.01	0.77	0.63	11.7	25.5	49.1
Maximum	0.25	1.64	1.80	107	1029	447
Range	0.24	0.87	1.17	94.8	1004	398
Five Mile						
Mean	3.81	11.3	8.03	2.90	19.2	17.3
Standard Deviation	3.73	5.61	3.33	2.06	10.8	10.5
Coeff. of Variation	0.98	0.50	0.42	0.71	0.56	0.60
Minimum	0.01	3.52	3.84	0.32	2.24	6.80
Maximum	14.6	24.3	17.6	10.2	41.3	47.5
Range	14.6	20.7	13.7	9.89	39.0	40.7

Cow Creek was the most variable site in terms of k_d. The k_d at this site spanned one, three, and two orders of magnitude for the BL, SD, and IT solutions, respectively. This high degree of variability in k_d at Cow Creek was expected due to its characterization as the site with the most erodible soil. Five Mile Creek was the most variable site in terms of τ_c with each solution producing a variation of one order of magnitude. Again, this was expected due to Five Mile Creek's characterization as the site with the most resistive soil. The τ_c results from Barren Fork Creek were the most uniform with every solution technique producing results within the same order of magnitude. There are a number of variables that could cause the presence or lack of variability, such

as the presence of gravel or roots at the JET site, differences in MC, or soil texture heterogeneity. This amount of variability causes less confidence in an average value being the most representative parameter for erosion predictions at a site.

To explore the variability further, summary statistics were calculated for results of each solution technique at each site (Table 1) and contour plots were generated to investigate spatial patterns in the data for each streambank layer (Figures 6-8). From the summary statistics there seems to be a moderate degree of variability in all six parameters at each site as the standard deviation is generally on the same order of magnitude as the mean. The high coefficients of variation also illustrate this point.

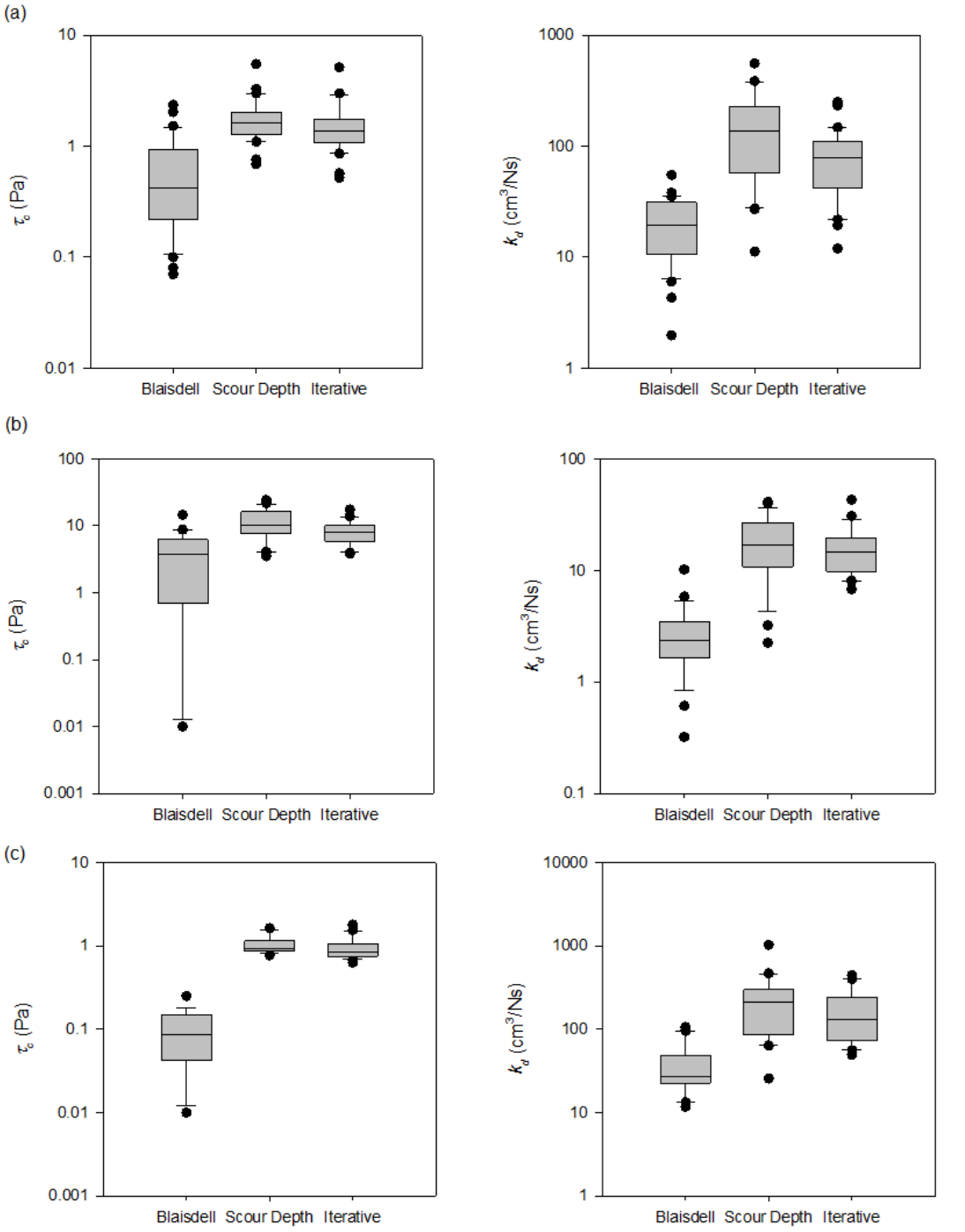

Figure 5.5. Range in erodibility parameters derived using the Blaisdell, scour depth, and iterative solution methodologies at (a) Barren Fork Creek, (b) Cow Creek, and (c) Five Mile Creek.

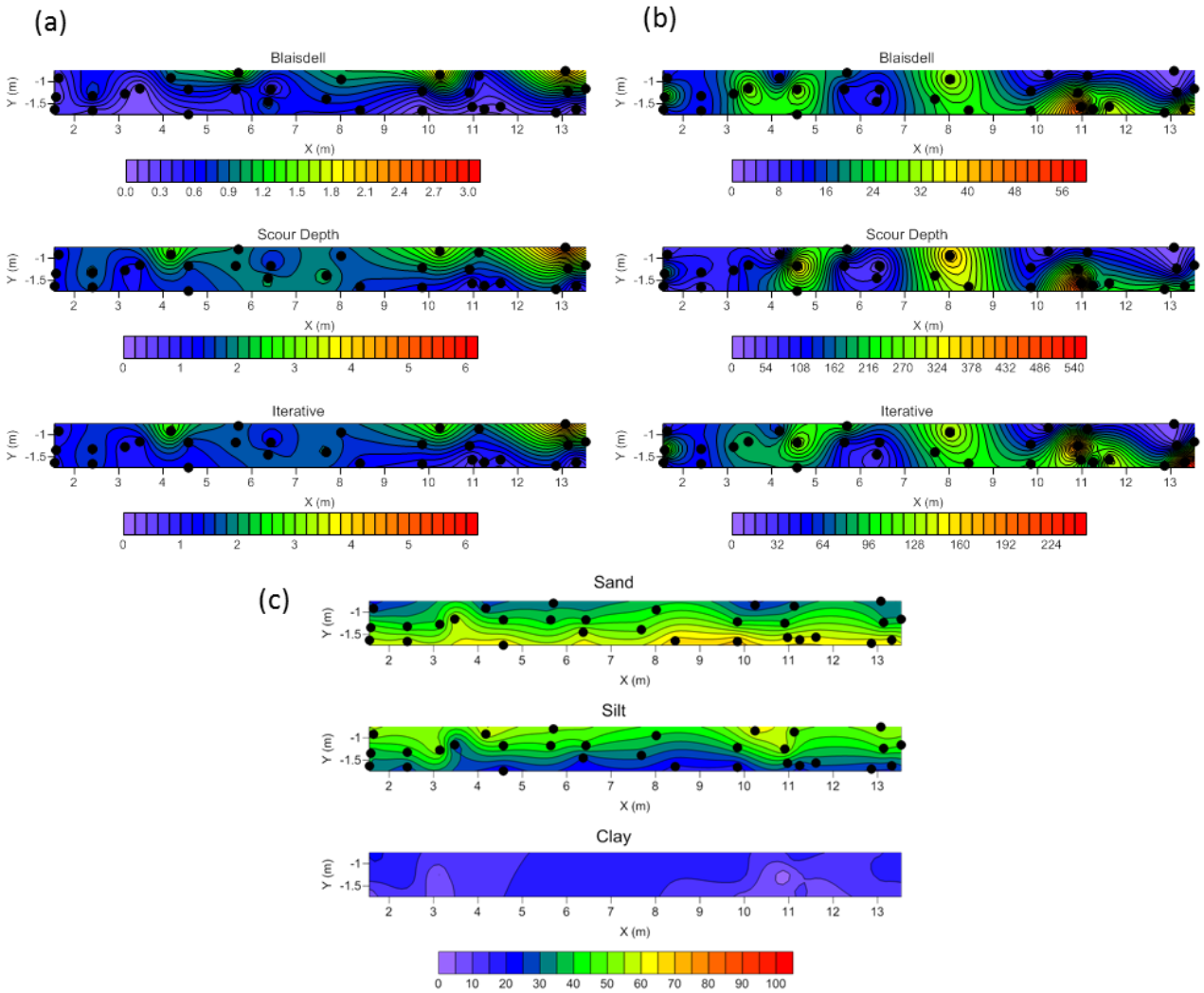

Figure 5.6. Contour plots showing (a) τ_c (Pa), (b) k_d (cm^3/Ns), and (c) soil texture at Barren Fork Creek.

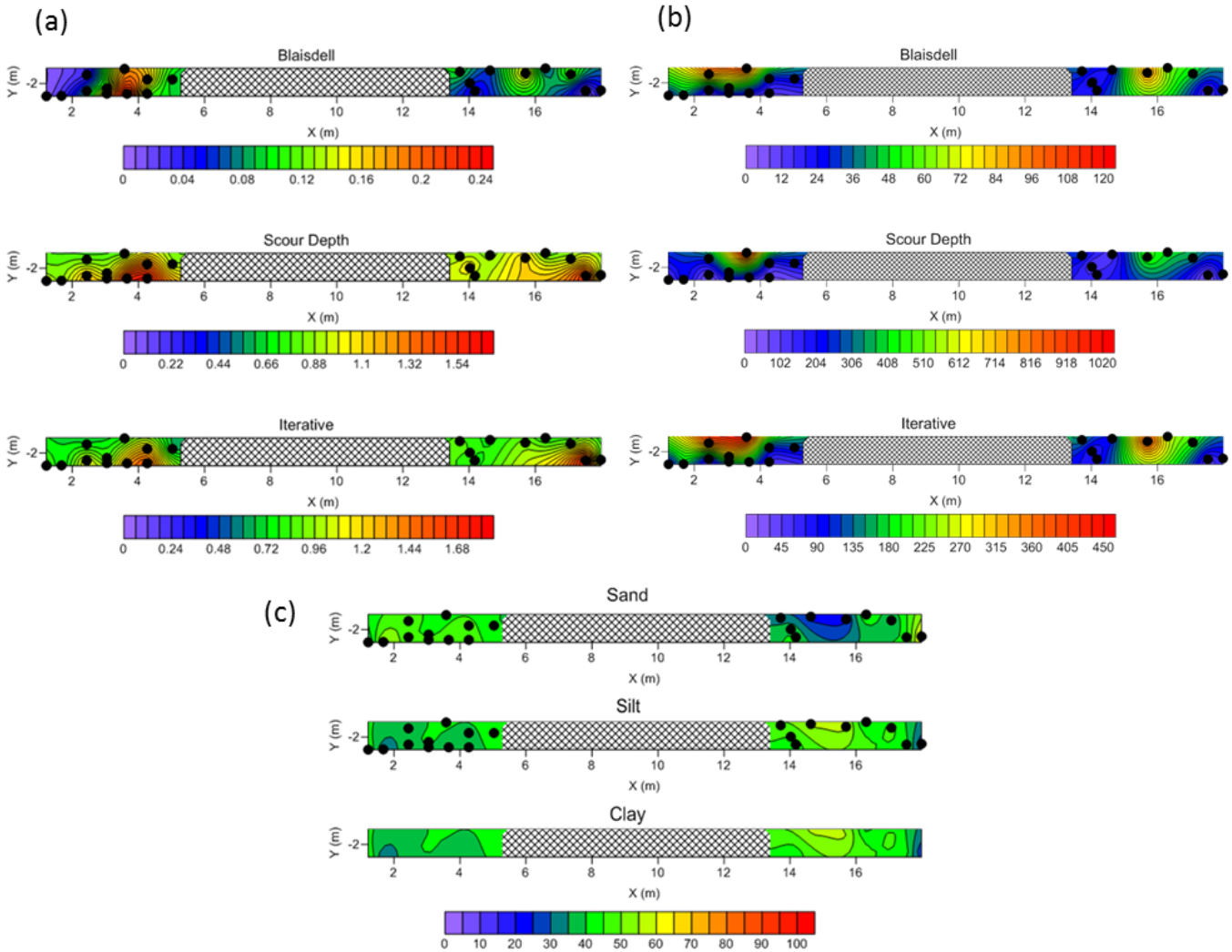

Figure 5.7. Contour plots showing (a) τ_c (Pa), (b) k_d (cm^3/Ns), and (c) soil texture at Cow Creek. The hatched area indicates an area of the bank that was heavily vegetated and thus not sampled.

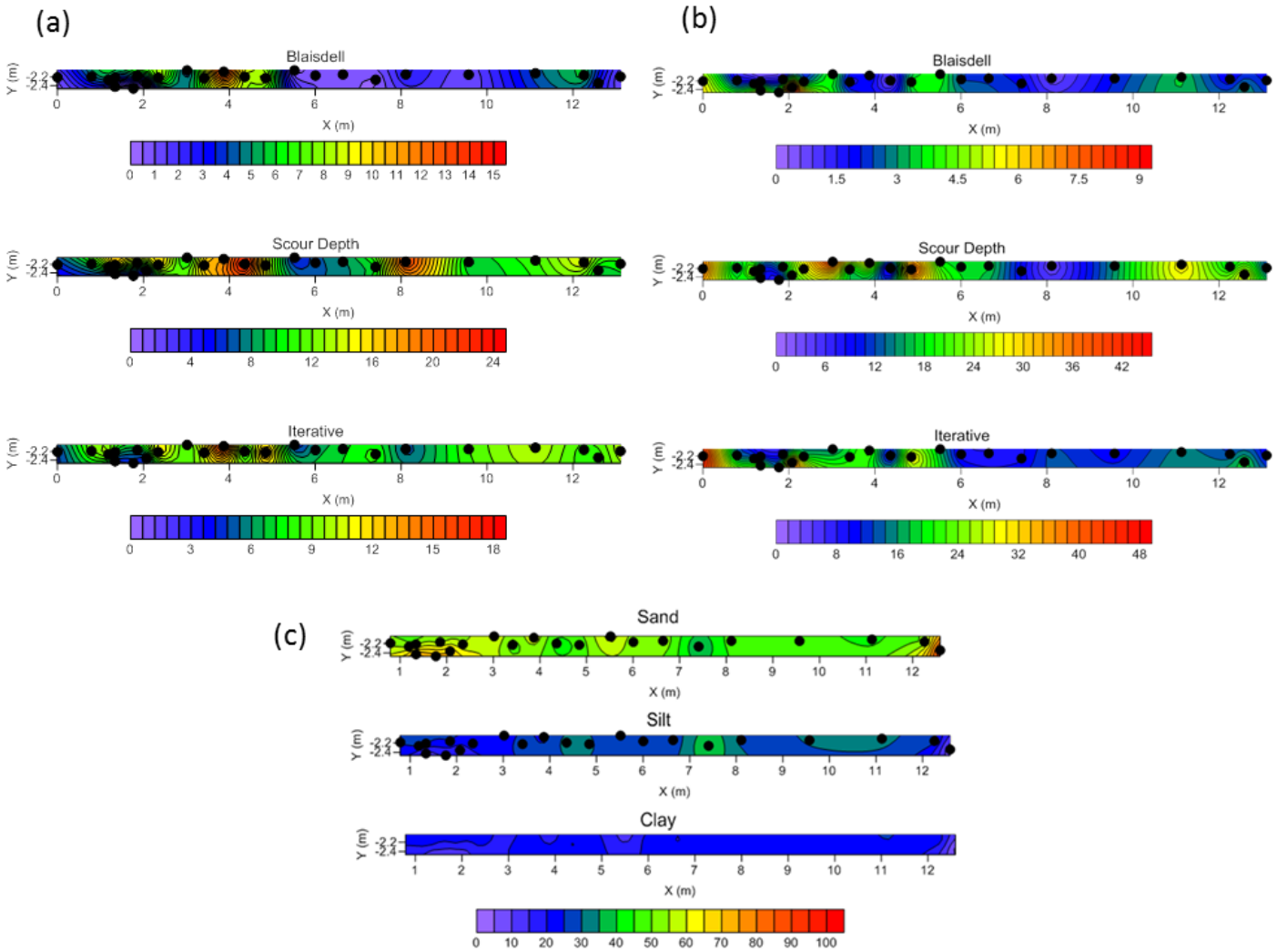

Figure 5.8. Contour plots showing (a) τ_c (Pa), (b) k_d (cm^3/Ns), and (c) soil texture at Five Mile Creek.

In order to determine if any correlations existed between the measured erodibility parameters and measured physical parameters, Spearman's rank correlation coefficient (r_s) was calculated. Correlations between k_d or τ_c for each solution technique and the spatial location, soil temperature, water temperature, *BD*, MC, *n*, *S*, *e*, *SN*, *SL*, *CL*, and *SC* were considered (Figures 9 to 11). The correlation coefficients ranged from -0.66 to 0.66, -0.59 to 0.62, and -0.53 to 0.64 for Barren Fork, Five Mile, and Cow Creek, respectively. Pairs of variables with positive correlation coefficients tend to increase together and those with negative coefficients tend to be inversely related.

All of the erodibility parameters measured with the JET were found to be significantly correlated with at least one measured variable with the exception of $\tau_{c\text{-}IT}$ at Five Mile Creek. Correlations were dependent on solution technique and site. Barren Fork had the highest number of correlations while the other two sites had few correlations between the erodibility parameters and measured parameters. Many of the correlations were expected and intuitive. For example, at Barren Fork the *SN* and τ_c from each solution technique were negatively correlated. Therefore, as the *SN* increased the τ_c decreased.

Further discussion of the correlations would be aided by a deeper analysis of the data through linear regression. At each site, parameters that were found to be correlated to the erodibility parameters were analyzed with a simple linear regression. Results from each site were reported and compared using the adjusted R^2 and PRESS (Tables 2 to 4). Following the simple linear regressions, standard stepwise multiple linear regressions were conducted using all measured parameters. There were no significant relationships found at any site using a multiple linear regression.

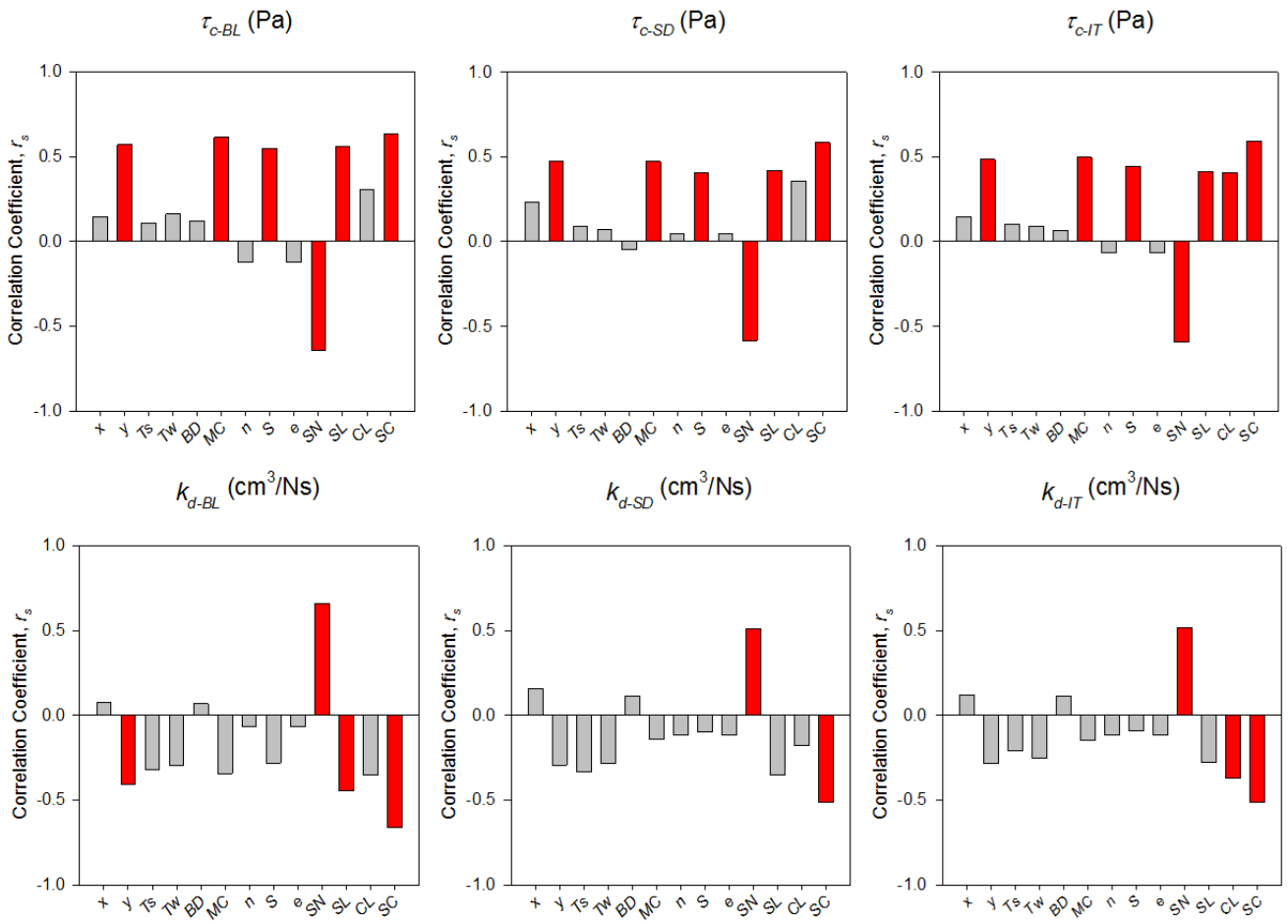

Figure 5.9. Spearman's rho (r_s) between τ_c or k_d for each solution technique and the horizontal coordinate (*x*), vertical coordinate (*y*), soil temperature (*Ts*), water temperature (*Tw*), bulk density (*BD*), volumetric moisture content (*MC*), porosity (*n*), degree of saturation (*S*), void ratio (*e*), % sand (*SN*), % silt (*SL*), % clay (*CL*), and silt-clay content (*SC*) for Barren Fork Creek. Parameters that are significantly correlated are shown in red.

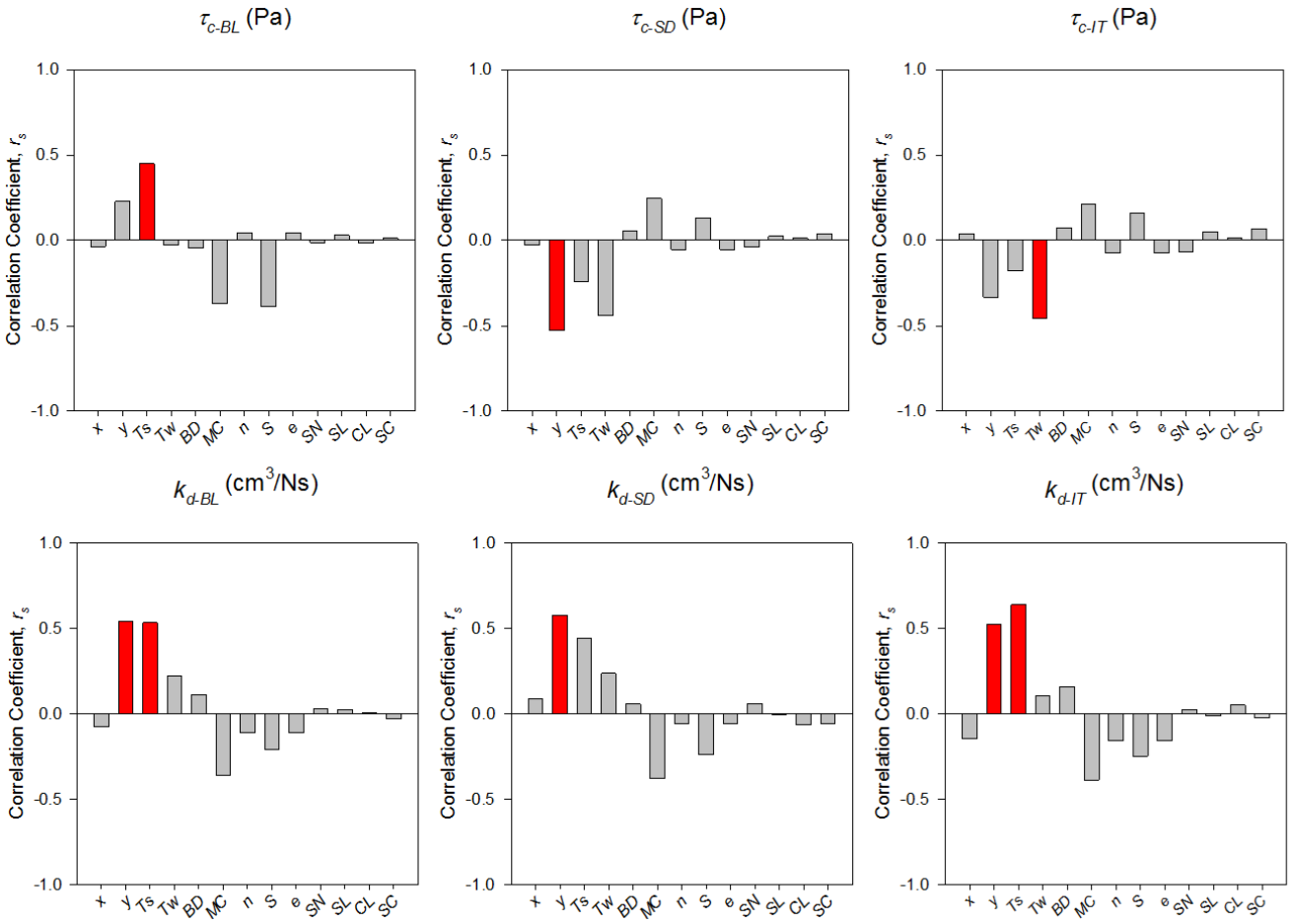

Figure 5.10. Spearman's rho (r_s) between τ_c or k_d for each solution technique and the horizontal coordinate (*x*), vertical coordinate (*y*), soil temperature (*Ts*), water temperature (*Tw*), bulk density (*BD*), volumetric moisture content (*MC*), porosity (*n*), degree of saturation (*S*), void ratio (*e*), % sand (*SN*), % silt (*SL*), % clay (*CL*), and silt-clay content (*SC*) for Cow Creek. Parameters that are significantly correlated are shown in red.

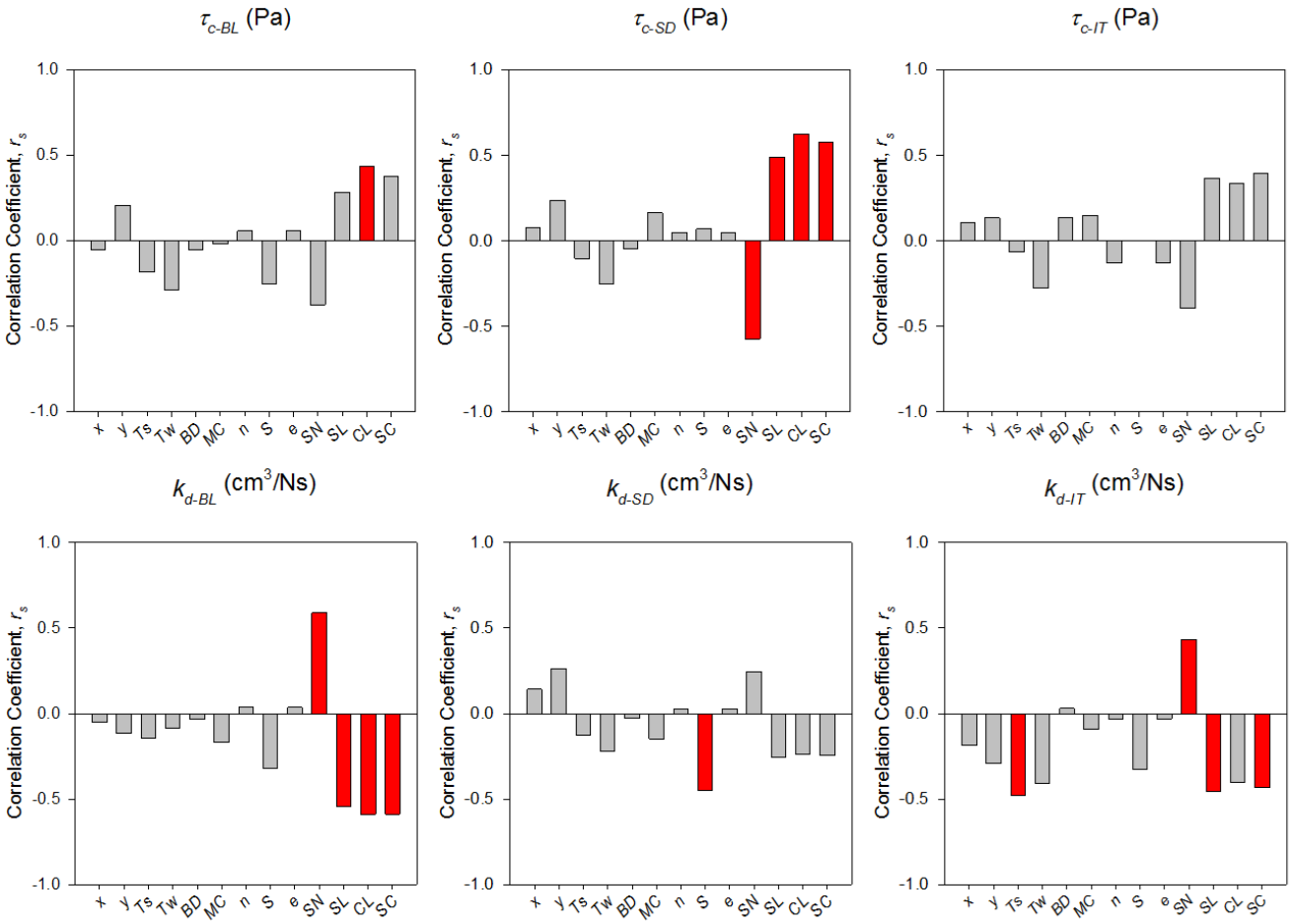

Figure 5.11. Spearman's rho (r_s) between τ_c or k_d for each solution technique and the horizontal coordinate (*x*), vertical coordinate (*y*), soil temperature (*Ts*), water temperature (*Tw*), bulk density (*BD*), volumetric moisture content (*MC*), porosity (*n*), degree of saturation (*S*), void ratio (*e*), % sand (*SN*), % silt (*SL*), % clay (*CL*), and silt-clay content (*SC*) for Five Mile Creek. Parameters that are significantly correlated are shown in red.

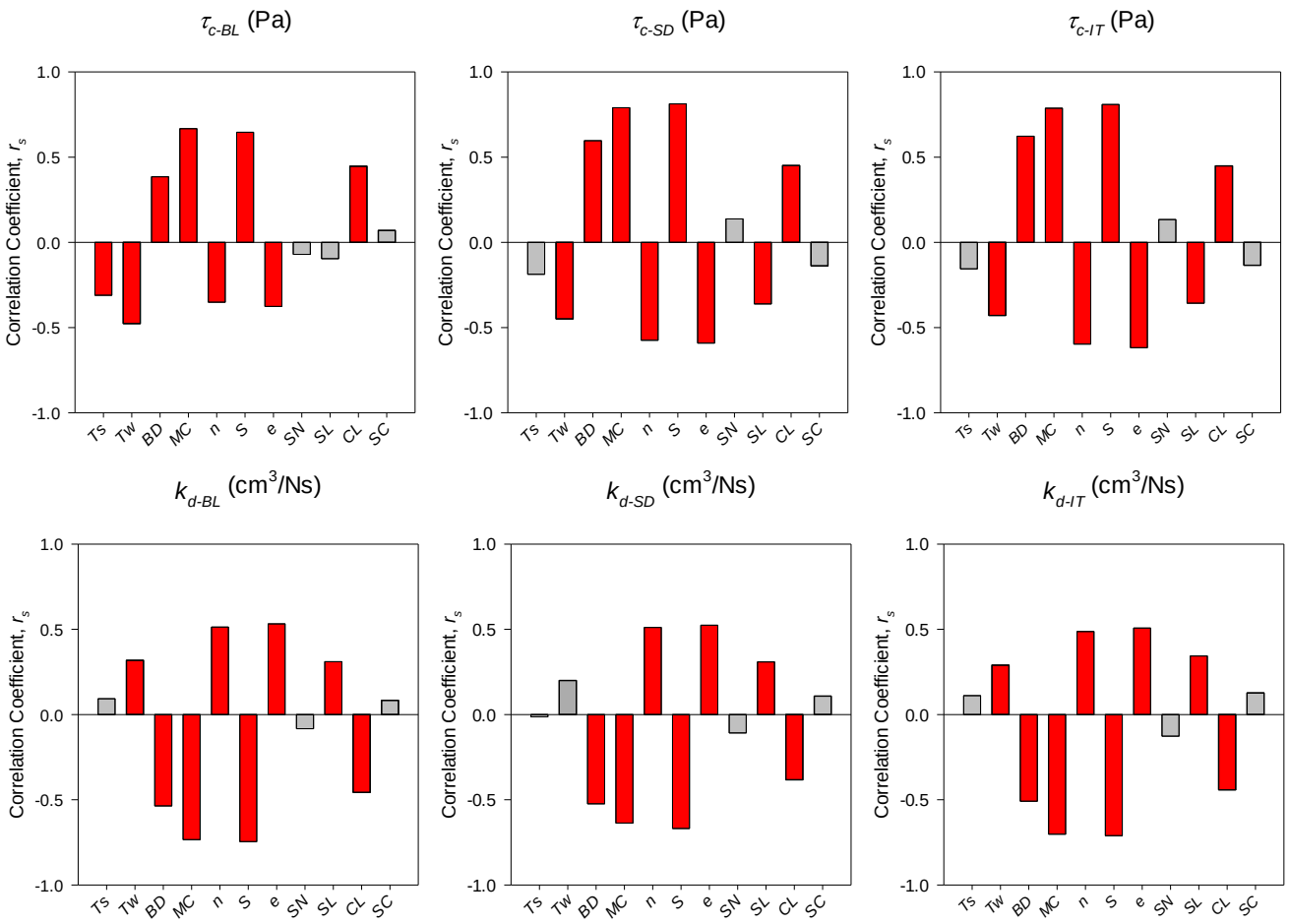

Figure 5.12. Spearman's rho (r_s) between τ_c or k_d for each solution technique and the horizontal coordinate (*x*), vertical coordinate (*y*), soil temperature (*Ts*), water temperature (*Tw*), bulk density (*BD*), volumetric moisture content (*MC*), porosity (*n*), degree of saturation (*S*), void ratio (*e*), % sand (*SN*), % silt (*SL*), % clay (*CL*), and silt-clay content (*SC*) for all three sites combined. Parameters that are significantly correlated are shown in red.

Table 5.2. Linear regressions for prediction of erodibility parameters at Barren Fork.

Parameter	Equation[1]	p-value	R^2 (adj)	PRESS
$\tau_{c\text{-}BL}'$	= 1.43 + 1.76 *y*	0.001	0.32	18.18
	= - 4.26 + 14.3 *MC*	0.000	0.42	15.69
	= - 6.39 + 8.08 *S'*	0.001	0.33	17.93
	= 5.06 - 1.65 *SN'*	0.000	0.39	16.78
	= - 2.46 + 0.0415 *SL*	0.001	0.32	18.58
	= - 3.12 + 0.0430 *SC*	0.000	0.40	16.55
$\tau_{c\text{-}SD}'$	= 1.54 + 0.797 *y*	0.001	0.31	4.12
	= - 0.681* + 4.95 *MC*	0.005	0.22	4.52
	= - 1.23* + 2.53 *S'*	0.027	0.13	4.95
	= 2.99 - 0.693 *SN'*	0.001	0.32	4.06
	= - 0.116* + 0.0160 *SL*	0.006	0.21	4.58
	= - 0.426* + 0.0177 *SC*	0.001	0.31	4.08
$\tau_{c\text{-}IT}'$	= 1.52 + 0.902 *y*	0.001	0.33	4.79
	= - 0.956 + 5.47 *MC*	0.005	0.23	5.37
	= - 1.60* + 2.85 *S'*	0.022	0.14	5.84
	= 3.09 - 0.764 *SN'*	0.001	0.32	4.86
	= - 0.326* + 0.0175 *SL*	0.006	0.21	5.49
	= - 0.121* + 0.0342* *CL*	0.056	0.09	6.19
	= - 0.680 + 0.0196 *SC*	0.001	0.32	4.85
$k_{d\text{-}BL}'$	= 1.75* - 1.95 *y*	0.016	0.16	50.49
	= - 3.53* + 2.18 *SN'*	0.001	0.30	41.33
	= 6.06 - 0.0460 *SL*	0.016	0.16	49.75
	= 7.15 - 0.0547 *SC*	0.002	0.28	42.54
$k_{d\text{-}SD}'$	= - 10.2* + 6.15 *SN'*	0.015	0.17	647.75
	= 19.9 - 0.153 *SC*	0.020	0.15	662.17
$k_{d\text{-}IT}'$	= - 3.54* + 3.43 *SN'*	0.025	0.14	246.06
	= 12.6 - 0.280 *CL*	0.014	0.17	242.72
	= 13.2 - 0.0844 *SC*	0.035	0.12	251.25

[1] Equation coefficients and constants statistically significant (α = 0.05) unless indicated by *. Variables marked with prime symbol (') are transformed: $\tau_{c\text{-}BL}' = \ln(\tau_{c\text{-}BL})$, $\tau_{c\text{-}SD}' = \ln(\tau_{c\text{-}SD})$, $\tau_{c\text{-}IT}' = \ln(\tau_{c\text{-}IT})$, $k_{d\text{-}BL}' = k_{d\text{-}BL}^{1/2}$, $k_{d\text{-}SD}' = k_{d\text{-}SD}^{1/2}$, $k_{d\text{-}IT}' = k_{d\text{-}IT}^{1/2}$, $S' = S^{1/2}$, $SN' = SN^{1/3}$.

Table 5.3. Linear regressions for prediction of erodibility parameters at Cow Creek.

Parameter	Equation[1]	p-value	R^2 (adj)	PRESS
$\tau_{c\text{-}BL}$	= - 1.19* + 0.0544* *Ts*	0.057	0.14	0.08
$\tau_{c\text{-}SD}$'	= 2.03 + 0.501 *y*	0.029	0.20	1.73
$\tau_{c\text{-}IT}$'	= - 7.33* + 0.363 *Tw*	0.035	0.18	0.35
$k_{d\text{-}BL}$'	= 6.13 + 1.44 *y*	0.005	0.33	7.89
	= - 16.9 + 0.850 *Ts*	0.004	0.34	8.00
$k_{d\text{-}SD}$'	= 37.3 + 11.4 *y*	0.007	0.30	585.78
$k_{d\text{-}IT}$'	= 28.7 + 8.20 *y*	0.008	0.29	300.73
	= - 121 + 5.65 *Ts*	0.001	0.42	246.08

[1] Equation coefficients and constants statistically significant (α = 0.05) unless indicated by *. Variables marked with prime symbol (') are transformed: $\tau_{c\text{-}SD}' = \tau_{c\text{-}SD}^{-3/2}$, $\tau_{c\text{-}IT}' = \tau_{c\text{-}IT}^{-1/2}$, $k_{d\text{-}BL}' = k_{d\text{-}BL}^{1/3}$, $k_{d\text{-}SD}' = k_{d\text{-}SD}^{1/2}$, $k_{d\text{-}IT}' = k_{d\text{-}IT}^{1/2}$.

Table 5.4. Linear regressions for prediction of erodibility parameters at Five Mile.

Parameter	Equation[1]	p-value	R^2 (adj)	PRESS
$\tau_{c\text{-}BL}$'	= 0.641* + 0.00263 *CL'*	0.033	0.17	23.26
$\tau_{c\text{-}SD}$	= 38.0 - 3.56 *SN'*	0.013	0.24	640.36
	= 9.20* + 0.000125* *SL'*	0.152	0.06	1090
	= 3.58* + 0.0194 *CL'*	0.002	0.37	511.92
	= 5.23* + 0.00300 *SC'*	0.012	0.24	648.94
$k_{d\text{-}BL}$'	= - 1.09* + 0.361 *SN'*	0.007	0.28	5.75
	= 1.90 - 0.000016 *SL'*	0.048	0.14	8.16
	= 2.33 - 0.00178 *CL'*	0.003	0.34	5.03
	= 2.25 - 0.000312 *SC'*	0.005	0.30	5.44
$k_{d\text{-}SD}$	= 51.3* - 38* *S'*	0.737	0.00	3134
$k_{d\text{-}IT}$'	= 2.92 - 0.0359* *Ts*	0.555	0.00	5.64
	= 0.875* + 0.215 *SN'*	0.032	0.17	3.15
	= 2.69 - 0.000011* *SL'*	0.058	0.13	3.37
	= 2.86 - 0.000184 *SC'*	0.028	0.18	3.08

[1] Equation coefficients and constants statistically significant (α = 0.05) unless indicated by *. Variables marked with prime symbol (') are transformed: $\tau_{c\text{-}BL}' = \tau_{c\text{-}BL}^{1/2}$, $k_{d\text{-}BL}' = k_{d\text{-}BL}^{1/2}$, $k_{d\text{-}IT}' = k_{d\text{-}IT}^{1/3}$, $S' = S^{1/3}$, $SN' = SN^{1/2}$, $SL' = SN^{3}$, $CL' = CL^{2}$, $SC' = SC^{2}$.

The Barren Fork Creek site had the greatest number of variable correlations with the erodibility parameters. The vertical direction on the bank, MC, *S*, *SN*, *SL*, *CL*, and *SC* were found to be correlated to the τ_c. The vertical direction on the bank, *SN*, *SL*, *CL*, and *SC* were found to be correlated to the erodibility coefficient. While most of these

relationships were significant, none of the linear regressions between these parameters produced relationships with high R^2 values. The PRESS values were also relatively large suggesting that the relationships do not have a powerful predictive capability. Barren Fork Creek was the most variable site in terms of soil texture. This may explain the correlations seen with the texture parameters. This site also had a defined root zone at the top of the bank and a visible wetting front within the root zone throughout the majority of testing (Figure 13). The correlations with the vertical direction on the bank and the MC and *S* could be indicative of these conditions. The τ_c increased with increasing MC. This is consistent with the results reported by Wynn and Mostaghimi (2006). This correlation could also be related to the vertical direction on the bank as both the τ_c and MC increased moving up the bank and into the root zone.

Cow Creek had very few correlations and the only correlated parameters were the vertical distance on the bank and the soil and water temperatures. This site had the most consistent soil texture and was vegetated throughout the bank. The consistency in soil texture may have prevented the texture from being a reliable predictor of the erodibility parameters at this site. The correlations between erodibility and soil temperature, although present, were not strong. Again, due to the consistency of the bank, soil temperature may have emerged as the most reliable predictor albeit not a good one.

Five Mile Creek was characterized as the most resistant site with the highest measured τ_c and highest amount of *CL*. The correlations at this site were almost solely dependent on texture. However, none of the relationships provide a strong predictive capability for any of the erodibility parameters.

Interestingly, *BD* was not correlated with either the τ_c or k_d at any of the sites. Wynn and Mostaghimi (2006) cited *BD* as one of the most highly significant parameters for determining both of the erodibility parameters. There was not a single parameter that was a significant predictor across sites and solution techniques for either the τ_c or erodibility coefficient. Because this study incorporates a relatively limited data set, continuing research is needed in order to confirm the lack of relationships over a wider range of conditions and soil textures.

The lack of significant relationships between measured parameters and the erodibility parameters in this study strengthens the argument that the τ_c and k_d are highly variable, sensitive, and must be measured in situ instead of estimated with empirical relationships. To further illustrate this point, data from all three sites were compared to the most widely used relationships to estimate the k_d and the τ_c. The Julian and Torres (2006) relationship correlating τ_c to the *SC* of cohesive soils (equation 5.2) was applied to the measured data at all three sites (Figure 14) and over predicted τ_c for the majority of the tests. In fact, the measured τ_c values spanned three orders of magnitude while the Julian and Torres (2006) relationship predicted a smaller range of values over a large range of *SC*. The Julian and Torres (2006) relationship was derived using a range of *SC* of approximately 5 to 95%. The *SC* in this study ranged between 28 and 93%. Even with this large range in *SC*, the Julian and Torres (2006) relationship predicted a small range in τ_c values. More research is needed in order to investigate the applicability of such relationships in a wide range of systems.

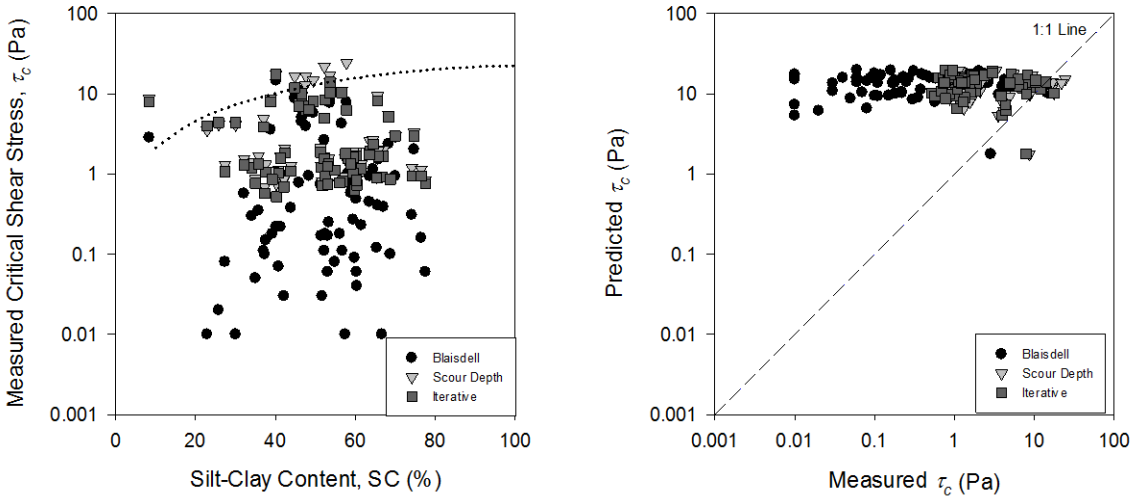

Figure 5.13. Measured τ_c and silt-clay content with the Julian and Torres (2006) relationship indicated by the dotted line (left), and measured versus predicted τ_c using the Julian and Torres (2006) relationship (right). Data compiled from all three sites, totaling 74 JETs.

The Hanson and Simon (2001) and Simon et al. (2011) equations (3 and 4) predicting the k_d from the τ_c were plotted alongside the measured erodibility parameters (Figure 14). While there was a similar trend between the measured data using the Blaisdell solution and the Hanson and Simon (2001) relationship (equation 3), k_d calculated using the Hanson and Simon (2001) relationship would have been generally underestimated. This result is similar to that found by Clark and Wynn (2007) and Karmaker and Dutta (2011). Similarly, there was a comparable trend between the measured data using the scour depth and iterative solutions and the Simon et al. (2011) relationship (equation 4), but k_d calculated using the Simon et al. (2011) relationship would have been underestimated as well. Erosion rate predictions would consequently have been underestimated as well using either solution technique or relationship. The updated Simon et al. (2011) relationship was a better predictor of k_d based on τ_c for this study although it would have still resulted in underestimation of the parameters.

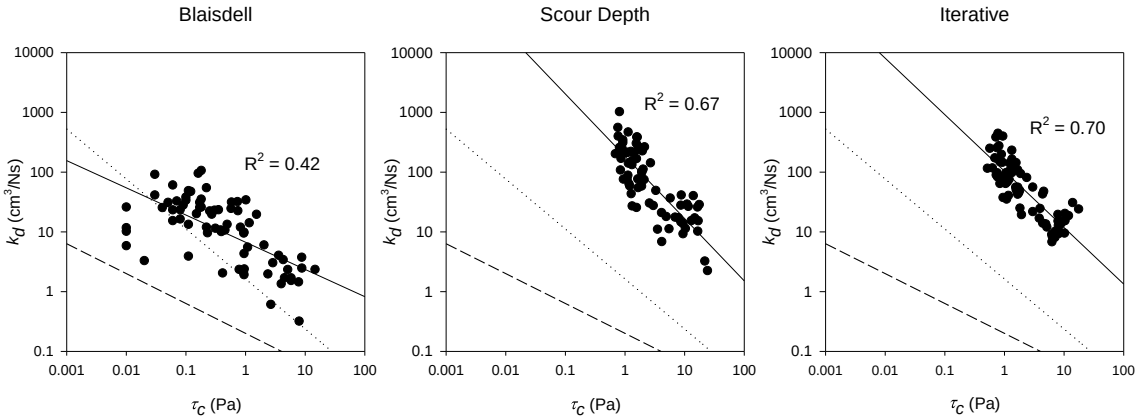

Figure 5.14. Correlations between k_d and τ_c for each solution technique from 74 JETs (circles) compiled from all three sites and comparison to previously proposed relationships by Hanson and Simon (2001) (dashed line) and Simon et al. (2011) (dotted line).

5.5 Conclusions

The objectives of this study were to address the variability in the erodibility parameters derived from JETs at a site scale with respect to soil parameter correlations, temporal variability, spatial variability, and testing variability. An intensive study of site scale parameter variability and correlations was undertaken at three separate sites in Oklahoma. A total of 74 JETs were completed and evaluated using the Blaisdell, scour depth, and iterative solution methodologies. At the site scale the critical shear stress and erodibility coefficients varied by up to three orders of magnitude, consistent with other studies. While there were correlations between the erodibility parameters and measured soil variables, there were no reliable relationships with strong predictive capabilities at any of the sites for any of the variables. Also, there were no significant multiple linear regressions to predict the erodibility parameters based on more than one soil parameter. Regression results showed that bulk density was not a significant predictor of erodibility. This was not consistent with other studies that showed bulk density being a highly significant predictor. Moisture content was also not a significant predictor of erodibility

in most cases. The texture at each site was responsible for most of the correlations to the erodibility parameters. At some sites, a vertical zoning trend was evident with higher critical shear stresses, and lower erodibility coefficients, occurring at the top or bottom of the bank. When assessing current relationships from the literature, it was found that the erodibility parameters measured in this study could not be predicted based on existing, widely used empirical models. This study illustrated that erodibility parameters must be measured *in situ* and cannot be estimated from empirical relationships due to the heterogeneous nature of soil and the variability in subaerial processes.More research is needed in order to quantify the role of vegetation and subaerial erosion in order to incorporate temporal and spatial variation in the erodibility of streambanks into channel evolution models.

5.6 Acknowledgements

The authors acknowledge the financial support of the Buchanan Family Trust through the Buchanan Endowed Chair at Oklahoma State University.

CHAPTER 6

MODELING STREAMBANK EROSION AND FAILURE ALONG PROTECTED AND UNPROTECTED COMPOSITE STREAMBANKS[4]

6.1 Abstract

Streambank retreat can be a significant contributor to total sediment and nutrient loading to streams. Process-based bank stability models, such as the Bank Stability and Toe Erosion Model (BSTEM), have been used to determine critical factors affecting streambank erosion and failure such as riparian vegetation and to estimate retreat rates over time. BSTEM has been successfully applied on a number of cohesive streambanks, but less so on composite banks consisting of both cohesive and noncohesive soils in highly sinuous streams. Composite streambanks can exhibit rapid and episodic bank retreat. The objectives of this research were two-fold: (i) develop and apply simplified procedures for estimating root cohesion based on above- and below-ground biomass estimates and (ii) systematically apply BSTEM to a series of 10 composite streambanks distributed along the Barren Fork Creek in eastern Oklahoma to assess model sensitivity to root cohesion and model performance in predicting retreat. This research aimed to document the influence of riparian conservation practices on bank retreat rates and

[4] Submitted to *Advances in Water Resources*:
Daly, E.R., R.B. Miller, and G.A. Fox. 2014. Modeling streambank erosion and failure along protected and unprotected composite streambanks. *Advances in Water Resources*.

evaluated simplistic methods for incorporating such practices into such process-based models. Sites modeled included historically unprotected sites with no riparian vegetation and historically protected sites with riparian vegetation present during all or part of the 2003 to 2010 study period. The lateral retreat ranged from 4.1 to 74.8 m across the 10 sites and was largest at the historically unprotected sites in which retreat averaged 49.2 m. Protected sites had less bank retreat but with more variability in retreat rates per year. With calibration focused on the erodibility parameters, the model was able to match both the observed total amount of retreat as well as the timing of retreat at both the protected and unprotected sites as derived from aerial imagery. During calibration BSTEM was not sensitive to the specific value of the soil cohesion or the additional soil cohesion added due to roots for the cohesive topsoil layer, suggesting the proposed simplified techniques could be used to estimate root cohesion values. The BSTEM modeling also provided an advantageous assessment tool for evaluating retreat rates compared to in situ bank retreat measurements due to the magnitude and episodic nature of streambank erosion and failures. Process-based models, such as BSTEM, may be necessary to incrementally model bank retreat in order to quantify actual streambank retreat rates and understand mechanisms of failure for the design of stabilization projects.

6.2 Introduction

Streambank erosion is an important global issue that affects infrastructure and stream-side property, in-stream habitat, and water quality. In response to streambank erosion, billions of dollars have been spent on stabilization projects of various kinds to help slow bank retreat (Bernhardt et al., 2005; Lavendel 2002) along with associated research on restoration practices (Khosronejad et al., 2013). It has recently been

recognized that bank retreat can be a significant contributor to the total sediment (Sekely et al., 2002; Simon and Rinaldi, 2006; Mukundan et al., 2010; Pizzuto, 2008) and nutrient (Laubel et al., 2003; Zaimes et al., 2008; Kronvang et al., 2012) loads to streams. These efforts commonly use empirical models based on factors such as measured erosion rates, soil types, and hydrographs (Laubel et al., 2003; Zaimes et al., 2008). Another approach in this effort is the use of process-based streambank erosion models to help determine the critical factors that affect bank retreat [Midgley et al., 2012; Jia et al., 2010; Tealdi et al., 2011; Duan, 2005).

From a process standpoint, the stability of a streambank is controlled by the relationship between the resisting force of the bank, which is a function of the soil strength and the driving forces within the bank, which are in turn functions of the soil weight, soil moisture, and geometry of the bank (Duan, 2005; Simon et al., 2000). The relationship between driving and stabilizing forces within the streambank change over time as the bank erodes and the pore-water pressure distribution changes within the bank (Fox and Wilson, 2010; Darby and Thorne, 1996; Darby et al., 2007; Rinaldi et al., 2008), leading to bank failures when the driving forces exceed the resisting forces along failure planes within the bank (Duan, 2005). One of the most commonly used and most advanced erosion process-based models is the Bank Stability and Toe Erosion Model (BSTEM), developed by the National Sedimentation Laboratory in Oxford, Mississippi (Midgley et al., 2012; Simon et al., 2000). The most current version of BSTEM (Dynamic Version 5.4, USDA ARS, Oxford, MS) has bank stability and toe erosion modules, and the capability to model a continuous hydrograph by sequentially applying

the various model components for a stream depth defined by a hydrograph, redrawing the bank profile, and then moving to the next step of the hydrograph.

6.2.1 BSTEM Model Description

As a process-based model, BSTEM uses as inputs the soil strength, erosional, and geometric characteristics of up to five bank layers, stream hydraulic characteristics including channel slope and Manning's *n*, and a stream stage hydrograph. The erosion component of BSTEM estimates bank undercutting as a result of fluvial erosion (Simon et al., 2000). Hydrodynamics plays a major role in determining the evolution of erosion processes. The model predicts erosion based on an excess shear stress equation originally proposed by Partheniades (1965). Erosion rate, ε (m s^{-1}), is calculated as

$$\varepsilon = k_d \left(\tau_o - \tau_c\right)^a \tag{6.1}$$

where k_d is the erodibility coefficient (m^3 N^{-1} s^{-1}), τ_o is the average shear stress (kPa), τ_c is the soil's critical shear stress (kPa), and a is an exponent usually assumed to be unity. The k_d and τ_c are functions of numerous soil properties. For non-cohesive soils, τ_c is typically estimated based on the median particle diameter (Garcia, 2008). To determine the applied shear stress and calculate erosion rate, BSTEM uses nodes that are specified along the bank face (Figure 6.1). The average boundary shear stress acting on each node of bank material is calculated ($\tau_o = \gamma RS$, where γ is the specific weight of water, R is the local hydraulic radius calculated from the water depth, and S is the channel slope). The uniform flow assumption of the boundary shear stress is an approximation of the actual shear stress when the energy slope differs from the bed slope. According to the BSTEM technical documentation (Figure 6.1), "average boundary shear stress exerted by the flow

on each node is determined by dividing the flow area at a cross-section into segments that are affected only by the roughness of the bank or bed and then further subdividing to determine the flow area affected by the roughness of each node. The line dividing the bed- and bank-affected segments is assumed to bisect the average bank angle and the average bank toe angle."

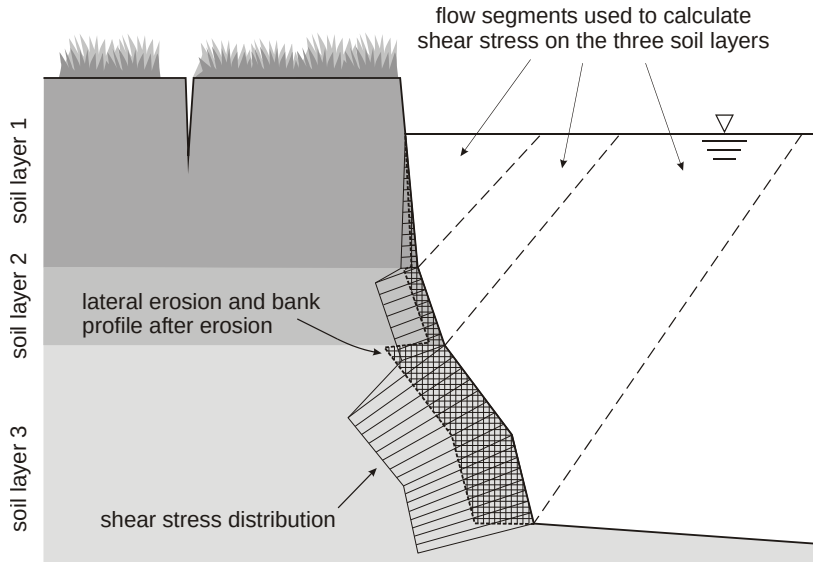

Figure 6.1. Segmentation of local flow areas and determination of the hydraulic radii in the calculation of the applied fluvial stress in the Bank Stability and Toe Erosion Model (BSTEM). Source: BSTEM technical documentation [20] and Simon et al. [34].

The bank stability module of BSTEM adjusts the pore-water pressure distribution according to the stage and groundwater elevation and soil properties, calculates the resulting soil weight, and calculates the stability of the bank based on the ratio of driving forces to the resisting forces expressed as a factor of safety (FoS). The FoS is determined through both horizontal layers and vertical slices. For horizontal layers, the model uses a limit equilibrium analysis in which the Mohr-Coulomb failure criterion is used for the saturated bank layers and the Fredlund criterion is used for the unsaturated bank layers.

The resisting forces in the model are defined by the modified Mohr-Coulomb equation:

$$s_r = c' + \psi \tan(\phi^b) + \sigma \tan(\phi') \quad (6.2)$$

where s_r is the shear strength of the soil (kPa), c' is the effective cohesion (kPa), σ is the normal stress (kPa), ϕ' is the effective internal angle of friction in degrees, ψ is the matric suction or the difference between the air pressure and pore water pressure (kPa), and ϕ^b is an angle that describes the relationship between shear strength and matric suction (degrees). Fredlund and Rahardjo (1993) assume ϕ^b to be between 10 and 20 degrees and that ϕ^b approaches ϕ' at saturation. The normal stress is defined as:

$$\sigma = W \cos(\beta) \quad (6.3)$$

The normal stress is modified by a hydrostatic confining force (P_i) when water is present in the channel and a hydrostatic-uplift force due to positive pore-water pressures on the saturated part of the failure plane (U_i). The hydrostatic-uplift force reduces the normal stress and therefore reduces the resistive force. Note from geometry that $P_i \cos(\alpha'-\beta)$ represents the component of the hydrostatic force acting into the bank and resisting motion. Therefore, the resistive forces (F_r) to failure are summed along the surface length of the failure plane (L) and summed across the number of horizontal layers, I:

$$F_r = \sum_{i=1}^{I} \left(c'_i L_i + \psi_i L_i \tan \phi_i^b + \left[W_i \cos \beta - U_i + P_i \cos(\alpha' - \beta) \right] \tan \phi_i' \right) \quad (6.4)$$

where c_i' is effective cohesion of i^{th} vertical layer (kPa), L_i is the surface length along the failure plane incorporated within the i^{th} vertical layer (m), W_i is weight of the i^{th} vertical layer (kN), P_i is the hydrostatic confining force due to external water level (kN m^{-1}) acting on the i^{th} vertical layer, β is failure-plane angle (degrees from horizontal), α' is local bank angle (degrees from horizontal), and ϕ'_i is the soil internal angle of friction of the i^{th} layer (degrees from horizontal).

Soil weight is the dominating driving force defined by

$$s_d = W\sin(\beta) \tag{6.5}$$

where s_d is the driving stress (kPa), W is the weight of the wet soil block per unit area of failure plane (kN m^{-2}), and β is the angle of the failure plane in degrees (Simon et al., 2000). This driving force is modified in cases where a hydrostatic confining force (P_i) is present. Note from geometry $P_i \sin(\alpha'-\beta)$ represents the component of the hydrostatic confining force acting upward along the failure plane and resisting the driving force. Therefore, the driving forces (F_d) leading to failure are summed across the number of horizontal layers, I, and represented by the following equation:

$$F_d = \sum_{i=1}^{I}\left(W_i \sin\beta - P_i \sin[\alpha'-\beta]\right) \tag{6.6}$$

Therefore, the FoS equation is given by the following equation:

$$FoS = \frac{\sum_{i=1}^{I}\left(c'_i L_i + \psi_i L_i \tan\phi_i^b + [W_i\cos\beta - U_i + P_i\cos(\alpha'-\beta)]\tan\phi_i'\right)}{\sum_{i=1}^{I}\left(W_i \sin\beta - P_i \sin[\alpha'-\beta]\right)} \tag{6.7}$$

Along vertical slices, the model examines the normal and shear forces active in slices of the failure blocks (portions of the bank above the failure surface). This model incorporates a four-step iterative process that includes the normal force acting at the base of a slice, N_j, interslice normal force, I_{nj}, and interslice shear force, I_{sj}, where j is the slice number and J is the total number of vertical slices. The F_r for vertical slices includes the cohesion force (c') quantified above over the specific length of the failure place in the vertical slice, Lj, the matric suction force, $\psi_j \tan\left(\phi_j^{\,b}\right)$, for each vertical slice, and the difference between the normal force and the hydrostatic-uplift force, $(N_j - U_j)\tan\phi_j'$, summed over the J vertical slices:

$$F_r = \cos\beta \sum_{j=1}^{J} \left(c'_j L_j + \psi_j \tan\phi_j^b + \left(N_j - U_j \right) \tan\phi_j^{'} \right) \tag{6.8}$$

The F_d for vertical slices is represented as the difference between the normal force (N_j) and the hydrostatic confining force (P_j), summed over the J vertical slices:

$$F_d = \sin\beta \sum_{j=1}^{J} \left(N_j \right) - P_j \tag{6.9}$$

Therefore, the FoS is given by the following equation:

$$FoS = \frac{\cos\beta \sum_{j=1}^{J} \left(c'_j L_j + \psi_j \tan\phi_j^b + \left(N_j - U_j \right) \tan\phi_j^{'} \right)}{\sin\beta \sum_{j=1}^{J} \left(N_j \right) - P_j} \tag{6.10}$$

For cantilever shear failures, *FoS* is merely a ratio of the shear strength of the soil layer(s) to the weight of the cantilever (overhanging soil layer or block) and similar to equation 6.7 above:

$$FoS = \frac{\sum_{i=1}^{I} \left(c'_i L_i + \psi_i \tan\phi_i^b - U_i \tan\phi_i^{'} \right)}{\sum_{i=1}^{I} \left(W_i - P_i \right)} \tag{6.11}$$

A complete derivation of the horizontal layer, vertical slice, and cantilever failure models can be found in the technical documentation or in a number of previous papers on the model (Midgley et al., 2012; Simon et al., 2000; Cancienne et al., 2008; Simon et al., 2009).

Failure is assumed to occur when the driving forces exceed the resisting forces (i.e. when *FoS* is less than one), and various combinations of failure plane angle and shear emergence elevation (on the bank face) are considered within the model in order to determine the failure plane with the lowest *FoS*. Following the completion of the bank stability component of BSTEM, the model redraws the bank (if failure has occurred) and then moves to the next time step of the hydrograph.

6.2.2 Influence of Riparian Vegetation

Because BSTEM is process-based, additional forces that affect bank stability can be added as components to the model. For instance, it is known that riparian vegetation can affect bank stability, and it is commonly assumed that the strength of plant roots anchored in the banks add some amount of strength to the soil which increases its resistance to mass failure. A force component termed root cohesion (c_r) (Simon and Collison, 2002; Pollen-Bankhead and Simon, 2009) is incorporated into the modified Mohr-Coulomb equation as an additive factor:

$$s_r = c' + c_r + \sigma \tan(\phi') + \psi \tan(\phi^b) \tag{6.12}$$

Pollen-Bankhead and Simon (2009) have added a c_r component to BSTEM, and discussed methods for estimating its magnitude, but these methods are dependent on intrusive and time-intensive root tensile-strength tests.

Most c_r studies involve direct shear testing of rooted soils in the laboratory (Gray and Ohashi, 1983) or *in situ* (Ziemer, 1981; Micheli and Kirchner, 2002). More recently, measurements of the root area ratio combined with tests of the tensile strength and/or pullout resistance of roots have been applied to calculating c_r (Easson and Yarbrough, 2002; Simon et al., 2006). These analyses have the advantage of directly measuring the parameters that affect the mechanical stability of banks, but the distinct disadvantage of requiring specialized equipment, time and expertise to conduct properly. Given that rapid assessment of stream sites is commonly conducted by personnel with moderate levels of specialized training, the possibility of collecting non-technical data for estimating c_r at streambank sites needs to be explored. For instance, it is a relatively simple field task to

estimate the above-ground biomass (AGB) at a site, and formulae exist to estimate root biomass from AGB. Intuitively, a relationship would seem to exist between root biomass and c_r, but there is little published literature that discusses such a relationship. Still, the question of the amount of bank stability added by roots remains an important question as landowners in many areas are encouraged to establish and maintain a riparian forest buffer next to their stream. This buffer improves wildlife habitat and water quality by acting as a treatment strip (Sabbagh et al., 2009; Fox and Penn, 2013), and these buffers may reduce streambank erosion and failure as well through c_r. A less intrusive method for estimating reasonable values of c_r for BSTEM simulations would be an important practical advance for collecting and utilizing c_r data.

6.2.3 Objectives

While BSTEM has been successfully tested and applied on a number of isolated cohesive streambanks (Cancienne et al., 2008; Simon et al., 2009), it has been less applied to composite banks with and without riparian vegetation on sinuous streams. For example, most streambanks in the Oklahoma Ozark ecoregion are composed of layers with contrasting textures, which have been labeled composite banks in the literature (Thorne and Tovey, 1981; Heeren et al., 2012). Erosion of these banks typically occurs in a sequence beginning when fluvial entrainment of the underlying, unconsolidated gravel layer produces an undercut upper bank, which eventually fails when the weight of the unsupported block exceeds the cohesive strength of the soil. These banks have shown very high rates of retreat, with a documented case of 20.9 m of bank retreat in a single flood event (Midgley et al., 2012; Heeren et al., 2012). Such erosion rates rule out

conventional methods for measuring erosion, such as erosion pins, while process-based modeling with BSTEM offers the possibility of deriving erosion data with detailed timing information that is based on site characteristics. One issue is that sinuosity is not explicitly considered in bank retreat estimation with BSTEM relative to increases in the applied shear stress. Adjustment approaches have been suggested in the literature but require further testing.

Understanding erosion in the watersheds of the Oklahoma Ozarks, with their composite streambanks, is important for resource conservation purposes, but is made technically challenging due to the magnitude and episodic nature of the erosion, and the high degree of variability of factors that affect erosion within the area. This study used a process-based bank erosion model to address three important research objectives. First, BSTEM was applied to a series of composite streambanks distributed along the Barren Fork Creek in eastern Oklahoma, in order to assess the ability of the model to simulate observed lateral retreat rates based on measured parameters with respect to composite banks and sinuous channels. Next, since there is currently a management effort in Oklahoma to maintain and expand riparian buffers for water quality protection and wildlife conservation, we attempt to develop simplified procedures for estimating root cohesion based on above- and below-ground biomass estimates and then determine the sensitivity of c_r for predicting lateral retreat on composite banks. Finally, we discuss the appropriateness of using erosion models rather than specific erosion study periods, such as with cross-sections surveys or erosion pins, in order to better estimate the episodic nature of erosion and failures for more informed long-term management decisions.

6.3 Materials and Methods

6.3.1 Description of Study Sites

Barren Fork Creek is a fourth order stream, originating in northwestern Arkansas, that flows west through the Boston Mountains and Ozark Highlands ecoregions, and reaches its confluence with the Illinois River at Lake Tenkiller near Tahlequah, OK (Figure 6.2). The Barren Fork Creek watershed is within the Illinois River watershed, which has many areas listed on the 303(d) list for nutrient and sediment related impairments. Barren Fork Creek has a natural meander and high degree of sinuosity, but land use changes over the past 150 years may have resulted in accelerated rates of streambank erosion and lateral channel migration. This watershed, which is typical of those in the Ozark ecoregion, is characterized by cherty soils and gravel bed streams (Midgley et al., 2012; Heeren et al., 2012). Streambanks within the watershed commonly are composed of two distinct layers with contrasting textures and properties (Figure 6.3). The top layer is typically a cohesive sandy loam or silt loam soil which can range in thickness from several centimeters to more than a meter (Figure 6.3 (a)). Underlying the topsoil, separated by a very sharp change in texture, is typically a packed gravel layer, similar in size to the streambed gravel, which also ranges in thickness from nonexistent to tens of centimeters or more (Figure 6.3 (b)). Also typically present is a gravel toe consisting of loose larger gravel particle sizes that have been detached from the packed gravel but not yet transported away (Figure 6.3 (c)). Previous research within the watershed has shown that the gravel bed extends downward to the bedrock which can be 10 m or more below the ground surface (Heeren et al., 2012).

Ten sites were selected at locations along Barren Fork Creek, which were designated by letters A-J (Figure 6.2, Figure 6.4). Several sites (B, C, D, G, H, I and J)

were known to have significant riparian tree coverage along their banks during all or part of the study period (2003-2010), and these sites will be referred to as historically protected sites (HP). The remaining sites (A, E, and F) had only pasture grasses during the study period, and will be referred to as historically unprotected sites (HUP). In the context of this study, riparian protection refers to the additional soil cohesion provided by tree roots which has the potential to reduce bank erosion. The HUP sites were distributed within the watershed, with Site B near the upstream end of the Oklahoma portion of the Barren Fork Creek watershed, and Sites E and F near the downstream end (Figure 6.2). Furthermore, several HUP and HP sites were paired; Sites A/B and Sites D/E were located within several hundred meters of each other (Figure 6.2).

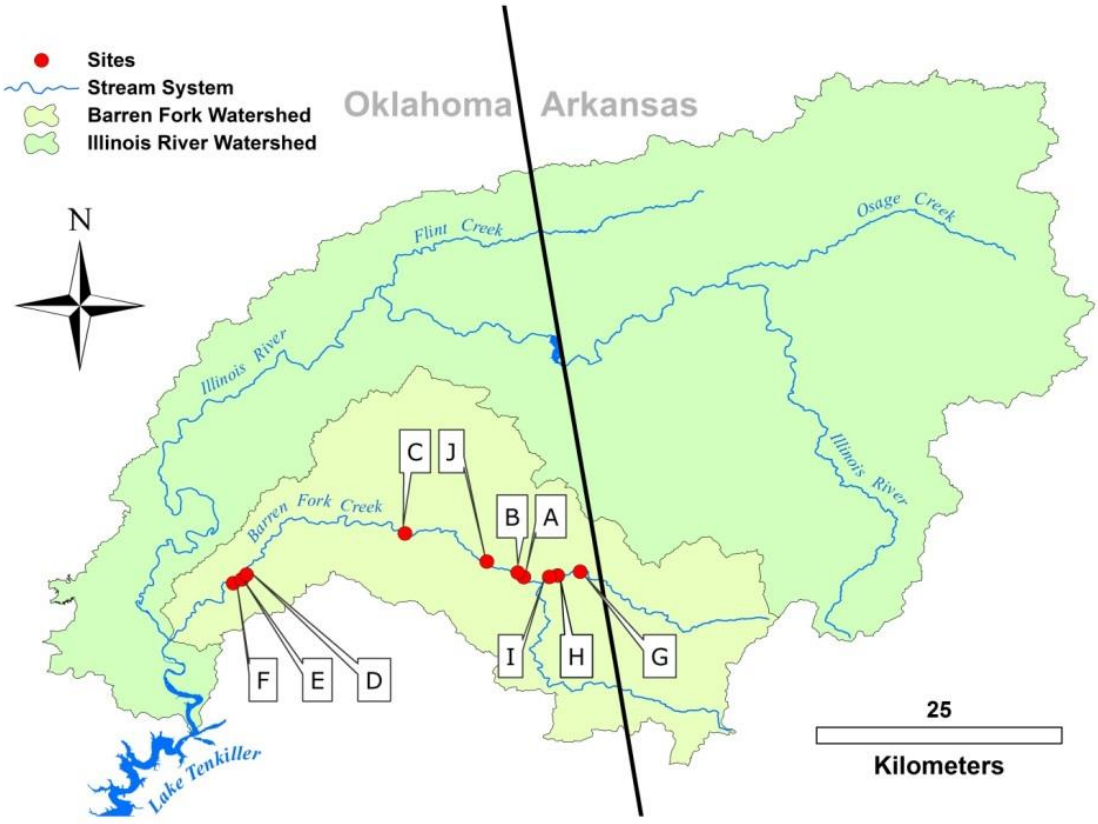

Figure 6.2. Barren Fork Creek watershed in Oklahoma and Arkansas, and study site locations.

Streambanks generally are either eroding (active), typified by steep banks that are close to the channel thalweg, or accreting (passive), typified by shallow gradients that are relatively distant from the channel thalweg. For this study only active banks were selected. A representative length of bank (reach) was identified at each site that had generally common characteristics including bank height, bank stratigraphy, and riparian cover. At each site a representative cross section was selected and a detailed bank stratigraphy prepared. A survey of the bank stratigraphy and stream channel was performed using a laser level or total station, and detailed notes kept of the thickness and texture of each bank layer, and the stream thalweg (deepest point in channel), as shown in Table 6.1. Additionally, a particle count was performed for each gravel-dominated layer in the cross-section, including the packed gravel, loose gravel toe and stream bed gravel. The stream slope along the reach was also measured by surveying the elevation drop along the thalweg from a riffle crest above the reach to one below the reach.

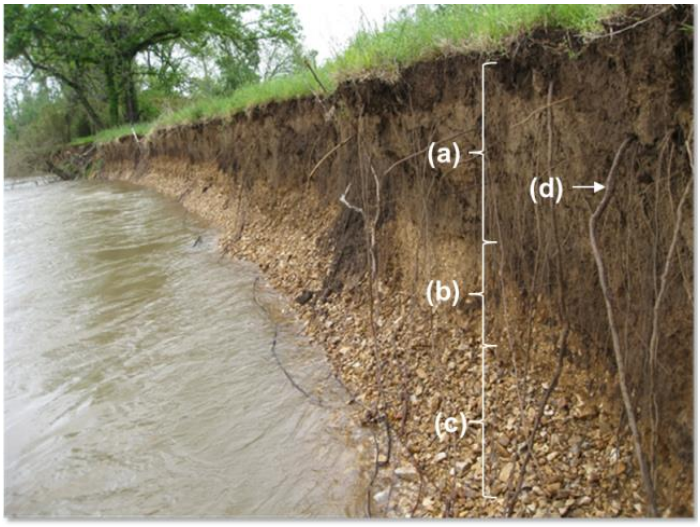

Figure 6.3. A Barren Fork Creek composite bank showing typical layers: (a) silt-loam topsoil, (b) packed gravel, and (c) loose gravel toe. Recent stream migration has eroded into (d) root zone of riparian tree near bank edge (not shown) (Midgley et al., 2012). Note that roots occupy only the cohesive soil layer, and do not extend into gravel layer. The steep bank profile is typical, and indicates that mass failure is the dominant mechanism of streambank erosion, which in this case is controlled by both the rate of fluvial undercutting of the gravel layers, and the strength of cohesive soil and tree roots (if present).

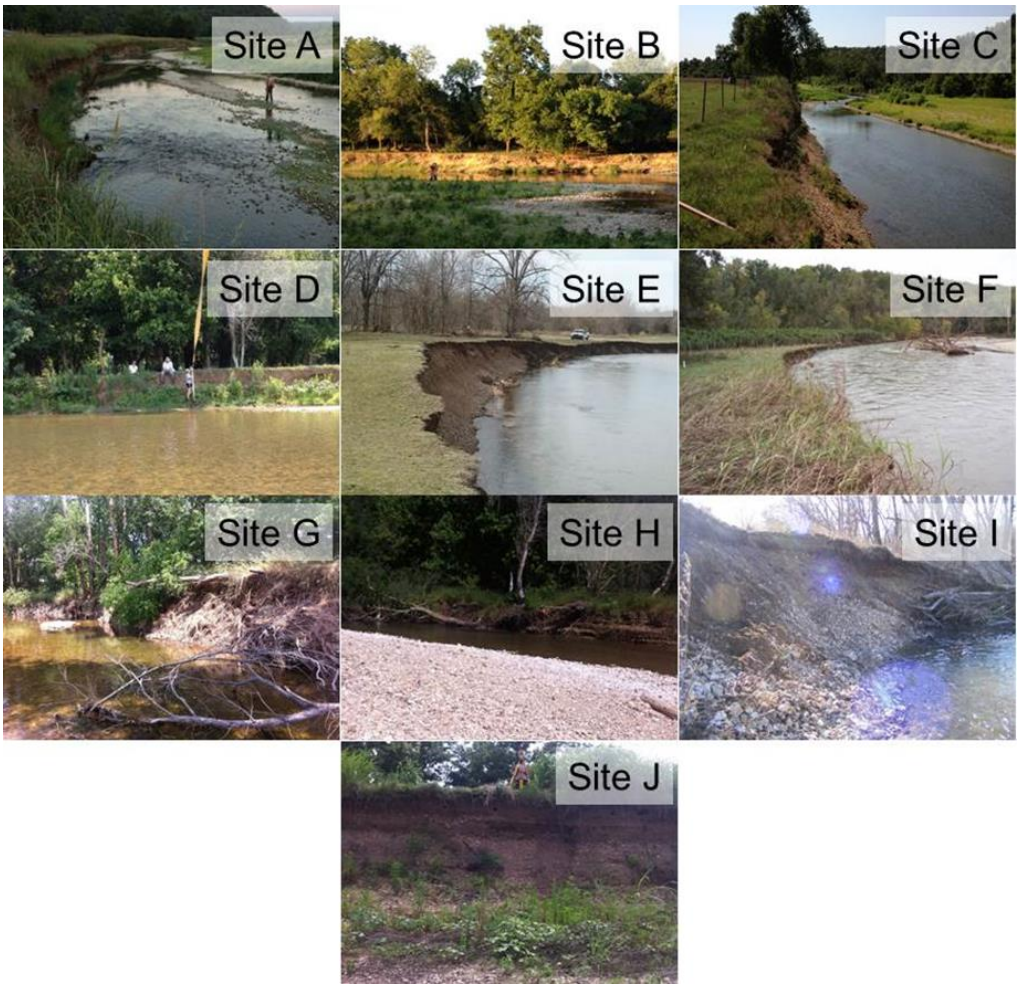

Figure 6.4. Pictures of Barren Fork Creek streambank sites, showing typically steep bank faces, cohesive topsoil, and coarse gravel subsoil. At some sites (G, H and I) riparian trees eroded from the bank top are visible at the bank toe.

6.3.2 Streambank Testing

The resistance of the streambanks to geotechnical failure and fluvial erosion were quantified at each site using *in situ* established field tests. The soil strength parameters *c'* and ϕ' of the cohesive soils were measured using the Borehole Shear Test (BST, Handy Geotechnical Instruments, Inc., Madrid, IA) in at least duplicate tests for the cohesive sandy loam or silt loam layer. The BST includes a shear head, which is inserted into a prepared borehole and expanded with a CO_2 pressure cylinder, which applies a known

normal force to a block of soil surrounding the shear head and causing it to consolidate. After allowing the soil water to re-equilibrate within the soil block, the test is performed by applying a shear force which pulls the consolidated soil block vertically through the borehole toward the BST. The shear force is increased until the soil block shears from the native soil, and that force is recorded. By sequentially increasing the normal stress and recording the shear stress a linear relationship is created in which the apparent cohesion corresponds to the y-intercept (kPa) and the ϕ' corresponds to the slope of the fitted line. The ψ was measured at a later time with a tensiometer from a sample acquired in the field, and the value applied to estimate c'. The unconsolidated gravels within the streambanks do not have cohesive strength and are only represented by a frictional resistance through ϕ', which was calculated from the median particle size (d_{50}) observed at each site.

Typically, the fluvial erosion rate of cohesive soils is quantified using an excess shear stress equation, dependent on the τ_c and k_d. A submerged jet test apparatus is one of the methods for measuring τ_c and k_d *in situ*, and has been used extensively for estimating τ_c and k_d for use in modeling streambank resistance to fluvial erosion (Hanson, 1990; Simon et al., 2010; Al-Madhhachi et al., 2013; Daly et al., 2013). In at least triplicate tests at each bank, the "mini" jet erosion test (JET) device was positioned on the face of the streambank in cohesive soil layers (i.e., sandy/silt loam above the gravel). Scour depth data versus time was analyzed using the scour depth solution from the automated spreadsheet routine of Daly et al. (2013). The τ_c for unconsolidated gravel layers was estimated based on the average gravel particle size using the following algorithm developed for noncohesive gravel particles on a slope (Millar, 2005):

$$\tau_c = 0.048 \tan(\phi')\rho g(s-1)d_{50}\sqrt{1-\frac{\sin^2\theta}{\sin^2\phi'}} \quad (6.13)$$

where ρ is the density of water (1000 kg/m^3), g is gravitational acceleration (9.81 m/s^2), s is the specific gravity of the bank soil (assumed to be 2.65 for all soils), d_{50} is the mean particle diameter of the soil (m), and θ is the bank angle (assumed to be 25°). Estimates of k_d for the unconsolidated gravel based on the estimated τ_c were derived from previous k_d-τ_c correlations (Simon et al., 2010; Hanson and Simon, 2001) and from previous bank modeling on similar sites (Midgley et al., 2012).

6.3.3 Aerial Imagery Analysis

Images from the National Agricultural Imagery Program (NAIP) from 2003, 2008 and 2010, all with 1 m horizontal resolution, were obtained for analysis. The images were georeferenced in ArcMap 10 (ESRI, Redlands, CA) and then used for determining bank erosion over time (Figure 6.5) following Heeren et al. (2012). A bounding rectangle, corresponding to the field-determined reach length (L_R), was created for each site. Within the rectangle, the bank edge for each NAIP image was digitized. Erosion was determined to have occurred when the digitized bank for the next NAIP appeared to be farther from the stream centerline than the previous bank. When erosion was determined to have occurred, a polygon was created using the two digitized bank locations, and the area calculated in m^2. For example in Figure 6.5, a polyline was drawn at the streambank profile in 2008, and this polyline was then overlaid onto the 2003 image. A polygon was then created showing the difference in the banks from 2003 and 2008. The same procedure was followed between the 2008 and 2010 images. The eroded area for an

elapsed interval (e.g. 2003-2008) was the area of a polygon (A_{2008}, m^2), and the bank retreat (R_{2008}, m) was calculated as A_{2008} divided by L_R. The total bank retreat (R_T) was the sum of R_{2008} and R_{2010}. Additionally, the aerial imagery was used to estimate the radius of curvature (e.g. ROC_{2008}) at each stream reach by drawing a circle with a perimeter overlying the bank edge and then adjusting the circle radius until the bank edge and perimeter matched as close as possible.

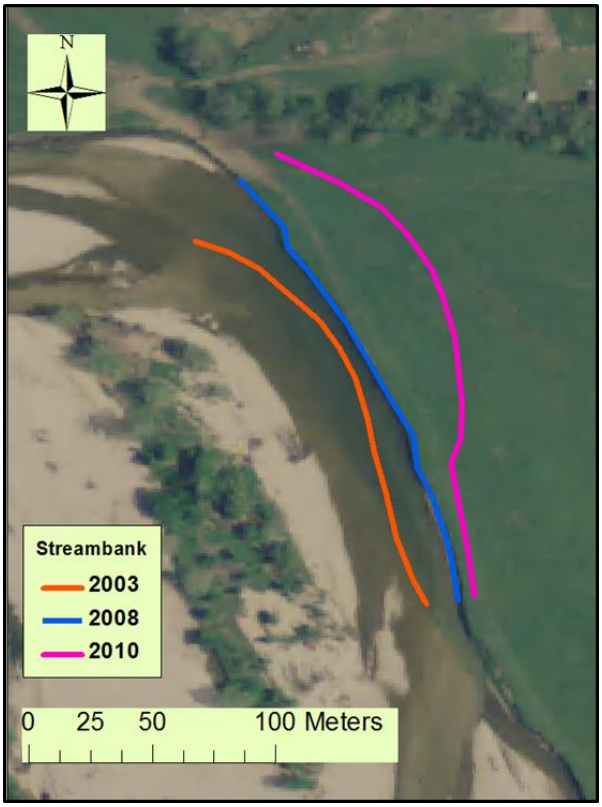

Figure 6.5. NAIP aerial imagery (2008) at Site A showing the bank retreat from 2003 to 2010.

6.3.4 Model Calibration

BSTEM input parameters included the soil strength parameters (W, c' and ϕ'), erosion resistance parameters (k_d and τ_c), and root cohesion parameters (c_r, if applicable and discussed below), as well as the stream hydrographs for the period 2003 to 2010.

Manning's *n* at each site was held constant and assumed to be 0.025. Site-specific rating curves were developed to determine the input stream stage at the thalweg. This rating curve was developed from discharges recorded at Barren Fork Creek USGS gauges and adjusted according to watershed area. The adjustment was made based on a weighting factor comparing the site watershed area to the gauge watershed area (Figure 6.6). The field-determined bank characteristics (i.e., erosion and geotechnical resistance parameters of the streambanks) were averaged and those values used as initial estimates for BSTEM. Bank retreat results from the BSTEM model runs were compared with the R_T as determined from the aerial imagery analysis.

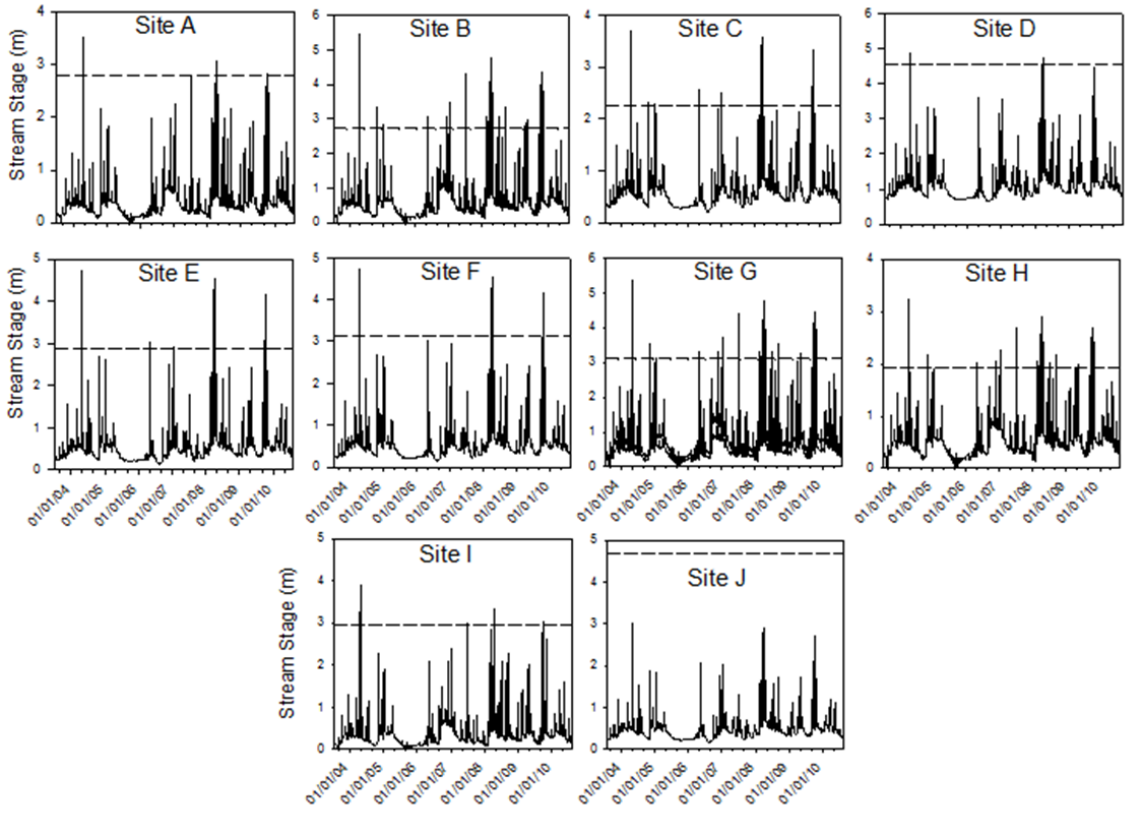

Figure 6.6. Site-specific hydrographs used for calibration. The dashed line represents bank height (m).

The main focus of the calibration process was on the fluvial erosion component of BSTEM because, as discussed later, BSTEM was insensitive to specific values of c' and c_r. Meander bends in rivers cause both curvature-driven and turbulence-driven secondary flows that alter the flow fields and the morphology of the bed and banks (Camporeale et al., 2007; Papanicolaou et al., 2007). River bends usually exhibit faster, deeper flows on the outside bend, and bank accretion and formation of point bars on the inside bend (Motta et al., 2012). These faster, deeper flows on the outside bend, along with the secondary flows, exert increased shear stresses on the streambank. Furthermore, spatial and temporal changes occur in the fluvial resistance of bank materials due to wetting/drying cycles, presence of roots, and moisture content over the simulation period. For example, fluvial resistance is typically quantified at a specific measurement time, but due to wetting/drying cycles and subaerial processes it has been observed that k_d and τ_c can change considerably over time. Therfore, a "lumped" adjustment factor (α, dimensionless) was used to modify equation 6.1 to account for the simplified hydraulics in BSTEM as well as potential changes in erodibility:

$$\varepsilon = k_d\left(\alpha\tau_0 - \tau_c\right) = \alpha k_d\left(\tau_0 - \frac{\tau_c}{\alpha}\right) \tag{6.14}$$

The α is directly proportional to k_d and indirectly proportional to τ_c, producing an increased k_d and decreased τ_c for any α greater than one. Previous studies have suggested that this adjustment factor represents the ratio of the applied shear stress at the bank site on the meander bend to the applied shear stress along the centerline of the channel, or the applied stress that would be expected without a meander bend (Langendoen and Simon, 2008), and has been utilized in previous studies with bank stability models (for examples, see Langendoen and Simon, (2008); Rousselot, 2009; Langendoen and Simon, 2009).

Proposed in this research is that α incorporates a number of different factors (hydraulics and erodibility characteristics) that are not easily separable.

Again, it is important to note that hydrodynamics plays a major role in determining the evolution of erosion processes. The current version of BSTEM utilizes a one-dimensional flow assumption; however, two-dimensional models have recently been integrated with bank stability models to attempt to more appropriately simulate the shear-stress distribution at the bank (Lai et al., 2014). For this study, erosion was so rapid that the stream cross-section changed rapidly (e.g., three-dimensional phenomena), and limited data was available at most of the ten sites to populate a two-or three-dimensional flow simulation at these sites. Some two- or three-dimensional models can predict changes in the stream cross-section but then data on incoming sediment loads and the sediment distributions are needed. Typical of many situations, such data is not available for the ten sites modeled in this research. Therefore, this research emphasized an approach for using a one-dimensional model. In cases where appropriate data exists to populate two- or three-dimensional flow codes, then modelers still need to account for spatial and temporal changes in the erodibility of the bank material. With that said, improved simulations of the imposed hydraulic stress may allow a focus on the estimation/modeling of spatial and temporal changes in erodibility. Future research should be performed with two- and three-dimensional hydraulic models combined with bank stability modeling to verify these statements.

The use of "lumped" calibration parameters have been utilized previously in modeling such dynamic systems. Millar (2000) suggests that the friction angle, ϕ', represents such a lumped calibration parameter when using an analytical model to study

alluvial channel patterns and bank stability. In this application, ϕ' accounts for several different processes (near-bank velocity, packing and imbrication, and others) that are not able to be accounted for individually. Millar equates this approach to the use of Manning's *n* to characterize hydraulic roughness (2000).

The α was used in situations where initial BSTEM modeled retreat was less than R_T. Also, calibration was guided by ensuring that the appropriate mechanism of failure, as observed during field monitoring, was predicted by BSTEM. Banks collapsed when fluvial erosion of the unconsolidated gravel undercut the streambank leading to mass failure. Specific α values may lead to unrealistic bank erosion and failure mechanisms, and so users of BSTEM should always confirm that field observed failure mechanisms are being adequately predicted. When the BSTEM bank retreat was greater than R_T, the τ_c of the cohesive soil layer was increased to no larger than the largest field-recorded value, and then the k_d of that layer was decreased until the BSTEM bank retreat was within 0.5 m of R_T. Additionally the topmost horizontal layer for all of the sites was modeled as an erosion-resistant thatch of grass at the floodplain surface following Midgley et al. (2012): that layer was given a thickness of 0.1 m, typical for the rooting depth of grass, a τ_c of 500 kPa, and a k_d of 0.004 $cm^3\ N^{-1}s^{-1}$. The high values for the topmost soil layer were used to ensure that the model does not erode the top layer during large flood events that overtop the bank. Grass layers are present at all bank sites with a large root area ratio that significantly influences the erodibility of the material. Therefore, high values of τ_c were used to prevent erosion from overtopping flows so that the model more appropriately predicted the failure mechanisms observed on the banks.

6.3.5 Root Biomass and Cohesion

The contribution of tree roots to the cohesion of the cohesive streambanks was not directly measured in this study. Instead the below-ground root biomass of live trees was estimated at each forested site (see a summary in Table 6.2). First, the species and diameter at breast height (DBH, m) was determined within a known area at each site; generally this included all trees within an area 100 m along the reach and 5 m of the bank edge. Next the above-ground biomass (AGB, kg) of each tree was estimated using the species-specific, diameter-based allometric equation (Jenkins, 2004), if available, or with a similar allometric equation intended for general hardwoods. The published R^2 for these equations ranged from 0.97 to 0.99 (Jenkins, 2004). The below-ground coarse root biomass (BGB, kg) per tree was estimated with the following equation (Jenkins, 2004):

$$BGB = ABG \times e^{-1.6911 + \frac{0.8160}{DBH}} \tag{6.15}$$

which calculates the BGB as a diameter-based ratio to AGB. Finally, the root biomass per soil volume (BGBv, kg m^{-3}) was estimated by calculating the sum of BGB for the surveyed area, then dividing by the biomass survey area times the cohesive soil depth from the channel cross section.

The root cohesion (c_r) calculation was based on the "RipRoot" subroutine in BSTEM. An assemblage of four floodplain hardwood species (Sycamore, Black Willow, Cottonwood and River Birch) was created in RipRoot, each of which was assumed to be 10 years old. A range of c_r values were calculated using that assemblage by varying the percent Bare Earth (%BA) from 0 (no trees) to 100% (no space between trunks). The calculated c_r using this method ranged from 0 to 6 kPa. The sum of the total BGB was divided by the product of surveyed area and mean topsoil thickness as calculated from

site surveys. This average root biomass per cubic meter was entered into the c_r model to estimate the root cohesion. To properly enter this value into the RipRoot module of BSTEM, the %BA was back-calculated, and the remaining percent area divided equally among each of the four floodplain trees species listed above. A summary of these equations are shown in Table 6.2.

Table 6.1. Equations used to calculate root cohesion (c_r).

	Equation	Units
General Hardwood Allometric Equation[1]	$\log_{10} AGB = -1.247 + 2.663\{\log_{10}(DBH)\}$	DBH = cm AGB = kg
Below Ground Biomass (BGB) per Individual Tree[1]	$BGB = ABG \times e^{-1.6911+\frac{0.8160}{DBH}}$	DBH = cm BGB = kg
Site Below-Ground Biomass (BGB_v)	$BGB_v = \sum_{1}^{n} BGB * (a \times d)$	BGB_v = kg m^{-3} a (survey area) = m^2 d (soil depth) = m
Modeled Root Cohesion (c_r)	c_r = -1.28x10^{-5}BGB$_v^5$ +8.77x10^{-4}BGB$_v^4$-2.10 x10^{-2}BGB$_v^3$ +1.88x10^{-1}BGB$_v^2$-7.15x10^{-2}BGB$_v$	c_r = kPa
Percent Bare Earth (%BA) Calculation	%BA = -16.778 c_r + 99.641	
10-yr Tree Percent (*10yr*) Calculation[2]	$10yr = \frac{100 - BA\%}{4}$	

6.3.6 Critical Study Period

Field measurement of streambank erosion can be a time-consuming and labor-intensive process, requiring repeated surveys utilizing permanent survey monuments or bank erosion pins. Both of these methods require the time of trained personnel over a period encompassing one or more years to assess the rate of erosion. Since bank erosion is linked to stream flow, and stream flow varies over time, shorter monitoring periods are likely to be much more variable in assessing bank erosion, with a particular period likely

to over- or under-estimate the rate of erosion. To quantify the impact of monitoring period on these banks that experience episodic extreme erosion events, the BSTEM modeled bank retreat over the 7-yr study period, which included years with flows both above and below the average flow, was divided into 1-, 2-, and 3-yr intervals and the BSTEM bank retreat totaled for those periods.

6.4 Results and Discussion

6.4.1 Aerial Imagery Analysis of Bank Retreat

The analysis of NAIP imagery from 2003, 2008, and 2010 noted bank erosion at every site almost each interval. The R_T ranged from 4.1 to 74.8 m and was largest at the HUP sites (A, E and F) which averaged 49.2 m, although the R_T at several HP sites (G and I) were close to or exceeded that magnitude (Figure 6.7, Table 6.1). The R_T at HP sites were generally less than 12 m over the study period, and averaged 17.5 m. While the difference in means was apparent, a t-test of the difference in means was not statistically significant ($P = 0.058$, $\alpha = 0.05$) because of the high variance in the HP sites. Episodic and massive bank failures occur when an erosive flow event occurs after the banks have been wet by previous storm events, removing matric suction as a component of the apparent cohesion of the streambanks (Midgley et al., 2012).

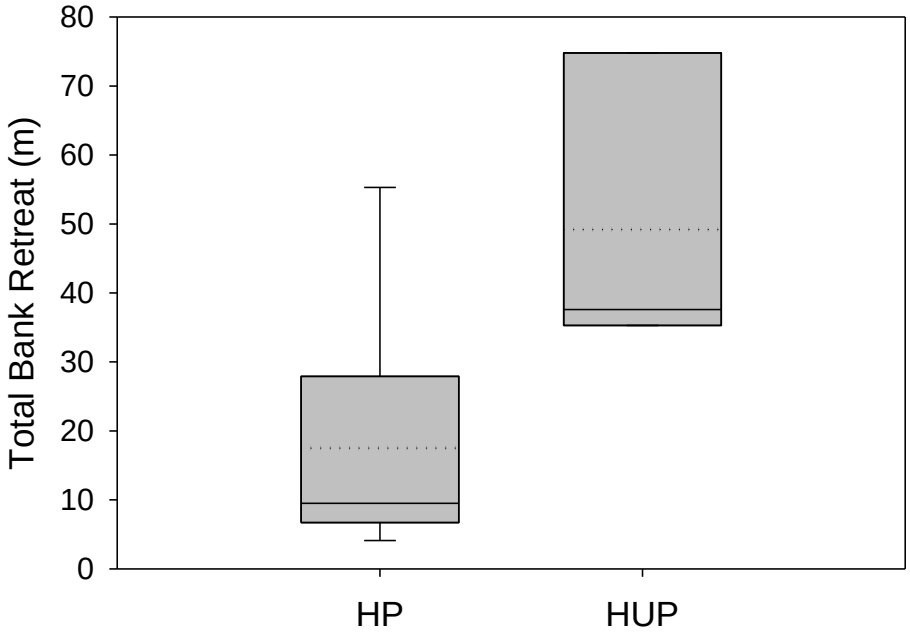

Figure 6.7. Box plot of the total bank retreat (RT) for the seven historically protected (HP) and three historically unprotected (HUP) study sites. The median value is designated by the solid, central line, the 1st and 3rd quartiles by the box extent, the whiskers indicate the 10th and 90th percentiles, and the mean value is shown as the dashed line. A t-test for the difference between the groups was not statistically significant (P = 0.067, α = 0.05).

Table 6.2. Surveyed characteristics of study sites.

Site	Latitude, Longitude	Historically Protected (HP) or Unprotected (HUP)[a]	Adjacent Land Use	Watershed Area, A (km^2)	Reach Length, L_R (m)	Total Retreat, R_T (m)	Total Bank Height, BH (m)	Cohesive Soil Thickness, D_{ts} (m)
A	35.91027, -94.58778	HUP	Pasture and Row Crops	363	190	35	2.80	1.58
B	35.91277, -94.59451	HP	Riparian Corridor	364	233	7	2.72	0.93
C	35.94878, -94.6993	HP	Pasture	544	138	7	4.57	2.16
D	35.91085, -94.8431	HP	Pasture	829	182	10	2.25	0.58
E	35.90633, -94.8465	HUP	Pasture	830	185	75	2.88	0.77
F	35.90276, -94.8548	HUP	Pasture	845	190	38	3.15	1.31
G	35.91352, -94.5373	HP	Riparian Woodland	150	105	28	3.10	0.76
H	35.90997, -94.55791	HP	Riparian Woodland	176	61	12	1.93	0.64
I	35.90877, -94.56565	HP	Riparian Woodland	178	87	55	2.95	0.37
J	35.92275, -94.62285	HP	Riparian Woodland	449	65	4	4.69	1.00

6.4.2 Bank Stability Modeling

Multiple regression of τ_c, k_d and c_r against bank retreat (m) was used to determine which BSTEM model inputs significantly affected bank retreat. For these composite banks, only k_d was a significant predictor ($\alpha = 0.05$). The sensitivity of c_r on the simulated bank retreat was further evaluated by increasing the c_r in the calibrated unprotected sites (A, E, and F). While c_r had no significant effect on the large amounts of bank retreat evident at those sites, increasing the c_r did seem to affect the variability of retreat. For instance, various magnitudes of c_r were added to the calibrated BSTEM model for Site A (R_T = 35.9 m), and the model re-run. The resulting R_T ranged from 29 to 70 m, with no systematic change with increasing c_r. Because c_r adds to soil strength, increasing c_r may either reduce retreat slightly by allowing the cohesive soils to form an overhanging shelf as the gravel layer is eroded away, or increase retreat by causing larger soil blocks to fail.

Sites B, C and D had riparian forest along the bank, and while the BSTEM initial calibrations for those sites included adding c_r, the final model was calibrated by decreasing the initial k_d, which suggested that the presence of tree roots in the bank soil affected soil erodibility. The effect of tree roots on streambank erodibility (k_d) has been addressed (e.g. Pizzuto et al., 2010), but no predictive relationships existed that could be used in BSTEM.

The BSTEM models were calibrated at each site by manipulating α, τ_c, and k_d (Table 6.3) until the BSTEM predicted R_T approached the aerial R_T. With the calibrated values, BSTEM was predicting the appropriate failure mechanisms of fluvial toe erosion of the unconsolidated gravel leading to bank undercutting and sloughing of the consolidated, cohesive sandy loam or silt loam layers (Figure 6.4), commonly observed

in a number of streambank studies at similar composite banks (Rinaldi et al., 2008). Evidence of this failure mechanism was visually observed during monitoring of erosion at several of the sites, and also Heeren et al. (2012) noted evidence of this failure mechanism (fluvial toe erosion and sloughing of consolidated, cohesive layers) at sites throughout this and similar watersheds while conducting rapid geomorphic assessments. Miller et al. (2014) also noted a helicopter video survey of the banks in the Barren Fork Creek watershed which again supported the modeled bank failure mechanisms. Good agreement existed between the total retreat predicted by the calibrated BSTEM models for each site and the R_T measured from NAIP aerial imagery for the entire simulation period from 2003-2010 (Figure 6.8). More importantly the observed/predicted agreement was also good for the interim time intervals 2003-2008 and 2008-2010 as well. Nearly all sites fall close to the 1:1 line, showing that BSTEM was generally good at predicting the timing of retreat. This shows that BSTEM is capturing the erodibility events in a realistic manner. Close examination of Figure 6.8a reveals outliers for both the 2003-2008 and 2008-2010 intervals. The distribution of bank retreat for each sampling interval and site type are displayed in boxplots (Figure 6.8b), and those outliers occurred in HUP sites and are most evident in the 2008-2010 interval, where the difference of means was significant ($P = 0.008$, $\alpha = 0.05$).

Table 6.3. Calibrated and original (base case) BSTEM model parameter values for Barren Fork Creek sites. Note that ϕ' is internal angle of friction, c' is cohesion, S_w is saturated weight of soil, τ_c is critical shear stress, k_d is soil erodibility, α is a factor that accounts for the stream radius of curvature at the site, and c_r is root cohesion based on the tree root biomass estimate. Historically unprotected sites have no c_r calibration.

Site		Material	ϕ' (°)	c' (kPa)	S_w (kN/m^3)	τ_c (Pa)	k_d (cm^3/Ns)	α	Bank Ht (m)	Soil Depth (m)	Root Depth (m)	c_r (kPa)
A	Calibrated	Soil	31.8	3.0	18	0.8	10.0	1.2	2.80	1.58	*	*
		Gravel	31.0	0.0	20	2.9	1.4					
A	Base Case	Soil	31.8	3.0	18	1.0	660.0	1	2.80	1.58	*	*
		Gravel	31.0	0.0	20	3.5	1.2					
B	Calibrated	Soil	35.9	5.0	18	3.9	8.1	1	2.72	0.93	0.90	1.5
		Gravel	34.8	0.0	20	5.5	1.0					
B	Base Case	Soil	35.9	5.0	18	2.4	35.5	1	2.72	0.93	0.90	1.5
		Gravel	34.8	0.0	20	5.5	1.0					
C	Calibrated	Soil	38.2	2.9	18	2.8	5.3	1	4.57	2.16	1.00	3.4
		Gravel	33.9	0.0	20	7.0	0.8					
C	Base Case	Soil	38.2	2.9	18	2.8	7.3	1	4.57	2.16	1.00	3.4
		Gravel	33.9	0.0	20	7.0	0.8					
D	Calibrated	Soil	26.0	6.3	19	5.5	5.4	1	2.25	0.59	0.58	6.8
		Gravel	32.0	0.0	20	6.1	0.9					
D	Base Case	Soil	26.0	6.3	19	0.8	148.9	1	2.25	0.59	0.58	6.0
		Gravel	32.0	0.0	20	6.1	0.9					
E	Calibrated	Soil	26.0	6.3	18	0.8	50.0	3	2.88	0.77	*	*
		Gravel	32.1	0.0	20	1.5	3.2					
E	Base Case	Soil	26.0	6.3	18	2.4	53.6	1	2.88	0.77	*	*

	Site	Material	ϕ' (°)	c' (kPa)	S_w (kN/m^3)	τ_c (Pa)	k_d (cm^3/Ns)	α	Bank Ht (m)	Soil Depth (m)	Root Depth (m)	c_r (kPa)
F	Calibrated	Soil	31.8	3.0	18	1.0	10.0	1.35	3.15	0.74	*	*
		Gravel	31.0	0.0	20	6.4	1.1					
F	Base Case	Soil	31.8	3.0	18	1.4	121.9	1	3.15	0.74	*	*
		Gravel	31.0	0.0	20	8.7	0.8					
G	Calibrated	Soil	38.0	10.4	18	1.0	20.8	3.7	3.10	0.76	0.75	5.4
		Gravel	32.4	0.0	20	1.3	3.8					
G	Base Case	Soil	38.0	10.4	18	1.0	67.8	1	3.10	0.76	0.75	5.4
		Gravel	32.4	0.0	20	4.8	1.0					
H	Calibrated	Soil	36.8	6.5	18	1.3	3.1	1	1.93	0.64	0.65	2.3
		Gravel	31.0	0.0	20	5.8	0.8					
H	Base Case	Soil	36.8	6.5	18	0.7	393.7	1	1.93	0.64	0.65	2.3
		Gravel	31.0	0.0	20	5.8	0.9					
I	Calibrated	Soil	35.1	1.0	18	0.8	111.5	1.25	2.95	0.37	0.36	5.4
		Gravel	32.8	0.0	20	4.3	1.2					
I	Base Case	Soil	35.1	1.0	18	1.1	89.2	1	2.95	0.37	0.36	5.4
		Gravel	32.8	0.0	20	5.3	1.0					
J	Calibrated	Soil	41.9	4.9	18	2.3	13.3	1	4.69	1.00	0.98	3.0
		Gravel	34.1	0.0	20	7.2	0.5					
J	Base Case	Soil	41.9	4.9	18	2.3	29.4	1	4.69	1.00	0.98	3.0
		Gravel	34.1	0.0	20	4.4	1.1					

HUP sites in general have the highest magnitude of R_T, and some factors that may help explain the disparity between observed and predicted erosion for the two outlier sites may be related to the BSTEM model. BSTEM uses a fixed bed location for the duration of the model hydrograph, so that bank retreat creates a bank profile with an extended bank toe. When R_T magnitudes are relatively small, the bank profile does not change much, and the distributions of erosive forces exerted by the water column over the wetted perimeter remain realistic. However, when R_T magnitudes are large, in our scenarios they reach up to 60 m, BSTEM draws an unrealistic bank profile with a bank toe that extends a large portion of that distance. This, in turn, will produce an unrealistic distribution of erosive forces along the wetted perimeter.

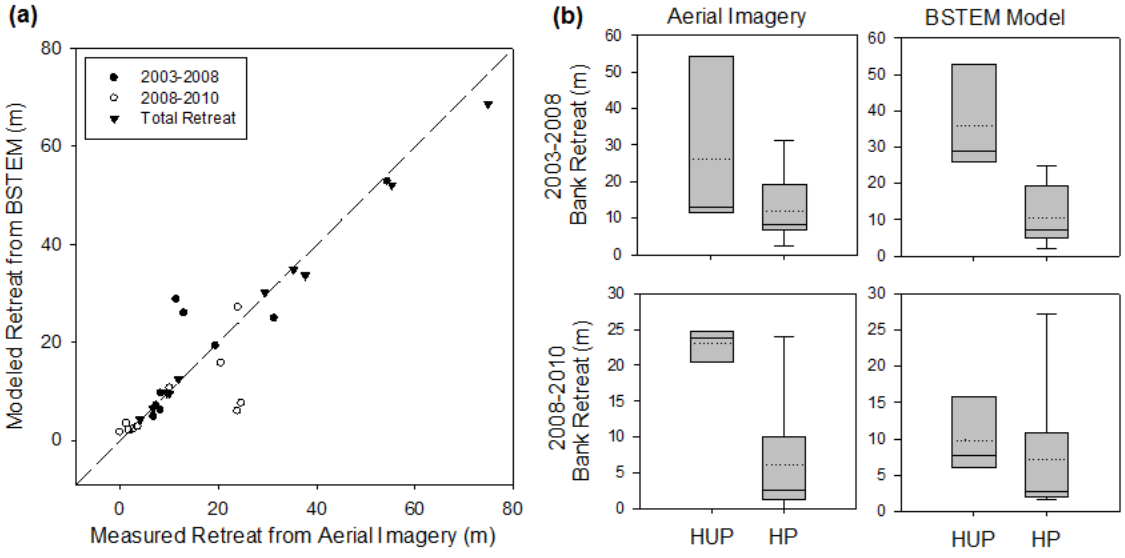

Figure 6.8. Comparison of measured bank retreat (R_T) from aerial imagery to predicted retreat estimates from BSTEM based on (a) linear regression and (b) box plots. Perfect agreement is shown as the dashed line in (a).

Additionally, R_T is a component of stream meandering whereby the planform of a stream, including the local radius of a stream bend, changes over time. When a stream reach undergoes large rates of R_T, such as those noted in this study, the reach will also

experience rapidly changing ROC and the associated local effects of turbulence. Thus, bank retreat may produce hydraulic conditions that further increase the rate of retreat. However, BSTEM assumes a straight stream reach, and the adjustment factor α (equation 6.14) was constant during a simulation. This disparity between variable field conditions and model constants was likely to be greatest when R_T was large. While there was no clear correlation between α and ROC, the sites with the most variability in ROC will have the highest standard deviation of ROC (ROC_{SD}), and a plot of α and ROC_{SD} shows that the highest α corresponded to the lowest ROC_{SD} and the largest R_T (Figure 6.9). This makes intuitive sense; a high ROC_{SD} implies that the ROC and hence the erosive characteristics of the curve also changed dramatically at the site; in contrast, α used in BSTEM to simulate those erosive characteristics was constant over the modeling period. Therefore, predictions of the timing of bank retreat were likely affected, and especially at sites with the highest ROC_{SD}. Future bank stability modeling over a long-term period may need to consider changes in the ROC through a time-dependent α if using a one-dimensional flow model or moving towards two- or three-dimensional flow modeling.

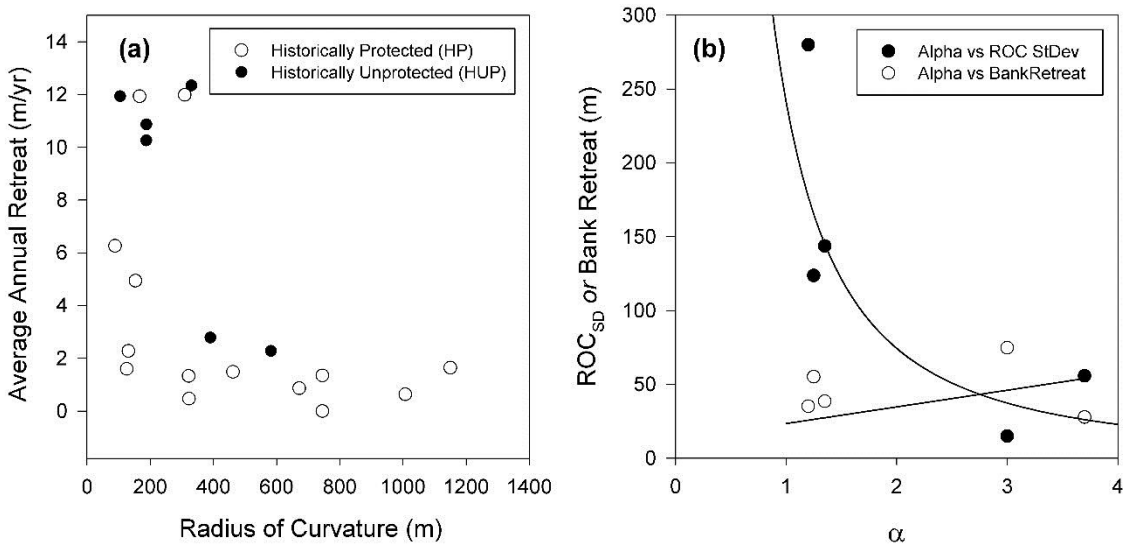

Figure 6.9. (a) Radius of curvature (ROC, estimated from aerial imagery) and the average annual bank retreat (m/yr) for historically protected (HP) and historically unprotected (HUP) sites, showing that the range of ROC and bank retreat was broad for both types of sites. (b) BSTEM α (dimensionless) versus the standard deviation of radius of curvature (ROC_{SD}, solid symbol) estimated from aerial imagery and BSTEM modeled bank retreat (hollow symbol).

As discussed, α not only incorporates hydraulic variability in terms of changes in the ROC, but also temporal and spatial variability of the erodibility parameters, τ_c and k_d. The lack of relationship between α and ROC suggests that α may be predominantly accounting for the spatial and temporal variability of the erodibility parameters. In some cases, large discrepancies existed between the field-measured erodibility parameters and those used in the calibrated model. The erodibility parameters were derived based on triplicate JETs assuming that the silt or sandy loam cohesive soil layer was uniform within a streambank profile. However, in many cases, sand lenses and additional heterogeneities may exist on a bank. Also, it is unknown whether triplicate JET tests accurately assess the actual spatial variability and adequately characterize the erodibility of the streambank. More research is needed to determine variability associated with JETs on streambanks and how appropriate derived parameters may be relative to the solution

approach. Furthermore, parameters from JETs are derived for the erodibility of the material at a discrete point in time. The temporal variability in erodibility parameters, much like the temporal changes in ROC, is not being captured by a constant α. As discussed earlier, even if a more advanced model (e.g., Lai et al., 2014) was used to simulate the applied boundary shear stress to account for changes in the ROC, a calibration factor may still be required to overcome the current limitations with representing temporal and/or spatial variability in erodibility parameters. Therefore, moving to a more sophisticated approach for estimating applied boundary stresses most likely will still require calibration of the model to adequately predict fluvial erosion in such a dynamic system. Future research should be performed to quantify changes in fluvial erosion potential over time.

6.4.3 Field Monitoring of Streambank Erosion Rates

As might be expected, a 1-yr monitoring period was highly variable for both HUP (Figure 6.10) and HP sites (Figure 6.11), with some HP sites having no erosion for one or more years. Erosion at the HUP sites was detected for each 1-yr period, but the rates varied, with some yearly rates as high as 24 m/yr (Figure 6.10, Site E). The 3-yr monitoring intervals were more consistent; however, there is a loss in resolution as the higher erosion rates are gradually averaged out over a longer period of time. For example, for the HP sites (Figure 6.11), a 1-yr monitoring record could produce a maximum retreat rate of nearly 25 m/yr at Site I while a 3-yr monitoring record may only show an averaged maximum retreat of less than 15 m/yr.

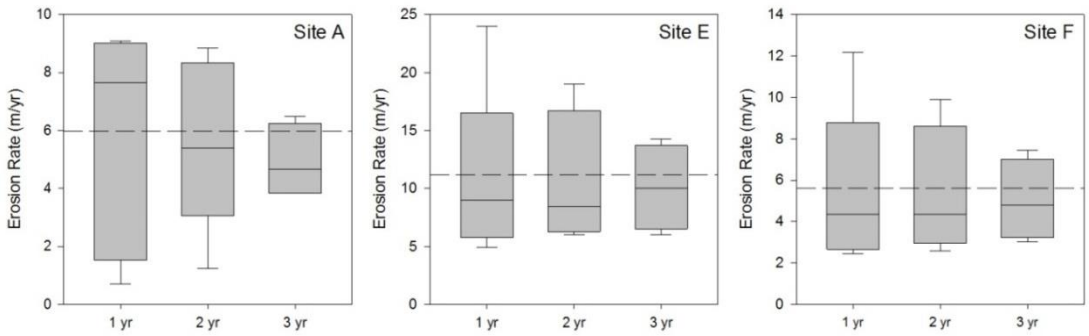

Figure 6.10. Erosion rates averaged over 1, 2, and 3 yrs at the historically unprotected sites. The dashed line represents the 6 yr averaged erosion rate.

Also, the period in which monitoring takes place can make a drastic difference on estimated annual bank retreats. Using Site I again as an example, if a 2-yr monitoring period was chosen to estimate the annual average retreat, the estimates would be drastically different if that survey was taken in 2006 to 2007 as opposed to 2008 to 2009. Estimates for a 2-yr monitoring period for 2006 to 2007 would be approximately 2 m/yr of bank retreat while estimates for 2008 to 2009 would be approximately 18 m/yr of bank retreat.

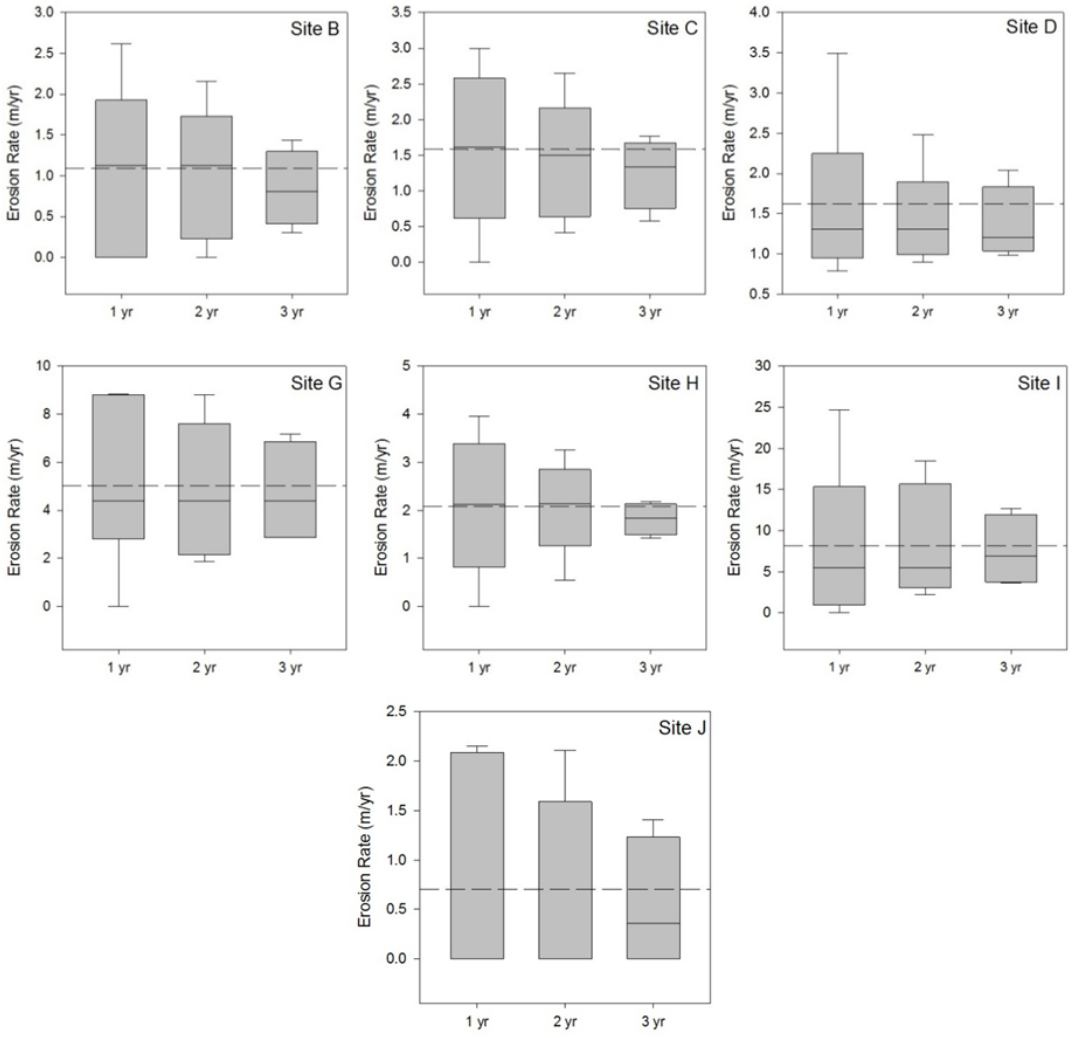

Figure 6.11. Erosion rates averaged over 1, 2, and 3 yrs at the historically protected sites. The dashed line represents the 6 yr averaged erosion rate.

These comparisons (Figure 6.10 and 6.11) illustrate the episodic nature of streambank erosion and bank retreat. Longer-term monitoring may not capture the active years of bank erosion while short-term monitoring may miss erosion events altogether. There is a need for the use of bank stability models such as BSTEM that use physical processes based on site characteristics to incrementally model bank retreat for long periods of time. This will provide a better set of tools for watershed managers to use

when making management decisions associated with site stability or sediment and nutrient loading.

6.5 Conclusions

Analysis of NAIP imagery from the streambank sites from 2003, 2008, and 2010 found that bank retreat at the historically unprotected sites averaged close to 50 m, while historically protected sites averaged approximately 18 m. When calibrating the BSTEM to match this observed NAIP retreat for these composite streambanks it was found that soil erodibility (k_d) was the only significant predictor of bank retreat. The riparian tree coverage at study sites was included in BSTEM as root cohesion (c_r), which increases the ability of soil to resist mass failure. This parameter was found to have no systematic effect on reducing bank retreat in these composite banks where the main mechanism of retreat was erosion of the underlying gravel layer. An important effect of streambank riparian tree cover was the ability of tree roots to reduce fluvial erosion, but there were no predictive models of this effect, so it was not included in BSTEM. However, a significant difference was found between historically protected and historically unprotected sites, which given that k_d was the significant retreat predictor, implies that the riparian forest reduced erosion where it was present. An accurate assessment of streambank retreat rates is important for many stream management decisions, but acquiring those data when retreat is both spatially and temporally variable can be problematic. An important factor was how long a period should be established for surveying. While the temporal sensitivity of the aerial imagery was limited to the acquisition frequency, the BSTEM model results allowed the simulation of various sampling durations. It was found that shorter sampling periods (1 to 2 yr) had high

variance while a 3-yr period had much less variance and the tendency for major retreat events to be averaged out over time. This highlights the importance of using bank stability models to conduct more long-term studies in order to properly capture the episodic nature of bank failures and retreat on composite banks such as those seen in this study. Process-based models, such as BSTEM, are needed for systems such as these where there is a high degree of variance in retreat rates from year to year. More research is needed to enhance the prediction abilities of the models, especially concerned with riparian vegetation and understanding the spatial and temporal variability of erodibility parameters.

6.6 Acknowledgements

The authors acknowledge the financial assistance of a 2012-2013 Oklahoma Water Resources Research Institute (OWRRI) and Oklahoma Water Resources Board (OWRB) grant through the USGS 104(b) grant program and FY 2012 319(h) Special Project #C9-00F56701.

CHAPTER 7

CONCLUSIONS

7.1 Conclusions

The overall objectives of this research were (1) to evaluate new solution methodologies for the derivation of the erodibility parameters, τ_c and k_d, from the JET, (2) investigate the erodibility parameters using all three techniques by considering parameter uniformity, correlations between the derived parameters and physical soil properties, and the applicability of currently proposed relationships to estimate the erodibility parameters at both a site and watershed scale, and (3) to apply the results from JET data to composite streambanks within a process-based modeling framework. The following conclusions were obtained from this dissertation:

1. The original Blaisdell technique for deriving the erodibility parameters from JETs did not always converge to a reasonable solution based on a visual observation of the dimensionless scour versus time. Therefore, a new spreadsheet tool was developed to incorporate an automated scour depth and iterative solution approach. This tool provides the Blaisdell solution, scour depth solution, and iterative solution approaches for use at the discretion of the user.
2. The scour depth solution was stable within the ranges tested and converged on the same solution despite different initial parameter estimates. The scour depth

solution fit the dimensionless scour function optimization better than the original Blaisdell solution, which tended to under predict the critical shear stress.

3. Results from the new scour depth solution showed similar trends in relationships between erodibility parameters as reported by previous research; however, these trends may need to be revisited with the alternative solution approach.
4. The results from a watershed scale study of JETs showed a wide range in variability throughout the watershed in both the estimated erosion parameters and the soil characterization. This highlights the fact that, while upon observation many of the soils seem uniform across the watershed, they are actually different from an erosion perspective and produce different values for τ_c and k_d or b_0 and b_1. This study demonstrated similarities between the excess shear stress parameters, k_d and τ_c, and the Wilson model parameters, b_0 and b_1, as applied to field data.
5. The variability observed at both a site and watershed scale in the erodibility and Wilson model parameters may be due to subaerial processes and more research is needed in order to quantify the spatial and temporal effects of these processes on the erodibility parameters.
6. Using default or general values to characterize erosion rates at multiple sites across a watershed may not produce the most representative result. Site-specific measurements are needed in order to properly quantify fluvial resistance to erosion.
7. The current relationships analyzed in these studies are used to estimate τ_c or k_d within the predictive framework of erosion models; however, they lack validation

outside of their original derivation and are largely applied for lack of a better estimate. Site-specific measurements are necessary when characterizing the erodibility of cohesive soils. Also, progress towards a mechanistic approach to modeling cohesive soil erosion is needed.

8. Determining the sample size needed to accurately estimate the erodibility parameters derived from the JET depends on the solution technique, the parameter being estimated, the degrees of precision and confidence necessary, and the presence of spatial dependency.
9. In general, the iterative and scour depth solutions may require more samples than the Blaisdell solution for the equivalent amount of precision and confidence due to the larger variance in parameter values.
10. Estimating k_d, regardless of solution technique, requires more samples than would be needed for estimating τ_c with the same amount of precision and confidence due to the larger magnitude and range in values.
11. Understanding the variability in these parameters and the amount of precision necessary is a major gap in this field of work at the current time.
12. At the site scale the critical shear stress and erodibility coefficients varied by up to three orders of magnitude, consistent with other studies.
13. While there were correlations between the erodibility parameters and measured soil variables, there were no reliable relationships with strong predictive capabilities at any of the sites for any of the variables.
14. There were no significant multiple linear regressions to predict the erodibility parameters based on more than one soil parameter.

15. Bulk density was not a significant predictor of erodibility. Moisture content was also not a significant predictor of erodibility in most cases. The texture at each site was responsible for most of the correlations to the erodibility parameters. Also a vertical zoning trend was evident at some sites.
16. Erodibility parameters must be measured in situ and cannot be estimated from empirical relationships due to the heterogeneous nature of soil and the variability in subaerial processes.
17. More research is needed in order to quantify the role of vegetation and subaerial erosion in order to incorporate temporal and spatial variation in the erodibility of streambanks into channel evolution models.
18. When calibrating the BSTEM to match this observed NAIP retreat for these composite streambanks it was found that soil erodibility (k_d) was the only significant predictor of bank retreat.
19. The riparian tree coverage at study sites was included in BSTEM as root cohesion (c_r), which increases the ability of soil to resist mass failure. This parameter was found to have no systematic effect on reducing bank retreat in these composite banks where the main mechanism of retreat was erosion of the underlying gravel layer.
20. An important effect of streambank riparian tree cover was the ability of tree roots to reduce fluvial erosion, but there were no predictive models of this effect, so it was not included in BSTEM. However, a significant difference was found between historically protected and historically unprotected sites, which given that

k_d was the significant retreat predictor, implies that the riparian forest reduced erosion where it was present.

21. This highlights the importance of using bank stability models to conduct more long-term studies in order to properly capture the episodic nature of bank failures and retreat on composite banks such as those seen in this study.
22. Process-based models, such as BSTEM, are needed for systems such as these where there is a high degree of variance in retreat rates from year to year. More research is needed to enhance the prediction abilities of the models, especially concerned with riparian vegetation and understanding the spatial and temporal variability of erodibility parameters.

7.2 Recommendations for Future Research

This research set the foundation for a large body of research necessary surrounding the JET, quantifying fluvial resistance of cohesive streambanks, and the use of this information in predictive modeling for improved watershed management. With the emergence of two new solution techniques, the scour depth solution and the iterative solution, for deriving the erodibility parameters from the JET, research into applying and verifying these solutions is needed. Beyond solution technique, more research is needed on the operation of the JET in the laboratory or in the field. Experience from this research suggests that there may be operating variables that could have an impact on the derivation of the erodibility parameters. Variables such as the head setting, the total duration of the test, and the measurement intervals used all have potential to effect the derivation of the erodibility parameters. These impacts could vary by solution technique as well. For example, the iterative solution makes the assumption that the equilibrium scour depth is

reached and, therefore, could be quite sensitive to the duration of the test. Simon et al. (2010) has suggested combatting this with the use of a dimensionless time filter, however more research is needed in this area. Research with respect to these operating variables could greatly enhance the use of the JET in terms of confidence in the parameter results.

This study also raised the question of how to accurately quantify soil erodibility on a site scale. With the wide range of variability that was shown in this and other studies, additional research is required in order to effectively use *in situ* measurements within the predictive framework of process-based models. The variability quantified in this research in terms of sample size requirements highlights the large degree of uncertainty present when inputting these parameters into models using current practices. Improvements in JET operation as discussed previously could aid in reducing this variability and uncertainty, but more research is also needed into quantifying the variability in soil erodibility due subaerial processes. Subaerial processes have been shown to have both a spatial and temporal component that is not captured by the JET at one discrete time and one discrete location. Quantifying these variations and their effects on soil resistance to fluvial erosion would greatly enhance the predictive capabilities of currently used models.

The BSTEM application in this study highlighted this fact. Currently, lumped calibration terms are used to account for temporal and spatial changes in the erodibility parameters of bank materials. There are currently no models that have the capability to handle spatial and temporal changes in erodibility parameters for streambanks. Erodibility parameters that are measured at a discrete point in time and space are being used to model streambank erosion over the course of many years and even decades. This

requires intensive calibration to account for changes in bank resistances that are not accounted for within the framework of the model. More research into quantifying spatial and temporal changes in the erodibility of cohesive streambanks would aid in advancing these models. This will require, specifically, a closer look at subaerial processes and their effects on reducing the ability of streambanks to resist fluvial erosion.

These advances, and others, in the field of cohesive soil erosion would work to augment our understanding of the complexities of streambank erosion. Working towards a greater understanding, and therefore more precise modeling, of streambank erosion would aid in making more informed watershed management decisions.

CHAPTER 8

REFERENCES

Abaci, O. and A. N. Thanos Papanicolaou. 2009. Long-term effects of management practices on water-driven soil erosion in an intense agricultural sub-watershed: monitoring and modeling. *Hydrol. Process.* 23, 2818-2837.

Al-Madhhachi, A. T., G. A. Fox, G. J. Hanson, A. K. Tyagi, and R. Bulut. 2014. Mechanistic detachment rate model to predict soil erodibility due to fluvial and seepage forces. *J. Hydraul. Eng. ASCE*, doi: 10.1061/(ASCE)HY.1943-7900.000836.

Al-Madhhachi, A. T., G. J. Hanson, G. A. Fox, A. K. Tyagi, and R. Bulut. 2013a. Measuring erodibility of cohesive soils using laboratory "mini" jet erosion tests. *T. ASABE* 56(3): 901-910.

Al-Madhhachi, A. T., G. J. Hanson, G. A. Fox, A. K. Tyagi, and R. Bulut. 2013b. Deriving parameters of a fundamental detachment model for cohesive soils from flume and jet erosion tests. *T. ASABE* 56(2): 489-504.

ASTM Standard D421 – 85. 2002. Standard practice for dry preparation of soil samples for particle size analysis and determination of soil constants. ASTM International, West Conshohocken, PA, 2002. Available www.astm.org.

ASTM Standard D422 – 63. 2002. Standard test method for particle size analysis of soils. ASTM International, West Conshohocken, PA, 2002. Available www.astm.org.

Bernhardt, E. S., M. A. Palmer, J. D. Allan, G. Alexander, K. Barnas, S. Brooks, J. Carr, S. Clayton, C. Dahm, J. Follstad-Shah, D. Galat, S. Gloss, P. Goodwin, D. Hart, B. Hassett, R. Jenkinson, S. Katz, G. M. Kondolf, P. S. Lake, R. Lave, J. L. Meyer, T. K. O'Donnell, L. Pagano, B. Powell, and E. Sudduth. 2005. Synthesizing U.S. river restoration efforts. *Science*, 308: 636–637. http://dx.doi.org/10.1126/science. 1109769.

Blaisdell, F. W., L. A. Clayton, and C. G. Hebaus. 1981. Ultimate dimension of local scour. *J. Hydraul. Div. ASCE* 107(3): 327-337.

Borradaile, G. 2003. Statistics of Earth Science Data: Their Distribution in Time, Space, and Orientation. Springer, New York, NY, 2003.

Briaud, J. L., C. K. Ting, H. C. Chen, S. W. Han, and K. W. Kwak. 2001. Erosion function apparatus for scour rate predictions. *J. Geotech. Geoenviron*. 127(2): 105-113.

Bunzl, K., W. Schimmack, and P. Jacob. 2001. Uncertainty analysis of the external gamma-dose rate due to the variability of the vertical distribution of 137Cs in the soil. *Jour. Environ. Radioactivity* 54(2): 243–252.

Camporeale C, P. Perona, A. Porporato, and L. Ridolfi. 2007. Hierarchy of models for meandering rivers and related morphodynamic processes. *Rev. Geophys.*, 45, RG1001. http://dx.doi.org/10.1029/2005RG000185.

Cancienne, R. M., G. A. Fox, and A. Simon. 2008. Influence of seepage undercutting on the stability of root-reinforced streambanks. *Earth Surface Proc. Land.* 33 (1):

1769-1786. doi: 10.1002/esp.1657.

Clark, L. A., and T. M. Wynn. 2007. Methods for determining streambank critical shear stress and soil erodibility: Implications for erosion rate predictions. *Trans. ASABE* 50(1): 95-106.

Cossette, D., K. A. Mazurek, and C. D. Rennie. 2012. Critical shear stress from varied methods of analysis of a submerged circular turbulent impinging jet test for determining erosion resistance of cohesive soils. In *Proc. 6th Intl. Conf. on Scour and Erosion (ICSE6)*, 11-18. Paris, France: Société Hydrotechnique de France (SHF).

Daly, E. R., G. A. Fox, A. T. Al-Madhhachi, and R. B. Miller. 2013a. A scour depth approach for deriving erodibility parameters from Jet Erosion Tests. *Trans. ASABE* 56(6): 1343-1351.

Daly, E. R., G. A. Fox, and A. T. Al-Madhhachi. 2013b. Application of excess shear stress and mechanistic detachment rate models for the erodibility of cohesive soils. ASABE Paper No. 131596568. St. Joseph, Mich.: ASABE.

Darby S. E., M. Rinaldi, and S. Dapporto. 2007. Coupled simulations of fluvial erosion and mass wasting for cohesive river banks. *J. Geophysical Res.*, 112, F03022. http://dx.doi.org/ 10.1029/2006JF000722.

Darby S. E., and C. R. Thorne. 1996. Numerical simulation of widening and bed deformation of straight sand-bed rivers. I. Model development. *J. Hydraulic Eng*, 122: 184–193.

Duan J. 2005. Analytical approach to calculate rate of bank erosion. *J. Hydraul. Eng.*, 131(11): 980–990.

Dunn, I. S. 1959. Tractive resistance of cohesive channels. *J. Soil Mech. Foundations Div. - ASCE* 85 (SM3): 1 – 24.

Easson G., and L. D. Yarbrough. 2002. The effects of riparian vegetation on bank stability. *Environ. Eng. Geosci.,* 8(4): 247–260.

Fox G. A, and C. J. Penn. 2013. Empirical model for quantifying total phosphorus reduction by vegetative filter strips. *Trans. ASABE,* 56(4): 1461–1469.

Fox, G. A. and G. V. Wilson. 2010. The role of subsurface flow in hillslope and stream bank erosion: a review. *Soil Sci. Soc. Am. J.* 74 (1): 717-733, doi: 10.2135/sssaj2009.0319.

Fox, G. A., D. M. Heeren, R. B. Miller, A. R. Mittelstet, and D. E. Storm. 2011. Flow and transport experiments for a streambank seep originating from a preferential flow pathway. *J. Hydrol.* 403(3-4): 360-366.

Fox, G. A., G. J. Sabbagh, W. Chen, and M. Russell. 2006. Uncalibrated modeling of conservative tracer and pesticide leaching to groundwater: Comparison of potential Tier II exposure assessment models. *Pest Mgmt. Sci.* 62(6): 537-550.

Fredlund D. G. and H. Rahardjo. *Soil Mechanics of Unsaturated Soils*. New York: John Wiley and Sons, Inc; 1993.

Garcia M. Sediment transport and morphodynamics. In: Garcia M, editor. *Sedimentation Engineering: Processes, Measurements, Modeling and Practice*, ASCE Manuals and Reports on Engineering Practice No. 110, Reston, VA: American Society of Civil Engineers; 2008, p. 21–164.

Grabowski, R. C., I. G. Droppo, and G. Wharton. 2011. Erodibility of cohesive sediment: The importance of sediment properties. *Earth-Science Rev.* 105 (1): 101 – 120,

doi: 10.1016/j.earscirev.2011.01.008.

Gray D. H. and H. Ohashi. 1983. Mechanics of fiber reinforcement in sand. *J. Geotech. Engrg.*, 109: 335–353.

Hale, W.E. 1972. Sample size determination for the log-normal distribution. *Atmospheric Environment*. 6(1): 419 – 422.

Hanson, G. J. 1990a. Surface erodibility of earthen channels at high stresses: I. Open channels testing. *Trans. ASAE* 33(1): 127-131.

Hanson, G. J. 1990b. Surface erodibility of earthen channels at high stresses: II. Developing an *in situ* testing device. *Trans. ASAE* 33(1): 132-137.

Hanson, G. J., and A. Simon. 2001. Erodibility of cohesive streambeds in the loess area of the Midwestern USA. *Hydrol. Proc*. 15(1): 23-28.

Hanson, G. J., and K. R. Cook. 1997. Development of excess shear stress parameters for circular jet testing. ASAE Paper No. 972227. St. Joseph, Mich.: ASAE.

Hanson, G. J., and K. R. Cook. 1999. Procedure to estimate soil erodibility for water management purposes. ASAE Paper No. 992133. St. Joseph, Mich.: ASAE.

Hanson, G. J., and K. R. Cook. 2004. Apparatus, test procedures, and analytical methods to measure soil erodibility *in situ*. *Applied Eng. in Agric.* 20(4): 455-462.

Hanson, G. J., K. M. Robinson, and D.M. Temple. 1990. Pressure and stress distributions due to a submerged impinging jet. ASCE National Conference on Hydraulic Engineering, New York: 252−530.

Hanson, G. J., K. M. Robinson, and K. R. Cook. 2002. Scour below an overfall: part II. Prediction. *Trans. ASAE* 45(4): 957-964.

Heeren, D. M., A. R. Mittelstet, G. A. Fox, D. E. Storm, A. T. Al-Madhhachi, T. L. Midgley, A. F. Stringer, K. B. Stunkel, and R. B. Tejral. 2012. Using rapid geomorphic assessments to assess streambank stability in Oklahoma Ozark streams. *Trans. ASABE* 55(3): 957-968.

Jenkins J. C., D. C. Chojnacky, L. S. Heath, and R. A. Birdsey. Comprehensive database of diameter-based biomass regressions for North American tree species. General Technical Report NE-319, USDA Northeastern Research Station; 2004.

Jia D., X. Shao, H. Wang, and G. Zhou. Three-dimensional modeling of bank erosion and morphological changes in the Shishou bend of the middle Yangtze River. *Adv. Water Res.* (2010), **33**(3): 348-360.

Julian, J. and R. Torres. 2006. Hydraulic erosion of cohesive riverbanks. *Geomorphology* 76(1): 193 – 206.

Karmaker, T., and S. Dutta. 2011. Erodibility of fine soil from the composite river bank of Brahmaputra in India. *Hydrol. Process* 25: 104-111.

Khosronejad A., C. Hill, S. Kang, and F. Sotirpoulos. Computational and experimental investigation of scour past laboratory models of stream restoration rock structures. *Adv. Water Res.* (2013), **54**: 191-207.

Kronvang B, J. Audet, A. Baattrup-Pedersen, H. S. Jensen, and S. E. Larsen. Phosphorus loads to surface water from bank erosion in a Danish lowland river basin. *J. Environ. Qual.* (2012), **41**: 304–313.

Lai, Y. G., R. E. Thomas, Y. Ozeren, A. Simon, B. P. Greimann, and K. Wu. Modeling of multilayer cohesive bank erosion with a coupled bank stability and mobile-bed model. *Geomorphology* (2014), doi: 10.1016/j.geomorph.2014.07.017.

Langendoen, E. J., and A. Simon. Closure to "Modeling the evolution of incised streams. II: streambank erosion". *J. Hydraul. Engr.* (2009), **135**: 1107–1108.

Langendoen, E. J., and A. Simon. Modeling the evolution of incised streams. II: Streambank erosion. *J. Hydraul. Engr.* (2008), **134**(7): 905–915.

Langendoen, E. J. 2000. CONCEPTS – Conservational channel evolution and pollutant transport system, stream corridor version 1.0. edited by U.S. Department of Agriculture, Agricultural Research Service. Oxford, MS: National Sedimentation Laboratory.

Laubel, A., B. Kronvang, A. B. Hald, and C. Jensen. Hydromorphological and biological factors influencing sediment and phosphorus loss via bank erosion in small lowland rural streams in Denmark. *Hydrol. Proc.* (2003), **17**(17): 3443–3463.

Lavendel, B. The business of ecological restoration. *Ecol. Res.* (2002), **20**: 173–178.

Layzell, A. L., and R. D. Mandel. 2014. An assessment of the erodibility of Holocene lithounits comprising streambanks in northeastern Kansas, USA. *Geomorphology* 213: 116-127.

Marot, D., P. L. Regazzoni, and T. Wahl. 2011. An energy-based method for providing soil surface erodibility. *J. Geotech. Geoenviron. Eng. ASCE* 137(12): 1290-1293.

Mazurek, K. A. 2010. Erodibility of a cohesive soil using a submerged circular turbulent impinging jet test. In *Proc. 2nd Joint Federal Interagency Conf. on Sedimentation and Hydrologic Modeling*. Reston, Va.: U.S. Geological Survey.

Micheli, E.R., and J. W. Kirchner. Effects of wet meadow riparian vegetation on streambank erosion. 2. Measurements of vegetated bank strength and consequences for failure mechanics. *Earth Surf. Proc. Land*. (2002), **27**: 687–697.

Midgley, T. L., G. A. Fox, and D. M. Heeren. 2012. Evaluation of the Bank Stability and Toe Erosion Model (BSTEM) for predicting lateral streambank retreat on composite streambanks. *Geomorphology* 145-146: 107-114.

Midgley, T., G. A. Fox, G. V. Wilson, R. M. Felice, and D. M. Heeren. 2013. In-situ soil pipeflow experiments on contrasting streambank soils. *Transactions of the ASABE* 56(2): 479 – 488.

Millar, R. G. 2000. Influence of bank vegetation on alluvial channel patterns. *Water Resour. Res.*, 36: 1109-1118.

Millar, R. G. 2005. Theoretical regime equations for mobile gravel-bed rivers with stable banks. *Geomorphology*, 64(3-4): 207–220.

Miller, R. B. 2012. Hydrogeophysics of gravel-dominated alluvial floodplains in eastern Oklahoma. Ph.D. Dissertation, Oklahoma State University, Stillwater, OK.

Miller, R. B., G. A. Fox, C. Penn, S. Wilson, A. Parnell, R. A. Purvis, and K. Criswell. 2014. Estimating sediment and phosphorus loads from streambanks with and without riparian protection. *Ag. Ecosyst. Environ.* 189: 70-81, doi: 10.1016/j.agee.2014.03.016.

Minitab, Inc. 2009. Minitab Statistical Software, Release 16 for Windows, State College, Pennsylvania. Minitab® is a registered trademark of Minitab, Inc.

Motta, D., J. D. Abad, E. J. Langendoen, and M.H. Garcia. 2012. A simplified 2D model for meander migration with physically-based bank evolution. *Geomorphology*, 163: 10–25. http://dx.doi.org/10.1016/j.geomorph.2011.06.036.

Mukundan, R., D. E. Radcliffe, J. C. Ritchie, L. M. Risse, and R. A. McKinley. 2010. Sediment fingerprinting to determine the source of suspended sediment in a southern piedmont stream. *J. Envion. Qual.*, 39: 1328–1337.

National Engineering Handbook (NEH). 2011. Erodibility parameter selection for soil material horizons (surface detachment coefficient and headcut erodibility index). Appendix 52D, Part 628, National Engineering Handbook (NEH), USDA-NRCS, 52D1 – 52D15.

Neitsch, S. L., J. G. Arnold, J. R. Kiniry, and J. R. Williams. 2011. Soil and water assessment tool theoretical documentation version 2009. Texas Water Resources Institute Technical Report No. 406.

Oklahoma Conservation Commission (OCC). 2010. Watershed Based Plan for the Illinois River Watershed. OCC Water Quality Division. Oklahoma City, OK.

Papanicolaou, A. N., M. Elhakeem, and R. Hilldale. 2007. Secondary current effects on cohesive river bank erosion. *Water Resour. Res.*, 43, W12418. http://dx.doi.org/10.1029/ 2006WR005763.

Partheniades, E. 1965. Erosion and deposition of cohesive soils. *J. Hydraul. Div. - ASCE* 91(HY1): 105-139.

Pizzuto, J. E., M. O'Neal, and S. Stotts. 2010. On the retreat of forested, cohesive streambanks. *Geomorphology*, 116: 341–352.

Pizzuto, J. E. Streambank Erosion and River Width Adjustment. In: Garcia M, editor. *Sedimentation Engineering: Processes, Measurements, Modeling and Practice*,

ASCE Manuals and Reports on Engineering Practice No. 110, Reston, VA: American Society of Civil Engineers; 2008, p. 387–438.

Pollen-Bankhead, N, and A. Simon. 2009. Advanced application of root-reinforcement algorithms for bank stability modeling. *Earth Surf. Proc. Land.*, 34: 471–480.

Rinaldi, M., B. Mengoni, L. Luppi, S. E. Darby, and E. Mosselman. 2008. Numerical simulation of hydrodynamics and bank erosion in a river bend. *Water Resour. Res.*, 44, W09428. http://dx.doi.org/ 10.1029/2008WR007008.

Rousselot, P. 2009. Discussion of "Modeling the evolution of incised streams. II: streambank erosion". *J. Hydraul. Engr.*, 135: 1107–1108.

Sabbagh, G. J., G. A. Fox, A. Kamanzi, B. Roepke, and J. Z. Tang. 2009. Effectiveness of vegetative filter strips in reducing pesticide loading: Quantifying pesticide trapping efficiency. *J. Environ. Qual.*, 38(2): 762–771.

Sekely, A. C., D. J. Mulla, and D. W. Bauer. 2002. Streambank slumping and its contribution to the Phosphorus and suspended sediment loads of the Blue Earth River, Minnesota. *J. Soil and Water Conserv.*, 57(5): 243–250.

Shields, I. A. 1936. Application of similarity principles and turbulence research to bed-load movement. In: Ott, W.P., van Uchelen, J.C. (Eds.), (Translators), Hydrodynamics Laboratory Publication, vol. 167. California Institute of Technology, Pasadena, CA.

Simon, A., and M. Rinaldi. 2006. Disturbance, stream incision, and channel evolution: The roles of excess transport capacity and boundary materials in controlling channel response. *Geomorphology*, 79(3-4): 361–383. http://dx.doi.org/10.1016/ j.geomorph.2006. 06.037.

Simon, A., and A. J. Collison. 2002. Quantifying the mechanical and hydrologic effects of riparian vegetation on streambank stability. *Earth Surface Processes and Landforms*, 27(5): 527–546.

Simon, A., A. Curini, S. A. Darby, and E. J. Langendoen. 2000. Bank and near-bank processes in an incised stream. *Geomorphology*, 35: 193–217.

Simon, A., N. Pollen, and E. Langendoen. 2006. Influence of two woody riparian species on critical conditions for streambank stability: Upper Truckee River, California. *J. Am. Water Res. Assoc.*, 42(1): 99–113.

Simon, A., N. Pollen-Bankhead, V. Mahacek, and E. J. Langendoen. 2009. Quantifying reductions of mass-failure frequency and sediment loadings from streambanks using toe protection and other means: Lake Tahoe, United States. *J. Am. Water Res. Assoc.*, 45: 170–186.

Simon, A., N. Pollen-Bankhead, and R. E. Thomas. 2011. Development and application of a deterministic bank stability and toe erosion model for stream restoration. In *Stream Restoration in Dynamic Fluvial Systems: Scientific Approaches, Analyses, and Tools*, 453-474. Geophysical Monograph Series, vol. 194. Washington, D.C.: American Geophysical Union.

Simon, A., R. E. Thomas, and L. Klimetz. 2010. Comparison and experiences with field techniques to measure critical shear stress and erodibility of cohesive deposits. In *Proc. 2nd Joint Federal Interagency Conf. on Sedimentation and Hydrologic Modeling*. Reston, Va.: U.S. Geological Survey.

Simon, A., R.E. Thomas, and L. Klimetz. 2010. Comparison and experiences with field techniques to measure critical shear stress and erodibility of cohesive deposits. In:

Proc. 2nd Joint Federal Interagency Conf. on Sedimentation and Hydrologic Modeling. Reston, Va.: U.S. Geological Survey.

Smeardon, E. and R. Beasley. 1961. Critical tractive forces in cohesive soil. *Agr. Eng.* 42(1): 26 – 29.

Stein, O. R., and D. D. Nett. 1997. Impinging jet calibration of excess shear sediment detachment parameters. *Trans. ASAE* 40(6): 1573-1580.

Stein, O. R., and D. D. Nett. 1997. Impinging jet calibration of excess shear sediment detachment parameters. *Trans. ASAE* 40(6): 1573-1580.

Storm, D.E., M.J. White, and S. Stoodley. 2003. Fort Cobb Basin—Modeling and land cover classification, final report to the Oklahoma Conservation Commission. Available online at http://storm.okstate.edu/reports/Fort%20Cobb%20report%20Final%20Report%202_262003.pdf.

Tealdi, S., C. Camporeale, and L. Ridolfi. 2011. Long-term morphological river response to hydrological changes. *Adv. Water Res.*, 34(12): 1643-1655.

Thoman, R. W. and S. L. Niezgoda. 2008. Determining erodibility, critical shear stress, and allowable discharge estimates for cohesive channels: case study in the Powder River basin of Wyoming. *J. Hydraul. Eng.* 134: 1677-1687.

Thorne, C. R., and N. K. Tovey. 1981. Stability of composite river banks. *Earth Surf. Proc. Land.*, 6: 469–484.

Ulrich, J. S. and J. L. Nieber. 2008. Streambank and bluff erosion modeling for the Knife River, Minnesota. ASABE Annual International Meeting, Providence, RI. June 29 – July 2.

USDA ARS. Bank Stability and Toe Erosion Model Homepage. USDA Agricultural Research Service National Sedimentation Laboratory. Oxford, MS. http://www.ars.usda.gov/research/docs.htm?docid=5044. Accessed January 23, 2014.

USEPA. 1998. Guidelines for Ecological Risk Assessment Washington, DC.*Impaired Waters and Total Maximum Daily Loads*, March 21, 2011 2011 [cited April 1. Available from http://water.epa.gov/lawsregs/lawsguidance/cwa/tmdl/.

Utley, B. and T. Wynn. 2008. Cohesive Soil Erosion: Theory and Practice. World Environmental and Water Resources Congress 2008 pp. 1-10. doi: 10.1061/40976(316)289.

Wahl, T. L., P. L. Regazzoni, and Z. Erdogan. 2008. Determining erosion indices of cohesive soils with the hole erosion test and jet erosion test. Report DSO-08-05, Bureau of Reclamation, Hydraulic Investigations and Laboratory Services.

Wan, C. F., and R. Fell. 2004. Investigation of rate of erosion of soils in embankment dams. *J. Geotech. Geoenviron.* 130(4): 373-380.

Wilson, B. N. 1993a. Development of a fundamental based detachment model. *Trans. ASABE* 36(4): 1105-1114.

Wilson, B. N. 1993b. Evaluation of a fundamental based detachment model. *Trans. ASABE* 36(4): 1115-1122.

Wilson, C. G., R. A. Kuhnle, D. D. Bosch, J. L. Steiner, P. J. Starks, M. D. Tomer, and G. V. Wilson. 2008. Quantifying relative contributions from sediment sources in

Conservation Effects Assessment Project watersheds. *J. Soil Water Cons.* 63(6): 523-531.

Wilson, C. G., R. A. Kuhnle, S. M. Dabney, R. N. Lerch, C. H. Huang, K. W. King, and S. J. Livingston. 2014. Fine sediment sources in conservation effects assessment project watersheds. *Journal of Soil and Water Conservation* 69(5): 402-413.

Wu, F.-C., C.-H. Yeh, and C.-H. Chen. 2013. Economical model of selecting an appropriate sample size of experiments. *International Journal of Information and Education Technology* 3(5): 567 – 570.

Wynn, T. M., and S. Mostaghimi. 2006. The effects of vegetation and soil type on streambank erosion, southwestern Virginia, USA. *Journal of the American Water Resources Association*: 69-82.

Wynn, T. M., M. B. Henderson, and D. H. Vaughan. 2008. Changes in streambank erodibility and critical shear stress due to subaerial processes along a headwater stream, southwestern Virginia, USA. *Geomorphology* 97: 260-273.

Zaimes, G. N., R. C. Schultz, and T. M. Isenhart. 2008. Streambank soil and phosphorus losses under different riparian land-uses in Iowa. *J. Am. Water Res. Assoc.*, 44(4): 935–947.

Ziemer, R. R. Roots and the stability of forested slopes. In: Davies TRH, Pearce AJ, editors. *Erosion and Sediment Transport in Pacific Rim Steeplands*, Proceedings of the Christchurch Symposium, 25-31 January 1981, Christchurch, New Zealand: Int. Assn. Hydrol. Sci. Pub. No. 132; 1981, p. 343–361.

VITA

Erin Rebecca Daly

Candidate for the Degree of

Doctor of Philosophy

Thesis: QUANTIFYING FLUVIAL RESISTANCE OF STREAMBANKS USING JET EROSION TESTS

Major Field: Biosystems and Agricultural Engineering

Biographical:

Education:

Completed the requirements for the Doctor of Philosophy in Biosystems and Agricultural Engineering at Oklahoma State University, Stillwater, Oklahoma in December, 2014.

Completed the requirements for the Master of Science in Biosystems and Agricultural Engineering at Oklahoma State University, Stillwater, Oklahoma in 2012.

Completed the requirements for the Bachelor of Science in Biosystems Engineering at Clemson University, Clemson, South Carolina in 2010.

Experience:

2012 – 2014: Graduate Research Associate, Buchanan Fellow, Oklahoma State University
2010 – 2013: Graduate Teaching Assistant, Oklahoma State University
2010 – 2012: Graduate Research Assistant, Oklahoma State University
2010: Research Assistant, Clemson University
2008 – 2010: Ernest F. Hollings Undergraduate Scholar, National Oceanic and Atmospheric Association

Professional Memberships:

American Society of Agricultural and Biological Engineers
Registered Engineer in Training in State of South Carolina